VOLUME **XXI** 2018
Évfolyam

HUNGARIAN NATIONAL REPORT ON INTERNATIONAL UNION OF GEODESY AND GEOPHYSICS

2015-2018

PUBLICATIONS IN GEOMATICS
Geomatikai Közlemények

HU ISSN 1419-6492

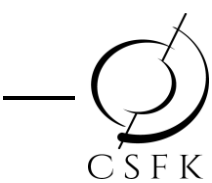

MTA CSFK GEODÉZIAI ÉS GEOFIZIKAI INTÉZET
9400 SOPRON, CSATKAI U. 6-8.

Hungarian National Report on International Union of Geodesy and Geophysics 2015-2018

PUBLICATIONS IN GEOMATICS
Geomatikai Közlemények

kiadja az

MTA CSFK GEODÉZIAI ÉS GEOFIZIKAI INTÉZETE

9400 Sopron, Csatkai E. u. 6-8. Pf. 5.
tel.: 99 / 508-340 fax.: 99 / 508-355
e-mail: geomatika@ggki.hu
web: www.geomatika.ggki.hu
web programozó: Lovranits Tamás

felelős kiadó:

Szarka László Csaba
főigazgató

főszerkesztő:

Papp Gábor

angol nyelvi szerkesztő:

Papp Gábor

technikai szerkesztő:

Rács Ágnes

készült a
LŐVÉR PRINT Kft. nyomdájában
9400 Sopron, Ady Endre u. 5.
tel.: 99 / 329-977

megjelent 100 példányban
Sopron, 2018

HU ISSN 1419-6492

HUNGARIAN NATIONAL REPORT ON INTERNATIONAL UNION OF GEODESY AND GEOPHYSICS

2015-2018

PUBLICATIONS IN GEOMATICS

Geomatikai Közlemények

XXI.

"Minden nemzet a maga
nyelvén lett tudós,
de idegenen sohasem."

(Bessenyei György)

GENERAL INFORMATION

Publications in Geomatics is a periodical journal since 1998 issuing generally one number a year. The purpose of the journal is to provide the home researchers and experts a forum to publish, mainly in Hungarian language, their new scientific results in the field of geosciences (geodesy, photogrammetry, geoinformatics, physical geodesy, geophysics, Earth magnetism, geodynamics, research of the inner structure of the Earth and the physics of its troposphere and solar-terrestrial environment) obtained from the analysis of spatial-temporal data using the methods of geomatics. The submitted papers are subject to an editorial procedure which is in compliance with the present-day standards, namely two independent referees form opinion about the manuscript. By default the names of the referees are known only to the editorial board, but their identity can be disclosed according to their wish. On the basis of reviews the editorial board decides whether it meets the requirements of the form, and content of the Publications in Geomatics and whether the eventual errors and shortcomings can be corrected and complemented by revision. The expert work of the editorial board is supported by an advisory board.

Editors, accomplishing the Journal's editing as a voluntary work, place emphases on rapid and high quality work. Therefore both the authors and the referees are expected to make efforts which are appreciated by the Editorial Board in advance. For this to do, it is suggested to peruse the instructions for authors and reviewers

Geomatikai_Közlemények_instrukciók_szerzőknek.docx,

Geomatikai_Közlemények_instrukciók_bírálóknak.pdf.

These files provide basic information for the use of the editorial system and for maintaining the high professional standards.

Publications in Geomatics is published by the Geodetic and Geophysical Institute of the Research Centre for Astronomy and Earth Sciences, Hung. Acad. Sci. Publishing costs are covered from grant money, the sponsorship of scientific organizations (e.g. Soproni Tudós Társaság) and from subsidy of the Seminar Series on Geomatics organized by the GGI in every two years.

The recent volume of Publications in Geomatics was sponsored by the Geodetic and Geophysical Institute of the Research Centre for Astronomy and Earth Sciences, Hungarian Academy of Sciences.

The association-, division- and commission reports were reviewed by Katalin Bene, Imre Bonta, Tamás Bozóki, Csenge Czanik, Lóránt Földváry, László Haszpra, Dávid Karátson, Ambrus Kenyeres, Árpád Kis, Károly Kis, Márta Kis, János Kiss, Rita Klébesz, István János Kovács, Péter Kovács, István Lemperger, János Lichtenberger, Gyula Mentes, Róbert Mészáros, Béla Paláncz, Szabolcs Rózsa, Péter Steinbach, József Szilágyi, Bence Takács, Péter Varga, Miklós Vincze, Viktor Wesztergom.

The editors in charge of the reports were László Bányai, Judit Benedek, Zoltán Gráczer, Katalin Gribovszki, János Kalmár, Ambrus Kenyeres, Árpád Kis, Gábor Papp, Szilárd Szabó, Gábor Ujvári.

PREFACE

The Hungarian National Committee of the International Union of Geodesy and Geophysics (IUGG, http://www.iugg.org) is pleased to present the 2015-2018 quadrennial Hungarian report to the membership of the IUGG. This report reviews the work accomplished in Hungary during the past four years and provides the record of the Hungarian contributions to the geodetic and geophysical research.

The Report covers the research and development performed by Universities, Scientific Institutions, and Government Agencies, subdivided by subjects in agreement with the following International Associations of IUGG: *a)* IACS (International Association of Cryospheric Sciences), *b)* IAG (International Association of Geodesy), *c)* IAGA (International Association of Geomagnetism and Aeronomy), *d)* IAHS (International Association of Hydrological Sciences), *e)* IAMAS (International Association of Meteorological and Atmospheric Sciences), *f)* IAPSO (International Association for the Physical Sciences of the Oceans), *g)* IASPEI (International Association of Seismology and Physics of the Earth's Interior) and *h)* IAVCEI (International Association of Volcanology and Chemistry of the Earth's Interior).

Since the last 26th General Assembly in Prague, Czech Republic, June 22-July 2, 2015 there has been some minor changes in the list of members of the Hungarian National Committee for IUGG. The members of the Hungarian National Committee for IUGG in the period of 2016-2019 are as follows. (National Correspondents of the Associations are indicated in brackets.) *President*: József ÁDÁM (IAG); *Secretary*: László BOZÓ (IAMAS); *Members*: Antal ÁDÁM, Péter BAKONYI, Judit BARTHOLY (IACS), István BONDÁR (IASPEI), László BÁNYAI, Gábor DOBOSI (IAVCEI), Attila GALSA, Zoltán GRIBOVSZKI (IAHS), Szabolcs HARANGI, Balázs HEILIG, László HORVÁTH (IAPSO), Péter MÁRTON, László SZARKA, József SZILÁGYI, Lajos VÖLGYESI, Tamás WEIDINGER and Viktor WESZTERGOM (IAGA).

In the past period the Hungarian National Committee for IUGG held three business meetings in Budapest at the following dates: *a)* 17 November 2015, *b)* 20 March 2018 and *c)* 20 November 2018.

This quadrennial Report is published by the Geomatikai Közlemények (Publications in Geomatics), a Journal issued by the Geodetic and Geophysical Institute of the Research Centre for Astronomy and Earth Sciences of the Hungarian Academy of Sciences, in the Volume XXI, 2018. Different parts of the Report are prepared by different Sections of the Hungarian National Committee for IUGG, and written and compiled by different authors. Therefore they are not quite balanced in size and the arrangements of the texts are not similar to each other. This Report would not be possible without the unselfish service of authors and editors.

We hope that this Report can provide to our foreign Colleagues a fairly clear picture of the development and what has been done in the past four years in the field of geodesy and geophysics in Hungary.

On behalf of the Hungarian National Committee for IUGG:

József Ádám
President

CONTENTS

Tartalomjegyzék

HUNGARIAN NATIONAL REPORT ON IACS (2015-2018)

Judit Bartholy[*]*, Rita Pongrácz*[*]

1 Introduction

The current reporting paper serves as a summary of the research activity related to the Cryosphere and carried out in Hungary during 2015-2018.

2 The Cryosphere-related research in Hungary

A large group of cryospheric research focuses on the analysis of ice-related climate proxy data from different locations (including samples from outside Hungary). For instance, Kern et al. (2016b, 2017b, 2018b) used the measurements of the radiocarbon and tritium activity in a 5.8 m long ice core from the Saarhalle Dachstein Mammoth Cave. The derived dataset is publicly available via PANGAEA at https://doi.org/10.1594/PANGAEA.881056. From another location, namely, the Velebit Mt. in Croatia, three cave ice deposits are evaluated in Kern et al. (2016a, 2017a, 2018a). The used methodology (i.e. ice core drilling in cave environment and the dating technique of ice deposits) is presented in Kern and Persoiu (2018) and Kern (2018). In addition, the data sets of annual freshwater ice phenology were compiled for the largest river (Danube) and the largest lake (Lake Balaton) in eastern-central Europe, extending regular river and lake ice monitoring data through the use of historical observations and documentary records dating back to AD 1774 (Takács and Kern 2017a) and AD 1885 (Takács and Kern 2017b), respectively. The analysis of the datasets is published in Takács et al. (2018), which concludes that the dates of the first appearance of ice and freeze-up have shifted later, namely by 12-30 days (Danube) and 4-13 days (Balaton) per 100 years. Furthermore, the analysis showed shifts in break-up and ice-off also, which occurred earlier by 7-13 and 9-27 days/100 years, respectively.

The publications of Hatvani and Kern (2015, 2017) and Hatvani et al. (2017) analyze ice core samples from Antarctica (i.e. meteorological stations Vernadsky and Halley Bay). Topál et al. (2017) used Greenland ice cores (from the North Greenland Traverse) to analyze the late Holocene climate variations. Ice core analysis is compared to other paleoclimatic techniques (e.g., tree rings) in a specific study (Kázmér et al. 2015).

In the framework of another major Cryosphere-related research activity Hungarian researchers from the Institute of Geography and Earth Science regularly organize in-situ measurement campaigns (https://atacama.expedicio.eu/en) in the high Andes mountains (the last two campaigns were in 2016 and 2018), and analyze the results from the arid climate of the Mt. Ojos del Salado (6893 m above sea level). In addition, satellite data is also used to analyze snow coverage of the region. Due to the extremely arid climatic conditions, surface ice is not widespread, although ice bearing permafrost is present above 5250 m, and the active layer of the permafrost becomes extremely thin around 6750 m. Their work appeared in several publications: Nagy et al. (2015, 2016a, 2016b, 2018a, 2018b).

Wet snow conditions in Hungary are analyzed by Somfalvi-Tóth et al. (2018a, 2018b, 2018c) and Simon et al. (2018). The research started with the forecasting problems associated to wet snow (Somfalvi-Tóth et al. 2015, 2016), namely evaluating a wet snow forecasting system using both operational numerical weather prediction models (ECMWF, AROME, ALADIN, WRF) and ensemble methods (AROME-EPS). Then the statistical-climatological background of wet snow in Hungary was investigated using meteorological station data from 1965–2016 and radiosonde data from 1980–2016 period with the following specific questions to be answered:

1) How is the vertical profile during wet snow events?
2) How are the 50- and 100-year return levels of wet snow?
3) How can the wet snow forecast be integrated into operative work?

[*]*ELTE Meteorológiai Tanszék, 1171 Budapest, Pázmány Péter sétány 1/a.*
E-mail: bartholy@caesar.elte.hu, prita@nimbus.elte.hu

The main conclusions of this PhD-related study can be summarised as follows, wet snow occurrences are likely when the following criteria are fulfilled:

(i) Temperature lapse rate between 1000 hPa and 925 hPa fluctuates within a narrow interval (–0.03 °C/km; –0.04 °C/km),
(ii) Positive temperature layer directly above the ground level,
(iii) The lowest atmospheric layer is usually not saturated hence the relative humidity is around 90%–95% at the 1000 hPa pressure level,
(iv) Wind speed is generally low, mostly below 5 m/s,
(v) Average relative topography for 850/1000 hPa is 1300 gpm, with the maximum of 1320 gpm, and the lower quantile of 1260 gpm. The trend analysis of the recent decades show that the number of wet snow cases generally increased in Hungary during 1965–2016.

The last group of publications includes the BSc and MSc thesis work of students specialised in meteorology at the Eötvös Loránd University. The focus of the students' work is on the forecast of precipitation phase in Cséke (2018) and Góth (2018). The role of ice particles within the clouds is discussed by Kordás (2015). The numerical modelling of snowflakes is discussed and attempted by Balogh (2017), which continued in Balogh and Geresdi (2018). A synoptical-climatological analysis of winter weather during Olympic Games can be found in Bata (2015), this research was further extended to winter mountain sports in general, with special emphasis on the impact of climate change to this sector (Bata 2017). Specific geographical locations within the Cryosphere (i.e. Alaska and Antarctica) are included in the climate change analysis carried out by Csobolya (2015). Finally, the Cryosphere in the northern polar region was analyzed by Herman (2016) using combined datasets with both in-situ and satellite measurements.

3 Conclusions

The present report includes 36 publications from Hungarian researchers and students. A large group of research focuses on the analysis of cryospheric proxy data from different locations. Another major Cryosphere-related research activity of Hungarian researchers includes the analysis of in-situ measurement campaigns in the high Andes mountains. The focus of the third group of research activities is wet snow conditions in Hungary. The last group of publications includes the BSc and MSc thesis work of students specialised in meteorology at the Eötvös Loránd University.

References

Balogh AJ (2017): Computer modelling of melting snowflakes (in Hungarian). BSc Thesis. Department of Meteorology, Eötvös Loránd University, Budapest, 30.

Balogh AJ, Geresdi I (2018): Computer modelling of melting snowflakes (in Hungarian). In: Pongrácz R, Mészáros R, Kis A (eds.), Aktuális környezeti problémák az időjárás és az éghajlat összefüggésében, Egyetemi Meteorológiai Füzetek, 30, 28-34, doi: 10.31852/EMF.30.2018.028.034.

Bata J (2015): Analysing the synoptic-climatological conditions during the past and future Winter Olympic Games (in Hungarian). BSc Thesis. Department of Meteorology, Eötvös Loránd University, Budapest, 36.

Bata J (2017): Mountain sports and tourism in the light of climate change (in Hungarian). MSc Thesis, Department of Meteorology, Eötvös Loránd University, Budapest, 44.

Cséke DCs (2018): Estimating the probability of various precipitation phases using ECMWF ensemble predictions. (in Hungarian). MSc Thesis, Department of Meteorology, Eötvös Loránd University, Budapest, 43.

Csobolya K (2015): Analyzing the projected climate change in different regions of the world (in Hungarian). BSc Thesis, Department of Meteorology, Eötvös Loránd University, Budapest, 49.

Góth R (2018): Presentation and evaluation of the precipitation phase forecasting methods used in Hungary (in Hungarian). MSc Thesis, Department of Meteorology, Eötvös Loránd University, Budapest, 74.

Hatvani IG, Kern Z (2015): Weighting alternatives (precipitation vs. accumulation) for water stable isotopes: implications for ice core records In: International Symposium on Isotope Hydrology: Revisiting Foundations and Exploring Frontiers (IAEA), Vienna, Austria, 31-34.

Hatvani IG, Kern Z (2017): Weighting alternatives for water stable isotopes: statistical comparison between station- and firn/ice records. Polish Polar Research, 38(2), 105-124.

Hatvani IG, Leuenberger M, Kohán B, Kern Z (2017): Geostatistical analysis and isoscope of ice core derived water stable isotope records in an Antarctic macro region. Polar Science, 13, 23-32.

Herman Á (2016): Analysis of the changes in the cryosphere in the northern polar region (in Hungarian). BSc Thesis, Department of Meteorology, Eötvös Loránd University, Budapest, 48.

Kázmér M, Major B, Kern Z, Harangi Sz (2015): The 1202 volcanic veil event - historical, tree-ring and ice-core data. In: Brönnimann S, Rohr C, Grosjean M, Joos F, Peter T (eds.) Volcanoes, Climate and Society - Bicentenary of the great Tambora eruption, University of Bern, p. 130.

Kern Z (2018): Dating cave ice deposits. In: Persoiu A, Lauritzen SE (eds.) Ice Caves, Elsevier Science, Amsterdam, 109-122.

Kern Z, Persoiu A (2018): Ice core drilling in cave environment – challenges and achievements over the past 70 years. In: IWIC VIII International Workshop on Ice Caves Potes, Universidad de Valladolid, 58.

Kern Z, Bocic N, Lázár E, Sipos G (2016a): Stratigraphy of the Kugina Ledenica (Central Velebit, Croatia) cave ice deposit and volume change over the past decade. In: Mihevc A, Zupan NH, Gostincar P (eds.) 7th International Workshop on Ice Caves: Program Guide and Abstracts, Karst Research Institute ZRC SAZU, Postojna, Slovenia, 50-50.

Kern Z, Molnár M, Pavuza R (2016b): Radiocarbon analysis of carbonaceous particulate matter from the Saarhalle ice block, Dachstein-Mammoth cave (Mammuthöhle), Austria. In: Mihevc A, Zupan NH, Gostincar P (eds.) 7th International Workshop on Ice Caves: Program Guide and Abstracts, Karst Research Institute ZRC SAZU, Postojna, Slovenia, 48-49.

Kern Z, Bocic N, Sipos, G (2017a): Contrasting mass balance periods in the ice caves of the Velebit Mt, Croatia documented by radiocarbon dated vegetal remains. In: 2nd Radiocarbon in the Environment Conference: Book of Abstracts, Debrecen, 88.

Kern Z, Molnár M, Palcsu L, Pavuza R (2017b): Age constraints on the deposition of the cave ice block of Saarhalle, Dachstein-Mammoth cave (Mammuthöhle, Austria) based on environmental radioisotopes. In: 2nd Radiocarbon in the Environment Conference: Book of Abstracts, Debrecen, 81.

Kern Z, Bočić N, Sipos Gy (2018a): Radiocarbon-Dated Vegetal Remains from the Cave Ice Deposits of Velebit Mountain, Croatia. Radiocarbon, 60(5), 1391-1402.

Kern Z, Palcsu L, Pavuza R, Molnár M (2018b): Age Estimates on the Deposition of the Cave Ice Block in the Saarhalle Dachstein-Mammoth Cave (Mammuthöhle, Austria) based on ^{3}H and ^{14}C. Radiocarbon, 60(5), 1379-1389.

Kordás N (2015): Ice in the clouds: the role of ice particles in the process of separating the charged particles in clouds (in Hungarian). BSc Thesis, Department of Meteorology, Eötvös Loránd University, Budapest, 37.

Nagy B, Kovács J, Mari L, Szalai Z (2015): Ice and water in the world's highest mountain desert, dry Andes, Ojos del Salado region. In: EUGEO Budapest 2015: Congress programme and abstracts. 162. Hungarian Geographical Society, Budapest. (ISBN:978-615-80307-0-0).

Nagy B, Kovács J, Mari L, Ignéczi Á, Szalai Z, Timár G, (2016a): At the edge of the cryosphere: the active layer in the highland desert of Ojos del Salado (Dry Andes, Chile) (in Hungarian). In: Pongrácz R, Mészáros R, Kis A (eds.), Kutatási és operatív feladatok meteorológusként, Egyetemi Meteorológiai Füzetek, 27, 112-118, doi: 10.31852/EMF.27.2016.112.118.

Nagy B, Mari L, Kovács J, Ignéczi Á, Weidinger T, Szalai Z, Timár G (2016b): Permafrost Melting as a Water Source in the Dryest Andes of the Earth (in Hungarian). In: Pajtókné Tari I, Tóth A (eds.) Magyar Földrajzi Napok 2016: Absztraktkötet: VIII. Magyar Földrajzi Konferencia : XVI. Geográfus Doktoranduszok Országos Konferenciája: Oktatás-módszertani és Földrajztanári Konferencia. 159: Eger, Magyarország, 2016. 08. 25-2016. 08. 27. Budapest: Magyar Földrajzi Társaság, 127. (ISBN:978-615-80307-1-7).

Nagy B, Igneczi A, Kovács J, Mari L, Szalai Z (2018a): Shallow ground temperature measurements on the highest volcano of the Earth, the Mt. Ojos del Salado, Arid Andes, Chile. Permafrost and Periglacial Processes, 30, 3-18, DOI: 10.1002/ppp.1989.

Nagy B, Kovács J, Ignéczi Á, Beleznai Sz, Mari L, Szalai Z (2018b): What's happening at the bottom of the Earth's highest-lying desert? - Temperature analysis of the active layer in the Dry Andes (in Hungarian). In: Pongrácz R, Mészáros R, Kis A (eds.), Aktuális környezeti problémák az időjárás és az éghajlat összefüggésében, Egyetemi Meteorológiai Füzetek, 30, 138-149, doi: 10.31852/EMF.30.2018.138.149.

Simon A; Somfalvi-Tóth K, Szűcs M (2018): Probabilistic forecasting of freezing rain and wet snow in Hungary. EMS Annual Meeting Abstracts 15, EMS2018-326.

Somfalvi-Tóth K, Tordai J, Simon A, Kolláth K, Dezső Zs (2015): Forecasting of wet- and blowing snow in Hungary. Időjárás - Quarterly Journal of the Hungarian Meteorological Service, 119(2), 277-306.

Somfalvi-Tóth K, Simon A, Kolláth K, Mészáros R (2016): Summary of Adhesive Snow Forecast at the National Meteorological Service (in Hungarian). In: Pongrácz R, Mészáros R, Kis A (eds.), Kutatási és operatív feladatok meteorológusként, Egyetemi Meteorológiai Füzetek, 27, 142-149, doi: 10.31852/EMF.27.2016.142.149.

Somfalvi-Tóth K, Mészáros R, Simon A (2018a): Comparison of 50-year return period wet snow loads based on weather station data between 1965-1990 and 1991-2016 in Hungary. In: Towards a better harmonization of snow observations, modelling and data assimilation in Europe. COST, ES1404, Harmosnow Workshop and Conference, 69-70.

Somfalvi-Tóth K, Simon A, Mészáros R (2018b): Modelling and operational forecast of hazardous wet snow load at the Hungarian Meteorological Service. In: Towards a better harmonization of snow observations, modelling and data assimilation in Europe. COST ES1404, Harmosnow Workshop and Conference, 64-65.

Somfalvi-Tóth K, Simon A, Mészáros R (2018c): Investigation of Vertical Layering of Adhesive Snow Based on 36 Years of Radiosonde Takeoff Measurements (in Hungarian). In: Pongrácz R, Mészáros R, Kis A (eds.), Aktuális környezeti problémák az időjárás és az éghajlat összefüggésében, Egyetemi Meteorológiai Füzetek, 30, 150-158, doi: 10.31852/EMF.30.2018.150.158.

Takács K, Kern Z (2017a): Long-term ice phenology records of Danube River (East Central Europe) between 1774 -2017 PANGEA, https://doi.org/10.1594/PANGEA/881055.

Takács K, Kern Z (2017b): Long-term ice phenology records of Lake Balaton (East Central Europe) between 1885-2017, PANGEA, https://doi.org/10.1594/PANGEA/881055.

Takács K, Kern Z, Pásztor L (2018): Long-term ice phenology records from eastern–central Europe. Earth System Science Data, 10(1), 391-404.

Topál D, Hatvani IG, Kern Z (2017): Detecting breakpoints in annual δ18 O ice core records from North Greenland. In: Hatvani IG, Tanos P, Cvetkovic M, Fedor F (eds.) Proceedings Book of the 20th Congress of Hungarian Geomathematicians and 9th Congress of Croatian and Hungarian Geomathematicians "Geomathematics in multidisciplinary science - The new frontier?" Pécs Regional Committee of the Hungarian Academy of Science, 20-27.

HUNGARIAN NATIONAL REPORT ON IAG (2015-2018)

József Ádám[*]

This report outlines the activities of Hungary in geodesy for the period January 2015 to December 2018. It has been prepared for submission to the International Association of Geodesy (IAG) at its General Assembly in Montreal, Canada during the 27th General Assembly of the International Union of Geodesy and Geophysics (IUGG) on July 8-18, 2019. It is issued on behalf of the IAG Section of the Hungarian National Committee for IUGG.

Since the last 26th General Assembly in Prague, Czech Republic, June 22-July 2, 2015 there have been some minor changes in the list of members of the IAG Section of the Hungarian National Committee for IUGG. Currently the National Correspondent to the IAG is also the Chairman of the IAG Section. The members of the IAG Section for the period of 2016-2019 are as follows: J Ádám (*Chairman*), L Bányai (*Secretary*), Gy Busics, L Földváry, T Jancsó, A Kenyeres, Gy Mentes, G Papp, Sz Rózsa, Gy Tóth, P Varga, and L Völgyesi. All are members of the Scientific Committee for Geodesy and Geoinformatics of the Hungarian Academy of Sciences (HAS).

Cooperating institutions in the field of IAG in Hungary are as follows: *a)* Department of Geodesy and Surveying, Budapest University of Technology and Economics (BME) (http://www.geod.bme.hu); *b)* Satellite Geodetic Observatory (at Penc) of the Department of Geodesy, Remote Sensing and Land Offices, Government Office of the Capital City Budapest (http://www.sgo-penc.hu); *c)* Geodetic and Geophysical Institute of the Research Centre for Astronomy and Earth Sciences of the Hungarian Academy of Sciences (HAS), Sopron (http://www.ggki.hu); *d)* Institute of Geoinformatics of the Alba Regia Technical Faculty of the Óbuda University at Székesfehérvár (http://www.uni-obuda.hu/geoinformatikai-intezet); *e)* Mining and Geological Survey of Hungary (MBFSZ), Budapest (https://mbfsz.gov.hu), and *f)* Geoinformation Service of the Hungarian Defence Forces, Budapest (https://honvedelem.hu/szervezet/mh_geosz).

The national report has been divided into commissions corresponding to the new structure of IAG. The commission reports are compiled by the leading authors indicated in brackets, who are responsible for the content of their corresponding reports, namely I. Commission 1 „Reference Frames" (A. Kenyeres and Gy. Busics), II. Commission 2 „Gravity Field" (L. Völgyesi), III. Commission 3 „Earth Rotation and Geodynamics" (P Varga and Gy Mentes), IV. Commission 4 „Positioning and Applications" (Sz Rózsa), V. Inter-commission Committee „Theory" (T Jancsó) and VI. Communication and Outreach Branch (J Ádám). This report would not be possible without their and co-authors' efforts.

[*]*Department of Geodesy and Surveying,*
Budapest University of Technology and Economics,
H-1521 Budapest, POB 91, Hungary ,
e-mail: jadam@epito.bme.hu

HUNGARIAN CONTRIBUTION TO THE RESEARCH ON NUMERICAL SOLUTIONS AND ITS THEORIES IN MATHEMATICAL GEODESY (2015-2018) – IAG INTER-COMMISSION COMMITTEE

Tamás Jancsó[*], Gábor Nagy[*], Lajos Völgyesi[**], Béla Paláncz[***], Erik Papp[****]

Currently available high-resolution Digital Elevation Models (DEM) permit computations of terrain-related gravitational parameters with an unprecedented accuracy. It is ±0.1 mGal (10^{-6} m/s^2) and ±10 E unit (10^{-8} s^{-2}) in terms of the first and second derivatives of the gravitational potential, respectively. These grid models, however, mean a huge number of elementary polyhedron volume elements (even ~100 million polyhedrons in case of a country as small as Hungary), the computation of the gravitational effect of which is a real challenge when fully analytical solution is preferred. Although the more detailed the better principle is generally accepted it is basically true only for errorless data. As soon as errors are present any forward gravitational calculation from the model is only a possible realization of the true force field on the significance level determined by the errors. As a consequence, the computational time can be significantly reduced by the optimization of the number of volume elements based on the accuracy estimates of the input data. Common gravity field modelling programs generate optimized models for every computation point (*dynamic approach*), whereas the *static approach* provides only one optimized model for all computational points. Based on the static approach, two different algorithms were developed which may reduce the number of volume elements efficiently by a factor of 5-10 if the known/estimated accuracy of the terrain data is interpreted as a threshold parameter (Benedek et al. 2018). The grid-based algorithm starts with the maximum resolution polyhedral model defined on a uniform grid and generates a new polyhedral surface. The other algorithm is more general, it works also for irregularly distributed data (points) connected by triangulation. Beyond the description of the optimization schemes Benedek et al. (2018) presents some applications of these algorithms in regional and local gravity field modelling too.

Monte Carlo simulation and geometrical analyses were developed to investigate triangular trihedral and rounded corner reflectors, which have areas without triple-bounced backscattering (Kalmár and Bányai 2017). Removing these blind areas, the surface and the material cost (and weight) can be significantly reduced without the loss of radar cross section (RCS).

A new robust LiDAR processing method was developed (Nagy et al. 2017). This method fits a regression plane to a point cloud in any horizontal position by fitting a disc on it, which contains a specified portion of points under the disc plane in all three sectors of the disc. This method can be used to create DEMs even without any filtering process. This article also describes an analysis, which compares the results of the fitting disc method using different parameters in processing of DEMs.

The geodynamic effects of extended and heavy rainfalls on the tilt observation in Conrad Observatory, Austria (alpine terrain), was investigated by Kalmár and Benedek (2017). A grid-based finite element model was developed to determine soil water loading, water catchment area and water separation lines. Considering proper terrain conditions, realistic loadings were estimated in this test area.

The application of moving statistical functions (mean, standard deviation, skewness, peak, convolution and regression) were investigated in the paper by Kalmár (2015) for automatic detections of different events in very long time series (several hundred thousand). Methods were developed for

[*]*Óbuda University, Alba Regia Technical Faculty*
E-mail: jancso.tamas@amk.uni-obuda.hu
[**]*Budapest University of Technology and Economics, Department of Geodesy and Surveying*
[***]*Budapest University of Technology and Economics, Department of Photogrammetry and Geoinformatics*
[****]*Szent István University, Ybl Miklós Faculty of Architecture and Civil Engineering*

detection of Q outbreaks in geomagnetic registration and for shift detections in geodynamic tilt registrations.

In the study of Bányai et al. (2015) a new generalized free network adjustment of GNSS baselines components has been implemented together with simultaneous estimation of seven parameters of similarity transformation relative to the coordinates of properly chosen stations estimated in the reference epoch. The similarity parameters are handled by constraint equations and the more stable singular value decomposition is used for the inversion of the extended normal equations. This procedure is proposed for estimation of relative displacements in local or regional networks if they are near to plate borders and only far GNSS fiducial stations are available.

The displacements in the line of sight directions between the SAR satellites and the moving persistent scatters, estimated by satellite radar interferometry, can be handled as geometric observables. Bányai et al. (2017) investigate the geometric features of ascending and descending changes - along with possible fusion of other geodetic observables, which can be used to estimate three-dimensional displacements. The accuracies, correlations and dilution of precisions of the fusion are estimated and the combination with GNSS displacements using the Kalman-filter is proposed.

Spherical harmonics are the most widely spread mathematical tool for describing the gravity field, generating a frequent need for spherical harmonic synthesis and spherical harmonic analysis. The huge amount of computational load can be efficiently reduced by certain numerically optimal solutions, which were efficiently implemented in a C++ script (Kemény and Földváry 2015).

Legendre polynomials of the spherical harmonics are defined in classical geodetic applications with the Rodriguez formula. It has been shown analytically that Legendre polynomials can also be considered as a finite set of periodic signals (Földváry 2015), which can efficiently simplify investigations of periodic component of the signal.

It is known that the averaging method makes smoother the extremes. Accordingly, estimation of the periodicity of an averaged time series is influenced by the smoothing property of the averaging, resulting in an underestimated amplitude of the periodicity. This can be partially recovered by an appropriate de-smoothing method (Földváry 2015). The same de-smoothing method can be interpreted for revoking of spatial smoothing effect of raster data, c.f. Digital Terrain Models (Földváry 2018).

The advantages of GIS software in handling, interpretation and analysis of geospatial data, have not been adopted for the satellite gravimetry before. First attempts for implementing satellite gravimetric data in GIS are provided by Földváry et al (2015). Also, the advantages of GIS has been implemented for describing the seismology of the Moon. As a result, an online GIS service has been developed under the name HGR.01, which contains all relevant information of the Moonquake observations so far (Lázár et al 2018a, b).

In the area of mathematical Geosciences, a new book was written and published about the hybrid symbolic-numeric methods in Mathematical Geosciences (Awange et al. 2018). Hybrid symbolic-numeric computation is a large and growing area at the boundary of mathematics and computer science. Three major areas of computation are covered in Awange et al, 2018. The first part discusses methods for computing all solutions to a system of polynomials. Purely symbolic methods e.g. via Gröbner bases tend to suffer from algorithmic inefficiencies, and purely numeric methods such as Newton iterations have trouble finding all solutions to such systems. One class of hybrid methods blends numerical calculations into the purely algebraic approach e.g. computing numeric Gröbner bases or Dixon resultants (the latter being extremely efficient e.g. for elimination of variables). Another hybrid technique mixes symbolic methods into more numerical approaches, e.g. finding initializations for numeric homotopy tracking to obtain all solutions. The second part goes into the realm of "soft" optimization methods, including genetic methods, simulated annealing, and particle swarm optimization, amongst others. These are all popular and heavily used, especially in the context of global optimization. While often considered as "numeric" methods, they benefit from symbolic computation in several ways. One is that implementation is typically straightforward when one has access to a language that supports symbolic computation. Updates of state, e.g. to handle

mutations and gene crossover, are easily coded. Indeed, this sort of thing can be so deceptively simple baked into the language so to speak, that one hardly realizes symbolic computation is happening. Amongst many applications in this part there is, again, that of solving systems of equations. Also, the mixed-integer programming is covered wherein some variables are discrete-valued and others continuous. This is a natural area for Hybrid symbolic-numeric computation since it combines aspects of exact and numeric methods in the handling of both discrete and continuous variables. This technique can be employed to solve GNSS phase ambiguity problem. The third part delves into data modelling. This begins with use of radial basis functions and proceeds to machine learning, e.g. via Support Vector machine methods. Symbolic Regression, a methodology that combines numerical calculations with evolutionary programming, is also introduced for the purpose of modelling data. Another area seeing recent interest is that of robust optimization and regression, wherein one seeks results that remain relatively stable with respect to perturbations in input or random parameters used in the optimization. Several hybrid methods are presented to address problems in this realm. Stochastic modelling is also discussed. This is yet an-other area in which hybrid methods are quite useful.

Symbolic computing languages have seen a recent trend toward ever more high-level support for various mathematical abstractions. This appears for example in exact symbolic programming involving probability, geometry, tensors, engineering simulation, and many other areas. Under the hood is a considerable amount of Hybrid symbolic-numeric computation. Naturally such support makes it all the easier for one to extend hybrid methods; just consider how much less must be built from scratch to support, say, stochastic equation solving, when the language already supports symbolic probability and statistics computations. Awange et al (2018) present to the reader some of the major areas and methods that are being changed, by the authors and others, in furthering this interplay of symbolic and numeric computation. The term Hybrid Symbolic-Numeric Computation has been with us for over two decades now.

A brief list of topics covered:

- Systems of polynomial equations with resultants and Gröbner bases
- Simulated annealing
- Genetic algorithms
- Particle swarm optimization
- Integer programming
- Approximation with radial basis functions
- Support vector machines
- Symbolic regression
- Quantile regression
- Robust regression
- Stochastic modelling
- Parallel computations

Most of the methods discussed in book will probably be implemented by the reader on a computer algebra system. The two most fully developed and widely used computer algebra system are Mathematica and Maple. Some of the polynomial computations here are better done on the specialized system Fermat. Other systems worthy of mention are Singular and SageMath.

The book by Awange et al. (2018) is not a reference manual for any system, and we have made an effort to keep the specialized commands to a minimum, and to use commands whose syntax makes them as self-explanatory as possible. More complete Mathematica programs to implement some of the examples are available online. Similarly, a program written in Fermat for the resultant method called Dixon-EDF is available online.

A novel RANSAC robust estimation technique has been investigated as an efficient method for solving the 7-parameter datum transformation problem in the presence of outliers (Paláncz et al. 2017). A new dual quaternion representation of the 3-point similarity transformation problem and

its non-iterative fast solution via linear homotopy has been developed. Paláncz at al. (2017) show how to build this model into a RANSAC shell and how to solve it in parallel way decreasing the computation time further. In addition, an efficient strategy based on the early stopping principle was given for adjusting automatically the threshold level of the robust algorithm properly. This method, which is frequently employed in geodesy has two sensitive features (i) the user adjusts some parameters of the algorithm making it subjective and a rather difficult procedure and (ii), its shell should repeatedly solve a nonlinear equation system. In this contribution the authors suggested an automatic adjustment strategy for the most important parameter ``the threshold value'' based on the "early stopping" principle of the machine learning technology. Using iterative numerical methods, they proposed the use of an algebraic polynomial system developed via dual quaternion technique and solved by non-iterative homotopy method thereby reducing the computation time considerably.

In order to illustrate the proposed method, the transformation parameters of the Western Australian Geodetic Datum (AGD 84) to Geocentric Datum Australia (GDA 94) was computed (Paláncz et al. 2017). The suggested algorithm requires longer running time than the standard Procrustes algorithm, however our optimal RANSAC is a robust method eliminating outliers. The novelty of the proposed approach lies in three major contributions (i) the provision for automatically finding the proper error limit parameter for RANSAC method, which has until now been an error-trial technique, (ii) employing algebraic polynomial form of the dual quaternion solution in the RANSAC shell thereby accelerating the repeatedly requested solution process and (iii) avoiding iterations via a heuristic approach of the scaling parameter.

Paláncz and Awange (2017) introduce the nonlinear homotopy in geodesy. Never had the concept of nonlinear homotopy been used by the geodetic community. This is partly attributed to the complexity of the involved equations and partly due to the computational time required. Recently, however, Nor et al. (2013) suggested the possibility of constructing nonlinear homotopy. The idea of vhich is developed for geodetic applications and an example of its use illustrated. Awange and Paláncz (2016) is dealing with the problem that the improved geo-spatial instrumentation and technology such as in laser scanning has now resulted in millions of data being collected, e.g., point clouds. It is in realization that such huge amount of data requires efficient and robust mathematical solutions that this third edition of the book extends the second edition by introducing three new chapters: Robust parameter estimation, Multiobjective optimization and Symbolic regression. Furthermore, the linear homotopy chapter is expanded to include nonlinear homotopy. These disciplines are discussed first in the theoretical part of the book before illustrating their geospatial applications in the applications chapters where numerous numerical examples are presented. The renewed electronic supplement contains these new theoretical and practical topics, with the corresponding Mathematica statements and functions supporting their computations introduced and applied. This third edition is renamed in light of these technological advancements.

In indoor and outdoor navigation, finding the local position of a sphere in mapping space employing a laser scanning technique with low-cost sensors is a very challenging and daunting task Lewis et al. (2018a) illustrate how Gröbner basis techniques can be used to solve polynomial equations arising when algebraic and geometric measures for the error are used. The effectiveness of the suggested method is demonstrated, thanks to standard CAS software like Mathematica, using numerical examples of the real world.

Improvements in computational and observational technologies in geoinformatics, e.g., the use of laser scanners that produce huge point cloud data sets, or the proliferation of GNSS and unmanned aircraft vehicles (UAVs), have brought with them the challenges of handling and processing this “big data”. These call for improvement or development of better processing algorithms. One way to do that is integration of symbolically presolved subalgorithms to speed up computations. Using examples of interest from real problems in geoinformatics Lewis et al. (2018b) discuss the Dixon-EDF resultant as an improved resultant method for the symbolic solution of parametric polynomial systems. The method itself is briefly described, then geoinformatics problems arising in minimum distance mapping (MDM), parameter transformations, and pose estimation essential for

resection are discussed. Dixon-EDF is then compared to older notions of "Dixon resultant", and to several respected implementations of Gröbner bases algorithms on several systems. The improved algorithm, Dixon-EDF, is found to be greatly superior, usually by orders of magnitude, in both CPU usage and RAM usage. It can solve geoinformatics problems on which the other methods fail, making symbolic solution of parametric systems feasible for many problems.

In the mathematical geodesy the different approaches of the tree-dimensional coordinate transformations are essential topics since they are frequently applied in the geodetic and surveying practice. Besides the traditional iterative solutions there are new closed form solutions, which consider the advantages of new mathematical algebra concept. Závoti and Kalmár (2016) present different solutions of the three-dimensional seven parameter Bursa-Wolf model which are based on quaternions and skew symmetric rotation matrices.

Quaternion-based geodetic datum transformation by iteration was developed (Papp 2015). Datum transformation is the most frequent problem in geodesy, photogrammetry, geoinformatics, and animation and computer vision. To overcome the drawback of traditional solution of the problem based on rotation angles this implementation adopts unit quaternion to represent three-dimensional rotation matrix. A quaternion-based iterative solution in terms of linearization in the Bursa-Wolf geodetic transformation model is described. The calculations show that the quaternion-based solution has no dependence on the initial values of the parameters. It provides reliable result with fast speed. The main advantage of this algorithm is that it can be applied in the case of arbitrary size rotation.

In Bursa-Wolf seven parameter similarity transformation model the transformation consists of three translation parameters, three rotation elements and one scale factor. Papp (2017) proposes a closed-form solution of datum transformation. In this solution, Clifford dual-number quaternions are used to represent the 3D rotation. Once the transformation parameters between the two data are established by identical point pairs, the rotation matrix, the scale parameter and the translation vector are simultaneously derived. The proposed algorithm seems better than the iterative algorithms. Most importantly, in contrast to unit quaternion-based algorithms, the presented algorithm solves seven unknown parameters simultaneously without the initial estimates of unknowns. The main advantage of this algorithm is that it can be applied in case of arbitrary size rotations. Consequently, the mathematical modelling of similarity transformation based on dual quaternions is an elegant method which is adaptable to present a compact formula for Bursa-Wolf model (Papp 2017).

An application aiming at coordinate transformation of LiDAR point clouds between the Hungarian Datum 1972 and the ETRS89 has been developed by Brolly (2018). The first step is a 7-parameter Helmert transformation with country-wide parameter set, which is refined by using a correction grid from accurate local transformations. The application allows direct read and write for ASPRS standard LAS file format and delivers transformation accuracy of a few centimetres throughout Hungary.

A new method for error detection with scale factors based on coordinates of model and control points was developed (Jancsó 2017). In photogrammetry the model coordinates of control points can be calculated, and they can be used effectively to detect gross errors located in control points. To reach this goal triangles are formed from points in every combination and the residuals of scale factors are calculated. The triangle where the sum of squared scale factor residuals is the smallest one can be found. Adding other points to this triangle one by one tetrahedrons are formed. Using the edges of these tetrahedrons equations of constraint conditions are compiled and the geodetic coordinates of the examined point can be determined. These calculated coordinates can be compared to the given geodetic coordinates and the allowable residuals are calculated. By this way all points can be filtered unanimously against gross errors.

References

Awange JL, Paláncz B (2016): Geospatial Algebraic Computations: Theory and Applications. New York, Springer - Verlag New York, Inc., p. 541.

Awange JL, Paláncz B, Lewis RH, Völgyesi L (2018): Mathematical Geosciences: Hybrid Symbolic-Numeric Methods. Springer International Publishing, Cham, 596, ISBN: 798-3-319-67370-7.

Bányai L, Mohamed A-M S, Szűcs E, Aboaly N, Mousa A, Khalil HA (2015): The relationship between global plate motion and intra-plate deformation analysis of Cairo network: Case study with simulated data. Arabian Journal of Geosciences, 9(1), 1-10.

Bányai L, Szűcs E, Wesztergom V (2017): Geometric features of LOS data derived by SAR PSI technologies and the three-dimensional data fusion. Acta Geod. Geoph., 52(3), 421-436.

Benedek J, Papp G, Kalmár J (2018): Generalization techniques to reduce the number of volume elements for terrain effect calculations in fully analytical gravitational modelling. Journal of Geodesy, 92(4), 361-381.

Brolly G (2018): Development of an application to transform spatial point sets produced by remote sensing between ETRS89 and EOV reference systems (in Hugarian). http://publicatio.uni-sopron.hu/1668/.

Földváry L (2015): Sine series expansion of associated Legendre functions. Acta Geod. Geoph., 50(2): 243-259.

Földváry L (2018): Desmoothing of block-wise gridded geoinformation. Journal of Geographical Society of Uzbekistan, Special Volume, 22-27, ISSN 0135-9614.

Földváry L, Kemény M, Huang XZ (2015): First results of implementing satellite-borne gravity data to GIS and future perspectives. 10th International Symposium on Applied Informatics and Related Areas - AIS2015, Székesfehérvár November 11, 2015, Paper P03. 6 p., ISBN: 978-615-5460-49-4.

Jancsó T (2017): Error detection with scale factors based on coordinates of model and control points (in Hungarian). Geomatikai Közlemények, 20, 41-46.

Kalmár J, Bányai L (2017): Material saving corner reflector design without blind areas (in Hungarian). Dimenziók: Matematikai Közlemények, 5, 51-56.

Kalmár J, Benedek J (2017**):** Determination of water loading, water catchment areas and water separation lines based on the modelling of rain seepage and leakage (in Hungarian). Dimenziók: Matematikai Közlemények, 5, 25-29.

Kalmár J (2015): Data analysis with moving statistics (in Hungarian). Dimenziók Matematikai Közlemények, 3, 5-13.

Kemény M, Földváry L (2015): Computational development for the processing of static gravimetric data (in Hungarian). Geomatikai Közlemények, 18(2), 53-62.

Lázár L, Kiszely M, Földváry L (2018a): HGR.01: Geographic Information System of the Moonquakes (in Hungarian). Űrtan Évkönyv: Az Asztronautikai Tájékozató 69(1), 49-60.

Lázár L, Kiszely M, Földváry L, Gribovszki K (2018b): HGR.01: Geographic Information System of the Moonquakes. Geophysical Research Abstracts 20: EGU2018-17555.

Lewis R, Paláncz B, Awange JL (2018a): Fitting a Sphere via Gröbner Basis. In: James, H. Davenport; Manuel, Kauers; George, Labahn; Josef, Urban (szerk.) International Congress on Mathematical Software - ICMS 2018 Cham (Svájc), 319 – 327.

Lewis R, Paláncz B, Awange JL (2018b): Solving geoinformatics parametric polynomial systems using the improved Dixon resultant. Earth Science Informatics, 1 – 11.

Nagy G, Jancsó T, Chen CH (2017): The Fitting Disc Method, a New Robust Algorithm of the Point Cloud Processing Acta Polytechnica Hungarica, 14(6), 59-73.

Nor HM, Ismail AM, Majid AA (2013): Quadratic bezier homotopy function for solving system of polynomial equations. Matematika, 29(2), 159–171.

Paláncz B, Awange JL (2017): Nonlinear homotopy in geodesy. Acta Geod. Geoph., 52(1) 1-4.

Paláncz B, Awange JL, Völgyesi L (2017): A novel RANSAC approach to robustly solve the 3D similarity transformation problem. Australian Journal of Earth Sciences, 64(4), 565-576.

Papp E (2015): Quaternion-based datum transformation by iteration (in Hungarian). Geomatikai Közlemények, 18(2), 23-41.

Papp E (2017): Geodesic datum transformation by dual quaternion (in Hungarian). Geomatikai Közlemények, 20, 99-109.

Závoti J, Kalmár J (2016): A comparison of different solution of the Bursa-Wolf model, and of the 3-D, 7 parameter datum transformation. Acta Geod. Geoph., 51, 245-256.

HUNGARIAN NATIONAL REPORT ON REFERENCE FRAMES (2015-2018) - IAG COMMISSION 1

Ambrus Kenyeres[*], *István Galambos*[*], *Bálint Magyar*[*], *Gábor Virág*[*]

1 Institutional background

In Hungary the Institute of Geodesy, Cartography and Remote Sensing (Hungarian abbreviation: FÖMI) was historically the responsible institution for geodetic reference networks, positioning services and the related research activities. Since January 2017 FÖMI has been moved under the Government Office of Capital City Budapest (Hungarian abbreviation: BFKH) as a department, but the professional work continued without significant disruption.

2 GNSS network (GNSSnet.hu) and related services

The Hungarian GNSS reference station infrastructure and services have been established and maintained by the GNSS Service Centre (GSC) acting as part of the BFKH Satellite Geodetic Observatory (SGO). The GNSSnet.hu network consists of 35 Hungarian and 19 stations from the neighbouring countries (Figure 1). The GNSS data is collected and processed in real time to provide nationwide homogeneous coverage with cm-accuracy services. The average inter-station distance is less than 60 km, enabling accurate modelling of distance-dependent errors like ionosphere, troposphere and orbits. All of the Hungarian stations and most of the integrated external sites are equipped with GPS+GLONASS sensors and individually calibrated chokering antennae. Seven receiver/antenna units are already Galileo capable.

The GNSS Service Centre uses the GNSMART network RTK software package (Geo++ GmbH) to provide reference data for both real-time and post-processing applications. Real-time data is distributed using the Ntrip protocol in all proprietary formats. RINEX and virtual RINEX data is provided for post-processing via the GSC website (www.gnssnet.hu) in RINEX version 2.11 format.

As of December 2018, more than 1500 organisations registered for the GNSS services and the number of registered user account exceeded 2900. The majority of land surveying tasks in Hungary are carried out using real-time GNSS technique.

GNSSnet.hu reference station coordinates are determined in ETRF2000 reference frame. Transformation to the Hungarian local grid (EOV) is supported in both real-time and post-processing mode. An online transformation service (EHT) is provided at the GSC website and a real-time transformation solution (VITEL) is available for most receiver brands as an extension of the RTK rover receivers' controller software.

The GSC concentrates its efforts on service quality improvements. Besides the automatic quality control of the GNSMART software, the GSC developed a number of real-time and post-processing quality monitoring tools for both internal use and information dissemination to the clients. The actual status of the service can be monitored online via the GSC website: http://www.gnssnet.hu. A special monitoring tool has been developed for mobile phones. This enables users working on the field to judge whether the system performs according to the expectations.

[*] *LTK Satellite Geodetic Observatory*
H-1149 Bosnyak square 5
E-mail: kenyeres.ambrus@gnssnet.hu

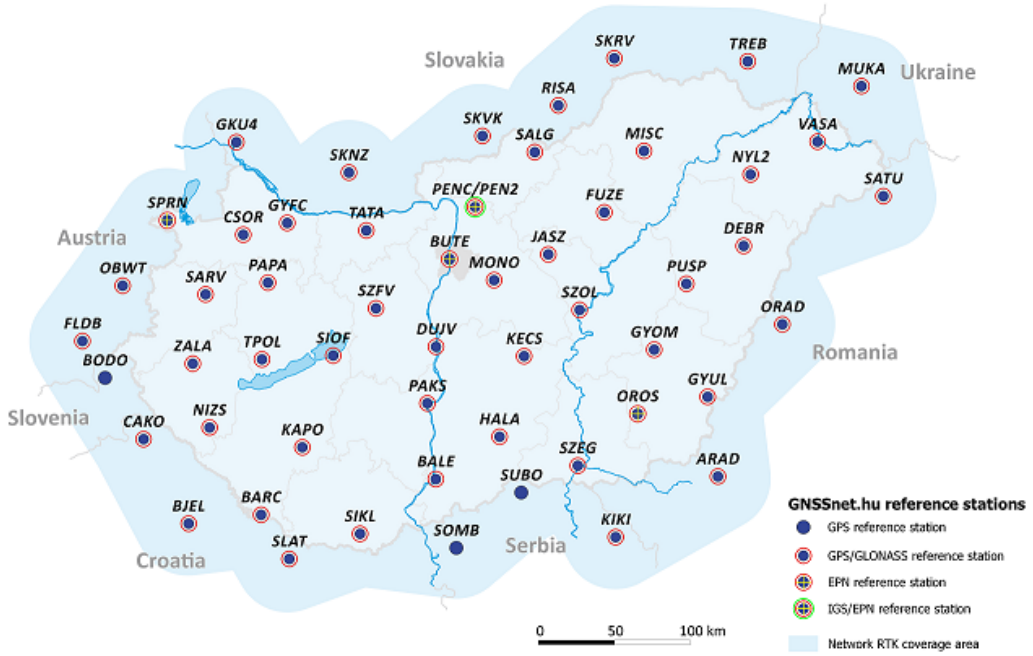

Figure 1. Sites of Hungarian Active GNSS Network

3 SGO GNSS Analysis Centre

Since December 2001 SGO is operating a GNSS Analysis Centre (AC), which routinely processes and analyses the following network data:

- A sub-network of EPN (EUREF Permanent Network) including 22 EPN stations. The daily and weekly EPN sub-network solutions are submitted to the EPN Combination Centre and used for the maintenance of EPN and ETRS89,
- 35 GNSSnet.hu sites and 41 additional permanent stations from the neighbouring countries. This analysis is being done both on hourly basis in near-real time mode (NRT) and daily/weekly basis using final IGS orbits. The results of the NRT analysis is submitted to E_GVAP as our contribution to support the European level weather forecast and climate research. The results of the routine daily analysis are used for the monitoring of the GNSSnet.hu station performance.

4 International collaboration

SGO supports the operation of EUREF and EPN. The Head of the SGO (Dr Ambrus Kenyeres) was the EPN Reference Frame Coordinator during the period of 2009-2017 and managed the maintenance of the ETRS89 (Bruyninx et al. 2015) using the periodically updated EPN multi-year solution and provided the official EPN coordinate and velocity estimates, which was updated in every 15 weeks (Kenyeres and Legrand 2017). In 2015 Ambrus Kenyeres was elected as the chair of the EUREF Governing Board.

SGO – as initiator of the EPN Densification – has started the integration of all European active GNSS network products to provide a high quality, homogeneous and dense position and velocity product in close cooperation with all national data providers. The first publication of the results was in 2018, the solution includes position SINEX results for almost 3200 stations and based on data from 2000 to 2017 (up to GPS week 1993). The position and velocity results are expressed in ITRF2014.

SGO is a partner of the EPOS IP (European Plate Observing System Implementation Phase) project and contributes to the long term EPOS service with GNSS product integration, time series generation and velocity results delivery (Caporali et al. 2015).

5 GPS geokinematics

SGO continued the investigations in the framework of the GPS crustal deformation monitoring program - commenced in 1991. The more than two decade long campaign style MGGA (Hungarian GPS Geokinematic Reference Network) measurement series had been merged with the long term analysis results of the GNSSnet.hu permanent data in the frame of EPN Densification. This allows us to extend our view and analysis over a larger area and interpret the displacement field as a complex tectonic environment. This new data enabled us to better constrain the 3D crustal deformation map of the Pannonian basin and estimate horizontal crustal motions and vertical tectonic signals to detect the main crustal blocks and faults and their present-day kinematics.

References

Bruyninx C, Altamimi Z, Brockmann E, Caporali A, Dach R, Dousa J, Fernandes R, Giannou M, Habrich H, Ihde J, Jivall L, Kenyeres A, Lidberg M, Pacione R, Poutanen M, Szafranek K, Söhne W, Stangl G, Torres JA, Völksen C (2015): Implementation of the ETRS89 in Europe: Current status and challenges. International Association of Geodesy Symposia. 146, Proceedings of the Symposium on Reference Frames for Applications in Geosciences (REFAG2014), Kirchberg, Luxembourg, 13-17 October, 2014, Springer, Editor: T van Dam, doi: 10.1007/1345_2015_130.

Caporali A, Bruyninx C, Ganas A, Kenyeres A, Lidberg M, Stangl G, Steffen H, Zurutuza J (2015): Stress drop at the Kephalonia Transform Zone estimated from the 2014 seismic sequence**.** Tectonophysics, 666, 164-172, doi: 10.1016/j.tecto.2015.11.004.

Kenyeres A, Legrand J (2017): Evolution of the ITRFyy Regional Densifications between Successive ITRS Realizations. 19th EGU General Assembly. Vienna, Austria, 04/23-04/28/2017, Geophysical Research Abstracts 15, EGU2017-15099.

HUNGARIAN CONTRIBUTION TO THE RESEARCH IN GRAVIMETRY, GRAVITY FIELD MODELLING AND GEOID DETERMINATION (2015-2018) - IAG COMMISSION 2

Lajos Völgyesi[*], József Ádám[*], Csaba Égető[*], Annamária Kiss[*], Szabolcs Rózsa[*], Gyula Tóth[*], Márta Kis[**], András Koppán[**], Krisztián Baracza[**], László Merényi[**], László Szabados[**], Judit Benedek[***], János Kalmár[***], Gábor Papp[***], Béla Paláncz[****], Mihály Dobróka[*****]

1 Introduction

This paper is made for the 27th International Union of Geodesy and Geophysics (IUGG) General Assembly 2019, Montreal, Canada as a quadrennial report of the Hungarian Contribution to the research in gravimetry, gravity field modeling and geoid determination (IAG Commission 2). In the past four years, we have conducted extensive and successful researches in the field of gravimetry, which are summarized below.

2 Hungarian Gravimetric Network

The Hungarian Gravimetric Network (MGH, Figure 1) is maintained by the Mining and Geological Survey of Hungary (the former Eötvös Loránd Geophysical Institute). According to the state in 2018, the MGH contains 24 absolute stations and 435 1st or 2nd order base points. The maintenance work includes the checking the status of base points as well as the substitution or installation of destroyed or new base points. Between 2015 and 2018, four absolute stations were installed, one base point was reinstalled, and one base point was newly installed. These stations were linked to the 3 nearest MGH base points by relative gravimetric measurements.

In order to improve the reliability and accuracy of the network, the gravity acceleration was redetermined (or newly determined in 4 cases) on 15 absolute stations between 2015 and 2018. The measurements were carried out by using the AXIS FG-5 No. 215 and 251 (H) absolute gravity meters operated by Vojtech Pálinkáš and Jakub Kostelecký (Výzkumný ústav geodetický, topografický a kartografický, v.v.i., Pecný, Czech Republic). Before the absolute measurements, vertical gravity gradient (VG) was determined on every station by LCR-G gravimeters, using a 3-level arrangement and at least 6 series of measurements.

Since the VG can deviate significantly from the normal value (–0.3086 mGal/m) in Hungary, vertical gradients were determined on further 26 base points between 2015 and 2018. Methodological examinations were also carried out by analyzing two-, three- and four-level VG measurements (Lévay and Koppán 2015).

Between 2017 and 2018 two newly installed INGA (Integrated Geodetic Point Network) base points were connected to the MGH network by comparative relative gravimetric measurements, the INGA stations were linked to the 3 nearest MGH base points.

In favour of the protection of MGH base points, recordings of base points were started into the Hungarian land and property registration system in 2018, according to the relevant rules of law.

[*]*Department of Geodesy and Surveying, Budapest University of Technology and Economics, E-mail:volgyesi@eik.bme.hu*
[**]*Mining and Geological Survey of Hungary*
[***]*Geodetic and Geophysical Institute, Research Centre for Astronomy and Earth Sci., Hungarian Academy of Sciences*
[****]*Department of Photogrammetry, Budapest University of Technology and Economics*
[*****]*Department of Geophysics, Faculty of Earth Science and Engineering, University of Miskolc*

Figure 1. Hungarian Gravimetric Network in 2018

3 Remeasurement of the first gravity reference station of Hungary

The first gravity reference station of Hungary was established by Károly Oltay, professor and head of former Department of Geodesy, Technical University of Budapest (Ádám et al. 2018). The station was located in the pendulum hall and its gravity value (g = 980 852 mGal) was derived in 1915 from relative pendulum measurements with respect to the reference station at Geodetic Institute in Potsdam. The network of European gravity reference stations was adjusted by C. Morelli in the 1940's and he got g = 980 853 mGal for the station established by Oltay. This value only slightly differs from the one obtained by Finnish professor R.A. Hirvonen (g = 980 853.3 mGal), who used isostatic reduction in his calculations.

The pendulum hall was reconditioned in 2016, during which the reference station was identified and restored. Gravity was measured at the reference station (see Figure 2) between 26 and 27 May, 2016 with the FG5X (No.251) absolute gravity meter by staff members of the Czech Geodetic Observatory (Pecny, Ondrejov).

Vertical gravity gradient was also required to be measured at the station to reduce gravity measurements to the benchmark and to compare with the old g value. The measured vertical gravity gradient (–0.3091 mGal/m) served on the one hand to calculate g for the benchmark (allowing our reference station to be fit into the present operative gravity base network of Hungary (MGH-2013). On the other hand it facilitated calculating g for the benchmark established by Oltay for comparisons. When the systematic difference of −14 mGal between the reference system of Potsdam and the absolute system (or the value of −13.94 mGal based on local studies) is accounted for, the value obtained by us in 2016 (g=980 839 431.55 μGal) agrees well with the value obtained by Oltay (Ádám et al. 2018).

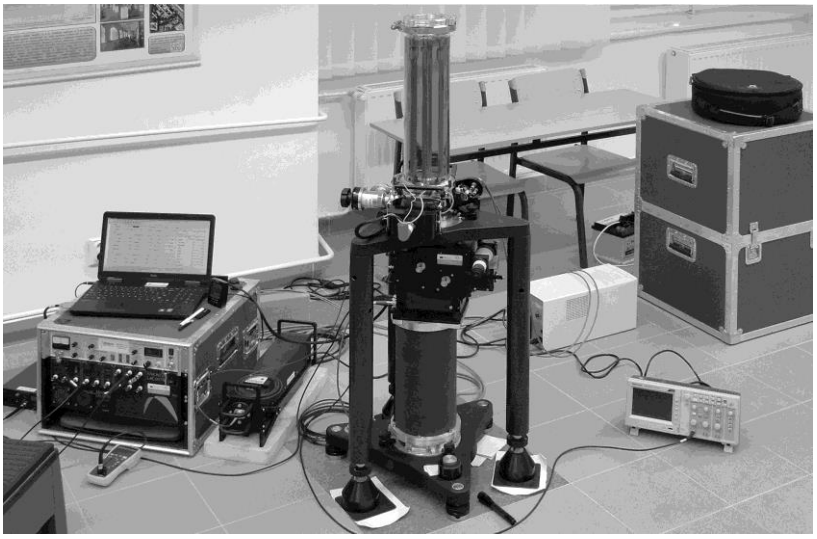

Figure 2. Measurement by the FG5X-251 absolute gravity meter at the Oltay-point

4 Torsion balance measurements

In the XX century, a large amount of torsion balance measurements have been carried out around the world. The measurements still provide a good opportunity to detect the lateral underground mass inhomogeneities and the geological fault structures using the so called edge effects in gravity gradients. Hitherto almost 60000 torsion balance measurements were made in Hungary mainly for geophysical purposes. Only the horizontal gradients were used for geophysical prospecting, the curvature gradients measured by torsion balance remained unused.

However, curvature gradients are very useful data in geodesy, using these gradients precise deflection of the verticals can be calculated by interpolation and using astronomical determination of

the geoid the fine structure of the geoid can be derived. In our test area a geoid with few centimeters accuracy was determined based on the curvature data.

Based on the horizontal and the curvature gradients of gravity the full Eötvös tensor (including the vertical gradients) can be derived by the 3D inversion method.

Following the first big success in the 1910s and the second „Golden Age" in the 1950s torsion balance measurements for geological exploration have practically finished in Hungary by the end of the 1960s (Szabó 2016). After a long pause geodesy needed further measurements. Applying the new technical opportunities we reconstructed and modernized our older instruments, one of these instruments is an Auterbal balance of the Department of Geodesy and Surveying, BME (Budapest University of Technology); the other one is an improved type E54 instrument of ELGI (Eötvös Loránd Geophysical Institute) and the 3rd one is an Eötvös-Pekar torsion balance of the Geodetic and Geophysical Institute of the MTA Research Centre for Astronomy and Earth Sciences (see on Figure 3.). Field torsion balance measurements have been restarted in 2007 and additional torsion balance measurements have been made to study the linearity of gravity gradients (Völgyesi 2015, Völgyesi et al. 2015b). To reach the linearity of gravity gradients between the former torsion balance stations new measurements need to be made, the linearity mainly depends on the topography and the subsoil mass inhomogeneities.

In 2017 we began to reanalysise and remeasure of the classic Eötvös, Pekár and Fekete (EPF) experiment (Völgyesi et al. 2018, Péter et al. 2018), in which we found a systematic error. The objective of this experiment was to test what is now known as the weak equivalence principle (WEP), that the behavior of an object in a gravitational field is independent of its chemical composition. We've already started the actual measurements with a modified Eötvös-Pekar torsion balance.

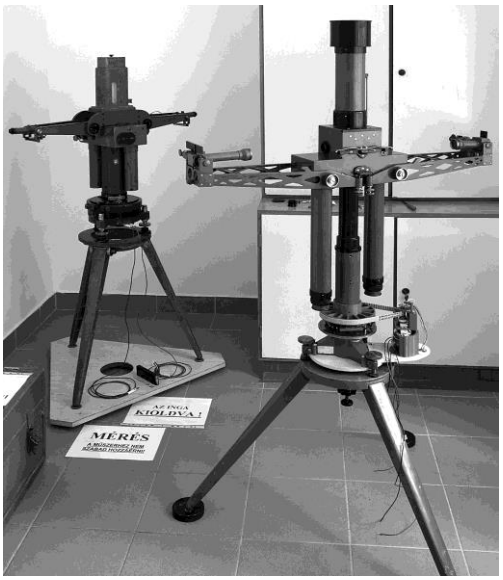

Figure 3. Renovated torsion balances at the Department of Geodesy and Surveying

5 Satellite gravity gradiometry

GRACE-borne temporal variations of the gravity field are proper tools for investigating mass redistribution processes on the seasonal and secular scales. It has been applied for investigating the water budget of the La Plata basin (Kiss and Földváry 2015a, Kiss and Földváry 2017b) resulting in an obvious change of periodicity along the river: while the upper sections are dominated by the annual periodicity of the water cycle, closer to the estuary due to the mixture with the runoffs of influents and subsurface waters, the periodicity vanishes.

GRACE monthly solutions are also used for monitoring present days ice mass variations at the polar caps. The most frequently used solution for Antarctica (Földváry et al. 2015a, 2015b) has been analyzed from error propagation perspectives. The efficiency of the ice mass balance investigations depend strongly on the reliability of the Glacial Isostatic Adjustment modelling (Földváry and Kiss 2016). All in all, it was found that over most area of Antarctica the accuracy of ice mass variations is not convincing, apart from the obvious melting process in West Antarctica and the mass accumulation in Enderby Land, no obvious mass variation can be detected (Kiss and Földváry 2017a).

By analysis of GRACE-derived mass time series, unexpected variations at multi-annual frequencies has been detected (Földváry and Kiss 2015). The locations of the multi-annual variations were identified with a combination of differently derived PSDs. The observed multi-annual variations were interpreted as consequence of large scale mass varying process, in most cases related to El Nino / La Nina events (Kiss and Földváry 2018).

6 Inversion reconstruction of 3D gravity potential function

Inversion reconstruction of 3D gravity potential based on gravity data measured by gravimeters, horizontal gravity gradients and curvature data measured by torsion balance and vertical gradients, including vertical deflection data have been obtained by our 3D solution. By applying this method the potential function – apart from an additive constant – and all the first and second derivatives of this potential function (elements of the full Eötvös tensor) can be determined not only at points of the region covered by measurements, but anywhere in the surroundings of these measurement points, using the coefficients of expansion in a series of a known set of basis function (Völgyesi et al. 2015a). The advantage of this method is that the solution can be performed by a significantly overdetermined inverse problem.

To verify the 3D inversion algorithm, test computations were made at the south part of Csepel Island in Hungary, where gravity, torsion balance and vertical gradient (VG) measurements have been performed, furthermore vertical deflection data were available from a new model. Torsion balance measurements were made here in 1950 and 30 new measurements were made in a denser net between the years 2006 and 2009, supplemented by gravity and vertical gradient observations. Deflections of the vertical have been determined for all points in the test area by the GGMPlus (Global Gravity Model, with plus indicating the leap in resolution over 149 previous 10 km resolution global gravity models) (Hirt 2013) model.

All the known horizontal gradients W_{zx}, W_{zy}, curvature data W_{xy}, W_{Δ}, vertical gradients W_{zz} and gravity values g were used as input data, but only a part of the known vertical deflection values were used as input data (as points for the training set) for the inversion; the remaining points (points of the validation set) were used for validating the computational results (15 points were considered for training, and 15 for the validation).

Different weights were applied for the input data: weights of the torsion balance measurements W_{zx}, W_{zy}, W_{xy}, W_{Δ} and the vertical deflection data were chosen to be 1 while the weights of gravity and VG measurements were chosen to be 10, as was the weight of the Laplace equation.

In our solution, comparing measured and computed data, we obtained practically the same horizontal gradients W_{zx}, W_{zy}, curvature data W_{xy}, W_{Δ}, vertical gradients W_{zz} and gravity values from the inversion as the input data of the measurements. In our study we focused mainly on how this inversion method can be applied to the determination of vertical deflections. From the 30 given vertical deflections 15 points were chosen as input data for the training set and are marked in Figure 4 by crosses; the remaining 15 points of the validation set as control points are marked by triangles. Differences $\Delta\xi = \xi^{(comp)} - \xi^{(GGMPlus)}$ and $\Delta\eta = \eta^{(comp)} - \eta^{(GGMPlus)}$ of the computed and given ξ, η components of the vertical deflections be seen in Figure 4. It can be seen that vertical deflections can be computed by this inversion method with $\pm 0.3 - 0.5''$ accuracy in our test area. Thus we have a very good possibility to compute vertical deflections with suitable accuracy based on the large amount and good quality of gravity and gravity gradient data in Hungary (Völgyesi et al. 2015a).

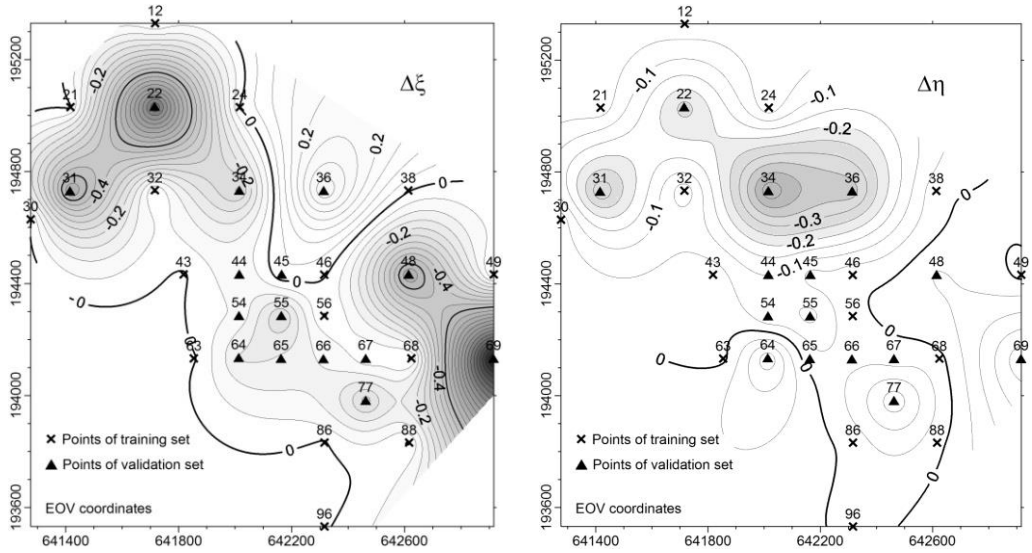

Figure 4. Differences between the computed vertical deflection components by inversion and the given ξ and η determined by the GGMPlus model within the test area. Points of training set are marked by crosses; points of validation set are marked by triangles. Contour interval is 0.05 arcsec

7 Correction of gravimetric geoid using symbolic regression

Unlike traditional linear and nonlinear regression methods that fit parameters to an expression (equation/relation) of a given form, symbolic regression (SR) searches both the parameters and the form of expression simultaneously. The proposed method could be of use to geodesy where regression analysis and functional approximation are often handled. For instance, SR could be used for gravimetric correction where they have been traditionally carried out using a wide variety of parametric and non-parametric surfaces such as polynomial models, spline interpolation, least squares collocation, kriging, combined least squares adjustments and thin plate spline (TPS) surface of solving the problem via finite elements method (Paláncz et al. 2015, see also http://library.wolfram.com/infocenter/articles/9444, 2019-10-01).

Some of these models are regression type global methods, e.g., linear parametric models and artificial neural network (ANN), while some of them are interpolating type local models as thin plate spline, support vector machines (SVM). Generally speaking local methods are more precise than global once on the training set, but their complexity is very high since they involve all of the measured data points in the model structure. In addition they proved to be less effective on the validation set since the overlearning affect the training set.

The result of this study indicates that SR can be a promising candidate to approximate functions and to find regression solutions in geodesy. However, the way to use SR method needs certain cautious, since there are many parameters which can be adjusted properly to get satisfactory result. According to our computational experiences, the best strategy is to let SR run until the structure of regression model has been found and then use standard nonlinear regression method to refine the parameters of the model. In addition finding a proper model structure depends strongly on the basic function-set used as building blocks of the SR. Therefore, one needs to select carefully these functions to find the proper solutions in an acceptable running time. Employing an intelligent guess for the initial population (i.e. Kreijzer expansion) is also indispensable. One should also keep in mind that the method is not a deterministic one therefore many repeated model generation runs were necessary. It is difficult to say which software package is the best choice, since the more effective package is the more sophisticated one and it is more difficult to adjust their parameters properly. So one should be cautious and not apply them blindly without prior study of their usage before (Paláncz et al. 2015, 2016).

8 Determinations of the vertical deflections

Our measurements and tests with QDaedalus predict revolutionary changes not only for the determination of deflections of the vertical (DOV) and local structure of the geoid but also for other fields of geodesy and surveying. This is corroborated by the fact that it is possible with the system in 30-60 minutes of measurement time only to get deflection of the vertical components which are accurate to 0.1 seconds of arc, or that it will be possible to determine geodetic astro-azimuths by luni-solar measurements with unprecedented accuracy (Völgyesi and Tóth 2015, 2016).

QDaedalus is an automated, computer-controlled astro-geodetic measurement system which has been developed at ETH Zurich, and is based on a transformed Leica Total Station that has been augmented with a GNSS receiver. This transformation mainly affects the optical part of the total station, and instead of its visual control it enables us to capture all CCD-assisted measurement data on the external controlling-processing computer hardware.

For the precise determination of deflection of the vertical, a very long sequence was measured at the point *Pistahegy*. The location of the measurements are shown in Figure 5, the WGS84 coordinates of point Pistahegy are, $\varphi = 47^{\circ}24'53.8112''$ and $\lambda = 19^{\circ}08'17.8948''$. From the autumn of the year 2015 for three years we performed 180 measurements taken at 83 nights at this point in different seasons, in the most diverse meteorological, temperature and refraction conditions.

Before the measurements, the most important step is to calibrate the instrument. Accordingly, it is necessary to establish a connection between the readings on the horizontal and vertical circle of the total station and the readings in the coordinate system of the CCD (Charge-coupled device) sensor. By the previous procedure at night in field conditions, the calibration was rather cumbersome and did not meet the exact measurement accuracy. To solve this problem, using a collimator we have developed a new method and tool for calibrating more easily and more accurately. Studies were performed on the optimal calibration measurements and raster size; additionally, the temperature dependence of the measurements was also investigated (Völgyesi and Tóth 2018). Our experiences are useful in all cases when installing a CCD sensor for geodetic instruments.

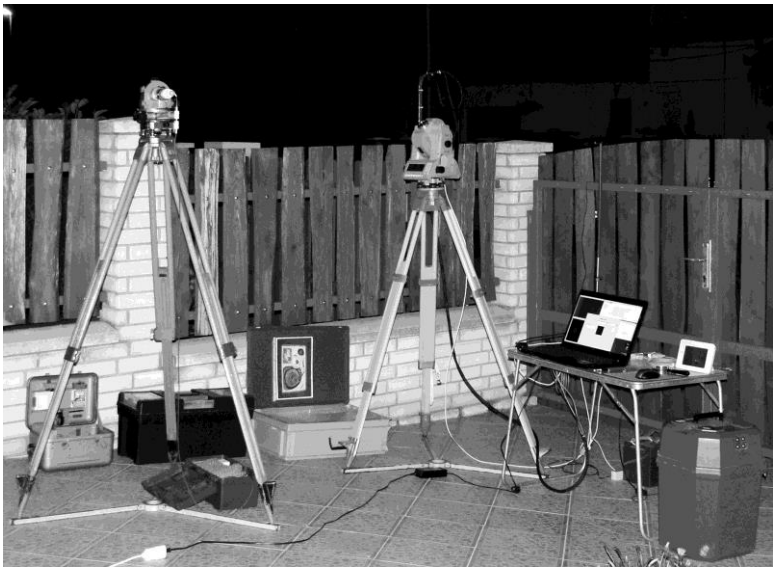

Figure 5. Night DOV measurement by QDaedalus system at Pistahegy point

We analyzed inversion residuals for the angles measured by the total station and found a horizontal angle bias for each new set of star observations. By incorporating the estimation of this bias in the least-squares Danish robust inversion procedure we reported 25% improvement in terms of standard deviation of the DOV components. On the other hand, inversion with Cauchy-Steiner weights by using bias estimation gave worst results by 5-10% in terms of standard deviation of DOV, and most

frequent value procedure with Cauchy-Steiner weights is still the best on average by 19%. We also analyzed the measurement residual time series by using ensemble averaging. We found that stationarity no longer holds for the residuals obtained with horizontal circle bias estimation (Tóth and Völgyesi 2017). We have compared two robust and resistant methods for the inversion of QDaedalus zenith direction determination. M-inversion using Cauchy-Steiner weights yielded consistently better inversion results in terms of accuracy and correlation norm based on more than 70 independent measurement series. This is probably due to the higher statistical efficiency of M-inversion in case of a non-Gaussian distribution of residuals compared with the robust E-estimation with Danish method commonly used in geodetic data processing. By analyzing the accuracy of deflection of the vertical components we can state that 15-30 minutes of measurement time by QDaedalus is probably enough to reach DOV accuracy below 0.1″.

9 Advances in forward gravity field modelling

The research related to the application of different volume elements in forward gravitational modelling and its optimization regarding both the computation time and modelling accuracy has been continued in the Geodetic and Geophysical Institute, MTA CSFK by the support of NKFIH-OTKA project K101603. Beyond the rectangular prism the polyhedron, as a discrete volume element, can also be used to model the density distribution inside 3D geological structures. The calculation of the closed formulae given for the gravitational potential and its higher-order derivatives, however, needs twice more runtime than that of the rectangular prism computations. Although the more detailed the better principle is generally accepted it is basically true only for errorless data. As soon as errors are present any forward gravitational calculation from the model is only a possible realization of the true force field on the significance level determined by the errors. So if one really considers the reliability of input data used in the calculations then sometimes the "less" can be equivalent to the "more" in statistical sense. As a consequence the processing time of the related complex formulae can be significantly reduced by the optimization of the number of volume elements based on the accuracy estimates of the input data.

Detailed analysis of the modelling accuracy based on the law of error propagation and supported by numerical tests was presented and new algorithms were proposed (Benedek et al. 2018) to minimize the number of model elements defined both in local and in global coordinate systems. Common gravity field modelling programs generate optimized models for every computation points (dynamic approach), whereas the static approach provides only one optimized model for all. Based on the static approach two different algorithms were developed. The grid-based algorithm starts with the maximum resolution polyhedral model defined by 3-3 points of each grid cell and generates a new polyhedral surface defined by points selected from the grid. The other algorithm is more general; it works also for irregularly distributed data (scattered points) connected by triangulation. Beyond the description of the optimization schemes some applications of these algorithms in regional and local gravity field modelling were presented too. The efficiency of the static approaches provided even more than 90% reduction in computation time in favourable situation without the significant loss of reliability of the calculated gravity field parameters.

10 Advances in gravimetry

In the framework of NKFIH-OTKA project K101603 (2012 – 2017) a new absolute calibration line was established in the vicinity of Sopron (Muck, Sopronbánfalva Geodynamical Observatory, and Fertőrákos Cave Theatre) with a maximum height- and gravity difference of 369.8 m and 80.149 mGal, respectively. The absolute g values were determined by Vojtech Pálinkáš and Jakub Kostelecký (Výzkumný ústav geodetický, topografický a kartografický, v.v.i., Pecný, Czech Republic) with an average accuracy of ±0.3 μGal. All the points can be easily reached by car and located in sheltered places. The stations can also be used to provide reference for the monitoring of the g variations in the tectonically active area of the Mur-Mürz fault system.

The team of NKFIH-OTKA project K101603 investigated also the characteristics and the metrological limits of the absolute calibration of spring type gravimeters using a cylindrical test mass moved vertically around the gravimeter by a lifting device operated in the Mátyáshegy Observatory (Koppán et al. 2016, 2017, Kis et al. 2018). The movement of the 3200 kg stainless steel mass generates a sinusoid-like calibrating signal having a peak-to-peak amplitude of 1102 nm/s^2. The careful determination of the geometrical and physical parameters of the test mass combined with the analytical modeling of its gravitational effect and the related uncertainties provides an accuracy of 3 nm/s^2 in absolute sense. The overall accuracy, however, is influenced by several environmental and instrumental factors which are investigated in detail. The conclusions are based on more than 400 experiments with 5 LCR G instruments. As a unique case a Scintrex CG-5 instrument was also involved in the tests what is probably the first attempt to the absolute calibration of this type of gravimeters ever done.

11 Updated Hungarian gravity field model with spherical radial base functions

GOCE has provided satellite-only global gravity field models with unprecedented spatial resolution (Földváry et al. 2015c). Updated gravity field solutions for Hungary were determined using the latest DIR R05 GOCE gravity field model. The solution methodology was least-squares gravity field parameter estimation using Spherical Radial Base Functions (SRBF). Regional datasets include deflections of the vertical (DOV), gravity anomalies, surface gravity gradients and quasigeoid heights by GPS/levelling (Tóth and Földváry 2015a, 2015b, 2015c).

Regional gravity field modeling in Hungary has a long history dating back to 1918, when first in the world a disturbing potential isoline map of Arad and its surroundings, based on astrogeodetic and torsion balance data was published by D. Pekár (Biró et al. 2013). Astrogeodetic geoid determinations starting from 1950 were followed by modern gravimetric geoid determinations at various institutions (Biró et al. 2013). The application of Least Squares Collocation (LSC) to include heterogeneous data in gravity field estimation resulted in the gravimetric-astrogeodetic-gradiometric solution HGTUB2007 (Tóth 2008) and an EGM2008-based astrogeodetic-gravimetric combined quasigeoid model (Tóth and Szűcs 2011).

Gravity field modelling by SRBFs has several merits:

- individual data-dependent weights can be introduced
- it is easy to incorporate different gravity field functionals (e.g. DOV or gravity gradients)
- computational burden is reduced with respect to LSC, where the number of unknowns equals the number of data
- rigorous parameter estimation and prediction with full covariance information is possible

The functional model of SRBF parameter estimation is

$$F(\mathbf{r}_i) + e(\mathbf{r}_i) = \sum_{k=1}^{k} x_k B^F(\mathbf{r}_i, \mathbf{r}_k) \tag{1}$$

Here F and e denote a measured gravity field functional and its error at point $\mathbf{r}_i$, $B^F(\mathbf{r}_i, \mathbf{r}_k)$ is the SRBF placed at point $\mathbf{r}_k$, k is the number of SRBFs and x_k are the unknown parameters. This equation can be written for the estimation of parameter vector $\boldsymbol{x}$ as a linear equation system with design matrix $\mathbf{A}$ and data vector $\mathbf{y}$ as

$$\mathbf{y} + \mathbf{e} = \mathbf{A}\mathbf{x} \tag{2}$$

The shape of the band-limited SRBF is defined by its coefficients b_n in the Legendre series

$$B(\mathbf{r}_i, \mathbf{r}_k) = \sum_{n=N_{\min}}^{N_{\max}} (2n+1) \left(\frac{\mathbf{r}_k}{\mathbf{r}_i} \right)^{n+1} b_n P_n(\hat{\mathbf{r}}_i, \hat{\mathbf{r}}_k) \tag{3}$$

where $P_n(\hat{\mathbf{r}}_i, \hat{\mathbf{r}}_k) = P_n(t_{ik})$ are Legendre polynomials of degree n, $t_{ik} = \hat{\mathbf{r}}_i, \hat{\mathbf{r}}_k$ is the cosine of the angle between $\hat{\mathbf{r}}_i, \hat{\mathbf{r}}_k$ unit vectors. From this expansion $B^F(\mathbf{r}_i, \mathbf{r}_k)$ can be obtained by applying the

particular differential operator D belonging to functional F on the SRBF $B(\mathbf{r}_i, \mathbf{r}_k)$.

The shape of SRBF depends on the chosen bandwidth and coefficients b_n. We have chosen the most simple band-limited Shannon radial basis functions (Figure 6).

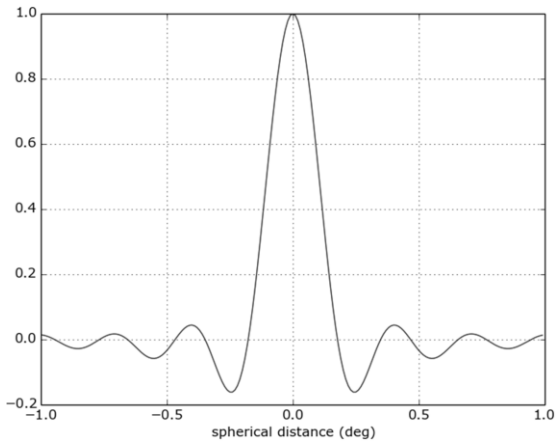

Figure 6. Shannon Radial Basis Function (bandwidth = 200-1200)

The positions of SRBF, i.e. points $\mathbf{r}_k$ were fixed to that of a Reuter grid. The distance between adjacent Reuter grid points is defined by the control parameter c. This parameter was chosen equal to the bandwidth of the base functions N_{max}.

Gravity field recovery from observed gravity data is an inverse problem. Instability of the inverse operator must be fixed by proper regularization to obtain a physically meaningful solution. For weighting and regularization the method of Variance Component Estimation (VCE) was used.

After the solution $\hat{\mathbf{x}}$ was estimated, the covariance matrix $\mathbf{C}_{\hat{\mathbf{x}}}$ of the parameters was determined from the law of covariance propagation as

$$\mathbf{C}_{\hat{\mathbf{x}}} = \sum_i \frac{1}{\sigma_i^2} \mathbf{N}^{-1} \mathbf{N}_i \mathbf{N}^{-1} \tag{4}$$

Prediction (synthesis) of gravity field functionals at non-measured points is possible by introducing $\hat{\mathbf{x}}$ into an equation similar to Eq. 2, $\mathbf{y}_S = \mathbf{A}_S \hat{\mathbf{x}}_S$. The full covariance matrix of predicted $\hat{\mathbf{y}}_S$ functionals is again computed by covariance propagation

$$\mathbf{C}_{\hat{y}_S} = \mathbf{A}_S \mathbf{C}_{\hat{x}} \mathbf{A}_S^T \tag{5}$$

The following 11 terrestrial datasets have been prepared for regional gravity field determination in the GRS80 system.

- Δg free-air anomalies of the MGH-50 gravity network (Renner and Szilárd 1959) (509 points)
- ξ, η astrogeodetic deflections of the vertical of the first-order control network (138 points)
- ζ quasigeoid undulations at OGPSH GPS control network:
  - ζ at points of the old Bendefy levelling network (87 points)
  - ζ at points of the EOMA levelling network (149 points)
  - ζ at points of the EOMA levelling network with recently levelled heights (97 points)
- v_{xz}, v_{yz} horizontal surface gravity gradients measured by torsion balance (37610 points)
- $v_{yy\text{-}xx}$, $2v_{xy}$ surface curvature gravity gradients measured by torsion balance (37272 points)

The last ζ dataset contains quasigeoid heights computed from a geopotential model (GPM) outside Hungary at points of a dense Reuter grid. The total number of data included in the solution was 154477. We have used three different GPMs. The GOCE DIR R05 model has been combined with the EGM20008 model according to optimal spectral content and has been evaluated in comparison with the EGM2008 and EIGEN-6C4 models to assess the performance of our regional gravity field solution.

All datasets have been reduced to contain information only between the chosen N_{min} and N_{max} SH degrees. First, frequencies above SH degree 2160 have been removed by the ERTM2160 model (Hirt et al 2013). Second, contributions of the GPM up to N_{min} and from N_{max} to 2160 have also been removed. Best data reduction is achieved by combined GOCE fifth generation models in bandwidth 200-1200. The bandwidth of the SRBFs, i.e. SH degrees N_{min} and N_{max} have to be chosen in accordance with extension of the data area and data density, respectively. We have chosen N_{min} =200 and N_{max} =1200.

The solution, i.e. the estimated SRBF parameters is shown in Figure 7 for the combined GOCE DIR R05 – EGM2008 GPM based model.

In Table 1 final variance factors as well as signal-to-noise ratios are shown for selected datasets. VCE iteration converges to these final variance factors σ_i^2 which indicate final relative weights of each dataset. Large variance factors show that those data were weighted down relative to others.

Another measure is the signal-to-noise ratio, SNR in dB, defined as the logarithmic ratio of the norm of the signal $\mathbf{y} = \mathbf{A}\hat{\mathbf{x}}$ with respect to norm of residuals $\hat{\mathbf{e}}$:

$$SNR = 10\log_{10}\frac{\|\mathbf{A}\hat{\mathbf{x}}\|}{\|\hat{\mathbf{e}}\|} \tag{6}$$

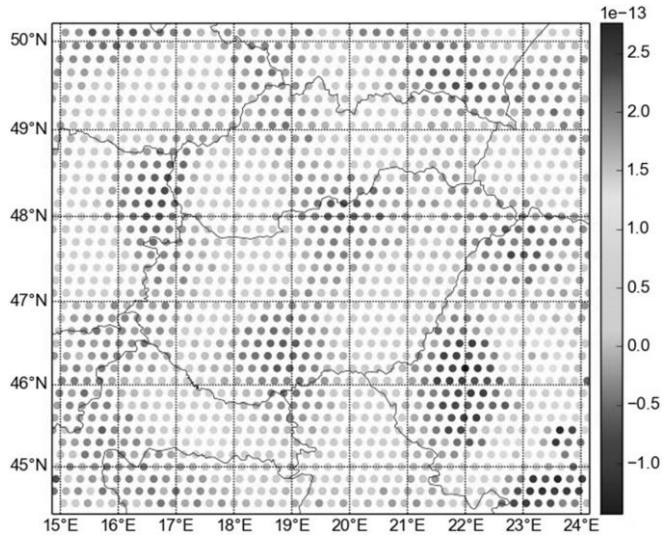

Figure 7. Estimated SRBF parameters of the geopotential according to Eq. 1. The parameters are normalized with the zero-degree term of the geopotential and hence unitless

Table 1. Variance factors σ_i and SNR ratios (dB) of selected datasets for GOCE DIR R05 based solution

dataset / GPM		ξ [“]	v_{xz} [E]	$\zeta_{\text{Bend.}}$	ζ_{EOMA}	ζ_{EOMARL}	$\zeta_{\text{GPM outside}}$	Δg
GOCE DIR R05 + EGM2008	σ_i	1.83	14.1	0.22	0.26	0.25	0.42	10.33
	SNR	1.91	-2.88	4.05	1.86	3.65	7.92	2.57

The relative accuracy of parameters can be defined as the ratio of parameter standard deviation and standard deviation of the solution vector. These relative accuracies are plotted on Figure 8 for the combined model.

The solution vector $\hat{\mathbf{x}}$ is used to predict quasigeoid heights and their covariances according to Eq. 5 on a regular grid. These predictions can be seen on Figure 9 and 10, respectively.

Finally to assess the accuracy of the solutions we predicted quasigeoid heights inside Hungary on a Reuter grid and compared the predictions with those of the GPMs in the frequency band 200-1200.

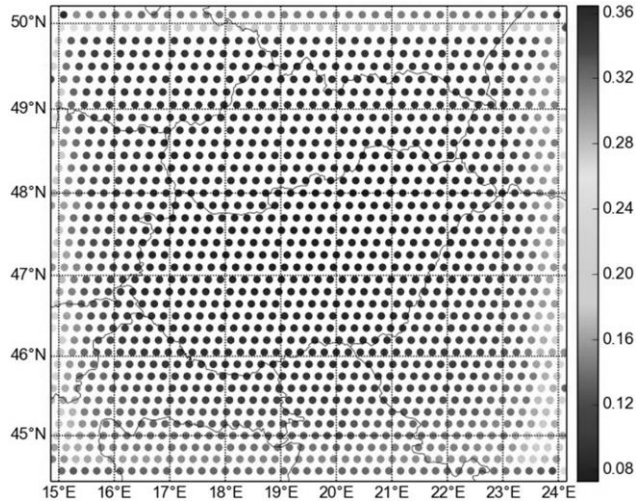

Figure 8. Relative accuracy of SRBF parameters

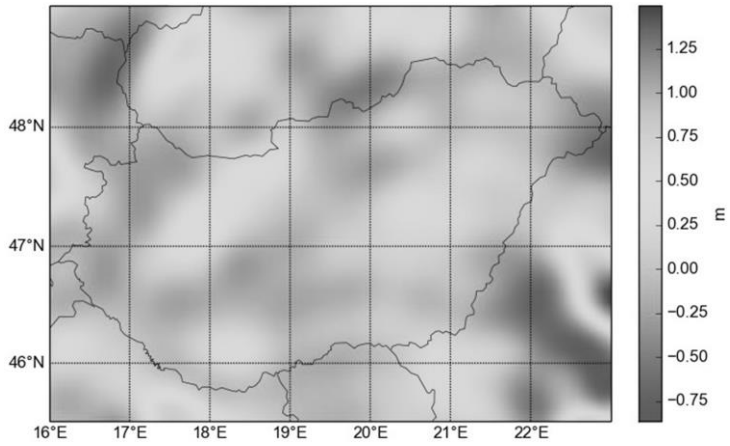

Figure 9. Estimated residual ζ quasigeoid in the SH band 200-1200

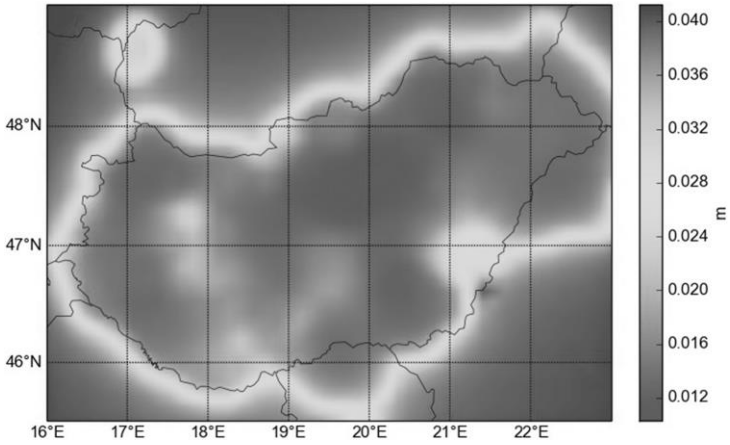

Figure 10. Estimated std error of residual ζ quasigeoid in the SH band 200-1200

Table 2 shows statistics of this comparison for the three tested geopotential models. These statistics show slightly better standard deviation of the residuals for the EGM2008 and EIGEN-6C4 models in the selected bandwidth of 200-1200, where residuals are defined as the differences of predicted SRBF and GPM quasigeoid heights. The mean of the residuals, however is the best for EIGEN-6C4 and our combined GOCE – EGM2008 model.

Table 2. Statistics of predicted quasigeoid height residuals at 1024 points of the three different SRBF gravity field models

GPM used	min	max	mean	std
EGM2008	-0.187	0.227	0.015	**0.051**
EIGEN-6C4	-0.189	0.224	**0.013**	**0.051**
GOCE DIR R05 and EGM2008	-0.206	0.219	**0.013**	0.056

The approach of regional gravity field modelling by SRBFs works quite well and provides reasonable results. One important merit of this technique is that data of different kind and heterogeneous distribution can easily be combined in a rigorous estimation procedure of gravity field parameters and their errors. We demonstrated this aspect by using DOV, gravity, gravity gradient and GPS/levelling data in combination with different geopotential models.

Since there is a direct connection one can easily compute SH coefficients from the estimated SRBF coefficients. This enables straightforward estimation of signal and error degree variances of regional datasets, which is another benefit of the regional gravity field modelling by SRBFs.

References

Ádám J, Rózsa Sz, Tóth Gy, Völgyesi L (2018): Remeasurement of the first gravity reference station of Hungary established 100 years ago at the Budapest University of Technology and Economics (BME) (in Hungarian). Geodézia és Kartográfia, 70(2), 4-14.

Benedek J, Papp G, Kalmar J (2018): Generalization techniques to reduce the number of volume elements for terrain effect calculations in fully analytical gravitational modelling. Journal of Geodesy, 92(4), 361-381.

Biró P, Ádám J, Völgyesi L, Tóth Gy (2013): Geodesy: Theory and Practice (in Hungarian). ISBN: 978-963-257-248-2. HM Zrínyi Nonprofit Kft, Budapest, Hungary. Reviewed by Allan, A.L., Survey Review, 46(339), 453.

Földváry L, Kiss A (2015): Determination the time variation of global geoid (in Hungarian). In: XVI. Földmérő Találkozó konferenciakiadványa (editor: J. Ferencz), Zilah, 2015.05.14-17., Erdélyi Magyar Műszaki Tudományos Társaság, 33-37.

Földváry L, Kemény M, Huang XZ (2015a): First results of implementing satellite-borne gravity data to GIS and future perspectives. 10th International Symposium on Applied Informatics and Related Areas - AIS2015, Székesfehérvár November 11, 2015, Paper P03. 6 p., ISBN: 978-615-5460-49-4.

Földváry L, Kiss A, Su ZX, Wang GC, Wang L (2015b): Accuracy investigations of GRACE-borne ice mass variations in Antarctica. Earth Science Frontiers, 22(4), 239-246.

Földváry L, Tóth Gy, Kiss A, Kemény M (2015c): GOCE Satellite: An Earth Orbiter Torsion Balance (in Hungarian). Magyar Tudomány, 176 (2015/9): 1063-1070.

Földváry L, Kiss A (2016): Accuracy analysis of Glacial Isostatic Adjustment models using for satellite gravimetry. 11th International Symposium on Applied Informatics and Related Areas (AIS 2016), Székesfehérvár November 11, 2016, 5-10, ISBN: 978-615-5460-92-0.

Hirt C, Claessens JS, Fecher T, Kuhn M, Pail R, Rexer M (2013): New ultrahigh-resolution picture of Earth's gravity field. Geophysical Research Letters, 40, doi: 10.1002/grl.50838.

Kiss A, Földváry L (2015): Annual hydrologic variations from GRACE gravity models (in Hungarian). Geomatikai Közlemények, 18(2) 43-52.

Kiss A, Földváry L (2017a): Uncertainty of GRACE-borne long periodic and secular ice mass variations in Antarctica. Acta Geodaetica et Geophysica, 52(4), 497–510.

Kiss A, Földváry L (2017b): Seasonal hydrologic variations in the La Plata basin from GRACE gravity field models. Acta Geodynamica et Geomaterialia, 14(2), 145–152.

Kiss A, Földváry L (2018): Multi-annual mass variations from GRACE monthly solution – preliminary results. Acta Geodyn. Geomater, 15(2), 165-172.

Kis M, Koppán A, Papp G, Benedek J, Baracza K, Szabados L, Csontos A, Meurers B (2018): Absolute calibration of relative gravity meters in tidal range - Determination of beam-position dependent transfer functions in the Mátyáshegy Gravity and Geodynamical Observatory. Geophysical Research Abstracts 20, EGU2018-15106.

Koppán A, Kis M, Merényi L, Papp G, Benedek J, Szűcs E, Meurers B (2016): Moving-mass calibration of LCR-G gravimeters- Determination of beam-position dependent transfer functions in the Mátyáshegy Gravity and Geodynamical Observatory Budapest. In: 18th International Symposium on Geodynamics and Earth Tides 2016, P07-02, 286-286. (https://g-et2016.units.it/node/286).

Koppán A, Kis M, Merényi L, Papp G, Benedek J, Szűcs E, Meurers B (2017): Determination of beam-position dependent transfer functions of LCR-G gravimeters by means of moving mass calibration device in the Mátyáshegy Gravity and Geodynamical Observatory Budapest. Geophysical Research Abstracts 19 (2017) Paper: EGU2017-17225.

Lévay E, Koppán A (2015): Comparison of vertical gradient determination techniques: first results. In: Proceedings of the 13th Students' Science Conference. Polanica Zdroj, Poland, 2015.09.17-2015.09.20. Wrocław, Wroclaw University of Technology, 108-113.

Paláncz B, Awange JL, Völgyesi L (2015): Correction of Gravimetric Geoid Using Symbolic Regression. Mathematical Geosciences, 47(7), 867-883, DOI 10.1007/s11004-014-9577-3.

Péter G, Deák L, Gróf Gy, Kiss B, Szondy Gy, Tóth Gy, Ván P, Völgyesi L (2019): Remeasurement of the Eötvös-Pekár-Fekete equivalence experiment (in Hungarian). Fizikai szemle, 69(4), 111-116.

Renner J, Szilárd J (1959): Gravity network of Hungary. Acta Technica Acad. Scient. Hung., 23(4), 365-395.

Szabó Z, (2016): The history of the 125 year old torsion balance. Acta Geodaetica et Geophysica, 51, 273-293.

Tóth Gy (2008): New combined geoid solution HGTUB2007 for Hungary. IAG Symposia Vol 133. Observing our Changing Earth, 405-412.

Tóth Gy, Földváry L (2015a): Updated Hungarian Gravity Field Solution Based on Fifth Generation GOCE Gravity Field Models. In: Ouwehand, L (szerk.) Proceedings of the 5th International GOCE User Workshop. ESA Communications - ESTEC, Paper: p_g11, 8 p.

Tóth Gy, Földváry L (2015b): Updated Hungarian gravity field solution based on fifth generation GOCE gravity field models (in Hungarian). Geomatikai Közlemények, 18(2), 63-74.

Tóth Gy, Földváry L (2015c): Hungarian Gravity Field Modeling by Spherical Radial Basis Functions. Poster presented at 26th IUGG General Assembly, Prague, June 22 to July 2.

Tóth Gy, Szűcs E (2011): On the determination of a new combined EGM2008 based quasigeoid model for Hungary. Acta Geod. et Geoph. Hung., 46(4), 417-430.

Tóth Gy, Völgyesi L (2017): Data processing of QDaedalus measurements. Geosciences and Engineering, 5(8), 149-166.

Völgyesi L (2015): Renaissance of the torsion balance measurements in Hungary. Periodica Polytechnica Civil Engineering, 59(4), 459-464, DOI: 10.3311/Ppci.7990.

Völgyesi L, Tóth Gy (2015): Possibilities of determinations of the vertical deflections (in Hungarian). Geomatikai Közlemények, 18(2), 75-83.

Völgyesi L, Tóth Gy, Dobróka M (2015a): Inversion reconstruction of 3D gravity potential function including vertical deflections. Geosciences and Engineering, 4(6), 81-92.

Völgyesi L, Tóth Gy, Ultmann Z (2015b): New chapter in the history of the Hungarian torsion balance measurements and their applications (in Hungarian). Magyar Geofizika, 56(2), 95-105.

Völgyesi L, Tóth Gy (2016): Possibilities of geodetic application of the QDaedalus system (in Hungarian). Geodézia és Kartográfia, 68 (9-10), 11-17.

Völgyesi L, Tóth Gy (2018): Calibration of the QDaedalus system (in Hungarian). Geodézia és Kartográfia, 70(6), 9-15.

Völgyesi L, Szondy Gy, Tóth Gy, Péter G, Kiss B, Deák L, Égető Cs, Fenyvesi E, Gróf Gy, Ván P (2018): Preparations for the remeasurement of the Eötvös-expriment (in Hungarian). Magyar Geofizika, 59(4), 165-179.

HUNGARIAN CONTRIBUTION TO THE RESEARCH OF PHENOMENA RELATED TO EARTH ORIENTATION, TIDES AND TECTONICS (2015-2018) - IAG COMMISSION 3

Péter Varga[*], Judit Benedek[**], Katalin Gribovszki[**], Márta Kis[***], Márta Kiszely[*], András Koppán[***], Gyula Mentes[**], Gábor Papp[**]

1 Earth Orientation (Earth rotation, polar motion, nutation and precession)

In the context of the dipole model of the Earth's magnetic field, the data from the international bank of digital information on the distribution of the virtual dipole moment (VDM) values in time, combined with the data obtained by subsequent investigations (7082 values in total), served as the basis for reconstructing its behaviour through the Paleoarchean–Phanerozoic. The VDM behavior is characterized by a positive linear trend in the interval of 4.1×10^{22} Am^2 (3.5 Ga ago) to 5.5×10^{22} Am^2 (now) (Figure 1). This background linear growth of the field strength is complicated by irregularly distributed VDM variations ranging in the amplitude from 1.7×10^{22} to 3.7×10^{22} Am^2 with the wavelength varying from 220 to 920 Ma. The average wavelength of such fluctuations is estimated to be 570 Ma, which is approximately equal by duration to the Wilson geological cycles. The interval of 0.84–1.3 Ga is first established to be characterized by the relatively calm VDM region of $4.7–4.9 \times 10^{22}$ Am^2. The first defined deep minimum described by 10 data points with the extreme of 2.3×10^{22} Am^2 (2.15 Ga ago) corresponds to the terminal phase in the formation of the earth's core geometry and initiation of the formation of the modern dipole field (Schreider et al. 2015, Varga 2015a).

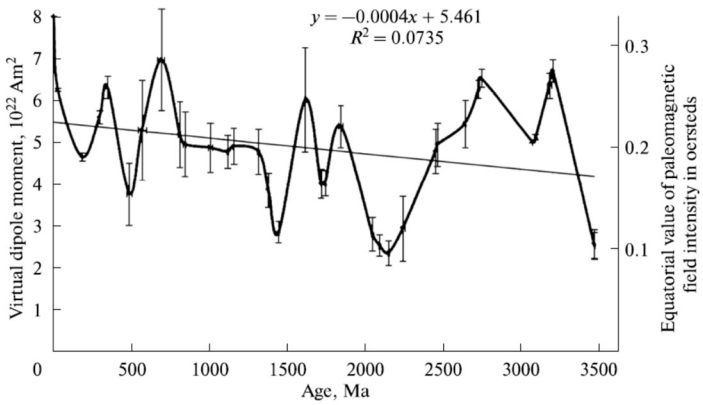

Figure 1. Distribution of the average values of the virtual dipole moment (10^{22} Am^2) over the past 3.500 Ma. The values are calculated by the method of a moving average in a window of 200 Ma with a step of 100 Ma. The plot shows the linear approximation of the values and reflects the growth of the value of the dipole component in the magnetic field of the Earth toward its modern values. The right vertical axis shows the VDM values recalculated into the equatorial intensity of the paleomagnetic field in oersteds. The vertical and horizontal bars designate the standard errors of the average in each calculation window

Our analysis has revealed that different literature sources often use different formulas for VDM calculation and these formulas do not coincide with each other, hence causing the differences between calculation results obtained by these formulas, with the same experimental values formally being used with them. To clarify this problem, development of the formula for VDM calculation has been verified and dimension of this formula has been estimated (Schreider et al. 2016).

[*] *MTA CSFK Geodetic and Geophysical Institute, Kövesligethy Radó Seismological Observatory, Budapest, Meredek 18, H-1112 E-mail: varga@seismology.hu*
[**] *MTA CSFK Geodetic and Geophysical Institute, Sopron, Csatkai E. 6-8 H-9400.*
[***] *Mining and Geological Survey of Hungary, Budapest Pf. 95, H-1590*

A statistical investigation of VDM data was carried out separately for the case of Archean+Proterozoic ($Arch + Ptz$) and for Phanerozoic (Pz). For the time interval 3.500 Ga - 0.570 Ga the time dependent slope is statistically different from zero ($VDM = a{\cdot}time + b$; $a = (0.00019{\pm}7.89{\cdot}10^{-5})$ Am^2/Ma), while for the Phanerozoic the temporal variation cannot be proven to be significant. The slope estimate is $a = (-0.00019{\pm}2.84{\cdot}10^{-4})$ Am^2/Ma.

The question whether the slope estimate reflects a significant trend in the change of VDM in the time-interval from 3.500 Ga to 0,570 Ga ($Arch + Ptz$) has been verified using a F statistical hypothesis test. Assuming identically normally distributed data the test statistics $T_a = \frac{a^2}{b^2} = 6.26$ follows an F-distribution with $n = 55$ degrees of freedom. Using a confidence level of $\alpha = 5\%$ the null hypothesis $H_0: a = 0$ is rejected on the basis of the critical value $F_{0.05}(1{,}55) = 4.0$. Consequently, the test supports that the slope is statistically significant. In case of time-interval from 0.570 to present $T_a = \frac{a^2}{b^2} = 0.40$ and $n = 136$ the value $F_{0.05}(1{,}136) = 3.9 > T_a$ and therefore the slope estimate a statistically is not significant. Consequently the magnitude of the VDM monotonously increased during the Archean and Proterozoic under the influence of some processes which took place in the liquid core of the Earth and which stopped at the beginning of Pz. The total energy of hydrodynamic currents generating the geomagnetic field and occurring inside the liquid core could not increase in time. The growth of VDM was caused presumably by a process which strengthened the dipolic character of the geomagnetic field. For example, this could happen by strengthening the dipolic nature of the geomagnetic field.

Based on a statistical analysis of paleontological and paleosedimentological data obtained from the sequences of different colorations in fossil corals, bivalves and brachiopods for the Pz, and stromatolites and tidal deposits (tidalites) for the Ptz, it has been found that during the Pz the LOD increased on average at a rate of 5.4 h/Ga (1.94ms/century), while during the Ptz, the average rate was only 1.24h/Ga (0.45ms/century), i.e. 4.4 times smaller (Figure 2).

The statistical study of LOD data base gives for the slope a ($LOD = a \cdot t + b$) $-(0.00124{\pm}0.00072)$ h/Ma for $Arch + Ptz$ and $-(0.0054{\pm}0.0006)$ h/Ma for Pz.

The significance of the trend estimate of LOD in the time-interval from 2.500 Ga to 0,570 Ga ($Arch + Ptz$) has been verified using again F statistical hypothesis test. Assuming identically normally distributed data the test statistics $T_a = \frac{a^2}{b^2} = 6.80$ follows an F-distribution with $n = 11$ degrees of freedom. Using a confidence level of $\alpha = 5\%$ the null hypothesis $H_0: a = 0$ is rejected on the basis of the critical value $F_{0.05}(1{,}55) = 3.36$. Consequently, the test supports that the slope is statistically significant. In case of time-interval from 0.570 to present $T_a = \frac{a^2}{b^2} = 46.25$ and $n = 55$ the value $F_{0.05}(1{,}136) = 2.8$ is smaller than T_a and consequently the slope estimate a statistically significant.

Consequently, at 3Ga BP, LOD was presumably of about (18.0 – 18.5) h. In contrast to the change rate ΔLOD during Pz, however, the rate during the Ptz cannot be proven to be statistically significant features of geodynamic processes VDM and LOD during the $Arch + Ptz$ and Pz were compared. The common feature of these processes is that they were different before and during the Phanerozoic (VDM stopped growing, the axial despinning rate became 4.4 times bigger). (Varga 2015a).

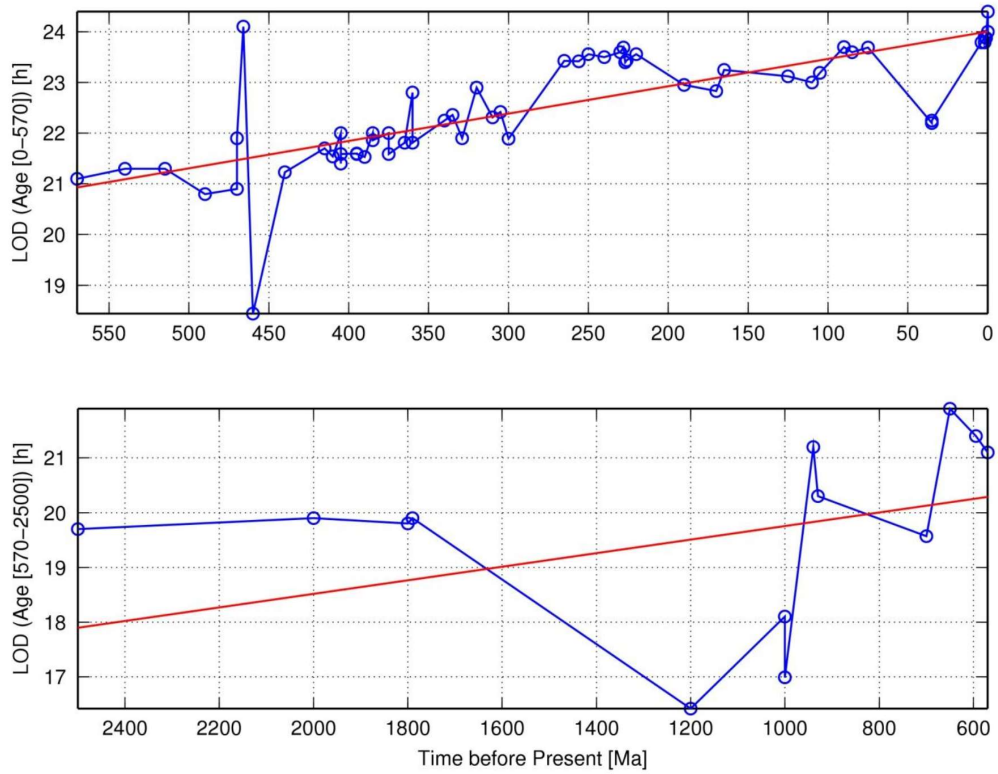

Figure 2. Length of day data for the time intervals from 0.570 Ga to present (above) and from 2.500 Ga to 0,570 Ga (below). The straight lines shows the regression line $LOD = a \cdot t + b$ with numerical values $a = (0.0054 \pm 0.0006)$) h/Ma and $a = (0.00124 \pm 0.00072)$ h/Ma for the Pz and $Arch + Ptz$ respectively

2 Earth tides, tidal stress, tidal triggering of earthquakes

Tidal stresses are generated in any three-dimensional body influenced by an external inhomogeneous gravity field of rotating planets or moons. A special case, stresses caused within the solid Earth by the body tides was investigated from viewpoint of their influence on seismic activity. The earthquake triggering effects of the Moon and Sun are usually investigated by statistical comparison of tidal variations and temporal distribution of earthquake activity, or with the use of mathematical or experimental modelling of physical processes in earthquake prone structures. In the investigation carried out by Varga and Grafarend (2016, 2018a,b), the magnitude of the lunisolar stress tensor in terms of its components along the latitude of the spherical surface of the Earth as well as inside the Earth (up to the core-mantle boundary) were calculated for the PREM (Preliminary Reference Earth Model). Results of calculations prove that stress increases as a function of depth reaching a value around some kPa at the depth of 900–1500 km, well below the zone of deep earthquakes. At the depth of the overwhelming part of seismic energy accumulation (around 50 km) the stresses of lunisolar origin are only $(0.0–1.0)10^3$ Pa. Despite the fact that these values are much smaller than the earthquake stress drops (1–30 MPa this does not exclude the possibility of an impact of tidal forces on outbreak of seismic events. Since the tidal potential and its derivatives are coordinate dependent and the zonal, tesseral and sectorial tides have different distributions from the surface down to the CMB (Core Mantle Boundary), the lunisolar stress cannot influence the break-out of every seismological event in the same degree. The influencing lunisolar effect of the solid Earth tides on earthquake occurrences is connected first of all with stress components acting parallel to the surface of the Earth. Reviewing the results of the calculations it can be concluded that the magnitude of trig-

gering effect of Earth tides is different in case of zonal (Z), tesseral (T) and sectorial (S) tides and also significantly depends on the latitude (Figure 3). The influence of load tides is limited to the loaded area and its immediate vicinity (Figure 4) (Varga and Grafarend 2018a,b).

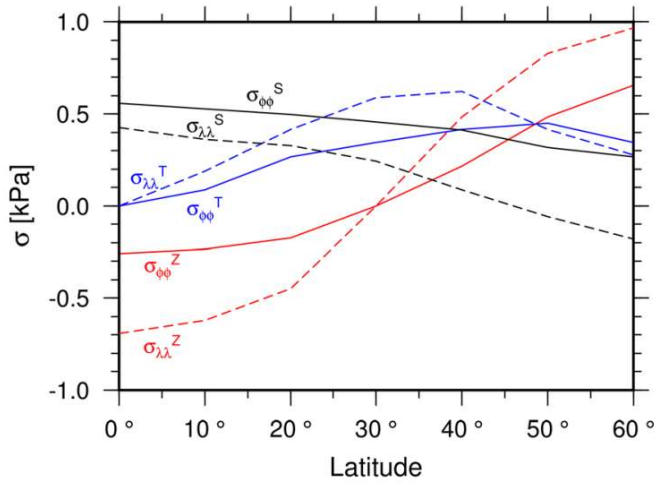

Figure 3. Latitude dependence of normal horizontal stress tensor components $\sigma_{\phi\phi}$ and $\sigma_{\lambda\lambda}$ along the surface of the Earth (Z zonal, T tesseral and S sectorial tides)

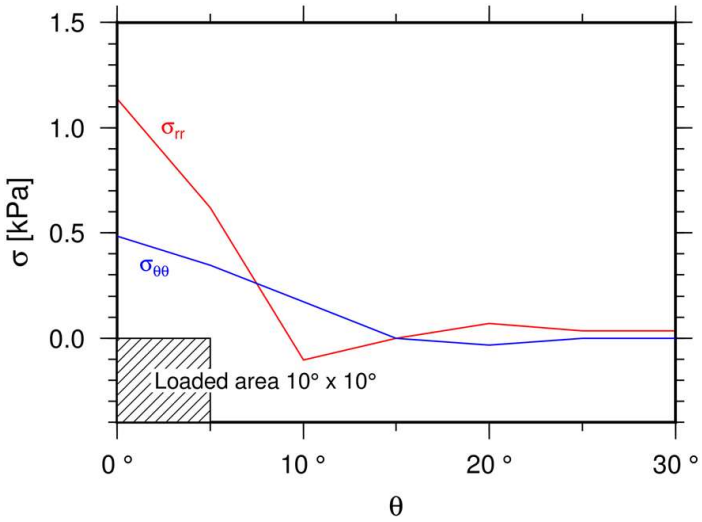

Figure 4. Radial normal (red line) and lateral (blue line) stress tensor components caused by 10^2 Pa normal load on a spherical segment function of spherical distance θ

In the framework of a national research project NKFIH-OTKA K101603 the location dependence of the bulk tidal gravity effect was investigated in the Pannonian basin (Papp et al. 2018). Some of the recent absolute g measurements in this area showed periodical change of the drop set means recorded during the observation days so it draw attention to the local tidal corrections of gravity measurements at μGal accuracy (=10^{-8} m/s^2) required by geodynamical research. Therefore 6 instruments (4 LCR G meters, a Scintrex CG-5, GWR SG025) at 5 different locations (Fig. 5) were operated for 3 – 9 months mainly in co-located configuration. Due to problem of the proper and accurate determination of the scale factors and functions of the applied spring gravimeters the ratio of the delta factors of O1 and M2 tidal constituents computed by ETERNA3.4 program package was investigated supposing that M2 is much more influenced by the ocean loading effect than O1. The slight detected increase of δ(O1)/δ(M2) (~0.2%) toward east obtained from the best selected time series does not

contradict to theory and the prediction provided by e.g. FES2014 ocean loading model. The measure of the increase is, however, significantly smaller than the expected (~0.8%) so further investigation is needed.

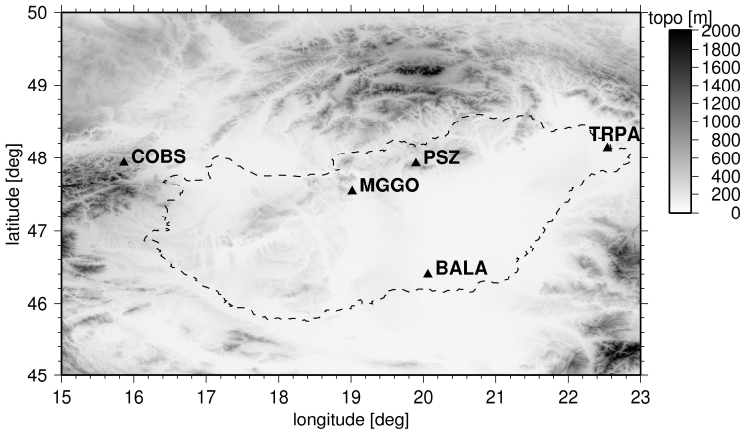

Figure 5. The map of the target area (Pannonian basin) and its orogenic environment (Eastern Alps, Carpathians) with the locations of the tidal stations. COBS – Conrad Observatory, Austria; MGGO – Mátyáshegy Gravity and Geodynamical Observatory, Hungary; PSZ – Piszkéstető Seismological Station, Hungary; TRPA – Tarpa Seismological Station, Hungary; BALA – Balástya, temporal station. The gray shaded map in the background shows the topography of the area. The black dashed line indicates the state border of Hungary

3 Tide generated deformations of the elastic Earth

3.1 Physical meaning of the zonal components of the geopotential

The physical meaning of the zonal components of the geopotential is closely related to the flattening and to the angular spin velocity of the Earth as well as to its equatorial (A) and polar (C) moments of inertia. Through these moments of inertia the gravitational potential V is connected to the mass density distribution within the Earth. A generalized form of the MacCullagh equation was obtained for even orders $n \geq 2$ by including the higher order zonal coefficients J_n connected with the higher ($n \geq 2$) degree moments of inertia C_n and A_n. It was shown that the higher the degree n, the higher is the weight of the near-surface (i.e. shallow) mass density distribution in J_n (Varga 2015b).

3.2 Properties of Love-Shida numbers

There are different equations to describe relations between different classes of Love–Shida numbers. In this study with the use of the time-varying gravitational potential an integral relation was obtained which connects tidal Love–Shida numbers (h, l, k), load numbers (h', l', k'), potential free Love–Shida numbers generated by normal (h'', l'', k'') and horizontal (h''', l''', k''') stresses. The equations obtained in frame of present study is the only one which

- holds for every type of Love–Shida numbers,
- describes a relationship not between different, but the same type of Love–Shida numbers,
- does not follow from the sixth-order differential equation system of motion usually applied to calculate the Love–Shida numbers.

The equation which is valid for all types of Love–Shida numbers is

$$k_n(a) = 4\pi G n/[\gamma(2n+1)a^{n+1}] \int_0^a -\rho(r) r^{n+1} [n(n+1) l_n(r) + h_n(r)] dr$$

here n is the order of spherical harmonics, a is the mean radius of the Earth, $0 \leq r \leq a$, $\rho(r)$ is the density function, γ is the mean gravity acceleration and G is the gravitational constant. In the r.h.s. of equation the first term describes the horizontal and the second the vertical displacement.
In case of $n = 2$

$$k_2(a) = \frac{3}{5}\int_0^a \varrho(r) \cdot r^3 \left[3l_n(r) + h_n(r)\right]$$

Based on the use of the above equation $k_2(a)$=0.3031, what is close to value observed by many authors. The importance of this equation is that it is the only relation which does not follows from the differential equation of motion usually used to calculate the Love–Shida numbers and contains the complete triplet h_n, k_n and l_n of the same type. They were obtained without any considerations concerning he boundary conditions, therefore it is valid both for tidal, load and potential free Love–Shida numbers (Varga et al. 2018a,b).

4 Research of tectonic movements, Earth's tides and related phenomena by extensometers and tilt sensors

In the Pannonian Basin extensometers are used for measurement of local tectonic deformations caused by Earth's tides and related phenomena. The locations of the extensometric stations are sown in Figure 6. Extensometric data obtained in three Hungarian observatories: Sopronbánfalva Geodynamic Observatory (SGO), Mátyáshegy (Budapest) Gravity and Geodynamic Observatory (MGGO), Pécs deep station and in the Vyhne (Slovakia) Tidal Station (VTS) were regularly preprocessed to eliminate short and long periodic seasonal disturbing effects (temperature, air pressure) and local effects depending on the properties of the measurement site (geology, cavity, etc.). To ensure the best data quality the instruments were yearly calibrated by the same calibration instrument, in addition to the daily calibration by the built-in calibrator. This method provides data of the same quality, allowing comparisons of data measured in each observatory, especially for the interpretation of tectonic movements (Brimich et al. 2016, Mentes 2016).

In this research period as tidal related phenomenon the effect of the Free Core Nutation (FCN) on the P1, K1, Ψ1 and Φ1 tidal waves were studied on the basis of tidal results obtained in four observatories. Since the SGO in Hungary is one of the few places where radon concentration and rock strain variations are simultaneously monitored the relationships between rock strain and radon concentration variations was also investigated.

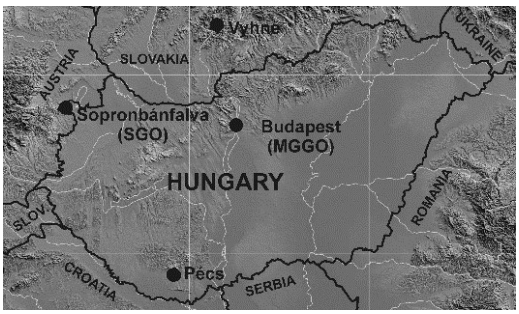

Figure 6. Locations of the extensometric stations in the Pannonian Basin

New sensors have been installed and operated in cooperation between Geodetic and Geophysical Institute MTA CSFK (Hungary), Zentralanstalt für Meteorology und Geophysik (Austria) and Finnish Geospatial Research Institute (Finland) in the Conrad Observatory (Austria) to test the capabilities of pendulum (biaxial Lippmann type) and interferometric hydrostatic (iWT) tiltmeters. Although the primary aim of the cooperation is to monitor the activity of the Mur-Mürz tectonic zone the recorded data can be also used for tidal research. Since 2016 the stable co-located and co-oriented operation of the sensors is ensured and tilt time series (visit http://kepujsag.ggki.hu) has been recorded continuously (Ruotsalainen et al. 2016). The data shows that both instruments pro-

vide high quality observations with a few nrad resolution. The first results, the most dominant environmental effects and a preliminary tidal model have been presented already during the IGETS 1st Workshop in 2018 in Potsdam. The cooperation has been extended and tilt data from The Peters Seismological Observatory (Victor Harbor, Australia) are also available for many kinds of investigations, especially for the analysis of ocean loading effects and its available models due to the location of TPSO.

5 Investigation of local tectonic movements and deformations

Extensometric data are usually evaluated every five years for investigation of local tectonics, since tectonic movements and deformations are slow processes with a rate of 1 nstr y^{-1} – 10 μstr y^{-1}. Figure 7 shows the fifteen-year long extensometric record obtained in the VTS. The gaps in the record are partly of instrumental origin (e.g. data logger was out of range) and the large distance between the observatory and the institute. To determine the average yearly rate of the tectonic movements a linear regression line was fitted to the measured extensometric data. The obtained strain rate is 38 nstr/year (1 nstr = 10^{-9} relative deformation). Figure 7 also shows the strain rates measured in the Slovakian GPS network (Hefty 2010). It can be seen that the velocities are small in the vicinity of Vyhne. The surface extension inferred from the horizontal velocities range from 8 to 45 nstr y^{-1} and in the vicinity of Vyhne is between 20 and 30 nstr y^{-1} (Brimich et al. 2016).

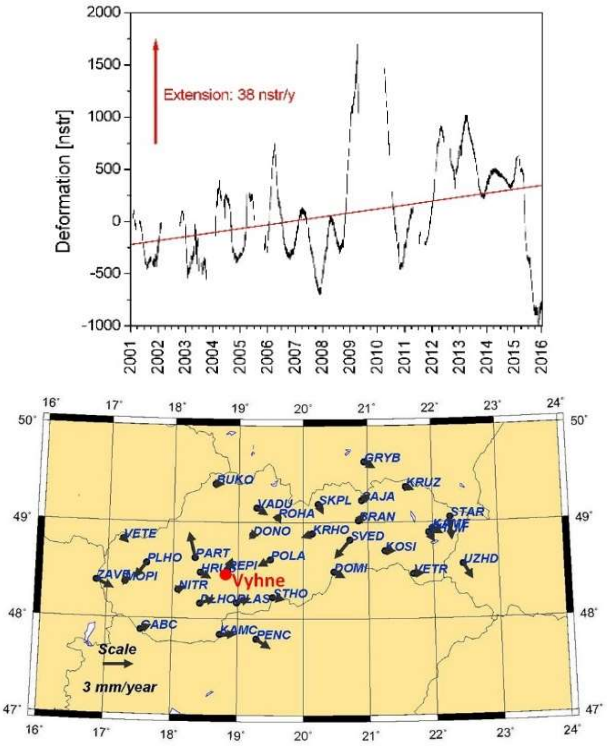

Figure 7. Long-term strain variations measured in the VTS (azimuth of the instrument: 55°) and the horizontal displacements measured in the Slovakian GPS network

Figure 8 shows both the "raw" strain data and the fitted polynomial measured in the SGO. The average strain rate measured in the 27-year long period was also determined as the steepness of the line fitted to the polynomial: -3.8 μstr/y (1 μstr = 10^{-6} relative deformation). We have investigated the reasons for the recorded strain with changing rate. We found that the measured compressive strain is in good accordance with the GPS and geophysical strain measurements in the region of the SGO. The local tectonic processes due to the uplift of the Alps and the push of the Pannonian Basin cause that the relative deformation measured by the extensometer in the SGO is approx. three orders

of magnitude higher than the deformation measured by the GPS in the region of the SGO (Mentes 2016).

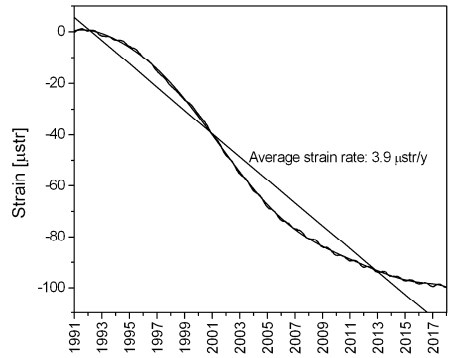

Figure 8. Long-term strain variations measured in the SGO (azimuth of the instrument: 116°)

Our investigations showed that earthquakes, with some exceptions, do not have a direct effect on the local strain rate variations measured in the SGO. They can relax or increase the rock strain depending on the geological and tectonic properties of their epicentres (Varga and Mentes 2016).

6 Investigation of the free core nutation by extensometers

The principle of our investigation was that tidal waves close to the FCN frequency are stronger influenced by the resonance than the farther. We calculated the ratio of the amplitude factors of the K1 (1.0027379 cpd), P1 (0.9972621 cpd), Ψ1 (1.0054757 cpd) and Φ1 (1.0082137) waves − being close to the FCN frequency (1.004915 cpd) − to the amplitude factor of O1 (0.9295357 cpd) which is far from resonance. However, this method does not take into account that local effects affect different tidal waves differently, but measurement errors are reduced. Therefore, both the amplitude factors and the ratios of the amplitude factors calculated from data series measured in different years in four observatories.

Observatories were compared with the theoretical values and with each other. The comparison was made by using amplitude factors and ratios obtained from uncorrected extensometric data series as well as corrected for temperature, barometric pressure and ocean load to investigate the effect of different corrections (Bán et al 2018a, b). Results obtained in the SGO are shown in Figure 9.

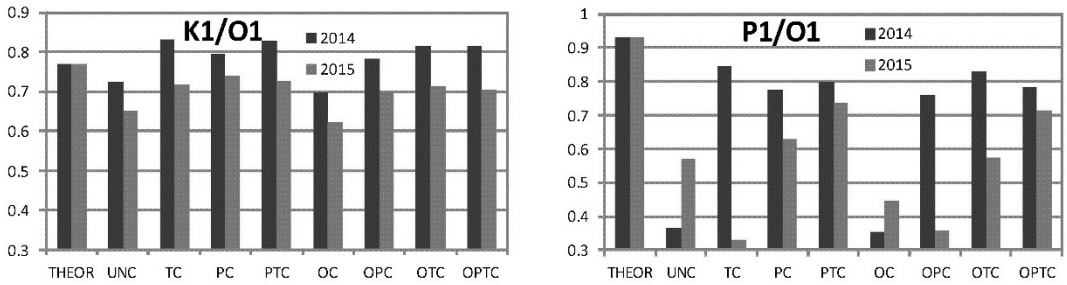

Figure 9. Comparison of the effect of different data corrections on the K1/O1 and P1/O1 amplitude factor ratios obtained from extensometric data recorded in the SGO in 2014 and 2015. THEOR denotes the theoretical amplitude factor ratios, UNC, TC, PC, PTC, OC, OTC, OPC, OPTC denote amplitude factor ratios obtained using uncorrected strain data, corrected for temperature, for barometric pressure, for temperature and barometric pressure, for ocean load, for ocean load and temperature, for ocean load and barometric pressure, and for ocean load, temperature and barometric pressure, respectively

With the exception of the Pécs station, the K1/O1 ratios are close to the theoretical values (Bán et al. 2018a, b, Brimich et al. 2016, Mentes et al. 2016). Except for MGGO in Budapest, there is a large difference between the obtained and theoretical P1/O1 ratios in each observatory. The Ψ1/O1 and Φ1/O1 ratios differ significantly from the theoretical values and have large errors. These discrepancies need further investigations. Our results have shown that the correction of temperature

effects does not affect the errors of the obtained amplitude factors, in contrast to the correction of the atmospheric pressure, which slightly reduces them.

7 Investigation of the relationships between rock strain and radon concentration variations

Changes in the radon gas concentration can precede geodynamic processes associated with tectonic, volcanic activities and earthquakes. For this reason the relationship between rock strain and radon concentration is an important scientific issue to be answered. According to the complexity of the radon emanation process influenced by environmental effects, the interpretation of radon concentration variation as a possible precursor of geodynamic processes is not yet resolved unambiguously. We investigated (Mentes 2018) the connection between indoor radon concentration and rock strain in the tidal frequency-range on the basis of seven-year long data series measured in years from 2009 till 2015. Since radon concentration also strongly depends on temperature and barometric pressure, the theoretical tide at the location of the measurement site and tidal components computed from strain, radon concentration, barometric pressure and temperature data were compared with each other (Figure 10).

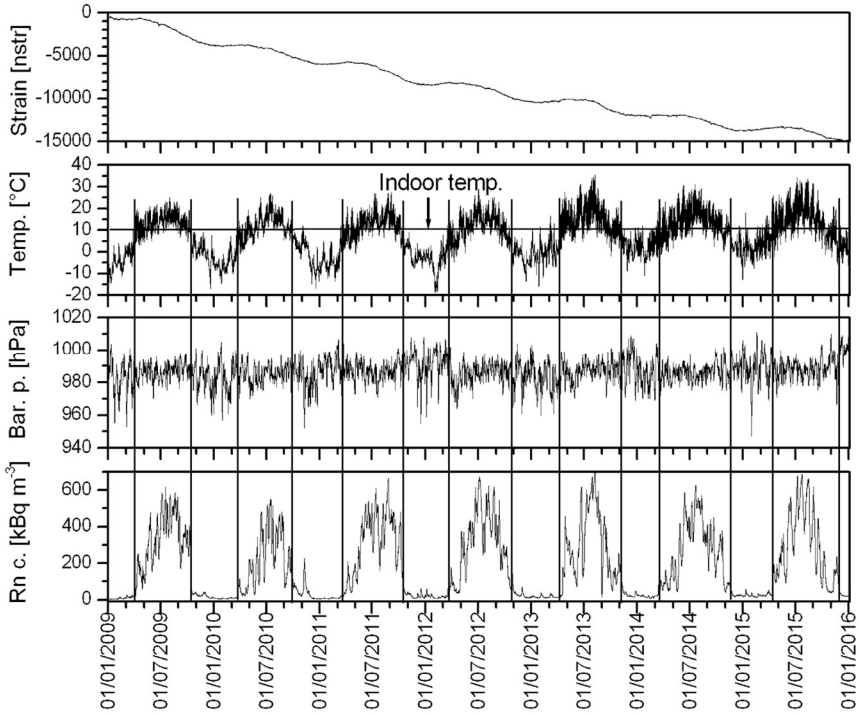

Figure 10. Strain measured by the extensometer (Strain), outdoor temperature (Temp.), barometric pressure (Bar. p.) and radon concentration (Rn c.) measured between 1 January 2009 and 31 December 2015

It was found that the strain induced radon concentration variations are in the order of 10–100 Bqnstr^{-1}, while the concentration variations bear more considerable similarity and relation to the temperature and barometric variations. Spectral and tidal analysis of data demonstrated that only the thermally induced solar components S1 and S2 are present in the radon concentration but their amplitudes hardly exceed the spectral noise level. The principal lunar semidiurnal M2 and diurnal O1 tidal waves cause the largest rock strain variations. The lack of the M2 and O1 tidal components in the radon concentration confirms the fact that the detected S1 and S2 tidal components appear due to the barometric tide and the daily variations of the temperature and barometric pressure (Figure 11).

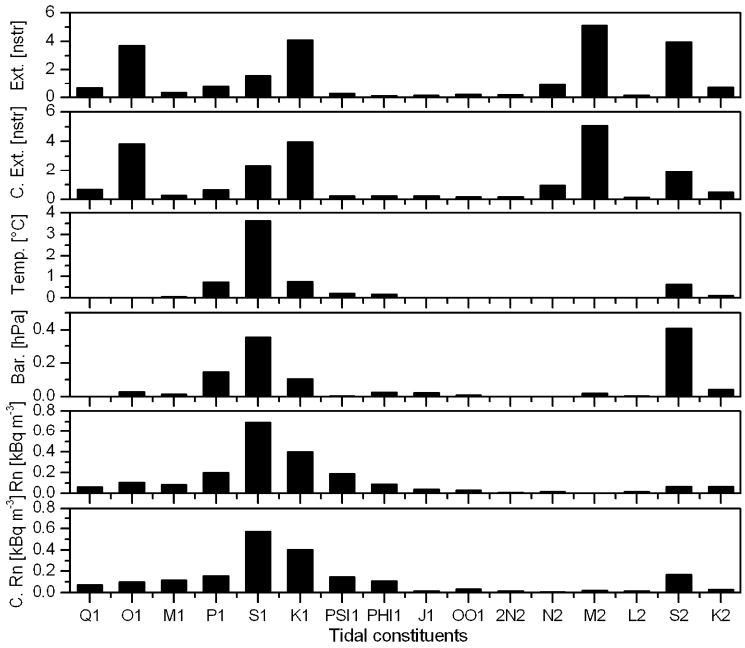

Figure 11. Amplitudes of tidal components obtained by tidal analysis of the strain (Ext.), corrected strain for the temperature and barometric pressure (C. Ext), temperature (Temp.), barometric pressure (Bar. p.), radon concentration (Rn) and radon concentration corrected for the temperature and barometric pressure (C. Rn) data

8 Analysis of earthquake signals appearing in rock deformation recordings

The rock-deformation data series collected by extensometers provide an opportunity for studying various changes in the geological, rock-physical environment, caused by earthquakes. Further information can be achieved about the nature of these effects, complementing the analysis with seismograms.

The appearance of effects of earthquakes in extensometric data were investigated on time series observed in the Mátyáshegy Gravity and Geodynamical Observatory (MGGO) in Budapest in the time of significant (M>6.5) earthquakes, and spectral analysis of the records were carried out (Kis et al. 2016, 2017). The results of the calculations were compared with the spectra of records of typical, undisturbed time interval, as well as with the spectra calculated from seismograms of Kövesligethy Radó Seismological Observatory (KRSO) in Budapest (the distance between MGGO and KRSO is less than 6 km).

Recordings of significant earthquakes observed by two long quartz-tube extensometers (azimuth angle difference is 76° as it is shown in Figure 12.) and a tidal monitoring LCR model G gravimeter operating in the MGGO , furthermore by a three component STS-2 in Budapest were compared with the use of spectral analysis. Three types of instruments were in use to record five significant (M>6.5) earthquakes (Figures.12 and 13):

- 2 long quartz-tube extensometers E1 and E2 operating in the MGGO with 76° azimuth angle difference, capable detect deformation of the order 10^{-11},
- 2 monitoring gravimeters (LCR G963 and LCR G1188 without and with Aliod 100 feedback system, respectively), operating also in the MGGO,
- Streckeisen STS-2 three component very broadband seismometer operating in KRSO.

Figure 12. M>6.5 earthquakes between 01/01/2015 and 31/04/2016. Red dots show the earthquakes analysed, green dots show the non-detectable ones by extensometers. Red lines represent the azimuth of E1 and E2 extensometers

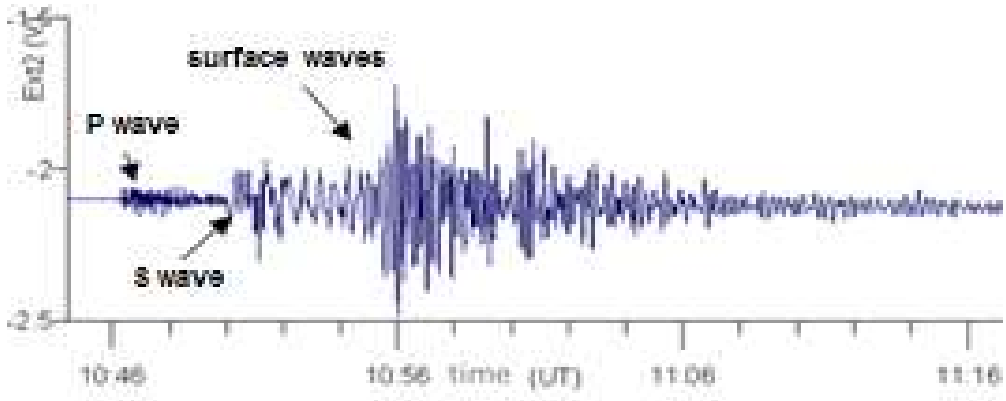

Figure 13. Displacements due to P, S and surface waves recorded by a quartz-tube extensometer in Mátyáshegy-Budapest (M7.1 2011/11/23 Turkey)

In order to compare the time series of teleseismic waves recorded by the extensometers and STS-2 the horizontal components (N-S and E-W) of the seismogram registrations were rotated with a certain angle to align with the azimuth of the extensometers (Kis et al. 2016, 2017). The gravity data were compared with the vertical component of the STS-2.

FFT and power spectral density were calculated to analyze the frequency response of the instruments and the seismic noise. In most cases good correlation was found in the response of the different types of equipment in case of the examined earthquakes (as an example the Japanese earthquake (M_W 7.0) of 2016 is presented on Figure.14.

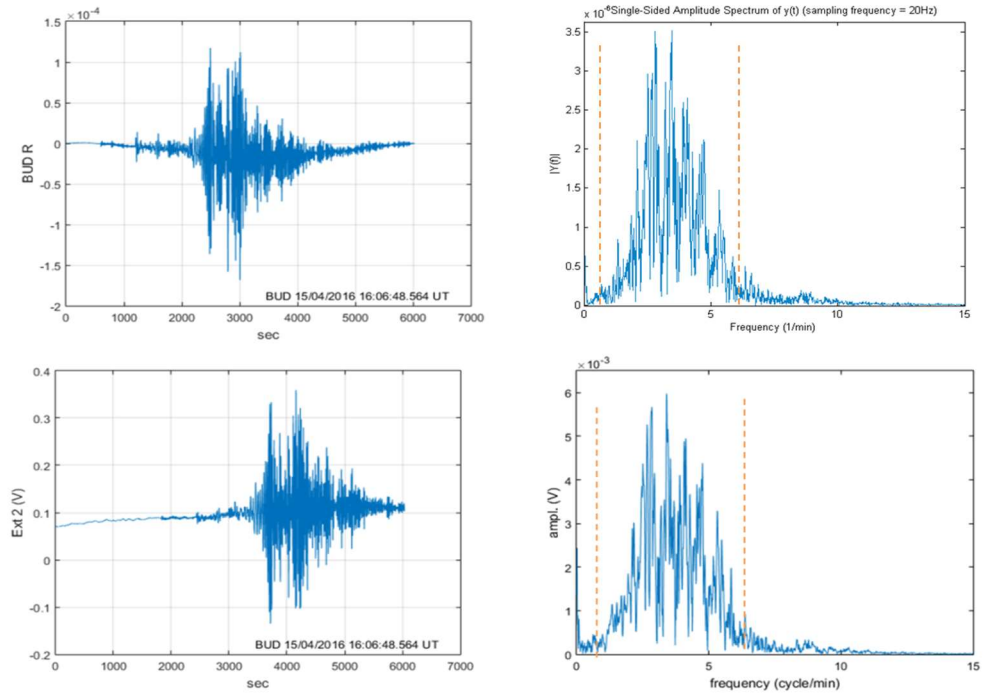

Figure 14. Recordings and amplitude spectra of M7.0 Japan 15/04/2016 16:25:06UT earthquake (depth: 10 km). BUD R is calculated from N and E components of STS-2 seismometer, rotated to the direction of E2 extensometer. In amplitude spectra figures disturbed interval is shown by dotted lines. In E2 recordings 1 [Volt] corresponds to 1064 [nm] displacement

In order to compare the frequency components of recorded teleseismic waves and seismic noise FFT and cross power spectral densities were calculated for channels of extensometer–R (radial horizontal) component of STS-2 and gravimeter–vertical component of STS-2. The cross power spectral densities due to seismic disturbances were obtained typically in the frequency band 0.05–150 (200) mHz /5 (10) s to 6 hr/ (Fig. 15).

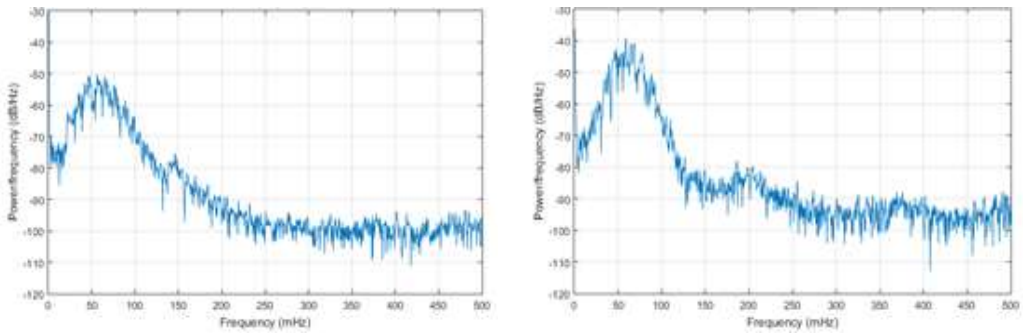

Figure 15. Welch cross power spectral densities, E2-BUD R, LCRG-BUD Z (M7.0 Japan 15/04/2016 16:25:06UT earthquake)

References

Bán D, Mentes Gy, Kis M, Koppán A (2018a): Observation of the Earth liquid core resonance by extensometers. Pure and Applied Geophysics, 175(5), 1631-1642.

Bán D, Mentes Gy, Kis M, Koppán A (2018b): Observation of the Earth liquid core resonance by extensometers. In: C Braitenberg, G Rossi (eds.), Geodynamics and Earth Tides Observations from Global to Micro Scale, Pageoph Topical Volumes Birkhäuser. Springer International Publishing AG, part of Springer Nature, 329, 37-48, https://doi.org/10.1007/978-3-319-96277-1.

Brimich L, Bednárik M, Bezák V, Kohút I, Bán D, Eper-Pápai I, Mentes Gy (2016): Extensometric observation of Earth tides and local tectonic processes at the Vyhne station, Slovakia. Contributions to Geophysics and Geodesy, 46(2), 75-90.

Hefty J, Hipmanová L, Gerhátová L, Igondová M. Droščák B (2010): Recent Geokinematics of Slovakia based on homogenized solutions of permanent and epoch GPS networks. Acta Geodyn. Geomater., 7(3), 303-315.

Kis M, Koppán A, Mentes Gy, Bán D, Kiszely M, Gribovszky K, Merényi L (2016): Analysis of effects related to earthquakes appearing in rock deformation and gravimeter recordings. In: 18th International Symposium on Geodynamics and Earth Tides 2016, P03-02, 282-282.

Kis M, Koppán A, Kiszely M, Gribovszki K, Mentes Gy, Bán D (2017): Analysis of earthquake signals appearing in rock deformation, gravimeter and seismological recordings. Geophysical Research Abstract: EGU2017-17371.

Mentes Gy (2016): Tidal strain variations recorded by a quartz-tube extensometer in the Sopronbánfalva Geodynamic Observatory, Hungary. In: World Multidisciplinary Earth Sciences Symposium: Abstract Collection Book, 18- 18. ISBN: 978-80-270-0316-7.

Mentes Gy, Bán D, Eperné Pápai I (2016): Detection of the near-diurnal period of the nutation of the Earth on the basis of the Sopronbánfalva extensometric data – Preliminary results (in Hungarian with English abstract). Geomatikai Közlemények, 18(2), 35-42.

Mentes Gy (2018): Investigation of the relationship between rock strain and radon concentration in the tidal frequency-range. Journal of Applied Geophysics, 155, 232-236.

Papp G, Benedek J, Varga P, Kis M, Koppán A, Meurers B, Leonhardt R, Baracza MK (2018): Feasibility study applied to mapping tidal effects in the Pannonian basin – An effort to check location dependencies at μGal level. Geodesy and Geodynamics, 9(3), 237-245.

Ruotsalainen H, Bán D, Papp G, Leonhardt R, Benedek J (2016): Interferometric water level tilt meter at Conrad Observatory. COBS Journal 4, 11-11.

Schreider AA, Screider AlA, Varga P, Denis C (2015): Evolution of the virtual dipole moment calculation for reconstruction of the oceanic inversion magnetic layer parameters. Oceanology, 55(2), 245-252.

Schreider AA, Ignatova AA, Screider AlA, Sajneva AA, Varga P, Denis C (2016): Evolution of the virtual dipole moment through the Paleoarchean–Phanerozoic. Oceanology, 56(3), 463-470.

Varga P (2015a): Long-term variations of the gravitational potential and of the geodynamical properties of a deformable Earth due to axial despinning. Zeitschrift der Leibniz-Sozietät, 19, 1-8.

Varga P (2015b) On the physical meaning of the zonal components of the geopotential. Geophysical Research Abstracts, 17, EGU2015-15409.

Varga P, Mentes Gy (2016): Deformation measurements and their relationships with earthquakes: "The relationship of man and the environment in the Carpathian Basin"(in Hungarian). Természet Világa, 147:(KSz), 12-16.

Varga P, Grafarend E (2016) Lunisolar tidal and tidal load elastic stress tensor components within the Earth's mantle and their influence on earthquake occurrences. Geophysical Research Abstracts 18, EGU2016-3297.

Varga P, Grafarend E (2018a): Influence of Tidal Forces on the Triggering of Seismic Events. Pure and Applied Geophysics, 175(5), 1649-1657.

Varga P, Grafarend E (2018b): Influence of Tidal Forces on the Triggering of Seismic Events. In: C Braitenberg, GRossi (eds.), Geodynamics and Earth Tides Observations from Global to Micro Scale, Pageoph Topical Volumes, Birkhäuser. Springer International Publishing AG, part of Springer Nature. 329, 55-63.

Varga P, Grafarend E, Engels J (2018a): Relation of Different Type Love–Shida Numbers Determined with the Use of Time-Varying Incremental Gravitational Potential. Pure and Applied Geophysics, 178(5), 1649-1657.

Varga P, Grafarend E, Engels J (2018b): Relation of Different Type Love–Shida Numbers Determined with the Use of Time-Varying Incremental Gravitational Potential. In: C Braitenberg, G Rossi (eds.), Geodynamics and Earth Tides Observations from Global to Micro Scale, Pageoph Topical Volumes, Birkhäuser, Springer International Publishing AG, part of Springer Nature, 329, 49-54.

HUNGARIAN CONTRIBUTION TO THE RESEARCH ON POSITIONING AND APPLICATIONS (2015 - 2018) - IAG COMMISSION 4

Szabolcs Rózsa[*], Ildikó Juni[*], Bence Ambrus[*], Bence Takács[*], Zoltán Siki[*], Márton Farkas[,**] , Bálint Vanek[**], Árpád Barsi[***], Vivien Potó[***], Tamás Lovas[***], József Árpád Somogyi[***], István Bozsó[****], Eszter Szűcs[****], László Bányai[****], Viktor Wesztergom[****]*

1 Introduction

The period of 2015-2019 brought many new results in the research of positioning techniques and the application of geodesy for engineering. The hottest topics are the application of continuously operating GNSS receivers for atmospheric remote sensing as well as the modelling of tropospheric delays in satellite navigation; the assessment of the integrity of satellite positioning services for safety-of-life applications such as airborne navigation; the localization of autonomous vehicles using GNSS/IMU/Lidar and sensor fusion techniques; the application of InSAR data for the estimation of cristal displacement. These research activities were carried out by the following research institutes: the Department of Geodesy and Surveying and the Department of Photogrammetry and Geoinformatics of the Budapest University of Technology and Economics, the Institute for Computer Science and Control and the Geodetic and Geophysical Institute of the Research Center of Astronomy and Earth Sciences of the Hungarian Academy of Sciences and the Satellite Geodetic Observatory at Penc.

The next sections introduce the most important results achieved in each topic. Due to the limitations of a review paper, further details can be found in the cited publications.

2 Remote sensing the atmospheric water vapour using GNSS

Continuously operating GNSS stations can provide valuable information on the spatial and temporal distribution of atmospheric water vapour. In 2013 a near-realtime GNSS processing facility was set up by the collaboration of the Satellite Geodetic Observatory Penc (SGO) and the Budapest University of Technology and Economics (BME). The applied computational strategy can be found in Rózsa et al. (2014). The processing center (SGOB later renamed to SGO1) joined to the EUMETNET's E-GVAP programme in 2013. Since then the ZTD estimates at the stations of the Hungarian GNSS Network are available for meteorological applications.

Hungary, with its representing institutions BME, SGO and the Hungarian Meteorological Service participated in the COST Action ES-1206 (GNSS for Severe Weather and Climate - GNSS4SWEC) studying the application of ground based GNSS observations for climatic studies and the modelling and forecasting of severe weather.

In the recent years Juni and Rózsa (2018) developed a new global model for the conversion of GNSS derived zenith wet delays (ZWD) to integrated water vapour (IWV) using a global archive numerical weather model dataset. The aim of this study was to provide an optimal solution for the conversion of ZWDs to IWVs, that takes into consideration the geographical variations of empirical conversion factors, since many recent studies still use the empirical models derived from North-American radiosonde observations. The studies showed that the coefficients of the empirical functions show a strong geographical variation. The conversion algorithm and data set is available at http://gpsmet.agt.bme.hu/zwd2iwv.

[*]*BME Department of Geodesy and Surveying, , 1111 Budapest, Műegyetem rkp. 3.*
E-mail: rozsa.szabolcs@epito.bme.hu
[**]*MTA SZTAKI , 1111 Budapest, Kende u. 13-17.*
[***]*BME Department of Photogrammetry and Geoinformatics, 1111 Budapest, Műegyetem rkp. 3.*
[****]*MTA CSFK GGI, 9400 Sopron, Csatkai E. u. 6-8.*

In Meteorology, the various atmospheric parameters are assimilated in numerical models. The first results of the application of GNSS derived ZTDs in numerical weather models in Hungary and the Carpathian Basin was reported in Mile et al. (2019). The results showed that the assimilation of GNSS ZTDs have a positive impact on the prediction of relative humidity as well as on the temperature. A significant improvement was observed in the short-term predictions (up to 5 hours) with a rather neutral on the longer predictions.

3 Studying the integrity of GNSS positioning

In safety-of-life navigation applications of GNSS the major concern of the user is not only the accuracy but the integrity of the positioning service. To assess the integrity, the protection level is calculated by overestimating the positioning error even at very rare probability levels. Recent studies show that - by the emerging multiple frequency civilian signals - the tropospheric delay becomes the most significant error source especially at low elevation angles. The RTCA MOPS (minimum operational performance standard) for GNSS systems in aeronautics specifies a global constant of ±0.12m for the maximum tropospheric residual error in the zenith direction in terms of standard deviation. Recent studies suggest that this value is too conservative in many regions of the globe leading to lower availability and continuity of the positioning service (Rózsa et al. 2017). To overcome this limitation, a new residual tropospheric error model was formulated in the frame of a ESA funded project by the colleagues of the Department of Geodesy and Surveying of the Budapest University of Technology and Economics together with the Hungarian Meteorological Service and Integricom.NL, that considers both the geographical and the seasonal variations of the tropospheric delay model performances. The advanced residual tropospheric delay error model (ARTE) was developed using the methodology of extreme value analysis of existing tropospheric delay models using 16 years of worldwide numerical weather model analysis (Rózsa 2018). The studied tropospheric delay models were the RTCA troposphere model, the ESA GALTROPO model and the GPT2W model.

The developed ARTE model was validated globally using IGS ZTD estimates, radiosonde observations and numerical weather models. Moreover they were tested in a case study under real extreme weather conditions in Central-Europe (Juni and Rózsa 2018). The results showed that the performance of the studied tropospheric delay models show strong seasonal variations (Figure 1-3). Thus various integrity models were formulated for the positioning applications. The most complex one considers both the seasonal and the geographical variations, while a simplified model was also developed that considers the geographical variations only. Finally a global constant model was also formulated that complies fully with the existing RTCA recommendations. The validation proved that the proposed model maintained the conservatism of the original model, nevertheless it provided a significantly lower residual error estimate in many regions of the globe (Figure 4). Among the studied three tropospheric delay models, GPT2W and ESA GALTROPO models provided significantly lower protection levels compared to the RTCA recommendations, that also means that the application of the developed models could improve both the availability and the continuity of satellite navigation services in safety-of-life applications.

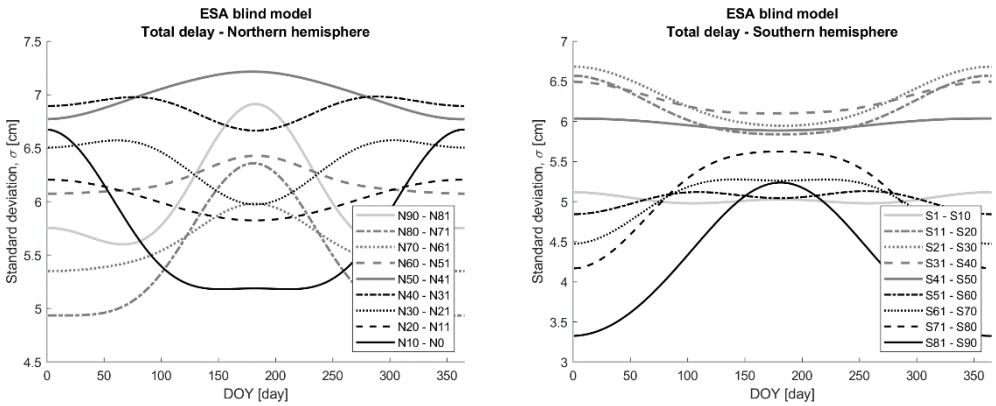

Figure 1. The seasonal variation of the sigma value of the ESA blind model in the different latitude bands

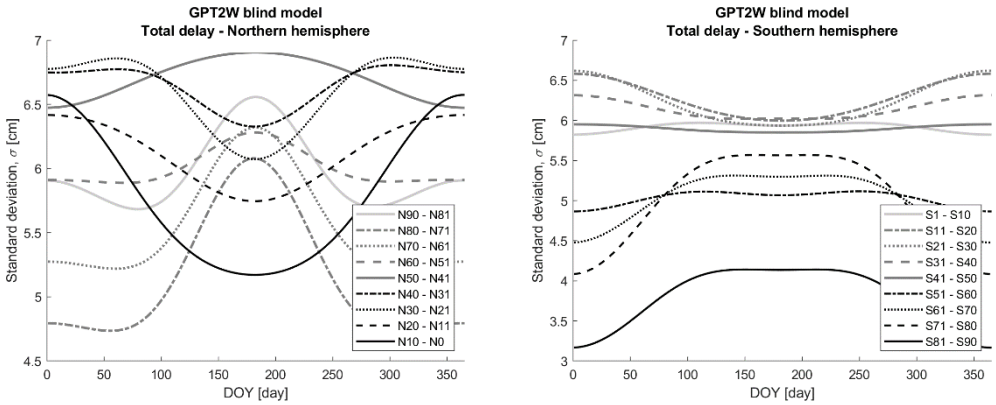

Figure 2. The seasonal variation of the sigma value of the GPT2w blind model in the different latitude bands

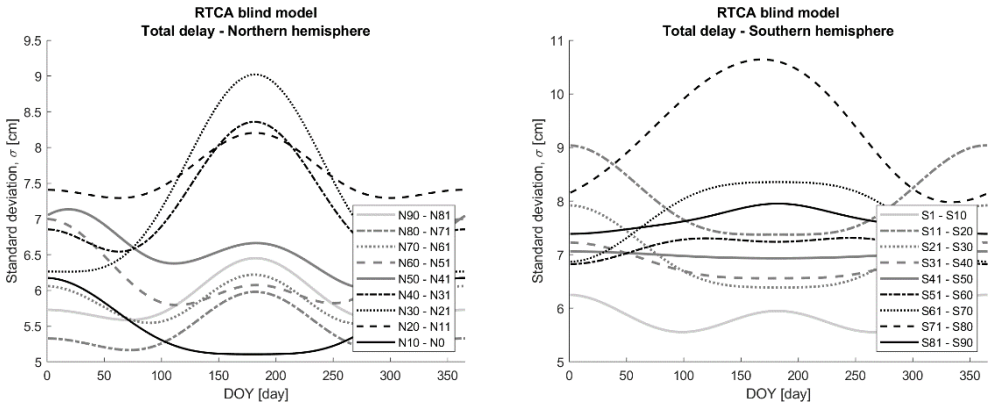

Figure 3. The seasonal variation of the sigma value of the RTCA blind model in the different latitude bands

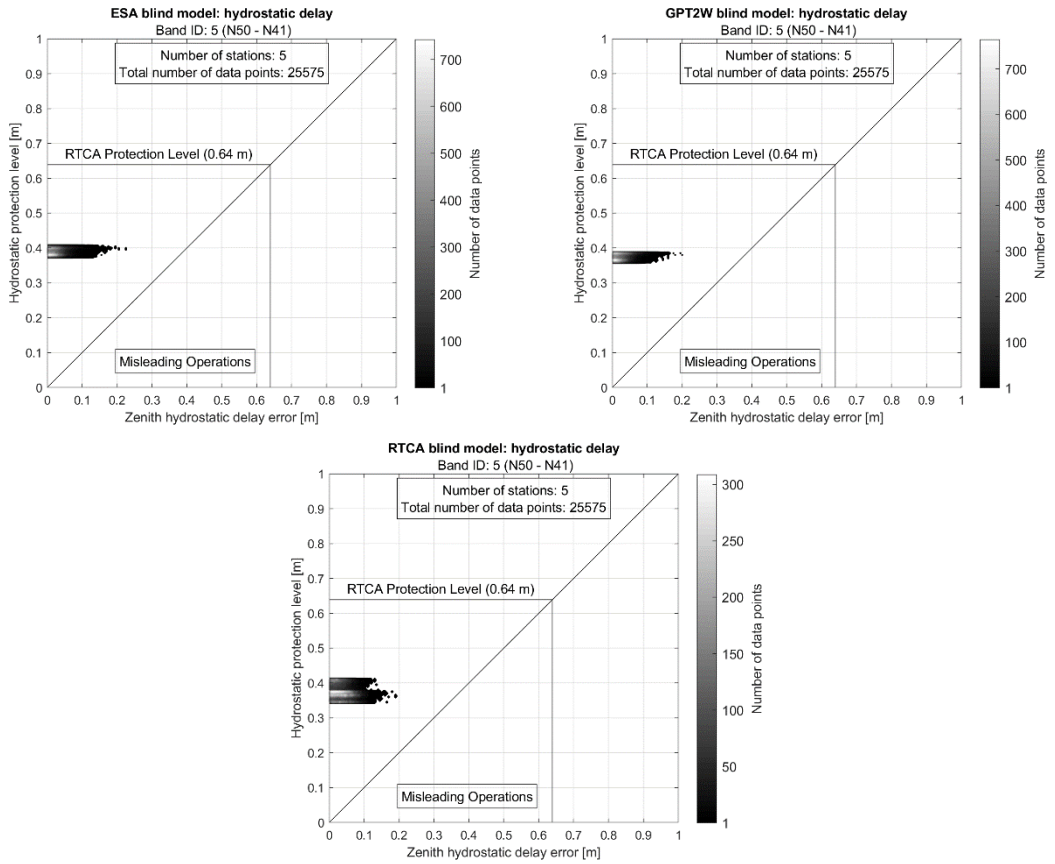

Figure 4. Validation of the residual tropospheric delay model using IGS ZTD products for the latitude band of N41°-N50°

The evaluation and monitoring of the integrity of GNSS positioning is inevitable for air traffic service providers and is an important research area (Markovits-Somogyi et al. 2017), too. In order to provide these professionals with open source software solutions, the well-known RTKLIB package (Takasu 2009) was extended with the calculation of protection levels based on the RTCA recommendations (Takács et al. 2017). The developed algorithm was tested with the commercial Pegasus and magicGemini softwares.

4 Position and orientation determination of autonomous platforms

The sensor fusion methods are getting more indispensable in the navigation. This information is the key of the high accuracy control of the moving platform used for mapping tasks. Although the low-cost inertial (INS) and Global Navigation Satellite Systems (GNSS) sensors are widespread, these equipment suffer from various significant error sources, which influence usability. The inertial sensors have bias, bias instability error, the single frequency GNSS receivers have clock error, multipath, inter-channel biases and the unknown integer ambiguity values of the carrier-phase measurements. Usually the higher sampling rate (50-2000Hz) of the inertial sensors complement the lower sampling rate (1-20Hz) of GNSS observations. The aim of a sensor fusion system is to provide high rate and high accuracy navigational data of the moving platform.

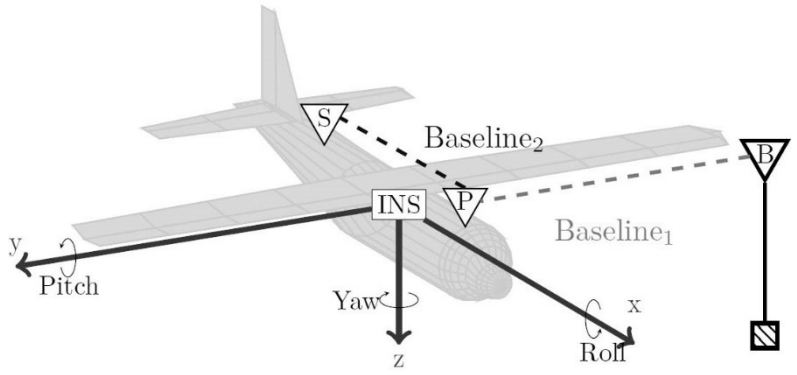

Figure 5. The onboard sensors (P, S: primary and secondary GNSS receivers; INS: inertial navigation sensor) of the UAV and the ground reference receiver (B)

Farkas et al. 2018 investigates a multi baseline GNSS positioning and attitude determination method, using low-cost differential GNSS, accelerometer and gyroscope data. The attitude angles are represented in quaternion form. The tightly coupled sensor fusion is accomplished by an EKF algorithm. The moving baseline's integer ambiguities are resolved by a quaternion constrained LAMBDA method. That sensor fusion method was based on inertial sensor data and non-differential GNSS code and Doppler measurements.

The key of the high accuracy GNSS positioning is to resolve the integer ambiguities of the carrier-phase measurements. The developed uses the least-squares ambiguity decorrelation adjustment method. The integer ambiguity resolution is applied only for the GPS measurements on both baselines.

The integer ambiguity resolution is different at the moving baseline. Giorgi and Teunissen (2010) use baseline length constrain, and a rotating matrix constrain based on Euler angles. Since our approach uses quaternion representation, the original ambiguity resolution method had to be modified with the constrain that the norm square of the quaternions is equal to one. The optimum is the integer ambiguity conditional quaternion vector, which has the smallest distance in the metric of the conditional covariance matrix with the norm square of one.

The method was tested with real flight data. The duration of the flight was nearly 3000 seconds. The base, the primary and the secondary receivers were u-blox NEO-M8T single frequency low-cost GNSS receivers with Tallysman 33-2405-05-0150 antennas (Figure 5).

These receivers were collecting GPS and GLONASS data. Integer ambiguities were resolved for GPS satellites, while float ambiguities were used for the GLONASS constellation. The maximal length of the first baseline was 11 kilometres and the second baseline was 0.29 meters long. The UAV was equipped with a PIXHAWK flight control computer with INS sensors, and a Sony ILCE-6000 camera for photogrammetric service. The onboard flight controller system uses a loosely coupled sensor fusion algorithm based on a single GNSS receiver and the INS sensor. The camera took 1200 pictures during the flight. The collected GNSS data was post processed with using the PPK technique for the position. Attitude angles were also estimated from the photogrammetric processing (PGP) of aerial images with known ground control points (GCPs) using the Pix4D software.

The developed EKF algorithm was used to process the raw INS and GNSS from observations. The position solution is compared to the PPK solution, and the attitude angle solution is compared to the PGP solution in the common epochs. Figure 6 depicts the comparison of the PPK and the EKF coordinate solutions. The mean value of the horizontal differences during the whole measurement is 0.007 meters in north and 0.002 meters in east with the root mean square (rms) value 0.01 and 0.003 meters. The mean vertical difference is -0.053 meters with 0.055 meters rms error. The ambiguity success rate is 99.12% for the first baseline.

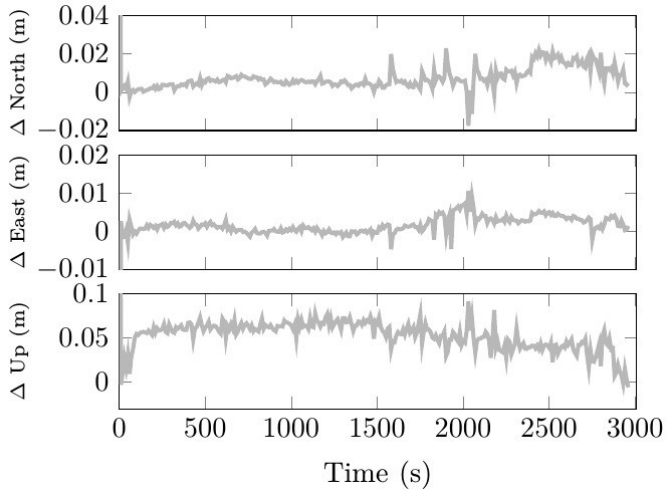

Figure 6. The comparison of the post-processed kinematic and the EKF sensor fusion coordinate solutions

Figure 7 depicts the comparison of the attitude solutions provided by the PIXHAWK onboard flight controller system and the developed EKF algorithm using the PGP orientation angles as references. The roll angle is estimated only by the angular velocities because there is no *y* axis lever arm component between the antennas of the moving baseline in the body coordinate frame. The two solutions have similar error magnitudes compared to the PGP results. However, the GNSS attitude estimation reduced the bias in the pitch angle compared to the PIXHAWK solution significantly. Moreover, the improvement in the yaw angle is significant, too. Moreover, the trend between 1500-2500 epochs is completely removed from the residuals. The mean value of the differences from the PGP solution is 0.27° with 0.62° rms compared to the PIXHAWK's mean value -3.06° with 3.52° rms. This result can be explained with the applied measurement configuration. Since GNSS observations provide lower accuracy in the vertical direction, its effect on the pitch angle is expected to be significantly lower than on the yaw angle. The ambiguity resolution success ratio for the moving baseline is 97.35%.

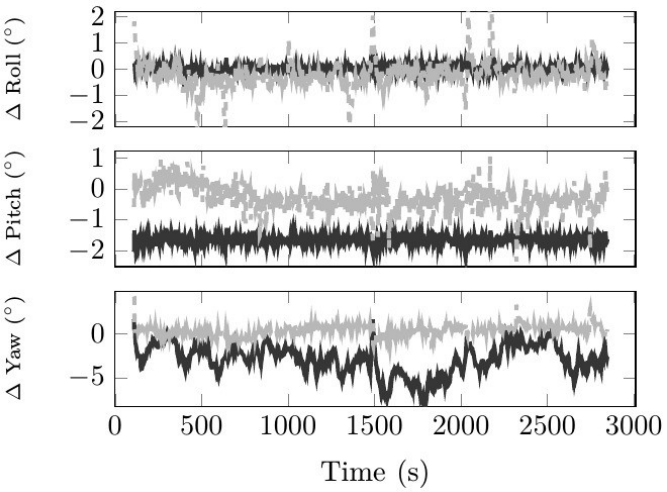

Figure 7. The comparison of the attitude solutions of the onboard flight controller and the developed sensor fusion algorithm wrt the photogrammetric processing (red: onboard sensor, green: developed EKF sensor fusion algorithm)

5 Supporting autonomous navigation by 3D maps

Intensive research has been conducted in the field of automated driving. The development of self-driving vehicles is a very hot topic in vehicular research currently. Such vehicles require effective and reliable decision mechanism to control the movement, which is expected by the development of artificial intelligence (AI). Beyond the AI-controlled driving, these vehicles have to collect very detailed information about their neighbourhood, that is realized by cutting-edge sensors, like vehicular Lidars, cameras and radars. Further data capture mechanisms are also welcome to increase the redundancy and reliability. Vehicles are nowadays already equipped with satellite based positioning systems, sometimes even with inertial measurement units, but there are still circumstances, when this technology has troubles in accuracy or even totally fail (urban canyons, tunnels etc.). In such situations alternative solutions are required, where prior captured 3D map data can help.

To establish highly detailed accurate 3D map database, several surveying technologies are involved. Among them terrestrial laser scanning and mobile mapping are the two flagship tools (Potó et al. 2017b, Potó and Barsi 2017a). Data acquisition by these modern technologies results huge amount of field data, which is the base not only for traditional mapping but also to derive products being able to support automated driving. The 3D map data is mainly point clouds (mostly colored, but at least with signal intensity values) and CAD models (created by the evaluation of the field surveys). New data sources are urban models, pavement descriptions or lane models. All these products can be extracted from the map data base (Potó et al. 2017a, Barsi et al. 2017, Potó and Barsi 2017b).

Scientific results of the last decades can be summarized in the data processing chain and development of non-existing neighbourhood model descriptions. Lane models, navigation aids or static occupancy maps are the most relevant new findings. The research group has focused on the collaboration with car maker industry, where simulator software packages can be fed by data taken from the reality. Strong efforts were made therefore in producing standard simulator inputs. The most important results were achieved with the OpenCRG models, where CRG stands for Curved Regular Grid. It is an efficient and highly potential model to bring information about the pavement surface.

6 Recent Application of Synthetic Aperture Radar Interferometry

The interferometric SAR observations play an important role in the monitoring and the analysis of recent crustal displacements in the Central-Europe, too. The Carpathian bend is amongst the tectonically most active areas in Europe where intraplate subduction triggers sub-crustal earthquakes releasing significant amount of seismic energy in a well-defined seismic zone. To constrain the deep processes by exploiting their linkage to the surface processes knowledge of surface deformations is required. Detection of small-magnitude tectonic processes with high reliability is challenging in which the recent space geodetic techniques may bright a breakthrough. A retrospective analysis of archive Envisat data set of the European Space Agency acquired in the frame of ESA CAT-1 project was used to investigate the feasibility limit of detecting crustal deformations in the region of the south Carpathian bend (Bozsó et al. 2017, Bozsó et al. 2018a, Szűcs et al. 2018), where past geodetic observations failed to unravel the tectonic processes with high details. Despite the inherent limitations of radar interferometry the results show that coherent velocity field can be estimated with a magnitude of few mm/yr. The vertical displacement suggest subsidence in the Brasov basin which is in agreement with former studies, however radar interferometry can provide more detailed picture.

In the framework of Integrated Sentinel-PSI and GNSS technical facilities and procedures for the determination of 3D surface deformations caused by environmental processes (4000114846/15/NL/NDe) ESA project the use of space geodetic methods and developments in the observation of tectonic processes was studied. So-called integrated benchmarks, equipped with GNSS adapter and corner reflectors for descending an ascending satellite passes, have been developed (Bányai et al. 2018), that provide a long-term stable reflection for Sentinel-1 twin satellites. Using exclusively the satellite observations of Sentinel-1, the surface deformation field in 3D can

only be determined with bias. Therefore a process based on Kalman filtering has been developed, that combines the absolute positioning provided by global navigation systems with relative surface changes based on interferometric processing of Sentinel-1 images (Bányai et al. 2017a, Bányai et al. 2017b). With this, it is possible to produce high-precision, 3D, absolute deformation data time series from the integrated points. Radar reflector networks can be utilized in areas where the traditional radar interferometry cannot be applied successfully. The developed procedure and benchmarks were tested (Bozsó et al. 2018b) in areas subjected to landslide of different intensity and characteristics (spatial distribution and time dependence) and proved its effectiveness.

7 Geodetic monitoring and early warning systems

At the Department of Geodesy and Surveying of the Budapest University of Technology and Economics a software system called Ulyxes has been developed for geodetic monitoring and early warning systems. Ulyxes is an open source project to drive robotic total stations as well as other sensors, collect their measurements in database and finally publish the results for authorized users on the web. On special requests the results are also presented with web based maps in the background (Siki 2015).

This project is like an instant coffee: three in one (coffee, sugar and milk). The coffee and the strongest part is the research and coding. The sugar is the application of the program in industrial environment and the milk on the top is the educational usage. The software development started in 2008 connected to a monitoring task in the Hungarian Nuclear Power Plant. Since then the development has been extended from total stations to different positioning capable sensors.

In 2012 the development of a new Python based object oriented framework started. The code is based on the results of some other open source projects, Python, PySerial, GNUGama, SQLite, OpenCV, etc. After connecting to the international Geo4All network in 2014, Ulyxes became a project of our Geo4All Lab. The project has its own home page (http://www.agt.bme.hu/ulyxes) and the source code is available on the GitHub portal (https://github.com/zsiki/ulyxes). The code is maintained by the colleagues at the Department of Geodesy and Surveying at the Budapest University of Technology, volunteers from all over the World are welcome. BSc and MSc students are also involved in the development and testing. More theses were connected to this project in the recent five years.

In the curriculum of an MSc subject called Surveying Automation, Ulyxes is used to demonstrate automatized tasks in engineering surveying. The system has been applied for several projects during the last 10+ years. Typical applications are the load tests of bridges and other engineering structures and on the other hand Ulyxes can be used to monitor the movements of buildings in the nearby of constructional works, like metro stations, underground garage and other buildings as well.

The source code is divided into three parts. The first one is the Ulyxes API which is the core of the system. The second one, Ulyxes Apps is a collection of applications based upon the API. The third part is the server side scripts to publish observation results through the Internet. The software has been extensively used in various monintoring and early warning systems (Kovács et al. 2016, Siki et al. 2018).

8 Geo-spatial mapping for engineering geology

Research has been conducted to support engineering geological studies with advanced geospatial mapping technologies (Terrestiral Laser Scanning – TLS and Remotely Piloted Aircraft System – RPAS). These techniques were used to obtain data on terrain morphology and to provide highly detailed geometry.

The investigations began with the survey of Sirok Castle and the cliff faces in its surroundings in 2016 (Török et al. 2016). The purpose of the study was to map the geologically dangerous areas, which led the strengthening of these areas. The investigation included both geology (field and laboratory) and remote sensing measurements, which were jointly processed in FEM analyses. The point

clouds obtained by spatial data acquisition were processed both separately and combined to test their applicability and to minimize the obscured surfaces. The spatial models proved to be suitable for providing information (e.g. through spatial sections) on steep, hardly accessible, extremely complex areas.

Later in 2017, measurements have been carried out in the Sárbogárd mine, which aimed to determine the dominant slips and layers and assess the potential of utilizing the intensity values obtained from laser scanning (Török et al. 2017). Also in an open pit mine in Bükkösd in 2018 the planning of the extraction of the coming years were supported by TLS and RPAS measurements (Török et al. 2018).

9 Conclusions and outlook

This paper introduced the most important achievements in the field of positioning and the application of geodesy in engineering in the past 4 years. Based on the reviewed results, one can see that the area of positioning is still in the forefront of actual research activities. The emerging techniques such as the introduction of autonomous driving inevitable relies on localization techniques and positioning services. Thus more and more accurate and reliable models are needed to take into consideration the systematic effects contaminating the position solution. Moreover, an optimal localization technique needs to be available under all circumstances. Not only under the clear sky, but also in urban canyons, underground, etc. Therefore the development of localization techniques of autonomous vehicles must rely on various, complementing positioning sensors and apply a proper sensor fusion algorithm to achieve the best results.

In the next years the introduced research topics will have a growing importance. Autonomous driving needs not only accurate, but also reliable positioning solution. Although the integrity assessment techniques exist for aerial navigation, these techniques need to be tailored to ground based applications. That is certainly one of the key challenges of the next four years.

Moreover, the understanding of Earth processes will remain in the forefront of geodetic research. The monitoring of the changing climate, the prediction of more and more frequent severe weather event require the combined assessment of all available observations of atmospheric parameters. A relatively new research field in this area is the study of the properties of the reflected GNSS signals to estimate further geophysical and hydrological parameters such as soil moisture, snow coverage, water levels, etc.

The availability of free InSAR imagery will further improve the understanding of surface processes, such as the recent crustal deformations, too.

Thus we are absolutely convinced that the successful period of 2015-2019 in the research of positioning in Hungary will provide a good basis for an even more prosperous future.

References

Á Barsi, V Poto, Á Somogyi, T Lovas, V Tihanyi, Z Szalay (2017): Supporting autonomous vehicles by creating HD maps. PRODUCTION ENGINEERING ARCHIVES / ARCHIWUM INZEYNIERII PRODUKCJI, 16(1), 43–46.

L Bányai, E Szűcs, A Hooper, V Wesztergom, I Bozsó (2017a): Descending and Ascending Persistent Scatterers Integration SYstem (DAISY) for Interpretation of Nearly Vertical and East-west Velocities Estimated by StaMPS Software in Geoinformation Systems In: Fringe 2017 Noordwijk, Hollandia (2017), Paper 236.

L Bányai, E Szűcs, V Wesztergom (2017b): Geometric features of LOS data derived by SAR PSI technologies and the three-dimensional data fusion. ACTA GEODAETICA ET GEOPHYSICA, 52(3), 421–436.

L Bányai, L Nagy, I Bozsó, E Szűcs, V Wesztergom (2018): Műholdradar-interferometriás alkalmazások fejlesztése a tektonikus folyamatok megfigyelésében. MAGYAR GEOFIZIKA, 59(1), 18-30.

I Bozsó, E Szűcs, L Bányai, V Wesztergom (2017): Attempts to investigate the dynamic surface changes in the Carpathian bend area using archive ascending and descending ENVISAT images processed by persistent scatterers interferometry. GEOPHYSICAL RESEARCH ABSTRACTS 19, EGU2017-1856.

I Bozsó, L Bányai, E Szűcs, V Wesztergom (2018a): An attempt to apply space-borne monitoring of recent tectonics in the Southern Carpathians. GEOLOGICA BALCANICA, Abstracts of the XXI International Congress of the Carpathian Balkan Geological Association (CBGA), 255.

Bozsó I, Szűcs E, Bányai L, Wesztergom V (2018b): Benchmark of C-band radar corner reflectors based on Sentinel-1 SAR images. First results in the monitoring of the Dunaszekcső landslide (Hungary) using corner reflectors. GEOPHYSICAL RESEARCH ABSTRACTS 20, EGU2018_714.

Farkas M, Vanek B, Rózsa Sz (2018): Pilóta nélküli repülőgép pozíciójának és orientációjának meghatározása low-cost GNSS, inerciális és mágneses szenzorok tightly coupled integrációjával. REPÜLÉSTUDOMÁNYI KÖZLEMÉNYEK, 30(1), 139-150.

Giorgi G, Teunissen PJG (2010): Carrier phase GNSS attitude determination with the multivariate constrained LAMBDA method. 2010 IEEE Aerospace Conference, 6-13. March 2010, Big Sky, MT, USA. 1-12.

Juni I, Rózsa Sz (2019): Validation of a New Model for the Estimation of Residual Tropospheric Delay Error Under Extreme Weather Conditions. PERIODICA POLYTECHNICA-CIVIL ENGINEERING, 63(1), 121-129.

Kovács N, Kövesdi B, Dunai L, Takács B (2016): Loading Test of the Rákóczi Danube Bridge. PROCEDIA ENGINEERING, 156(1), 191-198.

Markovits-Somogyi R, Takács B, de la Fuente A (2017): Introducing E-GNSS navigation in the Hungarian Airspace: The BEYOND experience and the relevance of GNSS monitoring and vulnerabilities. In Bacsárdi L; Kovács K (eds) Selected papers of the 3rd International Conference on Research, Technology and Education of Space (H-SPACE2017) Budapest, Hungary: Magyar Asztronautikai Társaság, 80-86.

Mile M, Benacek P, Rózsa Sz (2019): The use of GNSS zenith total delays in operational AROME/Hungary 3D-Var over a Central-European domain. ATMOSPHERIC MEASUREMENT TECHNIQUES, 12(3), 1569-1579.

Potó V, Barsi Á (2017a): Positioning of self-driving vehicles by 3D urban city models, "Theory meets practice in GIS" conference, Debrecen, 2017, 301–307.

Potó V, Somogyi Á, Lovas T, Barsi Á, Tihanyi V, Szalay Z (2017a): Creating HD map for autonomous vehicles - a pilot study. 34th International Colloquium on Advanced Manufacturing and Repairing Technologies in Vehicle Industry, 127–130.

Potó V, Barsi Á (2017b): "Applying Structure-from-Motion technique for visual odometry. AIS 2017 - 12th International Symposium on Applied Informatics and Related Areas, Óbuda University, 145–149.

V Potó V, Somogyi ÁJ, Lovas T, Barsi Á (2017b): Laser scanned point clouds to support autonomous vehicles. TRANSPORTATION RESEARCH PROCEDIA, 27(1), 531–537.

Rózsa Sz, Kenyeres A, Weidinger T, Gyöngyösi AZ(2014): Near real-time estimation of integrated water vapour from GNSS observations in Hungary. INTERNATIONAL ASSOCIATION OF GEODESY SYMPOSIA, 139(1), 31-39.

Rózsa Sz, Ambrus B, Juni I(2017)**:** Integrity analysis of the RTCA tropospheric delay model. In Orosz Gábor Tamás (ed) AIS 2017 – 12th International Symposium on Applied Informatics and Related Areas, Óbuda University, November 9, 2017. Székesfehérvár. 94-99.

Rózsa Sz (2018)**:** A new approach for assessing tropospheric delay model performance for safety-of-life GNSS applications. In A Heck, K Seitz, T Grombein, M Mayer, J-M Stövhase, H Sumaya, M Wampach, M Westerhaus, L Dalheimer, P Senger (Hrsg) (szerk.) (SchW)Ehre, wem (Schw)Ehre gebührt: Feitschrift zur Verabschiedung von Prof. Dr.-Ing. Dr. h.c. Bernhard Heck, Karlsruhe, Németország: KIT Scientific Publishing, 229-235.

Siki Z, Takács B, Égető Cs (2018): Ulyxes: an open source project for automation in engineering surveying. PEERJ PREPRINTS 6, e27226v1.

Siki Z (2015): Collecting and Processing Land Surveyors' Sensor Data. In: M A Brovelli, L Biagi, M Negretti (eds.) Geomatics Workbooks 12. Free and Open Source Software for Geospatial Como, Italy, Politecnico di Milano, 659.

Szűcs E, Bozsó I, Kovács IJ, Bányai L, Gál Á, Szakács S, Wesztergom V (2018): Probing tectonic processes with space geodesy in the south Carpathians: insights from archive SAR data. ACTA GEODAETICA ET GEOPHYSICA, 53(3), 331-345.

Takács B, Siki Z, Markovits-Somogyi R (2017): Extension of RTKLIB for the calculation and validation of protection levels. INTERNATIONAL ARCHIVES OF PHOTOGRAMMETRY AND REMOTE SENSING, 42(4/W2), 161-166.

Takasu T (2009): RTKLIB: Open Source Program Package for RTK-GPS, FOSS4G 2009 Tokyo, Japan, November 2, 2009

Török Á, Barsi Á, Bögöly Gy, Lovas T, Somogyi Á, Görög P (2018): Slope stability and rockfall assessment of volcanic tuffs using RPAS with 2-D FEM slope modelling. NATURAL HAZARDS AND EARTH SYSTEM SCIENCES, 18(2), 583-597.

Török Á, Barsi Á, Görög P, Lovas T, Bögöly Gy, Czinder B, Vásárhelyi B, Molnár B, Somogyi ÁJ (2017): Rockfall hazard assessment of nearly vertical rhyolite tuff cliff faces by using terrestrial laser scanner, UAV and FEM analyses. EGU General Assembly 2017, Conference Abstracts Vienna, EGU2017-10516.

Török Á, Bögöly Gy, Czinder B, Görög P, Kleb B, Vásárhelyi B, T Lovas T, Barsi Á, Molnár B, Koppányi Z (2016): Terrestrial laser scanner aided survey and stability analyses of rhyolite tuff cliff faces with potential rock-fall hazards, an example from Hungary. R Ulusay, O Aydan, H Gerçek, M A Hindistan, E Tuncay (eds) Rock Mechanics and Rock Engineering: From the Past to the Future: Eurock 2016 London, Great Britain, England, Taylor and Francis, 877-881.

HUNGARIAN CONTRIBUTION TO THE RESEARCH OF PALAEOMAGNETISM AND MAGNETIC ANISOTROPY (2015-2018) – IAGA DIVISION I: INTERNAL MAGNETIC FIELDS

*Emő Márton**

1 New statistical method for joint evaluation of magnetic anisotropy and mesotectonic data

A method was developed for the integrated interpretation of the orientation of the magnetic fabric (AMS) and stress axes in weakly deformed, "soft" sediments. In general, the most probable AMS and stress tensors that explain the observed data should be retrieved from the measured data, including the confidence region of the solution. In mathematical terms, the inherently non-linear problem is solved via multiple linear equations over the equidistantly discretized space of candidate solutions. In this way the confidence intervals of the most probable solution can be accurately computed. This idea extends the classical methods of AMS (anisotropy of the magnetic susceptibility) data evaluation to cases, where the AMS data sets define nearly rotational ellipsoids. The method was further developed to establish a new, stochastic stress-inversion method for fault-slip analysis, which is free from ad-hoc optimality conditions. Similarly to the classical stress-inversion procedures, this new method is also based on the so-called Wallace-Bott hypothesis (Wallace 1951, Bott 1959), but unlike the solutions in the literature, it provides statistical information for the data set, not just the principal directions of the best fit stress tensor. The two methods permitted to introduce a new statistical framework for integrated evaluation of AMS data sets with fault-slip data. The integrated evaluation is particularly useful, when the available AMS and/or fault-stria data are scarce. It helps to study the transition of ductile-to-brittle behaviour of progressively cemented sediments or solidifying rocks, as this was demonstrated on real data sets collected from the Pannonian Basin. The evaluated data clearly document, that the integrated evaluation tightens the range of possible extensional direction and it can be used to decide if the AMS fabric is of deformational origin. The method was presented at the international conference IUGG 2015 in Prague in the IAGA A10 section on 25th June, 2015 (Sipos et al. 2015) and subsequently published in Tectonophysics (Sipos et al. 2018). It is important to emphasize that in the course of the above elaborations the principal axes of the AMS data were treated as strictly precise. In order to satisfy this condition, AMS data must be filtered and data handicapped by statistical errors exceeding a certain limit should be rejected.

The algorithm was coded in Matlab environment by A. Sipos.

2 Paleomagnetic constraints on the mid-Jurassic – Eocene displacements of Adria

The Adria microplate has been in the focus of Mediterranean paleomagnetic research since the early 1970's and with the method evolving, the standard for quality data has been elevated. Thus, in order to construct a reliable APW (apparent polar wander) for stable Adria earlier published data were critically evaluated and the APW was extended with new Jurassic results. The new APW (Márton et al. 2017) is based on data which are coming from strictly autochthonous areas and represent geographically distributed localities of similar ages. The important aspects of the new APW are the tight age constraints of the large Late Jurassic CW rotation followed by equally large CCW rotation during the Early Cretaceous, the confirmation of a Late Cretaceous CW and the post-Eocene CCW rotation of Adria, with respect to Africa (Figure 1). The time of the latter is not con-strained directly, but the CCW rotations measured in several areas of the circum-Adriatic region and the tectonic inversion in the Pannonian basin s.l. point to its being very young, around 5-6 Ma.

**Mining and Geological Institute of Hungary, 1145 Budapest, Columbus u. 17-23.*
E-mail: paleo@mbfsz.gov.hu

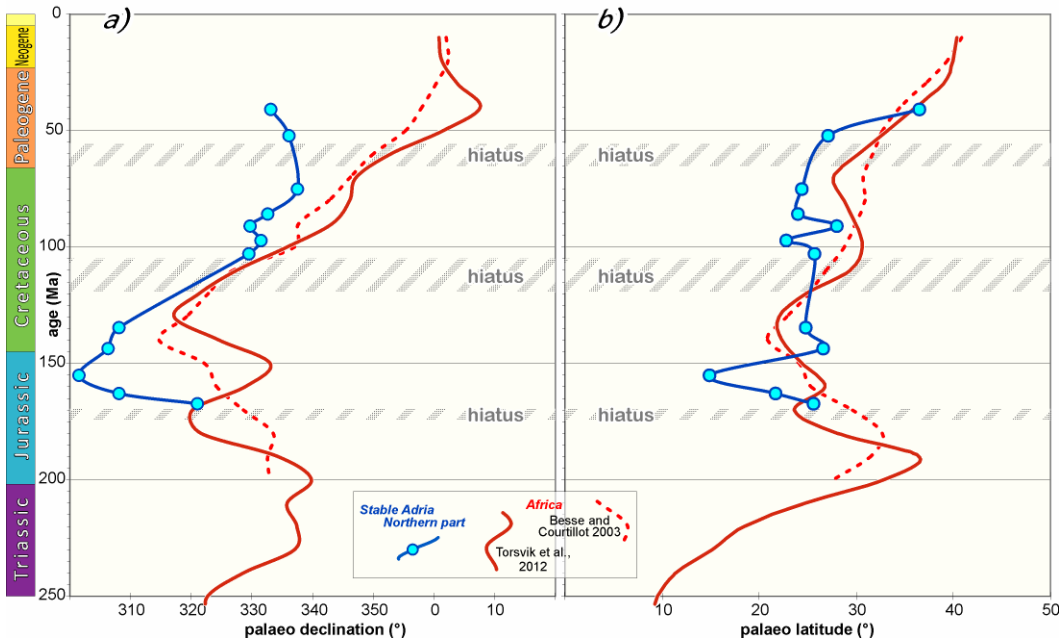

Figure 1. Comparison of paleomagnetic declinations (a) and paleolatitudes (b) from the APW of Northern segment of Stable Adria with declinations and paleolatitudes expected in an African framework from synthetic APWs by Besse and Courtillot (2002, 2003) and Torsvik et al. (2012). All data are recalculated for a reference location 45.3°N, 12.5°E. Stratigraphic gaps longer than 5Ma are indicated by shaded and numbered intervals

3 Intramontane basins in the External Dinarides

We carried out paleomagnetic and AMS measurements on oriented samples of Miocene age collected in Pag island and the Drnis-Sinj twin basin on the mainland. Following extension in the External Dinarides, the basins were filled with dominantly calcareous mud. Paleomagnetic results obtained by de Leeuw et al. (2012) from one section from each of the mentioned basins were interpreted as evidences for the absence of tectonic rotation after the deposition of the mud. We revisited the long Crnika section in Pag island, and documented, partly based on AMS results, partly on field observation of active slumping (the section was revisited after the AMS measurements revealing discrepancy between different segments of the section) that the palaeomagnetic results from this section are unsuitable for tectonic interpretation. In the Drnis-Sinj twin basin, we collected samples from several outcrops of Miocene sediments, including gently tilted as well as strongly deformed strata (including a plungig syncline). Our results, based on remanences acquired before the Pliocene deformation, suggest 13-20° CCW rotation. It is an open question at the moment if this rotation is connected to major neotectonic zones or represent a displacement involving a larger portion of the High Karst zone (Márton et al. 2016a).

4 Miocene basin evolution of the Western Carpathian–North Pannonian domain based on chronostratigraphic, stress field and paleomagnetic data

In recent years, important progress was made in the above research fields. Paleomagnetic results available till 2014 were critically reviewed and compiled by Márton et al. (2016b), and new ones were published for the Dukla nappe of the Outer Western Carpathians (Kiss et al. 2016) and for the Miocene Orava-Nowy Targ Intramontane basin of the Western Carpathians (Tokarski et al. 2016). In the last paper, a novel method was presented, namely the integrated interpretation of paleomagnetic declinations and the two peaks evident in the orientations of the fractures in the clasts.

Due to the enlarged data sets and reliable constraints on some events, it was possible to construct new palinspastic-paleogeographic and paleotopographic maps and relate the formations of basin depocentres to the CCW rotations of the ALCAPA Mega-Unit segments (Kováč et al. 2017, 2018). From palaeomagnetic point of view, the highlights are as follows. The openings of the basins started during the Early Miocene and lasted till the late Miocene in a roughly constantly oriented stress field and the present map view of the basins is due to significant amount of CCW rotations of different segments at different times, documented by paleomagnetic data. The most important features of the process are:

1. About 30° CCW "domino-style" rotation affecting the intramontane basins of the Eastern Alps
2. The about 50° "en bloc" CCW rotation of the crustal wedge built up from Northern Pannonian domain, from the Central Western Carpathians, from the Pieniny Klippen Belt and from the Outer Western Carpathians
3. During the Middle Miocene final stage of the collision of the Western Carpathians with the European Platform "domino-style" CCW rotations of about 30°, starting in the Northern Danube basin in the middle Miocene and ending in the Eastern Slovak Basin close to the Middle and Late Miocene boundary.

Acknowledgement. This work was supported by the National Research, Development and Innovation Office, Hungary - NKFIH K105245. Reviews by two anonymous referees are gratefully acknowledged.

References

Besse J, Courtillot V (2002): Apparent and true polar wander and geometry of the geomagnetic field over the last 200Myr. Journal of Geophysical Research, 107, B11, EPM 6-1–6-31.

Besse J, Courtillot V (2003): Correction to "Apparent and true polar wander and geometry of the geomagnetic field over the last 200Myr". Journal of Geophysical Research, 108, B10, EPM 3-1–3-2.

Bott MHP (1959) The mechanisms of oblique slip faulting. Geol. Mag. 96, 109–117.

de Leeuw A, Mandić O, Krijgsman W, Kuiper K, Hrvatović H (2012): Paleomagnetic and geochronologic constrains on the geodynamic evolution of the Central Dinarides. Tectonophysic, 530-531, 286-298.

Kiss D, Márton E, Tokarski AK (2016): An integrated paleomagnetic and magnetic anisotropy study of the Oligocene flysch from the Dukla nappe, Outer Western Carpathians, Poland. Geologica Carpathica, 57(6), 595-605.

Kováč M, Márton E, Oszczypko N, Vojtko R, Hók J, Králiková S, Plašienka D, Klučiar T, Hudáčková N, Oszczypko-Clowes M (2017): Neogene palaeogeography and basin evolution of the Western Carpathians, Northern Pannonian domain and adjoining areas. Global and Planetary Change, 155, 133-154, doi: 10.1016/j.gloplacha.2017.07.004.

Kováč M, Márton E, Klučiar T, Vojtko R (2018): Miocene basin opening in relation to the north-eastward tectonic extrusion of the ALCAPA Mega-Unit. Geologica Carpathica, 69(3), 254-263, doi: 10.1515/geoca-2018-0015.

Márton E, Pavelić D, Vranjković A, Ćosović V (2016a): Reapprisal of the palaeomagnetism of the Miocene intramontane Pag and Drniš-Sinj basin, External Dinarides (Croatia). Tectonophysics, 676, 125-134, doi: 10.1016/j.tecto.2016.03.033.

Márton E., Grabowski J, Tokarski AK, Túnyi I (2016b): Palaeomagnetic results from the fold and thrust belt of the Western Carpathians: an overview. In: Pueyo, E. L., Cifelli, F., Sussman, A. J. & Oliva-Urcia, B. (eds) Palaeomagnetism in Fold and Thrust Belts: New Perspectives. Geological Society, London, Special Publications, 425, 7-36.

Márton E, Zampieri D, Ćosović V, Moro A, Drobne K (2017) Apparent Polar Wander Path for Adria extended by new Jurassic paleomagnetic results from its stable core: tectonic implications. Tectonophysics, 700-701, 1-18, doi: 10.1016/j.tecto.2017.02.004.

Sipos AÁ, Márton E, Fodor L, Sipos Benkő K (2015): Towards an integrated reconstruction of the deformation field from simultaneous magnetic and mesotectonic data. 26th IUGG General Assembly, June 22 – July 2, 2015, Prague. 26th IUGG General Assembly Abstracts, IUGG-1601.

Sipos AÁ, Márton E, László F (2018): Reconstruction of early phase deformations by integrated magnetic and mesotectonic data evaluation. Tectonophysics, 726, 73-85, doi: 10.1016/j.tecto.2018.01.019.

Tokarski AK, Márton E, Swierczewska A, Fheed A, Zasadni J, Kukulak J (2016): Neotectonic rotations in the Orava-Nowy Targ Intramontane Basin (Western Carpathians): An integrated palaeomagnetic and fractured clasts study. Tectonophysics, 685, 35-43.

Torsvik TH, Van der Voo R, Preeden U, Mac Niocaill C, Steinberger B, Doubrovine PV, van Hinsbergen DJJ, Domeier M, Gaina C, Tohver E, Meert JG, McCausland PJA, Cocks LRM (2012): Phanerozoic polar wander, paleogeography and dynamics. Earth Sci. Rev., 114, 325–368.

Wallace RE (1951): Geometry of shearing stress and relation to faulting. J. Geol., 59,118–130.

HUNGARIAN CONTRIBUTION TO THE RESEARCH OF DYNAMIC PROCESSES COUPLED WITH THE UPPER-ATMOSPHERE/IONOSPHERE SYSTEM (2015-2018) – IAGA DIVISION II: AERONOMIC PHENOMENA

József Bór[*], Gabriella Sátori[*], Veronika Barta[*], Tamás Bozóki[,**], Attila Buzás[*,***], Karolina Szabóné André[*]*

1 Schumann resonances

Energetic emissions from the Sun can produce a varied influence on the modal frequencies, amplitudes and dissipation parameters of the Earth's Schumann resonances (SR). "Distinct differences are noted in the ionospheric depths of penetration for X-radiation and solar protons with correspondingly distinct signs of the frequency response" (Sátori et al. 2016). Enhanced fluxes of X-rays with wavelengths in the 0.1–0.8 nm range affect the upper characteristic height globally and manifest themselves by the increase of SR modal frequencies coherently in all SR modes and in both the electric and magnetic field components (Figure 1) while the energetic solar protons primarily influence the lower characteristic height of the SR cavity and cause the decrease of frequencies.

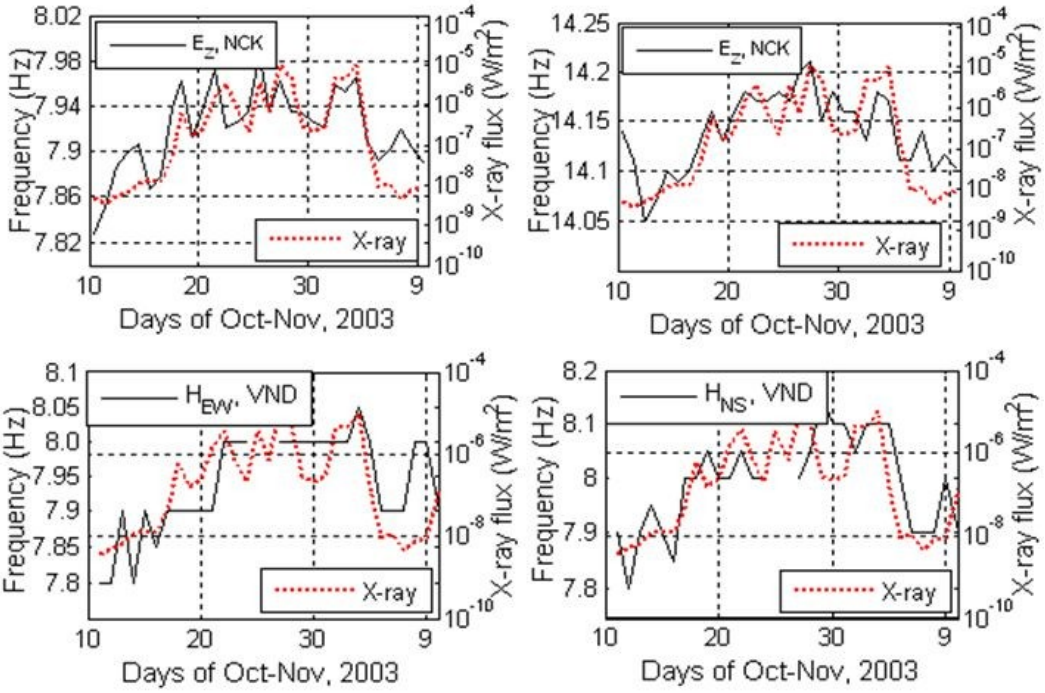

Figure 1. SR frequency response to the variation of the hard X-ray flux during the Halloween event in October/November, 2003 at Nagycenk (**top panels**: 1st and 2nd SR modes in the vertical electric field) and in the Antarctic station, Vernadsky (**bottom panels**: 1st mode in the two horizontal magnetic field components).
The figure is based on Figs 6 and 10 in Sátori et al. (2016)

The SR frequency response with opposite sign for the two kinds of energetic solar emission was demonstrated at multiple receiving stations for two extraordinary solar events from Solar Cycle 23: the Bastille Day event (July 14, 2000) and the Halloween event (October/November 2003). The preferential impact of the protons in the magnetically unshielded polar regions leads to a marked

[*]*MTA CSFK GGI, 9400 Sopron, Csatkai u. 6-8.*
E-mail: Bor.Jozsef@csfk.mta.hu
[**]*Doctoral School of Enviromental Sciences, University of Szeged, Szeged, Hungary*
[***]*Eötvös Loránd University, Budapest, Hungary*

anisotropic frequency response in the two magnetic field components. The general immunity of SR amplitudes to these extreme external perturbations serves to remind us that the amplitude parameter is largely controlled by lightning activity within the Earth–ionosphere cavity (Sátori et al. 2016).

The investigation of "background" SR measurements during the St Patrick Geomagnetic storm of 2015 indicated that sometimes not lightning-related ELF waves of magnetospheric origin can also contribute to the measured SR intensities. In the recovery phase of the storm, latitude-dependent, broadband intensifications of SR have been observed at ground observatories mainly in the NS propagation direction. At high latitudes, more than 250% of relative increment has been observed compared to geomagnetically undisturbed days. The intensifications, which lasted for several hours (sometimes even more than 10 hours) and were the most intense at resonance frequencies, appear simultaneously at latitudinally and longitudinally separated stations, which suggests a global change in SR. The observation could be explained with ELF waves entering the cavity at high latitude, while their interpretation through the amplification of lightning intensity or via the change of Earth-ionosphere cavity geometry can be excluded. The relative pattern of intensification in the horizontal magnetic components of the atmospheric electromagnetic field should constrain the direction of the entering region. This phenomenon might be the underlying reason for the observed 11 year periodicity of SR intensity at high latitude stations. The initial results about the possible origin of this external energy intrusion were reported at EGU 2018 (Bozóki et al., 2018).

2 Schumann resonance transients

The error of the ELF data-based source direction estimate of distant lightning strokes has been evaluated statistically (Bór et al. 2016). It was shown that the error of the source direction estimate is independent of the distance between the source and the detection site at least up to 11 Mm, i.e., the range covered by the available data.

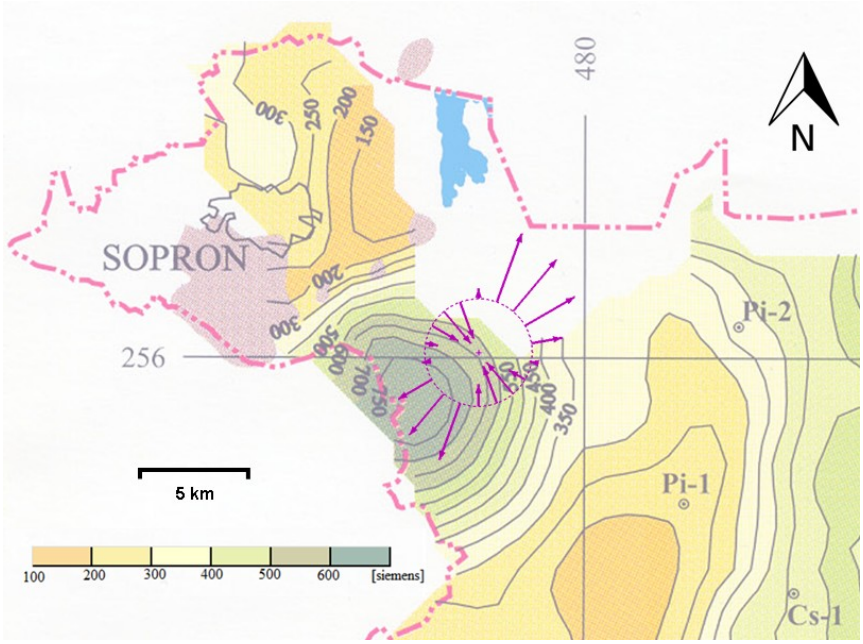

Figure 2. Conductance map near NCK station. The location of NCK station is marked by a small plus sign. Shaded area on the map shows the appearances of lower east-alpine Palaeozoic crystalline rocks at the surface near the town of Sopron. The white area without conductance data to north from NCK is part of Lake Fertő which is covered by reed. Deviations of ELF data-based source directions in terms of the true source azimuth are represented by arrows. Arrows are drawn by 20° starting at 0°. Arrows pointing inward and outward of the circle around NCK station correspond to negative and positive azimuth deviations, respectively. The length of the arrows is proportional to the absolute value of the average deviation. For example, the length of the arrow at 20° azimuth corresponds to +18.25° azimuth deviation.
(Re-printed from Bór et al. (2016), Figure 5.)

The results suggest that local anisotropic conductivity of the Earth's crust at the Széchenyi István Geophysical Observatory (NCK) can affect the polarization properties of ELF waves significantly (Figure 2). The effect depends on the azimuth of signal arrival and by correcting for it, the accuracy of ELF data-based source azimuth estimates can be improved significantly: the standard deviation of azimuth errors is lowered to 7.25° from 13.27° in the examined set of cases. This finding points at the rarely considered possibility of utilizing SR transients in surveying the electrical properties of the Earth's crust.

Transient signals bias the spectral properties of time series. Therefore, identification and proper handling of Schumann resonance (SR) transients (Q-bursts) in extremely low frequency (ELF) electromagnetic records is very much important from the point of view of the analysis of background SR properties. Q-bursts occurring in ELF records from Nagycenk (Hungary), Belsk (Poland), and Rhode Island (USA) were used to examine their effect on spectral properties of SR deduced from the corresponding continuous ELF time series. It was found that the integrated power spectral density (iPSD) obtained from an ELF data segment can be used to select those data segments which contain Q-bursts (Guha et al. 2017). An adaptive threshold can be given in the distribution of iPSD values (16 times the core width of the distribution). Data segments with iPSD higher than this threshold contain transients which significantly bias SR modal parameters, most significantly the resonant frequencies. Those data segments must be excluded from the analysis of the background spectral properties of SR. Applying this method to ELF data from several stations provides another possibility to geo-locate the sources of Q-bursts with time-of-arrival methods. This result is an important step forward for achieving standardized processing and evaluation of ELF data measured worldwide at several locations but by fairly different instrumentation.

3 Transient luminous events

A rare type of secondary transient luminous event (TLE), a so called troll (secondary jet) has been observed simultaneously by two low light cameras from Nydek (Czech Republic) and Sopron (Hungary) on 6 August, 2013. This faint emission terminated a series of red sprites (Figure 3) which was triggered by a corresponding sequence of positive polarity cloud-to-ground (+CG) lightning strokes (Mlynarczyk et al. 2015).

Figure 3. Brightness peak-hold image of the dancing sprite event produced from video footage recorded in Sopron. The event occurred between 22:34:06.959 – 07.399 UTC on 6 August, 2016 in Central Europe. The faint troll emission is marked by a dotted ellipse

Events in which several red sprites appear in a rapid sequence are called "dancing" sprite events. Location of the sprites and the troll could be determined by triangulation using video records from the two observation stations. Location, type, polarity and peak current of the parent lightning stroke of the sprites was provided by the LINET lightning detection network (Betz et al. 2008). A new method was used to reconstruct the current moment (CM) waveform and to deduce the charge moment change associated with the event. These characteristics were calculated from extremely low frequency electromagnetic signature recorded at the Hylaty station (Poland). The results showed that sprites were displaced up to 70 km from their parent lightning and that both short-delayed and long-delayed sprites can be generated by a single parent lightning stroke. The CM waveform revealed that the parent lightning stroke of this type in the examined case was followed by a strong but varying continuing current lasted for 200 ms. It is hypothesized that sprite current could also contribute to the detected enhancement on the CM waveform. It is discussed that the observed sequence of events supports the mechanism that had been suggested for the generation of secondary TLEs (Mlynarczyk et al. 2015).

Analysis of optical records of „dancing" red sprite events showed that subsequent sprite-parent lightning strokes occurred no further than 21 km from the closest preceding sprite entity in the considered cases (Bór et al. 2018). Joint analysis of simultaneously recorded video footages from Nydek, Czech Republic and from Sopron, Hungary, extremely low frequency (ELF) electromagnetic records from Poland, and lightning data from a European-scale lightning detection network was done. A working hypothesis has been set up which does not only provide an explanation for the experience described above, but it describes the formation of sprite producing lightning flashes in the stratiform region of mesoscale convective systems in a plausible and coherent way. The results shed light on the lightning activity from a new point of view. The analysis suggests that giant contiguous lightning flashes extending to hundreds of kms can develop in the stratiform cloud region of thunderstorms and can transport several hundred Coulombs of electric charge to the ground in discrete steps.

A linear relationship was found between the brightness of red sprites and the charge moment change (CMC) of their triggering lightning strokes (Nnadih et al. 2018). This relationship was deduced via joint analysis of the very first optical observations of red sprites in South Africa and extremely low frequency (ELF) electromagnetic signals produced by the triggering lightning strokes. The CMC of the lightning strokes was calculated from ELF data recorded at the Széchenyi István Geophysical Observatory.

Comparison of extremely low frequency (ELF) signals from not sprite-producing and sprite-producing lightning strokes demonstrated that sprite-triggering lightning strokes are more energetic (Spackova et al. 2018). Waveforms of ELF signals from sprite-producing lightning strokes indicate the presence of continuing current in the discharge process more often. The presence of continuing current, in accordance with earlier findings, indicates that large amount of charge flows through the discharge channel of sprite-parent lightning strokes.

4 Measurements of the quasi-static atmospheric electric field

The potential of the lower ionosphere with respect to the surface of the Earth is supposed to be mirrored by the atmospheric electrical potential gradient (PG) measured near the ground. On the other hand, near-surface electric field measurements are significantly affected by local conditions that change the conductivity of the air or otherwise bias the natural vertical electric field. Such conditions and effects must be quantified and corrected for in order for the measurements to be properly interpreted. A decreasing trend was found in PG values measured quasi-continuously since 1962 in the Széchenyi István Geophysical Observatory (NCK, 47°38' N, 16°43' E) (Märcz and Harrison 2003, 2005). The origin of this trend has been subject of yet unsolved scientific debates. In particular, the gradually increasing electrical shielding effect of trees growing not far from the location of measurements was suspected to cause the decrease in PG values over the decades of the measurements (Williams et al. 2005). However, the reliability of the model applied to justify the hypothesis has been criticized (Märcz and Harrison 2006). An attempt was made to accurately reconstruct the

shielding effect of surrounding trees on the measurement by setting up a carefully parameterised model that incorporates the heights, ages, type, and configuration of the trees and their exact distances to the measuring devices. The model was validated by the excellent matching of calculated and measured shielding factors for 2016-2017 with known actual tree heights (Buzás et al. 2017). A time-dependent correction factor has been produced (Figure 4) which will be used to correct the long term PG measurements so that correct analysis and interpretation of the PG measurements at NCK can be made (Buzás et al. 2018).

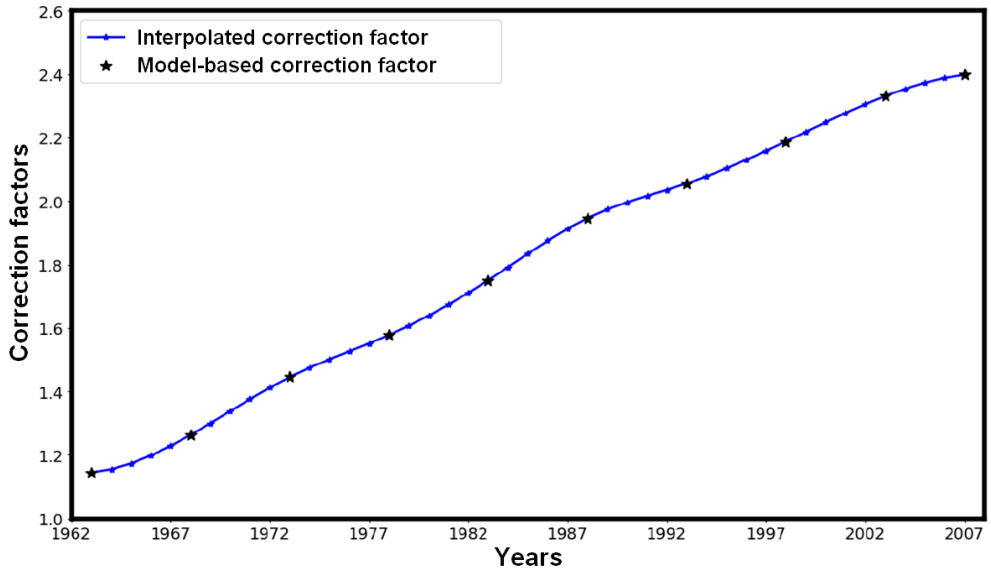

Figure 4. Time-dependent correction factor corresponding to the increasing shielding effect of trees surrounding the PG measuring site in the Széchenyi István Geophysical Observatory

Researchers from the MTA CSFK GGI contributed to an international database of atmospheric electric potential gradient (PG) measurements by providing PG and meteorological data recorded in the Széchenyi István Geophysical Observatory since 2016. The database has been established in the framework of the project 'GLObal Coordination of Atmospheric Electricity Measurements' (GloCAEM, https://glocaem.wordpress.com) run by University of Reading (UK). The aim of this project is to facilitate research on the DC Global Electric Circuit by collecting and sharing PG data in a standardized format. The database opens new horizons in studying the interactions between the atmospheric global electric circuit and various geophysical processes of the near-Earth space by joint analysis of PG data measured simultaneously at numerous recording sites around the globe.

5 Ionospheric research

The relation of electrical activity of thunderstorms and red sprites to the dynamics of overlying sporadic E (E_S) layers have been studied (Barta et al. 2017). The results suggest that thunderstorms may affect E_S layers primarily through subsequently produced atmospheric gravity waves (AGW) (Figure 5). AGWs may destroy or sometimes reinforce E_S layers. On the other hand, no direct physical mechanisms were unambiguously identified which could connect E_S layer variations to the simultaneously appearing red sprites.

A digital ionospheric radar system (DPS4D digisonde) has been installed at the MTA Széchenyi István Geophysical Observatory, Nagycenk in the framework of GINOP-2.3.2-15-2016-00003 project "Cosmic hazards and effects" (translated from the Hungarian title "Kozmikus hatások és kockázatok") and it is operating since June, 2018 (Figure 6). Ionospheric sounding is a ground-based measurement which provides important information on the state and evolution of the ionospheric plasma. More than 50 Digisonde DPS-4D ionospheric sounders

(http://www.digisonde.com/) worldwide produce real-time data in the international network GIRO (Global Ionospheric Radio Observatory, http://giro.uml.edu/) in order to monitor the ionosphere on regional and global scales.

The same type of digisonde that has been installed at Nagycenk operates in Pruhonice, Czech Republic since 2004. In collaboration with the Institute of Atmospheric Physics, joint analysis of short-term variability of the mid-latitude ionosphere has become possible. Ongoing studies are focusing especially on the occurrences and propagation of the Travelling Ionospheric Disturbances (TIDs) as well as occurrences and classification of various wave structures within the ionospheric plasma. The relatively short distance between Pruhonice, Czech Republic and Nagycenk allow us to perform special joint campaigns of vertical and/or oblique sounding using high sampling rate.

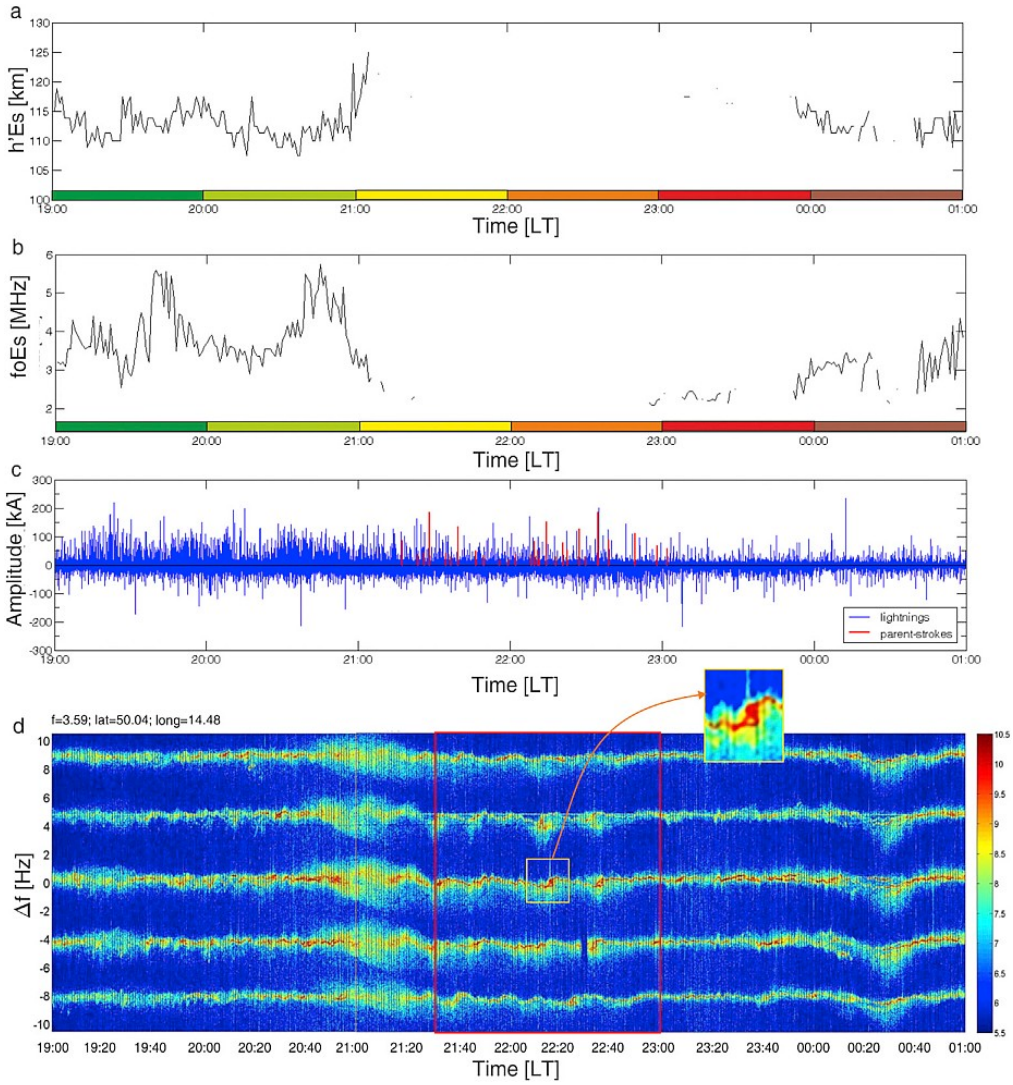

Figure 5. The reduction and disappearance of the ongoing E_S layer activity detected at Pruhonice during part of the time of a traversing thunderstorm. Temporal variations of (a) h'E_S; (b) foE_S; (c) peak current and polarity of CG strokes within 200 km from Pruhonice with the sprite-parent discharges shown in red; (d) the CDSS Doppler spectrogram. Doppler shifted signals in the time interval 21:30-23:00 LT, inside the red rectangular form S-like traces (as it is magnified in the inset), which are attributed to a wavelike modulation caused by atmospheric gravity waves. (Re-printed from Barta et al. (2017), Figure 3.)

Installation of the digisonde enabled the participation of MTA CSFK GGI in joint synchronized measurements in the framework of the Tech-TIDE H2020 project (http://techtide.space.noa.gr/)

which aims at detecting TIDs over the European region. Participation in the corresponding campaign measurements opens the possibility to make a detailed analysis of wave-like anomalies occurring in the ionosphere above Hungary and Czech Republic.

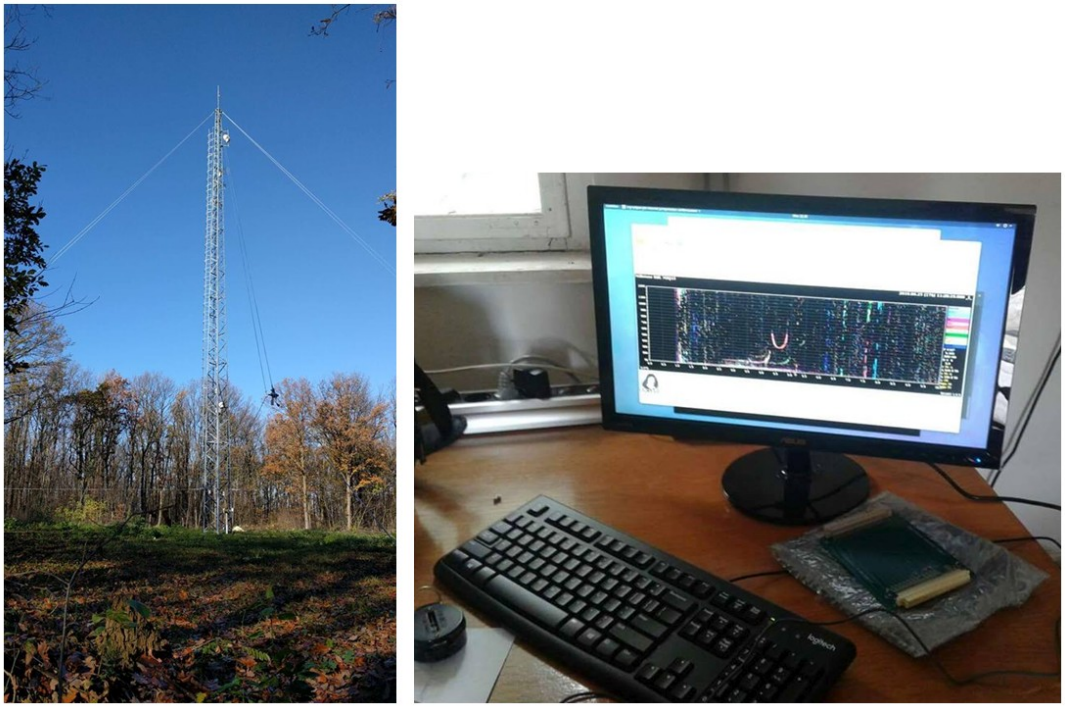

Figure 6. The transmitter antenna of the DPS4D digisonde at the MTA Széchenyi István Geophysical Observatory (left) and one of the first ionograms detected by the system (right).

Acknowledgements This work was supported by the National Research, Development and Innovation Office, Hungary-NKFIH, K115836. Contribution of J. Bór was supported by the János Bolyai Research Scholarship of the Hungarian Academy of Sciences (BO/00651/13/10h). Contribution of A. Buzás was supported by the ÚNKP-18-2 new national excellence program of the Ministry of Human Capacities. The work of Tamás Bozóki was supported by the ÚNKP-16-2, ÚNKP-17-2 and ÚNKP-18-3 New National Excellence Programs of the Ministry of Human Capacities. The authors appreciate support of the TEA-IS programme of ESF and the COST Action CA15211, ELECTRONET, in facilitating scientific communication. The installation of the DPS4D digisonde in the MTA Széchenyi István Geophysical Observatory was supported by the GINOP-2.3.2-15-2016-00003 project.

References

Barta V, Haldoupis C, Sátori G, Buresova D, Chum J, Pozoga M, Berényi AK, Bór J, Popek M, Kis Á, Bencze P (2017): Searching for effects caused by thunderstorms in midlatitude sporadic E layers. Journal of Atmospheric and Solar-Terrestrial Physics, 161, 150-159, doi:10.1016/j.jastp.2017.06.006.

Betz HD, Schmidt K, Oettinger WP (2008): LINET—An international VLF/LF lightning detection network in Europe. In Betz HD, Schumann U, Laroche P (Eds.), Lightning: Principles, instruments and applications, 115–140. Dordrecht (NL): Springer, doi:10.1007/978-1-4020-9079-0_5.

Bór J, Ludván B, Novák A, Steinbach P (2016): Systematic deviations in source direction estimates of Q-bursts recorded at Nagycenk, Hungary. J. Geophys. Res. Atmos., 121, 5601-5619, doi:10.1002/2015JD024712.

Bór J, Zelkó Z, Hegedüs T, Jäger Z, Mlynarczyk J, Popek M, Betz HD (2018): On the series of +CG lightning strokes in dancing sprite events. Journal of Geophysical Research: Atmospheres, 123, 11030-11047, doi:10.1029/2017JD028251.

Buzás A, Barta V, Steinbach P, Bór J (2017): Impact of local environmental conditions on atmospheric electrical potential gradient measurements. Geophysical Research Abstracts 19, EGU2017-1193-1.

Buzás A, Horváth T, Barta V, Bór J (2018): Revisiting the decreasing trend of atmospheric electrical potential gradient measured in Central Europe at Nagycenk, Hungary. Geophysical Research Abstracts 20, EGU2018-6723.

Bozóki T, Sátori G, Steinbach P (2018): Plasmaspheric hiss as an external excitation source of the Earth-ionosphere cavity. Geophysical Research Abstracts 20, EGU2018-7878.

Guha A, Williams E, Boldi R, Sátori G, Nagy T, Bór J, Montanyá J, Ortega P (2017): Aliasing of the Schumann resonance background signal by sprite-associated Q-bursts. Journal of Atmospheric and Solar-Terrestrial Physics, 165-166, 25-37, doi:10.1016/j.jastp.2017.11.003.

Märcz F, Harrison RG (2003): Long-term changes in atmospheric electrical parameters observed at Nagycenk (Hungary) and the UK observatories at Eskdalemuir and Kew. Annales Geophysicae, 21, 2193-2200, doi:10.5194/angeo-21-2193-2003.

Märcz F, Harrison RG (2005): Further signatures of long-term changes in atmospheric electrical parameters observed in Europe. Annales Geophysicae, 23, L12803, doi: 10.1029/2005GL025574.

Märcz F, Harrison RG (2006): Comment on „Shielding effects of trees on the measurement of the Earth's electric field: Implications for secular variations of the global electrical circuit" by E. Williams et al. Gephysical Research Letters, 33, 1987-1995, doi:10.1029/2005GL023717.

Mlynarczyk J, Bór J, Kulak A, Popek M, Kubisz J (2015): An unusual sequence of sprites followed by a secondary TLE: An analysis of ELF radio measurements and optical observations. J. Geophys. Res. Space Physics, 120, 2241-2254, doi: 10.1002/2014JA020780.

Nnadih S, Kosch M, Martinez P, Bor J (2018): First ground-based observations of sprites over southern Africa. South African Journal of Science, 114(9/10), #4272, doi:10.17159/sajs.2018/4272.

Sátori G, Williams E, Price C, Boldi R, Koloskov A, Yampolski Y, Guha A, Barta V (2016): Effects of Energetic Solar Emissions on the Earth-Ionosphere Cavity of Schumann Resonances. Surveys in Geophysics, 37(4), 757- 789. Paper GEOP-D-15-00044.2, 33.

Spackova H, Kolmasova I, Santolik O, Popek M, Bor J (2018): Properties of Sprite Parent Lightning for a Storm on 6 August 2013. in WDS'18 Proceedings of Contributed Papers - Physics (eds. J. Safrankova and J. Pavlu), Prague, Matfyzpress, 93-98, ISBN 978-80-7378-374-7.

Williams E, Markson R, Heckman S (2005): Shielding effects of trees on the measurement of the Earth's electric field: Implications for secular variations of the global electrical circuit. Geophysical Research Letters, 32, L19810. doi: 10.1029/2005GL023717.

HUNGARIAN CONTRIBUTION TO THE RESEARCH OF MAGNETOSPHERIC PHENOMENA (2015-2018) - IAGA DIVISION III: MAGNETOSPHERIC PHENOMENA

János Lichtenberger[,**], Balázs Heilig[***], Dávid Koronczay[*], Melinda Nagy[*], Orsolya Ferencz[*], Csaba Ferencz[*], Péter Steinbach[****], Péter Kovács[***], Antal Juhász[*****], Zoltán Németh[*****], Andrea Opitz[*****], Károly Szegő[****], Mariella Tátrallyay[*****], Anikó Timár[*****]*

1 Monitoring the Geospace by VLF waves

Artificial very low frequency (VLF, 3 to 30 kHz) signals have long been a useful tool in plasmaspheric research. They have been shown by ground-based measurements to be able to propagate in ducts in the magnetosphere. Continuous burst mode very low frequency (VLF) measurements were recorded on the Van Allen Probes satellites and are analyzed to detect pulses from the Russian Alpha (RSDN-20) ground-based navigational system between January and March 2016 (Koronczay et al. 2018). Based on the wave characteristics of these pulses and on the position of the spacecraft, the signals propagated mostly in ducted mode in the plasmasphere.

Knowledge of the propagation path allowed us to carry out a monochromatic wave propagation inversion to obtain plasmaspheric electron densities. We compared the obtained densities with independent in situ measurements on the spacecraft. The results show good agreement, validating our inversion process (Figure 1). This contributes to validating the field-aligned density profile model routinely used in the inversion of whistlers detected on the ground. Furthermore, our method can provide electron densities at regimes where no alternative measurements are available on the spacecraft. This raises the possibility of using this method as an additional tool to measure and monitor plasmaspheric electron densities.

Lightning discharges radiate electromagnetic waves in a wide frequency range, with maximum energy in extremely low frequency/very low frequency band. A part of the radiated extremely low frequency/very low frequency wave energy is trapped in the Earth–ionosphere waveguide and travels thousands of kilometers in different modes with lower attenuation. Amplitude, frequency and phase of these waves are used to study the less explored D-region ionosphere at lower latitudes. Extremely low frequency/very low frequency observations are recorded continuously by automatic whistler detector setup installed at low-latitude Indian station Lucknow (Geom. lat. 17.6N; long. 154.5E). In total, 149 cases of tweeks having modes ranging from 3 to 6 have been recorded by automatic whistler detector during December 2010 and analyzed (Singh et al. 2015). Result shows that the propagation distance in the Earth–ionosphere waveguide lies between 1.1 and 9.4 Mm. The electron density in the lower D-region varies between 25 and 150 cm-3. The upper boundary of the waveguide varies between 80 and 95 km. The reported results are in good agreement with the earlier measurements at different latitudes and longitudes.

The analysis of more than 2000 lightning-generated whistlers recorded at a low-latitude station, located at Allahabad (geographic latitude, 25.40°N; geographic longitude, 81.93°E; L = 1.081), India, during December 2010 to November 2011. The main focus of this work is on the correlation between observed low-latitude whistlers and lightning activity detected by the World-Wide Lightning Location Network near the conjugate point (geography 9.87°S, 83.59°E) of Allahabad.

[*]*ELTE, 1117 Budapest Pázmány Péter sétány 1/A.*
E-mail: lityi@sas.elte.hu
[**]*MTA CSFK GGI, 9400 Sopron, Csatkai u. 6-8.*
[***]*MBFSz, 1145 Budapest, Columbus u. 17-23.*
[****]*MTA-ELTE, 1117 Budapest Pázmány Péter sétány 1/A.*
[*****]*MTA Wigner FK, 1121 Budapest, Konkoly-Thege Miklós út 29-33.*

Whistler occurrence is higher in the postmidnight period as compared to the premidnight period. Whistlers were observed in the daytime only on 2 days that too before 8:30 LT (morning). Seasonally, occurrence is maximum during winter months, which is due to more lightning activity in the conjugate region and favorable ionospheric conditions.

About 63% of whistlers were correlated with lightning strokes in the vicinity of the conjugate point within spatial extent of 1000 km (conjugate area). Most (about 53%) whistlers were found to be associated with lightning strokes that were offset to the southeast of the conjugate point. The results indicate that an energy range of 7.5–17.5 kJ of lightning strokes generate most of whistlers at this station. The L shell calculations show that propagation paths of the observed whistlers were embedded in the topside ionosphere. Based on these results we suggest a possibility of ducted mode of propagation even for such very low latitude whistlers.

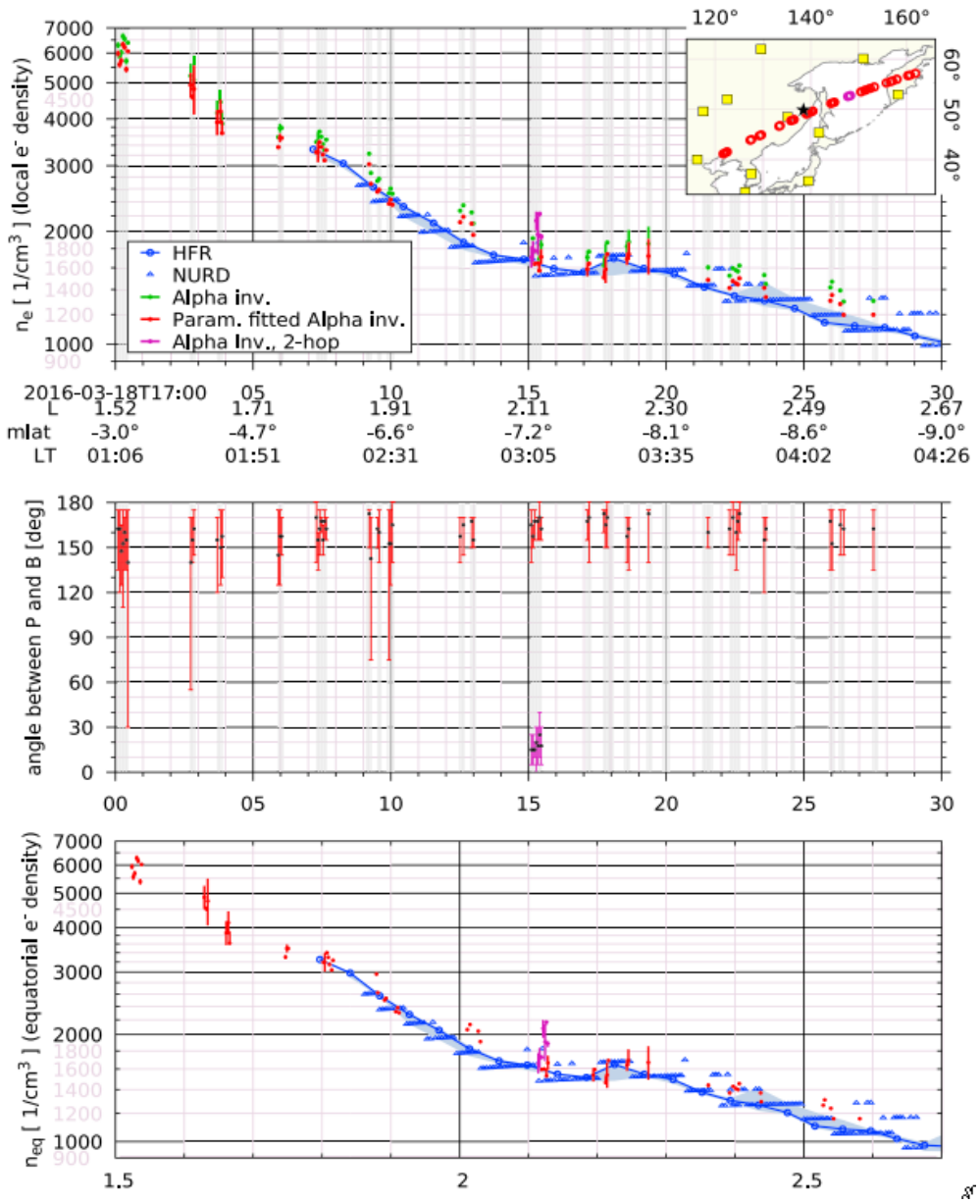

Figure 1. (top) Comparison of local electron densities obtained with our VLF signal inversion method (green dots using Ozhogin et al., 2012 model with default parameters; red dots = with fitted parameters; error bars shown stem from uncertainty of pulse arrival time determination) to densities from upper hybrid frequencies as a reference (blue triangles = NURD; blue circles = HFR analysis; blue-shaded area = uncertainty). Shaded gray areas are the periods when EMFISIS WFR continuous burst mode measurements were turned on. (inset) Map of satellite footprints (red circles), source transmitter (star shape), and ionosonde stations (squares). (middle) Angle of Poynting vector of each signal with respect to the field lines. (bottom) Comparison of inversion results and reference measurement, both converted to equatorial electron densities, against L value. Only the parameter fitted results are shown. VLF = very low frequency; HFR = High Frequency Receiver; EMFISIS = Electric and Magnetic Field Instrument and Integrated Science; WFR = Waveform Receiver. Some Poynting vectors (middle panel, purple bars) show parallel propagation in the opposite direction, that is, toward the transmitter. This is a result of signal reflection from the Southern Hemisphere ionosphere, similar to two-hop whistlers. Inversion results of these signals, assuming such two-hop propagation are shown in purple

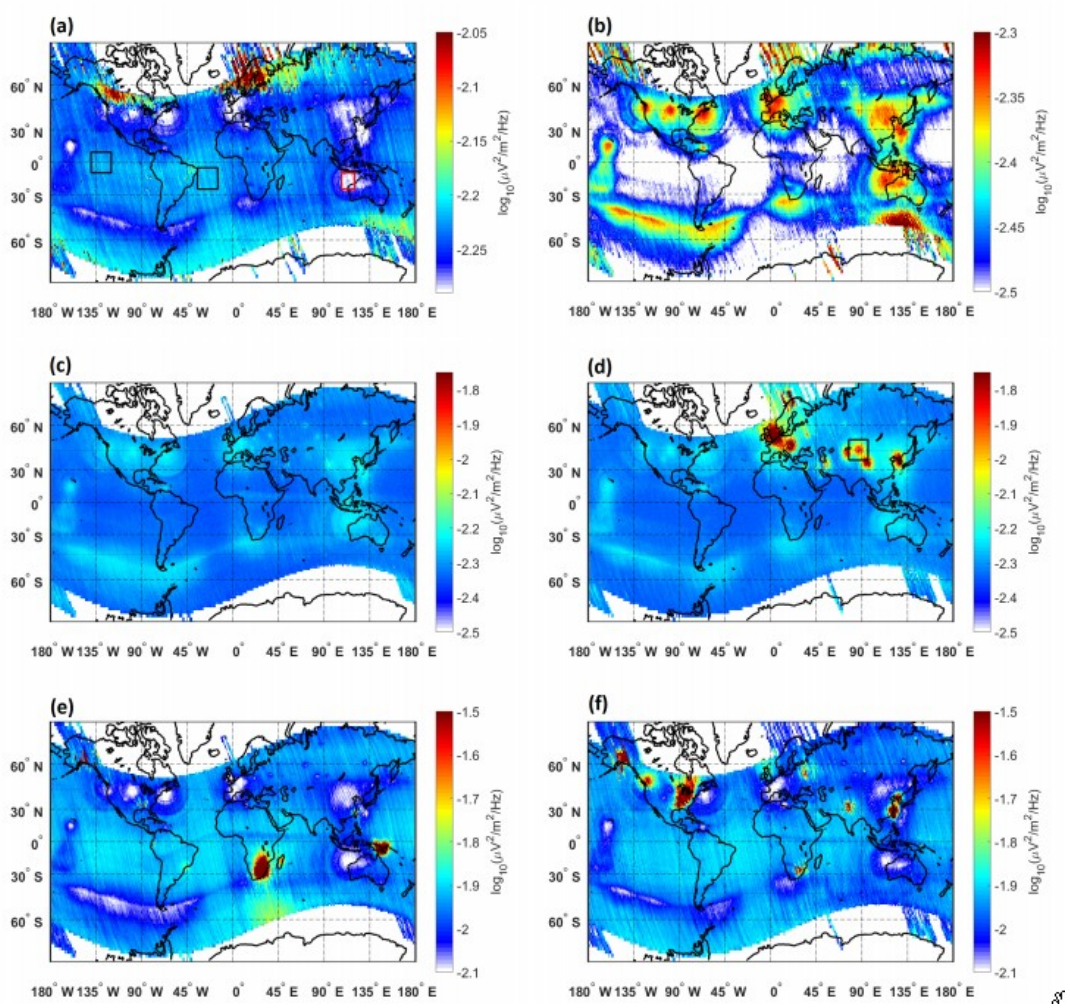

Figure 2. Intensity map of HF waveband averaged for different 100 kHz frequency ranges recorded between 2006 and 2009. In panel (a-b) we plot average intensities for the whole 4 years interval. In panel (a) we show measurements in the 1.3-1.4 MHz waveband. Red box illustrates the area selected above NWC transmitter, black boxes indicate the background regions detailed in the text. Panel (b) shows the same, but the signal is averaged for the 2.3-2.4 MHz frequency range. In panels (c-f) we plot measurements separated to northern summer season (April-August) and northern winter (November-February). Panels (c-d) shows data recorded between 2.6-2.7 MHz during the summer (c) and winter (d). Panels (e-f) follows the same order for the 3.2-3.3 MHz frequency range (Note that the four frequency ranges are plotted with different colorscales due to visualizing purposes.)

Creating statistical maps of MF signatures seen on HF DEMETER data for narrow (100kHz) frequency window and for seasonal variations, we found further signatures have not presented earlier (Nagy et al 2018). Signal enhancements between 1.8-2.9MHz above the powerful VLF transmitters can be attributed to the effect of heating of the ionosphere by the VLF waves that results through increased collision frequencies to widened transmission cones (Figure 2). The same effect may result the opposite (narrowed transmission cone and thus decreasing signal level) below 1.8MHz and above 2.9MHz - but this needs to be confirmed to extend the model of for these frequencies.

However, the low level of the seasonal variation on signal enhancement and decrease above the VLF transmitter seen in MF DEMETER data may question the origin of the variation that thought to be attributed to high frequency part of terrestrial lightnings, because the seasonal variation of

lightning occurrence around the VLF transmitters are much higher, it reaches one-one and a half order of magnitudes. We have found signatures of increased signal level over certain areas above 2.7MHz for local winter periods. They may be attributed to MF radio broadcast transmitters and can propagate through the ionosphere as during the local winter, the fof2 generally below 2.7MHz. However some of the area found are not expected to exhibit radio broadcasting activity (Himalaya, Tibet, North sea), while there are areas spatially close the ones found, that do not exhibit such signatures (East US cf. West US or Central Europe cf. Western Europe). The absence of signal increase/decrease above the three Russian Alpha transmitters is not yet understood. Finally, the sources of the MF signatures could be lightnings and MF radio broadcast transmitters, however, based on "anomalies" found in the signatures, this cannot be confirmed yet, further analysis of existing and future experimental data is needed accompanied with extended model calculations.

2 ULF wave observations at low-Earth orbit and on the ground

The observation of ULF waves at low-Earth orbit (LEO) became possible with the launch of the German CHAMP and the Danish Ørsted magnetic field missions in 2000. Especially, the observations made by the CHAMP satellite with its magnetic data of unprecedented quality led new results. Heilig et al. (2007) demonstrated that ULF waves generated by interaction of the magnetosphere and the upstream solar wind can penetrate deep in the magnetosphere and can even reach the equatorial and low latitude ionosphere. This somewhat unexpected result led to the revision of theoretical considerations on ULF wave propagation in the magnetosphere (Pilipenko et al. 2008). Since then, the initial results, the existence of ULF waves in the topside ionosphere have been confirmed by series of authors. LEO satellites are also good in providing observations of various phenomena with global coverage within a few months. This makes them suitable for the statistical investigation of the spatial distribution of the considered phenomena. CHAMP contributed significantly to our knowledge on different ULF wave types, such as compressional Pc3 waves (Heilig at al. 2007), field line resonances (Vellante et al. 2004; Ndiitwani and Sutcliffe 2009, 2010; Heilig et al. 2013), Pi2 waves (Sutcliffe and Lühr 2003, 2010; Han et al 2004), Pc2 waves (Yagova et al. 2015), and Pc1 waves (Park et al. 2013), first of all on their spatial structure.

With the advent of ESA's Swarm mission, a constellation of three identical satellites at LEO launched on 22 November 2013, these possibilities were multiplied, not only because of the more data and the better spatial coverage, but also by the possibility to make simultaneous multipoint measurements. This is essential for discriminating between spatial and temporal variations and also for mapping the spatial structure of various wave types yielding information on phase relations and coherence that could not have been observed directly before.

Based on 21 months (Jan 2014-Sep 2015) of Swarm observations, Heilig and Sutcliffe (2016) published the very first coherence and phase maps of compressional Pc3 pulsations as it appears in the topside ionosphere. Here (Figure 3) we present an updated version of their figure based on an extended dataset. They concluded that the Pc3 waves of upstream origin populate practically the whole sunlit hemisphere. The wave activity is the largest near the geomagnetic equator peaking somewhat before the local noon (Figure 3 top). The dimension of the coherent region exceeds 10000 km (or 90°) in latitudinal and 20000 km in longitudinal sense (bottom left). The whole coherent region is close to in-phase (bottom right), but in antiphase with ground observations (not shown).

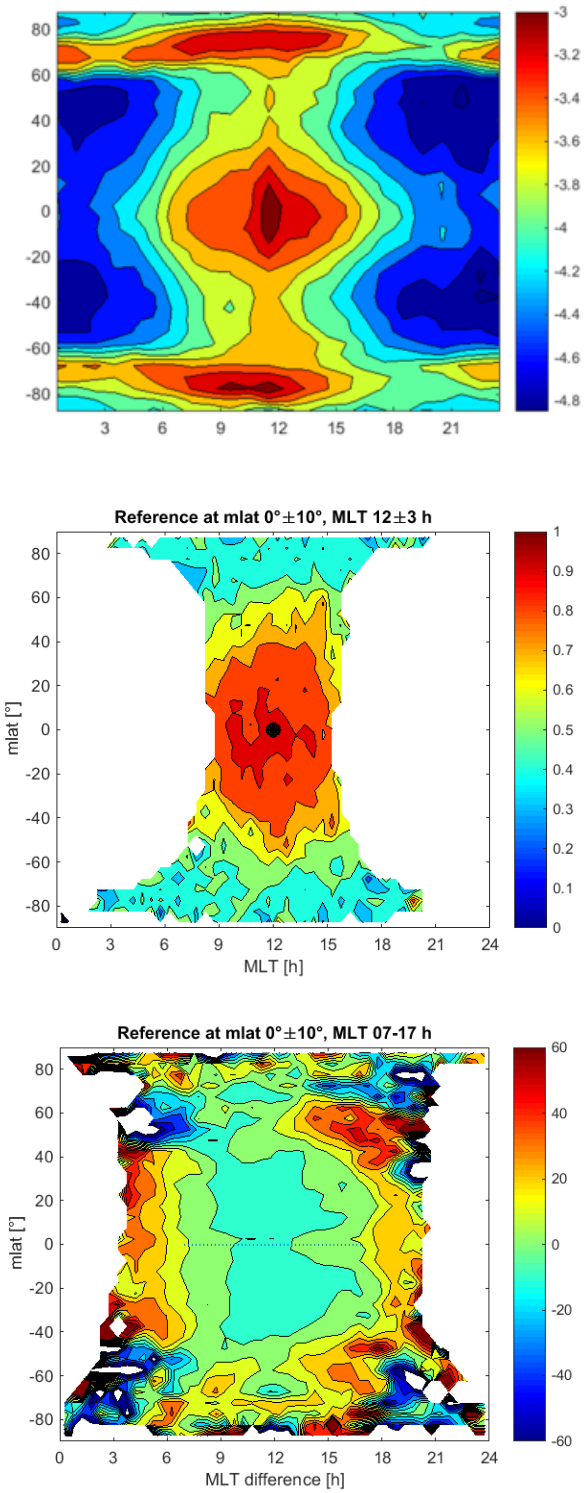

Figure 3 (top) Magnetic latitude vs. magnetic local time distribution of the compressional signal power in the Pc3 band (middle) coherence related to a reference point on the magnetic equator at local noon (bottom) phase difference from the reference point

At higher mid-latitudes Doppler shifted compressional waves were observed, providing the first observational evidence to support the prediction by the inductive thin ionosphere model that incident Alfvén mode waves are partially converted into compressional mode waves by the inductive ionosphere. The resulting waves are evanescent and can be observed exclusively at LEO.

Pilipenko and Heilig (2016) reviewed recent LEO observations of ULF waves, as well as the recent improvements of the thin ionosphere model that aims at accounting for the observed wave characteristics.

The importance of ground observations of ULF waves has increased since the availability of space measurements. Ground magnetometer networks provide continuous time series from fixed locations, while the separation of spatial and temporal fluctuations in satellite data is mostly not straightforward. Space-ground comparisons are very useful for understanding and supporting the proper interpretation of satellite data. In 2012 a new European quasi-Meridional Magnetometer Array (EMMA) was established, first of all to monitor ULF wave activity. Since then, EMMA observations are coordinated by the Mining and Geological Survey of Hungary (MGSH) (Lichtenberger et al. 2013). EMMA now consists of 25 magnetometers spanning from Northern Finland to Italy, covering the L-shell range: 1.5-6.1.

Yagova et al. (2017) investigated night time Pc3 events and found that these pulsations can be divided in two groups. The first group is in fact a spatiotemporal extension of the dayside Pc3 activity to the dark side. These Pc3 waves can be detected on the night side when the solar wind speed exceeds 500 km/s. The other type appearing at moderate solar wind speed is believed to be generated locally. Their preferred occurrence is near midnight and at middle latitudes. They seem to be associated with auroral activations, however, their generation mechanism is unknown.

Takahashi et al. (2018) analysed magnetospheric observations by the NASA's THEMIS and Van Allen Probes satellites in conjunction with EMMA recordings to investigate a Pi2 pulsation event (8 Nov 2014). The analysis revealed the radially standing structure of the Pi2 wave, its relation to the location of the plasmapause. The spatial structure of the event was consistent with that of plasmaspheric virtual resonances triggered by an impulsive source. On the other hand, the low coherence between the magnetotail plasma flow fluctuations and the Pi2 signal does not support the bursty bulk flow model of Pi2 generation. Dayside Pi2 waves were attributed to ionospheric currents connecting the night side resonance region to the day side.

A high azimuthal wave number ($m \sim -49$, i.e. wesward propagating) odd mode standing Pc4 wave and associated oscillations of energetic (>50 keV) protons were identified in Arase satellite observations by Yamamoto et al. (2018). The event occurred on the night side (LT ~ 03) on 15 April 2017. The phenomenon is known as the drift resonance of poloidal Alfvén waves with drift-bouncing ring current ions. Unlike earlier studies that linked the growth of these giant pulsations to the bump-on-tail structure on proton phase space density distribution, a steep earthward phase space density gradient was found to be responsible for the observed waves.

The study of magnetohydrodynamic (MHD) oscillations in the solar corona is an emerging topic. Although there are several similarities (and differences) between MHD phenomena observed in the solar corona and in the terrestrial magnetosphere, the two research areas have developed independently from each other, with hardly any communication, creating their own independent terminology. As a product of an International Space Science Institute team effort, Nakariakov et al., (2016) reviewed the most important topics in both discipline, including the phenomenology, MHD theory and modelling, the use of MHD waves in plasma diagnostics, etc.

MGSH and European Organization for Nuclear Research (CERN) launched a collaboration aiming at studying the possible stray magnetic fields that may affect the operation of the planned compact linear collider (CLIC). According to modelling studies carried out in CERN fluctuating magnetic field as low as a nT/s may change the orbit of charged particles so that leads to a significant loss of effective luminosity of the beam. Dynamic stray fields can be produced by natural, as well as by technical (originating from the environment or from the collider components themselves) sources. First, the natural sources, including the occurrence of extreme events and their potential amplitudes were reviewed by Heilig et al. (2018) concluding that at the planned side, the natural phenomena do not pose a significant risk on the experiment, except for some really extreme

and infrequent events. The authors also called the attention for the induced effect of geomagnetic storms and close-by lightning strikes that can easily reach the machine through its electrically connected components or by the induced electric field. The conclusions were incorporated into the CLIC Sumary Report (CLIC and CLICdp collaborations, 2018).

3 Monitoring the dynamic plasmasphere

By establishing EMMA in 2012, the direct goal was to develop a ground-based plasmaspheric density monitoring system that can be run in real time. The plasma mass density monitoring is based on the detection of geomagnetic field line resonances by applying an improved phase gradient method on magnetic data recorded at closely separated (few hundred km) meridional station pairs. The inversion of the observed resonance frequencies are realized through the numerical solution of the MHD wave equation in a realistic magnetic field topology (Tsyganenko model), assuming a simple field-aligned density distribution. The monitoring system was developed by an international consortium in the frame of an EU funded FP7 project (PLASMON).

EMMA density estimates were used by Jorgensen et al. (2017) to improve the Dynamic Global Core Plasma Model (DGCPM), a plasmasphere model widely used by the space research community. DGCPM is a simple physical model where the quiet plasmasphere is filled from the underlying sunlit ionosphere and emptied into the dark ionosphere along magnetic field lines by diffusion. Geomagnetic storms occasionally deplete the outer plasmaspheric shells through the increased convection in the outer magnetosphere driven by the solar wind.
Comparison of observed and model values revealed that both the night time loss and daytime refilling rates in the original model are insufficiently low. By adjusting these global model parameters the model fitted the observations not only in the latitude range where the data were taken from but also deeper in the magnetosphere and even outside the plasmapause. The modification resulted in an order-of-magnitude faster daytime refilling and night time loss.

EMMA density data have been exploited for statistical studies, as well as for case studies on some special events. Del Corpo et al. (2018) derived an empirical density model based on 165 days of data, valid for the L=2.4-5.5 range and for a wide range of geomagnetic conditions.

Piersanti et al. (2017) investigated the effects of the 21 June 2015 coronal mass ejection (CMO) on the coupled terrestrial magnetosphere-plasmasphere-ionsophere system. The CMO triggered an intense geomagnetic storm on the following day causing a strong erosion (an order of magnitude at L=5.5) of the plasmasphere reaching as deep as L=2.5. Two erosion period separated by a day were identified. While for the first depletion, the recovery of the plasmasphere took place very fast, within a day, after the second erosion episode the refilling was much slower.

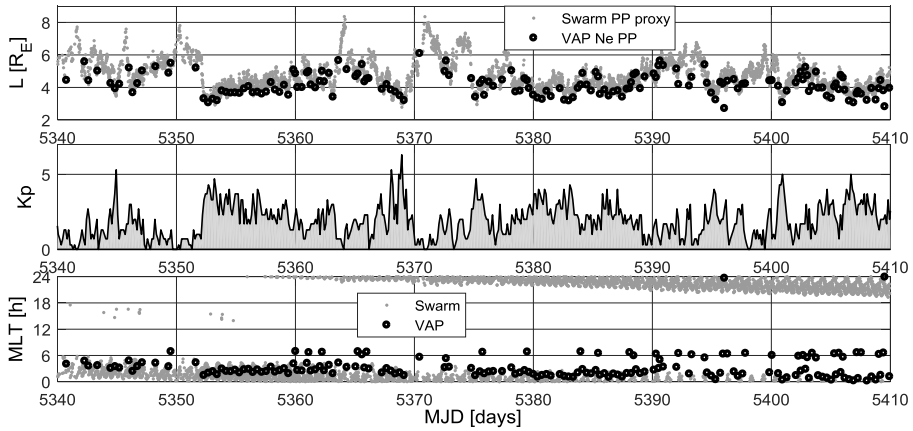

Figure 4 (top) Swarm PP proxies for 70 consecutive days and simultaneous VAP PP crossings (middle) time evolution of the Kp index (bottom) magnetic local time of the satellite observations

LEO satellites, albeit orbiting in the topside ionosphere, still can provide us with information on the dynamics of the plasmasphere. Heilig and Lühr (2013) showed that the termination latitude of nightside small-scale field-aligned currents observed by the CHAMP satellite is closely coincident with the ionospheric footprint of the plasmapause (PP). Based on this finding they developed a monitoring technique to follow the dynamics of the nightside PP. Heilig and Lühr (2018) applied the technique to the Swarm mission data. Their PP proxy was validated by in-situ observed Van Allen Probe electron densities. Figure 4 is an illustration of the validation process presenting 70 day of simultaneous Swarm PP proxy and in-situ PP crossings. A new finding of Heilig and Lühr (2018) was that the dayside PP position correlates with the delayed time history of the SSFAC boundary location. They attributed this behaviour to the result of the localized nightside formation of the new plasmapause and its corotation with the solid Earth. The new results pave the way toward an efficient PP monitoring tool based on an SSFAC index derived from vector magnetic field observations at low-Earth orbit.

4 Nonlinear analysis of spaceborne magnetic and geomagnetic time-series

The space and terrestrial magnetic observations exhibit signatures of deterministic nonlinear physical phenomena in the solar-terrestrial system. The plasma dynamics is governed by the equations of magnetohydrodynamics (MHD). Though the MHD description is deterministic, the dynamics of the plasma is completely unpredictable, if the magnetic Reynolds number, i.e. the ratio between the nonlinear and viscous terms of the momentum equation, is high. At high Reynolds number the flow is termed turbulent. The behaviour of turbulent dynamics can be revealed via statistical approach by using empirical observations of the multi-scale fluctuations. It is emphasized that the solar-system plasma is regarded as an excellent natural laboratory for studying MHD turbulence in collision-less environment extending to a quasi-infinite space.

The high Reynolds number in turbulent dynamics means the dissipation free cascade of energy transfer between consecutive spatial and temporal scales in the magnetohydrodinamic (MHD) scale range. It follows that the spectra of the physical properties of the plasma, like magnetic field, or plasma velocity, exhibit scale-free power-law behaviour with scaling exponent of -5/3 (Kolmogorov (K) scaling) or -3/2 (Iroshnikov-Kraichnan (IK) scaling). Additionally, the MHD equations show that the fluctuations of turbulent physical fields should exhibit self-similar, fractal character. However, most of the experimental studies of turbulence invalidate this conjecture and suggest that self-similarity appears only in local subsets of the turbulent space and the interwoven fractal subsets are ordered into a space possessing multifractal symmetry. Multifractality implies intermittent variations in the turbulent dynamics that exhibit non-Gaussian statistical features, thus the statistical description of the dynamics needs the knowledge of higher-order statistical moments of the fluctuating physical quantities.

4.1 Planetary magnetospheres and solar wind

Between 2013 and 2015 we have participated in the STORM EU FP7 consortial project (Echim et al. 2016). The main project's objectives were the systematic experimental investigation of energy cascade and dissipation processes, as well as of multiscale intermittent dynamics and anisotropies in the solar system plasma by using data of three main space missions, Cluster, Ulysses and Venus Express (VEX). Besides space data, we also analysed geomagnetic data recorded along the chain of meridional EMMA network (Del Corpo et al. 2018). The target regions of our studies were the solar wind, the different regions of Earth's magnetosphere (magnetosheath, cusp, plasma sheet, lobe) and the magnetosheath surrounding the induced magnetosphere of Venus. Magnetic and plasma time-series of the different regions were selected from the different space and geomagnetic data bases and compiled into systematic data catalogues. Our main contribution concerned the spectral, probability density function and high-order multifractal spectrum analyses of the time records. In order to ease the analyses of hundreds of time-series, we developed for the first time a routine for the automatic detection of power-law frequency and time-scale ranges of analysing functions, such

as frequency spectra or partition functions of multifractal spectrum analysis. Besides the study of solar system data, the STORM project also aimed at the development of a Matlab library of Integrated Nonlinear Analysis (INA) tools, along with an interface for its user-friendly application in data analysis. The tool is freely available for the space science community.

In this review, some of the scientific impact of the project is highlighted. Vörös et al. (2015) investigated the statistical parametric approach of multiscale solar wind processes composed of a mixture of corotating streams, corotating interaction regions, solar ejecta, discontinuities, and turbulence. The analysed data represented the plasma behaviour near the solar cycle minimum 2008. It was conjectured that the multiscale processes were best modelled by log-kappa distributions and the kappa parameter of the statistics was supposed to vary as the occurrence frequencies of multiplicative solar wind processes (stream/ejecta interactions, and consequently, in terms of the solar cycle. The turbulent dynamics of the solar wind was also studied be Teodorescu et al. (2015), who analysed the spectra of 156 slow and 48 fast stream solar wind magnetic time-series recorded by VEX at 0,72 AU. They argued that the spectra exhibited an inertial frequency range relying to dissipation-free energy cascade among the different turbulent scales. The statistical analyses of the obtained inertial range spectral slopes indicated that the spectra of slow wind were close to the Kolmogorov type of spectrum of fully-developed hydrodynamic turbulence. However, it was also stressed that the dynamics was anisotropic, thus the direct comparison between HD and slow solar wind was not reliable. Comparison with results of spectral analyses of Wind spacecraft data (Chen at al. 2013) showed that the slow wind spectra in the inertial range steepened between 0,72 and 1 AU that was an indication of the radial evolution of turbulence along the solar wind path. Interestingly, such finding was not observed for the fast streams of solar wind. The spectral slopes of the fast solar wind were, on average, closer to the slope of the Iroshnikov-Kraichnan spectrum, -1,5. Besides, the fast wind spectra exhibited more power in the transversal than compressional magnetic components. The two findings relied to the Alfvénic character of the fluctuations and the dominance of sheet-like structures in the formation of turbulence in the fast solar wind.

Venus Express was designed to study the atmosphere and ionosphere of Venus. However, along its orbit, the spacecraft also carries out particle and magnetic field measurements in the induced magnetosphere and magnetosheath regions of the planet. Dwivedi et al. (2015) have studied the spectral properties of Venusian magnetosheath time-series, with special consideration to their power-law scaling related to turbulent dynamics. The spectra have been analysed both in frequency and wave number domains, by considering the validity of the Taylor hypothesis. By using the automated routine (see above) compiled to identify scaling regions and slope of the spectra, it was shown that Venusian magnetosheath spectra exhibited dominantly three scaling regions, the middle of which indicated fully developed plasma turbulence with spectral exponent close to -1.6. The upper limit of the turbulent scaling range was close to the ion cyclotron frequency. Similar analysis was carried out for the Earth' magnetosheath by using 337 time-series recorded by the Cluster mission (Echim et al. 2018). Contrary to the Venusian spectra, the Kolmogorov type of scaling was apparently missing in the spectra of the terrestrial magnetosheath. For the explanation of the different observations, it was suggested that in front of the induced magnetosphere of Venus the bow shock represents a weaker barrier towards the solar wind than for the case of Earth possessing an intrinsic magnetosphere. Therefore, the turbulent properties of the solar wind dynamics can penetrate into the Venusian magnetosheath, while at the terrestrial bow shock the solar wind develops into a completely new dynamical structure. It was also conjectured that the limited spatial extension of the magnetosheath hinders the appearance of fully developed turbulence in the new dynamical regime.

The dynamical properties of the terrestrial magnetosphere and its relation to the solar wind driver was further investigated via the systematic nonlinear analysis of 1 Hz sampling frequency geomagnetic data recorded in eight observatories (Kilpisjärvi, Sodankylä, Hankasalami, Nurmijärvi, Tartu, Belsk, Tihany, L'Aquila) of the chain of meridional EMMA network (Del Corpo et al. 2018). The analyses concerned one year long X component time-series from the years of solar maximum (2001, 2002, 2003) and solar minimum (2007, 2008). The probability density function analyses proved that the time-series exhibited non-Gaussian intermittent fluctuations in the time-scale range

of 1-2000 sec., i.e. in the typical range of geomagnetic substroms. This range was independent from the geomagnetic latitude, but the level of intermittency exhibited a decreasing trend from the polar region towards the mid-latitudes. The solar cycle dependence of the intermittency level was also obvious, that is, the time-series were, in average, more intermittent during solar maximum than minimum years. This finding was confirmed by the results of higher-order structure function analyses. The statistical analyses of power-spectral density function of the time-series also proved a scaling region in the scales of substroms relying to turbulent energy cascade processes in the magnetosphere. Note that the spectral exponents were different from the K or IK scaling for the cases of all observatories.

4.2 Nonlinear analysis of Swarm mission data

A statistical analysis was carried out on the high-resolution (50 Hz) vector field magnetic (VFM) time records of Swarm spacecraft triplet in order to discriminate between Gaussian and non-Gaussian magnetic fluctuations in the ionosphere at two altitudes, 460 km (Swarm-C) and 530 km (Swarm-B) (Kovács et al. 2018). We applied probability density function (PDF) analysis of incremental magnetic field time-series of the individual Swarm records. Non-Gaussian behaviour of the difference time-series could reveal multiscale intermittent magnetic fluctuation in the studied plasma region. The level of intermittent dynamics was measured by the fourth statistical moments of the incremental time-series, i.e. by their flatness. Our aim was to investigate the variation of the flatness parameter in terms of the positions of the Swarm spacecraft. Swarm data from the years between 2014 and 2016 were analysed by a sliding-window method, and the spatial distribution of the mean flatness values were mapped in terms of geomagnetic coordinates. The magnetic field recorded in spacecraft frame was transformed to mean-field aligned (MFA) system so that the intermittent behaviour of the compressional and transversal fields could be separately investigated. It was shown that the transversal field exhibited the strongest intermittency in the auroral oval, presumably due to the magnetic effect of intensive field-aligned currents. This conjecture was confirmed by the finding that the geomagnetic latitude of the most intermittent region fluctuated in terms of the geomagnetic activity, that is, it moved towards the equator during disturbed period and vice versa. On the other hand, for the case of the mean-field aligned (i.e. compressional) magnetic variations the most intermittent region was found at around +-10° from the dip equator (Figure 5.). It was argued that the equatorial intermittent events corresponded to ionospheric plasma irregularities, such as equatorial spread F (ESF) events or substorm induced pulsations (Burke et al. 2004).

5 The environment of comet 67P/Churyumov-Gerasimenko

The Rosetta spacecraft of ESA performed the first ever orbital insertion and landing on a comet in 2014. Between August 2014 and September 2016, the orbiter was continuously measuring different parameters in the environment surrounding the nucleus of the comet. It followed the variation of the activity from its very beginning to its maximum and through the declining phase observing the properties and interactions of the gas, dust, plasma and electromagnetic fields in the coma.

Until the beginning of 2015, the spacecraft observed a low activity comet with a tenuous neutral atmosphere and relatively few dust grains around it. The solar wind reached the spacecraft orbiting in the inner regions of the induced magnetosphere, and probably also reached the nucleus. The interaction of the solar wind with the cometary matter caused solar wind deflection, acceleration of cometary ions and electrons as well as some instabilities generating persistent low frequency waves near the comet. The team of the Rosetta Plasma Consortium (including researchers of the Wigner RCP) presented the first results about this unique environment in several scientific papers (Nilsson et al. 2015a, Richter et al. 2015, Edberg et al. 2015).

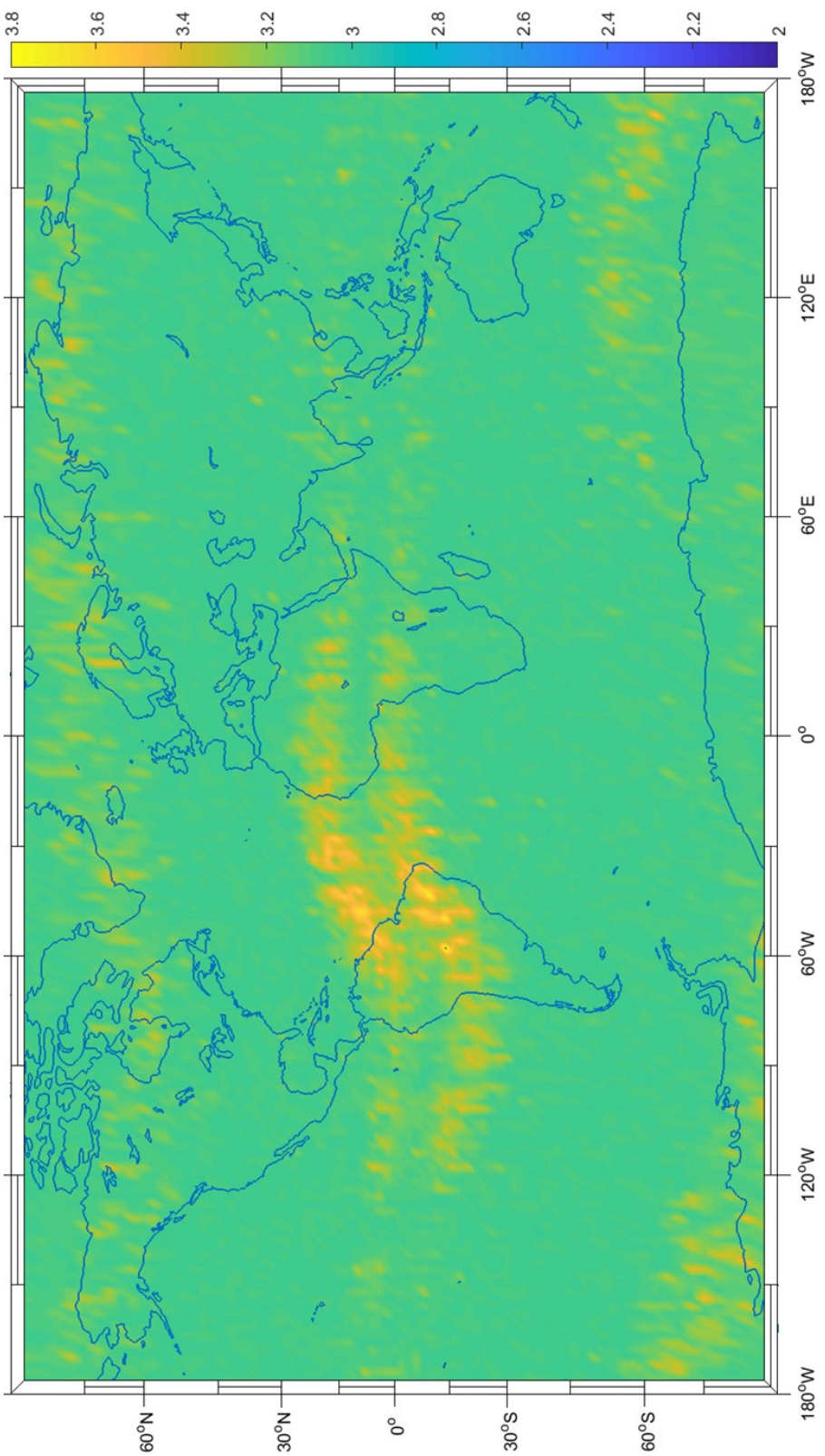

Figure 5. Global spatial distribution of nonlinear intermittent magnetic events observed in the B_z mean-field aligned longitudinal magnetic record of the SWARM-C spacecraft. The colours represent the mean flatness values obtained for the SWARM magnetic records in 1°×1° latitude and longitude grid

Later in 2015 the density of the cometary plasma increased and this plasma expelled the solar wind out of the inner magnetosphere (Nilsson et al. 2015b). Strange ion events occurred frequently during this period, in which the measured ion energy first increased then decreased. Near the perihelion of comet 67P/Churyumov-Gerasimenko in August 2015 the cometary activity reached its maximum. Most accelerated ion events disappeared and the spacecraft observed a calmer inner region. During this period Rosetta discovered the diamagnetic cavity of the comet: a region around the nucleus, from which the strong cometary activity 'blows away' the magnetic field – a phenomenon observed earlier once at comet 1P/Halley (Goetz et al. 2016). Nemeth et al. (2016a) developed a method to find diamagnetic cavity crossing events on a magnetically dirty spacecraft, where residual fields render the usual methods very difficult. Using this method, more than a hundred cavity crossing events were detected and an 'event database' was set up. Nemeth et al. (2016a) analyzed these events, revealed and explained the plasma signatures accompanying the crossing of the cavity boundary, described the probable shape of the cavity. It was shown that an old model – refined and with proper input parameters – provides a good fit for the average extent of the cavity. The diamagnetic cavity boundary distance around Comet 67P/Churyumov-Gerasimenko was calculated using various methods. Timar et al. (2017) found that the global outgassing rate determines the position of the boundary with local pressure variations being suppressed, while the rapid changes in the external solar wind pressure at the position of the comet can explain the intermittent nature of the cavity crossing events.

After more than 2 years in orbit around comet 67P/Churyumov-Gerasimenko, the Rosetta spacecraft provided sufficient information about the plasma environment in order to separate temporal and spatial effects. Several papers discussed the different plasma regions and boundaries including the mass-loading effect, the induced magnetosphere, and the innermost diamagnetic cavity (Mandt et al. 2016, Madanian et al. 2017, Henri et al. 2017, Hajra et al. 2018).

Behar et al. (2016) investigated the interaction of the solar wind with the cometary plasma, and found several relationships between the angular distributions of the interacting plasma populations. Egberg et al. (2016) studied the response of the cometary environment to the arrival of abrupt solar wind disturbances. Broiles et al. (2016) analyzed suprathermal electron drivers at the comet, Volwerk et al. (2016) studied the magnetic pile-up and mirror-mode waves.

The Grain Impact Analyzer and Dust Accumulator (GIADA) instrument on board Rosetta was able to constrain the origin of the dust particles detected within the coma of comet 67P/Churyumov–Gerasimenko (Fulle et al. 2015). The collected particles belong to two families:

(i) compact particles (ranging in size from 0.03 to 1 mm), witnessing the presence of materials that underwent processing within the solar nebula and

(ii) fluffy aggregates (ranging in size from 0.2 to 2.5 mm) of sub-micron grains that may be a record of a primitive component, probably linked to interstellar dust. The dynamics of the fluffy aggregates constrain their equivalent bulk density to <1 kg/m3. These aggregates are charged, fragmented, and decelerated by the spacecraft negative potential and enter GIADA in showers of fragments at speeds <1 m/s. The density of such optically thick aggregates is consistent with the low bulk density of the nucleus. The mass contribution of the fluffy aggregates to the refractory component of the nucleus is negligible and their coma brightness contribution is less than 15%.

6 The plasma environment of the Earth

The four identically equipped Cluster spacecraft of the European Space Agency have been studying the small-scale spatial and temporal characteristics of the terrestrial plasma environment in three dimensions since February 2001. Processes of different scales can be studied by changing the separation distances between the spacecraft. As the originally polar orbit is evolving, different regions of the terrestrial plasma environment can be studied which were not sampled earlier in the mission. The Cluster mission is now extended until the end of 2020.

The Hungarian Data Centre (operated by the Wigner RCP) (http://hdc.rmki.kfki.hu/cdms/) is preparing the Auxiliary parameters for the Cluster Science Data System and for the Cluster Science Archive (http://cosmos.esa.int/web/csa/) which has been the public interface of the mission since November 2013. The archive provides online access to high quality, validated, high-resolution data from the Cluster instruments together with auxiliary and support data products.

7 The plasma environment of Venus as a function of the solar wind variations

Venus is an unmagnetized planet with a thick atmosphere and important ionosphere. As a result of its interaction with the solar wind, there is an induced magnetosphere, which is trivially highly sensitive on solar wind variations. These interactions were studied based on observations from the Venus Express spacecraft. Vech et al. (2015) performed a statistical study on the interaction between interplanetary coronal mass ejections (ICMEs) and the induced magnetosphere of Venus, where the solar wind parameters, the position of the bow shock, the size and plasma properties of the magnetic barrier, and the position of the ion composition boundary (ICB) were analyzed. When the interaction between magnetic clouds and the induced magnetosphere of Venus was observed, the small magnetosonic Mach numbers inside the magnetic clouds caused the bow shock to appear at anomalously large distances from the planet. The position of the ICB on the nightside was found closer to the planet during ICME passages which is attributed to the increased solar wind dynamic pressure.

Vech et al. (2016) presented the first statistical analysis on the effects of heliospheric current sheet crossings on the induced magnetosphere of Venus. These events are of particular interest because they lead to the reconfiguration of the induced magnetosphere with opposite polarity. A statistical approach was performed in order to study the spatial distribution of the heavy ion flux measurements in the plasma environment of Venus. The average and median heavy ion flux measurements are compared before and after the polarity reversal events. The results show that after the events the average and median heavy ion fluxes in the magnetotail are reduced. Even if a passage of a current sheet is a short time scale event lasting about 10 min, its effect on the near-Venus plasma environment lasts for a few hours. The conclusion is that the observations show similarities to comet studies and the polarity reversal of the induced magnetosphere might be accompanied by dayside reconnection and magnetic disconnection of the plasma tail from the planetary ionosphere.

8 The environment of Saturn and Jupiter

Nemeth et al. (2015) used numerical ion velocity moments derived from the measurements of the Cassini Plasma Spectrometer to reveal the latitudinal structure of the nightside outer magnetosphere of Saturn. It turns out that the magnetosphere consists of shells rotating with different velocities; the innermost shell is rotating with the highest speed and the speed is decreasing as moving outward.

Szego et al. (2015) was taking a leading part in a review of the magnetodiscs and aurorae of giant planets. The magnetodisc is a complex magnetized plasma phenomenon, which influences almost every property of the magnetospheres of Jupiter and Saturn. Based on the observations of the Cassini spacecraft, the magnetodisc of Saturn was studied. Nemeth et al. (2016b) found that the complex time dependence of the magnetic and plasma measurements in the vicinity of the magnetodisc can be simultaneously explained by a simple model, which takes into account the planetary period oscillations (PPO) of the magnetodisc and the position of the spacecraft relative to the central sheet of the magnetodisc.

The Cassini spacecraft detected rock nanograin dust particles in the Kronian system. Based on an extensive, four-year analysis of data from the spacecraft, combined with computer simulations and laboratory experiments, Hsu et al. (2015) concluded that the tiny dust particles most likely form when hot water containing dissolved minerals from the moon's rocky interior travels upward, coming into contact with cooler water. It is exciting that these tiny grains of rock, spewed into space

by geysers on Enceladus can tell us about the conditions on - and beneath - the ocean floor of an icy moon in the Kronian system.

Using Cassini observations, the orbital evolution of E-ring dust particles was followed through their entire lifetime, starting from moon Enceladus, and ending in: a) a collision with the A-ring or any of the satellites; or b) losing all their mass due to sputtering; or c) leave the magnetosphere of Saturn. Using an updated version of the model of Juhász and Horányi (2002) and Juhász et al. (2007) by including a noon-midnight electric field in the magnetosphere and a refined asymmetric plasma model, the deposition rates and maps of E-ring particles were calculated to surfaces of the moons of Saturn. The active geysers in the south polar region of Enceladus are sources of dust particles that sustain the vast E-ring of Saturn, extending out beyond Titan at 20 Saturn radii. The dynamics of the small micron and submicron particles escaping from Enceladus is primarily set by Saturn's gravity, plasma drag, radiation pressure, and electromagnetic forces. Simulations were developed to follow different sized (0.1-5 micron) dust particles from Enceladus till their ultimate demise: being ejected from Saturn's magnetosphere, or hitting one of its moons. The expected size, speed, and spatial distributions of the impacting particles were determined and their predicted anisotropies were identified when bombarding the leading/trailing hemispheres of the moons, possibly offering an explanation for their observed brightness features (Kempf et al. 2018).

References

Behar E, Nilsson H, Wieser Stenberg G, Nemeth Z, Broiles TW, Richter I (2016): Mass loading at 67P/Churyumov-Gerasimenko: A case study. Geophys. Res. Letters, 43(4), 1411-1418, doi: 10.1002/2015GL067436.

Broiles TW, Burch JL, Chae K, Clark G, Cravens TE, Eriksson A, Fuselier SA, Frahm RA, Gasc S, Goldstein R, Henri P, Koenders C, Livadiotis G, Mandt KE, Mokashi P, Nemeth Z, Odelstad E, Rubin M, Samara M (2016): Statistical analysis of suprathermal electron drivers at 67P/Churyumov–Gerasimenko. MNRAS, 462 (Suppl_1), S312-S322, doi: 10.1093/mnras/stw2942.

Burke WJ, Gentile LC, Huang CY, Valladares CE, Su SY (2004): Longitudinal variability of equatorial plasma bubbles observed by DMSP and Rocsat-1. J. Geophys. Res., 109, A12301.

Chen CHK, Bale SD, Salem CS, Maruca BA (2013): Residual energy spectrum of solar wind turbulence. The Astrophysical Journal, 770:125, doi:10.1088/0004-637X/770/2/125.

CLIC and CLICdp collaborations (2018): The Compact Linear e+e- Collider (CLIC) Summary Report., CERN Yellow Reports: Monographs 2/2018, Geneva, 2018, 112 p, CERN-2018-005-M, ISBN: 978–92–9083–506–6, ISSN: 2519-8068, doi: 10.23731/CYRM-2018-002.

Del Corpo A, Vellante M, Heilig B, Pietropaolo E, Reda J, Lichtenberger J (2018): Observing the cold plasma in the Earth's magnetosphere with the EMMA network. Annals of Geophyisics 61, doi: 10.4401/ag-7751.

Echim M. and the FP7 STORM Team (2016): Solar system plasma Turbulence: Observations, inteRmittency and Multifractals. EGU General Assembly 2016, Geophysical Research Abstracts, 18 EGU2016-13412-2.

Echim M, Kovacs P, Dwivedi NK, Yordanova E, Teodorescu E (2018): Comparative statistical analysis of magnetosheath turbulence/variability at Venus and Earth. 15th European Space Weather Week, November 5-9, Leuven, Belgium.

Dwivedi NK, Schmid D, Narita Y, Kovács P, Vörös Z, Delva M, Zhang T (2015): Statistical investigation on the power-law behavior of magnetic fluctuations in the Venusian magnetosheat. Earth, Planets and Space, 67(137), doi:10.1186/s40623-015-0308-x.

Edberg NJT, Eriksson AI, Odelstad E, Henri P, Lebreton J-P, Gasc S, Rubin M, André M, Gill R, Johansson EPG, Johansson F, Vigren E, Wahlund JE, Carr CM, Cupido E, Glassmeier K-H, Goldstein R, Koenders C, Mandt K, Nemeth Z, Nilsson H, Richter I, Wieser GS, Szego K, Volwerk M (2015): Spatial distribution of low-energy plasma around comet 67P/CG from Rosetta measurements. Geophys. Res. Letters, 42(11), 4263-4269, doi: 10.1002/2015GL064233.

Edberg NJT, Eriksson AI, Odelstad E, Vigren E, Andrews DJ, Johansson F, Burch JL, Carr CM, Cupido E, Glassmeier K-H, Goldstein R, Halekas JS, Henri P, Koenders C, Mandt K, Mokashi P, Nemeth Z, Nilsson H, Ramstad R, Richter I, Wieser Stenberg G (2016): Solar wind interaction with comet 67P: Impacts of corotating interaction regions. J. Geophys. Res. Space Phys., 121(2), 949-965, doi: 10.1002/2015JA022147.

Fulle M, Corte VD, Rotundi A, Weissman P, Juhasz A, Szego K, Sordini R, Ferrari M, Ivanovski S, Lucarelli F, Accolla M, Merouane S, Zakharov V, Epifani EM, López-Moreno JJ, Rodríguez J, Colangeli L, Palumbo P, Grün E, Hilchenbach M, Bussoletti E, Esposito F, Green SF, Lamy PL, McDonnell JAM, Mennella V, Molina A, Morales R, Moreno F, Ortiz JL, Palomba E, Rodrigo R, Zarnecki JC, Cosi M, Giovane F, Gustafson B, Herranz ML, Jerónimo JM, Leese MR, López-Jiménez AC, Altobelli N (2015): Density and charge of pristine fluffy particles from comet 67P/Churyumov–Gerasimenko. Astrophys. J. Letters 802(1) Paper L12.

Goetz C, Koenders C, Richter I, Altwegg K, Burch J, Carr C, Cupido E, Eriksson A, Güttler C, Henri P, Mokashi P, Nemeth Z, Nilsson H, Rubin M, Sierks H, Tsurutani B, Vallat C, Volwerk M, Glassmeier K-H (2016): First detection of a diamagnetic cavity at comet 67P/Churyumov-Gerasimenko. Astronomy & Astrophysics 588, A24, 6, doi: 10.1051/0004-6361/201527728.

Gokani, SA, Singh R, Cohen MB, Kumar S, Venkatesham K, Maurya AK, Selvakumaran R, Lichtenberger J (2015), Very low latitude (L = 1.08) whistlers and correlation with lightning activity. J. Geophys. Res. Space Physics 120, 6694–6706, doi:10.1002/ 2015JA021058.

Hajra R , Henri P, Vallieres X, More J, Gilet N, Wattieaux G, Goetz C, Richter I, Tsurutani BT, Gunell H, Nilsson H, Eriksson AI, Nemeth Z, Burch JL, Rubin M (2018): Dynamic unmagnetized plasma in the diamagnetic cavity around comet 67P/Churyumov-Gerasimenko. MNRAS, 475(3), 4140-4147.

Han DS, Iyemori T, Nose M, McCreadie H, Gao Y, Yang F, Yamashita S, Stauning P (2004): A comparative analysis of low-latitude Pi 2 pulsations observed by Oersted and ground stations. J. Geophys. Res., 109, A10209.

Heilig B, Lühr H (2013): New plasmapause model derived from CHAMP field-aligned current signatures. Ann. Geophys, 31, 529-539, doi:10.5194/angeo-31-529-2013.

Heilig B, Lühr H (2018): Quantifying the relationship between the plasmapause and the inner boundary of small-scale field-aligned currents, as deduced from Swarm observations. Ann. Geophys., 36, 595-607, doi: 10.5194/angeo-36-595-2018.

Heilig B, Sutcliffe PR (2016): Coherence and phase structure of compressional ULF waves at low-Earth-orbit observed by the Swarm satellites. Geophys. Res. Let. 43, 945-951, doi:10.1002/2015GL067199.

Heilig B, Beggan C, Lichtenberger J (2018): Natural sources of geomagnetic field variations. CERN, Geneva, CERN-ACC-2018-0033, CLIC-Note-1083, 16, 10 Oct 2018, cds.cern.ch/record/2643499.

Heilig B, Lühr H, Rother M (2007): Comprehensive study of ULF upstream waves observed in the topside ionosphere by CHAMP and on the ground. Ann. Geophys., 25, 737–754.

Heilig B, Sutcliffe PR, Ndiitwani DC, Collier AB (2013): Statistical study of geomagnetic field line resonances observed by CHAMP and on the ground. J. Geophys. Res., 118, 1934-1947.

Henri P, Vallières X, Hajra R, Goetz C, Richter I, Glassmeier K-H, Galand M, Rubin M, Eriksson AI, Nemeth Z, Vigren E, Beth A, Burch J, Carr C, Nilsson H, Tsurutani B, Wattieaux G (2017): Diamagnetic region(s): structure of the unmagnetized plasma around Comet 67P/CG. MNRAS, 469, S372-S379.

Hsu H-W, Postberg F, Sekine Y, Shibuya T, Kempf S, Horányi M, Juhász A, Altobelli N, Suzuki K, Masaki Y, Kuwatani T, Tachibana S, Sirono S-I, Moragas-Klostermeyer G, Srama R (2015): Ongoing hydrothermal activities within Enceladus. Nature, 519(7542), 207-210.

Jorgensen AM, Heilig B, Vellante M, Lichtenberger J, Reda J, Valach F, Mandic I (2017): Comparing the Dynamic Global Core Plasma Model (DGCPM) With Ground-Based Plasma Mass Density Observations. J. Geophys. Res. Space Physics, 121, doi:10.1002/2016JA023229.

Juhász A, Horányi M (2002): Saturn's E ring: A dynamical approach. J. Geophys. Res. Space Phys., 107(A6), 1066, p. 10, doi:10.1029/2001JA000182.

Juhász A, Horányi M, Morfill GE (2007): Signatures of Enceladus in Saturn's E ring. Geophys. Res. Letters, 34(9), L09104, p. 5, doi: 10.1029/2006GL029120.

Kempf S, Horányi M, Hsu HW, Hill TW, Juhász A, **Smith HT** (2018): Saturn's Diffuse E Ring and Its Connection With Enceladus. In Schenk et al. (Eds.), Enceladus and the Icy Moons of Saturn, 195-210, Univ. Arizona Press, Tucson.

Koronczay D, Lichtenberger J, Juhász L, Steinbach P, Hospodarsky GB (2018). VLF transmitters as tools for monitoring the plasmasphere. Journal of Geophysical Research: Space Physics 123. doi:10.1029/2018JA025802.

Kovács P, Heilig B, Vadász G, Koppán A, Echim M (2015): Study of intermittent dynamics in the geomagnetic fluctuations of different geomagnetic latitudes. 26th IUGG General Assembly, Prague, June 22 – July 2.

Kovacs P, Heilig B, Echim M, Koppan A (2018): Study of spatial distribution of nonlinear anomalous magnetic fluctuations along the orbit of the Swarm spacecraft. EGU General Assembly 2018, Geophysical Research Abstracts, 20, EGU2018-14128, 2018.

Lichtenberger J, Clilverd M, Heilig B, Vellante M, Manninen J, Rodger C, Collier A, Jørgensen A, Reda J, Holzworth R, Friedel R (2013): The plasmasphere during a space weather event: first results from the PLASMON project. J. Space Weather Space Clim. 3, A23.

Madanian H, Cravens TE, Burch J, Goldstein R, Rubin M, Nemeth Z, Goetz C, Koenders C, Altwegg K (2017): Plasma environment around comet 67P/Churyumov-Gerasimenko at perihelion: model comparison with Rosetta data. Astronomical Journal, 153(1), 30, p. 10.

Mandić I, Vujić E, Heilig B, Pelajić I, Herak D (2016): Recent efforts toward the establishment of the Lonjsko Polje Geomagnetic Observatory. Acta Geophysica 64, 1311-1339, doi: 10.1515/acgeo-2016-0051.

Mandt KE, Eriksson A, Edberg NJT, Koenders C, Broiles CT, Fuselier SA, Henri P, Nemeth Z, Alho M, Biver N, Beth A, Burch J, Carr C, Chae K, Coates AJ, Cupido E, Galand M, Glassmeier K-H, Goetz C, Goldstein R, Hansen KC, Haiducek J, Kallio E, Lebreton J-P, Luspay-Kuti A, Mokashi P, Nilsson H, Opitz A, Richter I, Samara M, Szego K, Tzou C-Y,Volwerk M, Simon Wedlund C, Stenberg Wieser G (2016): RPC observation of the development and evolution of plasma interaction boundaries at 67P/Churyumov-Gerasimenko. MNRAS, 462 (Suppl_1), S9-S22, doi: 10.1093/mnras/stw1736.

Nagy M, Steinbach P, Lichtenberger J (2018)**:** What are the Source of MF Signatures Recorded on DEMETER Satellite? 2018 2nd URSI Atlantic Radio Science Meeting (AT-RASC), Meloneras, 2018, 1-4. doi: 10.23919/URSI-AT-RASC.2018.8471630.

Nakariakov V, Pilipenko VA, Heilig B, Jelínek P, Karlický M, Klimushkin DY, Kolotkov DY, Lee DH, Nisticò G, Van Doorsselaere T, Verth G, Zimovets IV (2016): Magnetohydrodynamic Oscillations in the Solar Corona and Ultra-Low Frequency Oscillations in the Earth's Magnetosphere: Towards Consolidated Understanding. Space Science Reviews 200, 75-203, doi: 10.1007/s11214-015-0233-0.

Ndiitwani DC, Sutcliffe PR (2009): The structure of low-latitude Pc3 pulsations observed by 587 CHAMP and on the ground. Ann. Geophys., 27, 1267– 1277.

Ndiitwani DC, Sutcliffe PR (2010): A study of L-dependent Pc3 pulsations observed by low Earth orbiting CHAMP satellite. Ann. Geophys., 28, 407–414.

Nemeth Z, Szego K, Foldy L, Kivelson MG, Jia X, Ramer KM, Cowley SWH, Provan G, Thomsen M (2015): The latitudinal structure of the nightside outer magnetosphere of Saturn as revealed by velocity moments of thermal ions. Annales Geophys., 33(9), 1195-1202, doi: 10.5194/angeo-33-1195-2015.

Nemeth Z, Burch J, Goetz C, Goldstein R, Henri P, Koenders C, Madanian H, Mandt K, Mokashi P, Richter I, Timar A, Szego K (2016a): Charged particle signatures of the diamagnetic cavity of comet 67P/Churyumov–Gerasimenko. MNRAS, 462 (Suppl_1), S415-S421, doi: 10.1093/mnras/stw3028.

Nemeth Z, Szego K, Foldy L, Cowley SWH, Provan G, Thomsen M (2016b): Periodic motion of the magnetodisk as a cause of quasi-periodic variations in the Kronian magnetosphere. Planet. Space Sci., 130(1), 54-59.

Nilsson H, Stenberg WG, Behar E, Wedlund CS, Gunell H, Yamauchi M, Lundin R, Barabash S, Wieser M, Carr C, Cupido E, Burch JL, Fedorov A, Sauvaud JA, Koskinen H, Kallio E, Lebreton JP, Eriksson A, Edberg N, Goldstein R, Henri P, Koenders C, Mokashi P, Nemeth Z, Richter I, Szego K, Volwerk M, Vallat C, Rubin M (2015a): Cometary science. Birth of a comet magnetosphere: a spring of water ions. Science, 347(6220), paper id: aaa0571, 5 pp.

Nilsson H, Stenberg Wieser G, Behar E, Simon Wedlund C, Kallio E, Gunell H, Edberg NJT, Eriksson AI, Yamauchi M, Koenders C, Wieser M, Lundin R, Barabash S, Mandt K, Burch JL, Goldstein R, Mokashi P, Carr C, Cupido E, Fox PT, Szego K, Nemeth Z, Fedorov A, Sauvaud J-A, Koskinen H, Richter I, Lebreton J-P, Henri P, Volwerk M, Vallat C, Geiger B (2015b): Evolution of the ion environment of comet 67P/Churyumov-Gerasimenko: Observations between 3.6 and 2.0 AU. Astronomy & Astrophysics, 583, A20, 8 pp, doi:10.1051/0004-6361/201526142.

Park J, Lühr H, Rauberg J (2013): Global characteristics of Pc1 magnetic pulsations during solar cycle 23 deduced from CHAMP data. Ann. Geophys., 31, 1507–1520.

Piersanti M, Alberti T, Bemporad A, Berrilli F, Bruno R, Capparelli V, Carbone V, Consolini G, Cristaldi A, Del Corpo A, Del Moro D, Di Matteo S, Ermolli I, Fineschi S, Giannattasio F, Giorgi F, Giovannelli L, Guglielmino SL, Laurenza M, Le Preti F, Marcucci FM, Martucci M, Merge' M, Pietropaolo E, Romano P, Sparvoli R, Stangalini M, Vecchio A, Vellante M, Villante U, Zuccarello F, Heilig B, Reda J, Lichtenberger J (2017): Comprehensive Sun-to-Earth analysis of the Geoeffective Solar event of June 21, 2015: Effects on the Magnetosphere - Plasmasphere - Ionosphere system. Sol. Phys. 292, 169, doi: 10.1007/s11207-017-1186-0.

Pilipenko VA, Heilig B (2016): ULF waves and transients in the topside ionosphere, A. Keiling, D.H. Lee, V. Nakariakov (eds.). Low-frequency waves in space plasmas (AGU Geophysical Monograph Series 216), Wiley, 15-29, doi: 10.1002/9781119055006.

Pilipenko V, Fedorov E, Heilig B, Engebretson MJ (2008): Structure of ULF Pc3 waves at low altitudes. J. Geophys. Res., 113, A11208, doi:10.1029/2008JA013243.

Richter I, Koenders C, Auster HU, Fruhauff D, Gotz C, Heinisch P, Perschke C, Motschmann U, Stoll B, Altwegg K, Burch J, Carr C, Cupido E, Eriksson A, Henri P, Goldstein R, Lebreton JP, Mokashi P, Nemeth Z, Nilsson H, Rubin M, Szego K, Tsurutani BT, Vallat C, Volwerk M, Glassmeier K-H (2015): Observation of a new type of low-frequency waves at comet 67P/Churyumov-Gerasimenko. Annales Geophys., 33(8), 1031-1036, doi: 10.5194/angeo-33-1037-2015.

Singh A, Verma P, Singh R, Lichtenberger J (2015). Remote sensing of D-region ionosphere using multimode tweeks. Indian Journal of Physics, 90, 1-7. 10.1007/s12648-015-0727-3.

Sutcliffe PR, Heilig B (2016): Comparison of ULF wave studies using Swarm and CHAMP magnetic field data. In European Space Agency, (Special Publication) ESA SP (Vol. SP-740). European Space Agency.

Sutcliffe PR, Lühr H (2003): A comparison of Pi2 pulsations observed by CHAMP in low Earth orbit and on the ground at low latitudes. Geophys. Res. Lett., 30, 2105, doi:10.1029/2003GL018270.

Sutcliffe PR, Lühr H (2010): A search for dayside geomagnetic Pi2 pulsations in the CHAMP low-Earth-orbit data. J. Geophys. Res., 115, A05205, doi:10.1029/2009JA014757.

Szego K, Achilleos N, Arridge C, Badman S, Delamere P, Grodent D, Kivelson MG, Louarn P (Eds.) (2016): The Magnetodiscs and Aurorae of Giant Planets. Space Sciences Series of ISSI, 50. New York: Springer Verlag, ISBN:978-1-4939-3394-5.

Takahashi K, Hartinger MD, Vellante M, Heilig B, Lysak R, Lee DH, **Smith ChW** (2018): Roles of Flow Braking, Plasmaspheric Virtual Resonances, and Ionospheric Currents in Producing Ground Pi2 Pulsations. J. Geophys. Res. Space Physics, 123, doi: 10.1029/2018JA025664.

Teodorescu E, Echim M, Munteanu C, Zhang T, Bruno R, Kovacs P (2015): Inertial Range Turbulence of Fast and Slow Solar Wind at 0.72 AU and Solar Minimum. The Astrophysical Journal Letters, 804:L4,. doi:10.1088/2041-8205/804/2/L41.

Timar A, Nemeth Z, Szego K, Dosa M, Opitz A, Madanian H, Goetz C, Richter I (2017): Modelling the size of the very dynamic diamagnetic cavity of comet 67P/Churyumov–Gerasimenko. MNRAS, 469 (Suppl_2), S723-S730, doi: 10.1093/mnras/stw2628.

Vech D, Szego K, Opitz A, Kajdic P, Fraenz M, Kallio E, Alho M (2015): Planetary space weather effects on the bow shock, magnetic barrier, and the ion composition boundary at Venus. J. Geophys. Res. Space Phys., 120(6), 4613-4627, doi: 10.1002/2014JA020782.

Vech D, Stenberg G, Nilsson H, Edberg N, Opitz A, Szego K, Zhang T, Futaana Y (2016): Statistical features of the global polarity reversal of the Venusian induced magnetosphere in response to the polarity change in IMF. J. Geophys. Res. Space Phys., 121(5), 3951-3962, doi: 10.1002/2015JA021995.

Vellante M et al. (2004): Ground/satellite signatures of field line resonance: A test of theoretical predictions. J. Geophys. Res., 109, A06210, doi:10.1029/2004JA010392.

Volwerk M, Richter I, Tsurutani B, Götz C, Altwegg K, Broiles T, Burch J, Carr C, Cupido E, Delva M, Dósa M, Edberg NJT, Eriksson A, Henri P, Koenders C, Lebreton J-P, Mandt KE, Nilsson H, Opitz A, Rubin M, Schwingenschuh K, Stenberg Wieser G, Szego K, Vallat C, Vallieres X, Glassmeier K-H (2016): Mass-loading, pile-up, and mirror-mode waves at comet 67P/Churyumov-Gerasimenko. Annales Geophys., 34(1), 1-15, doi: 10.5194/angeo-34-1-2016.

Vörös Z, Leitner M, Narita Y, Consolini G, Kovács P, Tóth A, Lichtenberger J (2015): Probability density functions for the variable solar wind near the solar cycle minimum. Journal of Geophysical Research, 120(8), 6152-6166, doi: 10.1002/2015JA021257.

Yagova N, Heilig B, Fedorov E (2015): Pc2-3 geomagnetic pulsations on the ground, in the ionosphere, and in the magnetosphere: MM100, CHAMP, and THEMIS observations. Ann. Geophys., 33, 117–128.

Yagova NV, Heilig B, Pilipenko VA, Yoshikawa A, Nosikova NS, Yumoto K, Reda J (2017): Nighttime Pc3 pulsations: MM100 and MAGDAS observations. Earth, Planets and Space 69, 61, doi:10.1186/s40623-017-0647-x.

Yamamoto K, Nosé M, Kasahara S, Yokota S, Keika K, Matsuoka A, Teramoto M, Takahashi K, Nomura R, Vellante M, Heilig B, Fujimoto A, Tanaka Y, Shinohara M, Shinohara I, Miyoshi Y (2018): Giant pulsations excited by steep radial gradient of phase space density of proton: Arase observation. Geophys. Res. Lett., 45. doi: 10.1029/2018GL078293.

HUNGARIAN CONTRIBUTION TO THE RESEARCH OF SOLAR WIND AND INTERPLANETARY MAGNETIC FIELD PHENOMENA (2015-2018) - IAGA DIVISION IV: SOLAR WIND AND INTERPLANETARY FIELD

Árpád Kis[*], Melinda Dósa[**], Géza Erdős[**], Antal Juhász[**], Károly Kecskeméty[**], Andrea Opitz[**], István Lemperger[*], Veronika Barta[*], Zoltán Vörös[*]

1 Heliosphere

The heliospheric magnetic field was investigated by the analysis of near-earth interplanetary measurements. It was shown, that structures recurrent with the solar rotation are persistent for a long time, both in the polarity (magnetic sectors) and the magnitude of the magnetic field. The origin of those structures are different, and also, the rotation period of the magnetic field enhancements associated to Corotating Interaction Regions is slightly smaller than that of the magnetic sectors. The different rotation period suggests a major re-arrangement of the solar magnetic field during the declining phase of the solar cycles (Dósa and Erdős 2017).

Solar wind propagation is a key to predict space weather parameters at certain distances from the Sun. Background solar wind and transients have to be handled separately. At the Wigner RCP, a database was created which contains identified transient events as seen on different space-based instruments. Dósa et al. (2018) developed a new solar wind propagation method, called Magnetic Lasso propagation. This is a problem-tailored propagation tool that concentrates on the exact location where the prediction should be most accurate. The method works ballistically, but compared to the simple ballistic approach, the Magnetic Lasso method is based on reconstructing the ideal Parker spiral connecting the target with the Sun by testing a previously defined range of heliographic longitudes. The model takes into account the eventual evolution of stream–stream interactions and handles these with a simple model based on the dynamic pressure difference between the two streams. The model has the advantage that it can be coded easily and fitted to the problem; it is flexible in selecting and handling input data and requires little running time.

As part of the EU H2020 Europlanet-RI project, there are Planetary Space Weather Services (PSWS) developed (Andre et al. 2018) that extend the concepts of space weather and space situational awareness to other planets in our Solar System and in particular to spacecraft that voyage through it. A variety of tools (e.g. web applications or numerical models) are available for tracing propagation of solar events through the Solar System and modelling the response of the planetary environment (surfaces, atmospheres, ionospheres, and magnetospheres) to those events. These tools are now tailored for planetary event prediction and space weather applications. PSWS review, test, improve and adapt methods and tools available within the partner institutes in order to make prototype planetary events and space weather services operational. Besides the above described contribution of the magnetic lasso method, the Wigner RCP has performed thoroughful testing of these services and provided reliability estimates.

2 Energetic particles

In spite of efforts to understand it, the origin of suprathermal ions in the heliosphere still remains an open problem: where, when and via what mechanisms they are accelerated. Zeldovich et al. (2018) compared the interplanetary quiet-time flux data of ^{3}He, ^{4}He, C, O, Fe ions in the 40 keV to 2 MeV/nucleon energy range measured aboard the ACE (ULEIS), WIND (EPAM), and SOHO (EPHIN) spacecraft during the ascending phase of Solar Cycle 24 with those obtained earlier for SC 23.

[*]*Geodetic and Geophysical Institute, Hungarian Academy of Sciences, Sopron, Csatkai u. 6-8.*
[**]*Wigner Research Centre for Physics, Hungarian Academy of Sciences, Bp, Konkoly-Thege u. 29-33.*

The new data confirmed that the energy spectra of these ions and their relative abundances are governed by their first-ionization potential with substantial differences in the ion energy spectra during the two consecutive solar cycles. Except for the solar activity minimum, the Fe/O ratio during quiet-time periods correspond either to the abundances of ions accelerated in impulsive solar flares or to the mean abundances of elements in the solar corona. At the activity minimum, this ratio assumes values characteristic for the solar wind. Based on SWICS/ACE data, Zeldovich et al. (2016) found that the ratios of suprathermal iron and carbon ions to oxygen are similar to the relative abundances of the corresponding thermal ions in the fast and slow (Maxwellian) solar wind while the ^{4}He/O ratio exceeds the corresponding ratio in the solar wind by a factor of two. The intensities of all suprathermal ions in outflows from coronal holes (CHs) increase with the speed of the solar wind. This indicates that at low solar activity suprathermal ions from CHs represent a high-temperature "tail" of the solar wind. Although relativistic electrons are very rarely observed in the distant magnetotail of the Earth (at 30 to 40 Earth radii), their behavior is important for understanding the mechanisms of solar particle penetration into the magnetosphere. Daibog et al. (2016) analyzed the fluxes of MeV energy electrons registered aboard the IMP-8 satellite inside and outside the terrestrial magnetosphere, as well as upon entering and leaving it. In addition to galactic and solar flare electrons, Daibog et al. (2016) found Jovian electrons which easily penetrate the magnetotail; electrons of solar origin not associated with flares; as well as bursts of electrons in the magnetosphere and magnetosheath accelerated in auroral zones during substorms.

Variations in the flux of Jovian electrons near the Earth in two synodic cycles of the Earth-Jupiter system were compared. Whereas in the 1974–1975 cycle Jovian electrons were observed by IMP-8 during 13 successive solar rotations; in the 2007–2008 very low activity minimum they recurred in 14 solar rotations (SOHO). The electron fluxes in each solar revolution were periodic with a characteristic time scale of ~27d, the maximum flux appearing near the middle of the rotation. The mean period of the variations significantly differs from the 27.3d synodic period for the Sun–Earth system: for the electron fluxes Daibog et al. (2017a) found 26.8d in 1974–1975 and 26.1d in 2007–2008. The detected variations are interpreted in terms of reflecting variations in the structure of the solar wind speed and associated magnetic traps, the confinement time of the electrons in these magnetic traps, and the influence of the relative positions of the Earth and Jupiter in space (Daibog et al. 2017b).

3 Ion acceleration and at the Earth's quasi-parallel bow shock

The Earth's bow shock and the IP shocks are capable to accelerate particles to high energies. This has been known for a long time, however the details of the acceleration mechanism are not yet completely understood. According to the theory of shock acceleration, the first order Fermi acceleration to work efficiently there are several important conditions to be satisfied. One condition is that the particles (ions and electrons) need to be efficiently pitch-angle scattered by waves through wave-particle interaction. The scattering ensures that the accelerated particles are turned back to the shock front where they can gain further energy. The consequence of the pitch-angle scattering – or the consequence of the diffusion against convection- is that the partial density of energized particles falls of exponentially in the upstream direction. The "steepness" of the density profile provides information about the efficiency of the scattering and the diffusion coefficient can be determined.

The new results demonstrate that when a strong reflected ion beam, the so-called field-aligned beam (FAB) is formed on the quasi-perpendicular side of the bow shock, it can significantly influence the scattering process. The waves generated by the FAB are convected deep in the foreshock region where they can scatter the bow shock accelerated energetic ions. This results in a more efficient scattering, leading to a smaller e-folding distance and smaller diffusion coefficient (Kis et al. 2018). This is the first time when such a strong interaction between the physical processes at the quasi-perpendicular and at the quasi-parallel side of the Earth's bow shock is recorded. These

results are strongly supported by simulation results which demonstrates the universality of the observed interaction (Otsuka et al. 2018).

4 Dust particles

O'Brian et al. (2018) investigated the effect of interplanetary coronal mass ejections (ICMEs) on the transport and delivery of nano-dust to 1 AU. Charged nanometer-sized dust particles are expected to be generated close to the Sun and interact strongly with the solar wind as well as with solar transient events. Nano-dust generated outside of ~0.2 AU are picked up and transported away from the Sun due to the electromagnetic forces exerted by the solar wind. O'Brian et al. (2018) extended an earlier developed numerical model to calculate the trajectories of nano-dust particles in the solar wind by including their interaction with interplanetary coronal mass ejections. According to this study ICMEs can greatly alter nano-dust trajectories and the smallest particles (<10 nm) can be delivered to 1 AU in high concentration. Their presence near the Earth's orbit could potentially be revealed by simultaneous measurements of nano-dust fluxes and solar wind particles/magnetic fields.

5 Turbulence and magnetic reconnection in space plasmas

In order to study the electron scale processes associated with magnetic reconnection in the turbulent magnetosheath, high resolution data from ESA-NASA Magnetospheric Multi Scale (MMS) mission were used for estimation of the terms in the generalized Ohm's law (Yordanova et al. 2016). The observations also confirmed the theoretical expectations according to which the separatrix region of magnetic reconnection is associated with particle acceleration, agyrotropic velocity distributions and plasma heating.

Vörös et al. (2017) investigated turbulent reconnection in the magnetosheath by using MMS data. It was found that the physical signatures of turbulent reconnection resemble those of the most studied 2D laminar cases including reconnection signatures such as parallel electric fields, Hall fields, demagnetized ions and electrons, dissipation and wave particle interactions in a proper coordinate system. Both electron and ion outflows have been observed indicating that the reconnection jets were not destroyed by turbulent motions.

The existing nonlinear models of turbulence predicting the decay rate of turbulent fluctuations were compared to decay rate of fluctuations measured by Cluster in the solar wind (Narita and Vörös 2017). It has been found that magnetic fluctuations decay much faster than the predicted decay rates by turbulence models. Therefore, part of the magnetic field energy over smaller temporal and spatial scales has to be converted to other forms of energy via e.g. wave-particle interactions and/or magnetic reconnection.

In Xiao et al. (2018) plasma turbulence was investigated near Venus. Venus has no intrinsic magnetic field, the plasma and magnetic structures in the planetary environment appear to be the result of direct interaction between the solar wind and the ionosphere. The interplanetary magnetic field (IMF) is also draped around the ionospheric obstacle and in these processes the induced magnetosphere of Venus is formed. Although there exist strong fluctuations and turbulence near Venus, however, the effects of the bow shock geometry on fluctuations was not systematically studied so far. Venus Express magnetic data were used to study fluctuations downstream of quasi-parallel (Qpar) and quasi-perpendicular (Qperp) shocks. The shape of the bow shock was determined from a semiempirical model, the magnetosheath flow pattern was obtained from an analytical streamline model. The study of power spectral densities showed that in both Qpar and Qperp cases there exist periodic, noisy and turbulent fluctuations, however, the developed turbulence is associated more frequently with Qpar shock. This resembles the spectra in the terrestrial magnetosheath downstream of Qpar shock.

References

Kis Á, Matsukiyo S, Otsuka F, Hada T, Lemperger I, Dandouras I, Barta V, and Facsko G (2018): Effect of Upstream ULF Waves on the Energetic Ion Diffusion at the Earth's Foreshock. II: Observations. The Astrophysical Journal, 863, Issue 2, article id. 136, 9-9.

Andre N, Grande M, Achilleos N, Barthélémy M, Bouchemit M, Benson K, Blelly PL, Budnik E, Caussarieu S, Cecconi B, Cook T, Génot V, Guio P, Goutenoir A, Grison B, Hueso R, Indurain M, Jones GH, Lilensten J, Marchaudon A, Matthiä D, Opitz A, Rouillard A, Stanislawska I, Soucek J, Tao C, Tomasik L, Vaubaillon J (2018): Virtual Planetary Space Weather Services offered by the Europlanet H2020 Research Infrastructure. Planetary and Space Science, 150, 50-59.

Daibog EI, Kecskeméty K, Lazutin LL, Logachev YI (2016): Jovian electrons as an instrument of investigation of the interplanetary medium structure. Journal of Physics: Conference Series, 675 (3), article id. 032024, 4-4.

Daibog EI, Kecskeméty K, Lazutin LL, Logachev YI (2017a): Registering Jovian electrons in the Earth's orbit. Bull. Russian Academy of Sciences: Physics, 81, 136-139.

Daibog EI, Kecskeméty K, Lazutin LL, Logachev YI, Surova GM (2017b): A 27-Day Period in the Flux of Jovian Electrons at the Earth's Orbit. Astronomy Reports, Maik Nauka/Interperiodica Publishing (Russian Federation), 61, 1073-1081.

Dósa M, Erdős G (2017): Long-term longitudinal recurrences of the open magnetic flux density in the heliosphere. Astrophysical Journal, 838, 104, 8-8, doi:10.33847/1538-4357/aa657b.

Dósa M, Opitz A, Dálya Z, Szegő K (2018): Magnetic lasso: a new kinematic solar wind propagation method. Solar Physics, 293, 127, doi:10.1007/s11207-018-1340-3.

Otsuka F, Matsukiyo S, Kis Á, Nakanishi K, Hada T (2018): Effect of Upstream ULF Waves on the Energetic Ion Diffusion at the Earth's Foreshock. I. Theory and Simulation. The Astrophysical Journal, 853(2), article id. 117, 11-11.

Narita Y, Vörös Z (2017): Lifetime estimate of plasma turbulence, Nonlin. Processes in Geophysics, 24, 673-679, https://doi.org/10.5194/npg-24-673-2017.

O'Brien L, Juhász A, Sternovsky Z, Horányi M (2018): Effects of interplanetary coronal mass ejections on the transport of nano-dust generated in the inner solar system. Planetary and Space Science, 156, 7-16.

Vörös Z, Yordanova E, Varsani A, Genestreti KJ, Khotyaintsev YuV, et al. (2017): MMS observation of magnetic reconnection in the turbulent magnetosheath. Journal of Geophysical Research: Space Physics, 122, 11442-11467, https://doi.org/10.1002/2017JA024535.

Xiao SD, Zhang, TL, Vörös Z (2018): Magnetic fluctuations and turbulence in the Venusian magnetosheath downstream of different types of bow shock. Journal of Geophysical Research: Space Physics, 123, 8219-8226. https://doi.org/10.1029/2018JA025250.

Yordanova E, Vörös Z, Varsani A, Graham DB, Norgren C, et al. (2016): Electron scale structures and magnetic reconnection signatures in the turbulent magnetosheath. Geophysical Research Letters, 43, 5969-5978, doi:10.1002/2016GL069191.

Zeldovich MA, Logachev YI, Surova GM, Kecskeméty K, Veselovskii IS (2016): Suprathermal ions in solar-wind outflows from coronal holes at 1 AU. Astronomy Reports, 60, 687-693.

Zeldovich MA, Logachev YI, Kecskeméty K (2018): Quiet-time 0.04 – 2 MeV/nucleon ions at 1 AU in Solar Cycles 23 and 24. Solar Physics 293(1), article id. 3, 21.

HUNGARIAN CONTRIBUTION TO THE RESEARCH ON OBSERVATORY, INSTRUMENTS, SURVEYS AND ANALYSIS (2015-2018) - IAGA DIVISION V: OBSERVATORY, INSTRUMENTS, SURVEYS AND ANALYSIS

István Lemperger[*], Péter Kovács[**], András Csontos[**], Gergely Vadász[***], Balázs Heilig[**], András Koppán[**], László Merényi[**], László Szabados[**], Árpád Kis[*], Attila Novák[*], Viktor Wesztergom[*]

1 Introduction

In line with the aims of the quadrennial IUGG national committee reports, the present paper gives a short review on the Hungarian contribution to the main objectives of IAGA Division V (see www.iaga-iaga.org), achieved between 2014 and 2018. Our contribution is primarily relied on two Hungarian geomagnetic observatories located in Tihany and Nagycenk, and on our geomagnetic country survey and repeat-station survey networks. The following three main sections of the paper are devoted to the presentation of the current infrastructural status, and the main developments and tasks carried out in relation to our geomagnetic infrastructures during the last IUGG report period. We also present our main scientific achievements obtained with the processing and analyses of our geomagnetic observations as well as of public geomagnetic data sources.

2 Repeat-station (RS) survey in Hungary

In Hungary, the geomagnetic survey campaigns possess a long tradition. The first magnetic network survey was carried out by Karl Kreil between 1847 and 1857, with the occupation of 52 stations on the territory of Hungary. Later, eight further country surveys (CS) were carried on. Between 1950 and 1995, the surveys were completed in regular intervals of 15 years. Since 1965, a so-called repeat-station (RS) network comprising 15 non-anomalous stations (Aczél and Stomfai, 1969) has also been surveyed in 2-3 years of periodicity. The main objective of maintaining the RS network is to monitor the spatial distribution of the secular change of the magnetic field and to regularly update the field measured in the dense country network. In 2003, we became the founding member of MagNetE (Magnetic Network of Europe), a European scientific association dedicated to the harmonization of RS campaigns carried out throughout Europe. The member countries undertake to carry out RS survey regularly, in every second year, and to provide their RS observations to the public via the world data-centre (WDC) of Edinburgh.

2.1 Campaign measurements and data processing

During the last IAGA period, two RS campaigns were completed, in 2016 and 2018. In the survey practice, we use one-axial fluxgate magnetometer mounted on the telescope of a Theo020A Zeiss theodolite to measure the magnetic declination and inclination in the null mode (Newitt et al. 1996), and GSM 19 Overhauser type of magnetometer to record the total field. In each station, the measurements are carried out in the morning and afternoon hours in consecutive days in order to minimize the error of the temporal reduction. Basically, the temporal reduction is carried out with the use of the magnetic recording of the Tihany Geophysical Observatory (IAGA code: THY). Additionally, we also installed a three-component dIdD magnetometer in the Baradla cave (near to Aggtelek RS) and use its record for the reduction of the nearby measurements. The limestone cave environment ensures low level of magnetic and mechanical noise, as well as temperature stability.

[*]*MTA CSFK GGI, 9400 Sopron, Csatkai u. 6-8.*
E-mail: geomatika@ggki.hu
[**]*MBFSz, 1145 Budapest, Columbus u. 17-23.*
[***]*MTA-ELTE Statistical and Biological Physics Research Group, 1117 Budapest, Pázmány Péter s. 1A*
E-mail: gvadasz@t-online.hu

For our practice of data reduction by using on-site variometer recording (Kovács et al. 2012). It is shown, that, by applying the on-site recording, the gain in the temporal reduction accuracy can exceed 2 nT in X, Y or Z components and this profit depends on the geomagnetic activity conditions.

The normal field models of Hungary are compiled by the first- or second-order polynomial of the geographic coordinates. The polynomial fitting is carried out separately for each of the vector component, thus this solution ignores the Laplace's condition. To avoid this shortcoming, recently, we have developed a Matlab code for the application of the adjusted spherical harmonic analysis (ASHA), introduced by De Santis (1992) for the modelling of the geomagnetic field for a spherical cap domain. To improve the model accuracy for Hungary, we involve RS and observatory data of neighbouring countries, from the database of WDC for Geomagnetism. Moreover, in empty area we also set up "virtual stations" and fill them with magnetic values derived from the recent IGRF (*International Geomagnetic Reference Field*) model (Thébault et al. 2015). The X, Y and Z component magnetic models compiled by ASHA for the epoch of 2016.5 are shown in Figure 1.

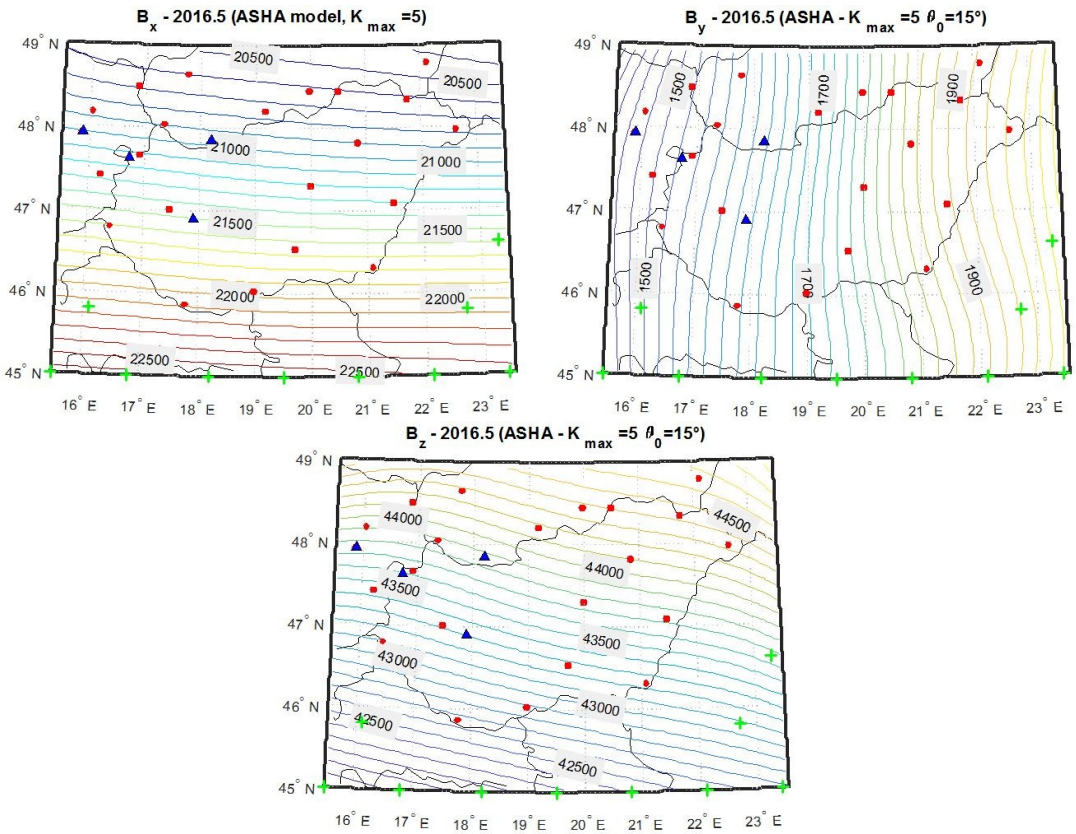

Figure 1. The X (upper left), Y (upper right), and Z (bottom) component model field for Hungary compiled according to ASHA (see text). The red dots, blue triangles and green crosses show the locations of repeat stations, observatories (Tihany, Nagycenk, Hurbanovo, Conrad) and "virtual stations" (see text), respectively, from where data have been used in the model computation. The contour lines are labelled in nT unit

2.2 MagNetE workshop, Budapest, 2015

The 7th European MagNetE workshop was hosted by the Geological and Geophysical Institute of Hungary (now Mining and Geological Survey of Hungary, MBFSZ), between 16 and 18 September, 2015. 43 attendees have participated from 14 countries. The scientific part of the workshop consisted of four oral sessions and one poster session. The oral and poster sessions concerned the

following themes: (1) National reports on repeat station survey and Survey methods (3 oral presentations, and 8 posters), (2) Geomagnetic data and data archives (5 oral presentations and 4 posters), (3) Scientific use of ground and spaceborne magnetic data (5 oral presentations), (4) New observation techniques, instruments and methods, future perspectives (3 oral presentations and 3 posters). Two invited talks have been presented by R. Leonhardt (title: Historical magnetic records and the past geomagnetic field evolution) and I. Wardinski (title: Models and forecasts of geomagnetic secular variation), respectively. As part of the workshop schedule, two time-slots have been allocated for discussions on the following main topics: (1) Coordination of the RS activity at European level, (2) Enhancing the visibility of the RS efforts, (3) Launching new coordinated campaigns and measurements adapted for the joint scientific use of spaceborne and ground-based geomagnetic observations. On 17th of September, the participants visited the Tihany Geophysical Observatory.

2.3 Archeomagnetic and volcanic database

As a project partner, Mining and Geological Survey of Hungary (MBFSZ) contributed to the HISTMAG historical, archeomagnetic and volcanic database (Arneitz et al. 2017). HISTMAG compiled data mostly but not exclusively from the former territory of the Austro-Hungarian Empire. Hungary's main contribution was the newly discovered 17-19th magnetic declination data from historical Selmecbánya (now Banska Stiavnica in Slovakia) and the digitization of the declination data recorded in the 18th century by meteorological observatories participating in the network Societas Meteorologica Palatina.

3 Tihany Geophysical Observatory

The Tihany Geophysical Observatory (THY) is maintained by the Mining and Geological Survey of Hungary (MBFSZ). Our Survey was established by the Hungarian Government in July 2017, uniting the Geological and Geophysical Institute of Hungary (MFGI) Hungarian Office for Mining and Geology. The Survey is a central governmental body with separate functions and competence. The observatory is situated in a national park on the Tihany peninsula of Lake Balaton. Since 1955 the observatory has continuously recorded geomagnetic data. Tihany is a founding member of the INTERMAGNET (*Inte*rnational *R*eal-time *Mag*netic Observatory *Net*work). The geomagnetic data gathered here are published yearly on the INTERMAGNET CD-ROMs and on the DVDs.

3.1 Instrumentation and data acquisition

During the last IAGA period two fluxgate variometers and two Overhauser effect based magnetometers were operating for continuous recording at the observatory: a suspended DMI FGE triaxial fluxgate magnetometer with XYZ orientation, a Narod triaxial ring-core fluxgate magnetometer installed in HDZ orientation, a GSM-19 Overhauser magnetometer (GEM-Systems) for recording the total field and a dIdD (delta inclination delta declination vector overhauser magnetometer) system. The fluxgate magnetometers are installed in the variation pavilion of the observatory. The temperature in this hut is being controlled within $\pm 0.2^{\circ}$C. Nevertheless the temperature of the sensor and the electronics is monitored by the built-in temperature sensors of the FGE magnetometer.

The GSM-19 Overhauser magnetometer is installed in the absolute house of the observatory. The distance between the absolute pillar and the sensor of the magnetometer is about five meters.

The dIdD system is installed in the old variation house. This building is a cellar that is why the yearly temperature variation is attenuated there.

The FGE magnetometer is equipped with an OBSDAQ type, 24-bit A/D converter. Its output signal is transmitted to the recorder through a 120 m long optical cable. Optical cable is applied for protection against lightning hazard. Accuracy of time synchronizing to GPS time is ±2 msec. The applied sampling rate is 128Hz. After digital filtering 1-second resolution data are also recorded in

addition to the 1-minute mean values required by INTERMAGNET. FGE magnetometer is the main recording system of the observatory since 1999.

The high resolution NAROD fluxgate magnetometer belongs to the EMMA geomagnetic pulsation recording array.

The dIdD system registers inclination and declination, as well as total field data in every five seconds. When these data are used as input to a task-oriented digital acquisition (DAQ), they produce real-time XYZF 1-minute means. Of course, all the original readings are stored, as well. Thus, the dIdD instrument can serve as back-up systems for our base FGE magnetic recording system.

The observatory has two absolute instruments: a Zeiss 20A theodolite and a Zeiss 10A theodolite equipped with a DMI D&I sensor. The absolute measurements are taken weekly according to the null reading method. A set of absolute observations consists of two independent measurements of D and I. Total field is continuously recorded by a GSM-19 and even by the dIdD. All the baselines are derived from standard absolute observations.

In order to apply some convenient networking technologies (i.e. remote control, file transfer, secured connections, etc.) a Linux based data logger was developed. The DAQ in THY (realized by DIMARK family) is able to acquire magnetic data and housekeeping data from one or more different instruments, including fluxgate, Overhauser, dIdD magnetometers or temperature sensors (through A/D converters or RS-232 protocol). GPS PPS is used for sample triggering and time labeling of magnetic data.

All of our data acquisition units are linked into a local network, while communication between the observation site and the office is realized by a microwave (2.4 GHz) transmitter. For data security reasons, the recorded data are stored parallel on three different computers located in different buildings.

3.2 Observatory data and database

Since 2013 data from the main observatory system have been quasi real time transmitted to Edinburg GIN server instead the previously used e-mail transmission. The data are also available to partner researchers through a real time ftp server. The observatory developed a website where the recordings of all instruments are plotted near real time. Since 2005 the second sampled XYZ variation data have been real time transmitted to National Institute of Information and Communication Technology (Japan) Space Environment Information Service. In 2015 the observatory joined to the quasi-absolute minute mean data transmission to the INTERMAGNET website in order to support the work of satellite missions. Since 2009, the metadata base of the definitive data sets of the observatory is available on the GEOMIND (www.geomind.eu) and KINGA (kinga.elgi.hu) Internet information services.

The relation of three geomagnetic indices, the AE (indicating the surface effect of the auroral electrojet), ap (a planetary index derived from K [activity] index) and Dst (disturbance storm time index, indicating the intensity of the ring current) was also studied for the period of 24th solar cycle (Csontos 2017).

3.3 Additional measurements and activities in Tihany Geophysical Observatory

- Coordinator and PI of EMMA (European quasi-Meridional Magnetometer Array ranging from Finland to Italy) for space weather studies (by monitoring global ULF wave activity and plasmaspheric density)
- Since 1968 onwards whistlers have been detected in the Observatory as a joint project with the Space Research Group of Eötvös Loránd University (ELTE), Budapest.
- Seismological recording is performed using Güralp CMG-3T seismometer. The instrument belongs to the network of permanent seismograph stations in Hungary. The

station is operated by Geodetic Institute, Research Centre for Astronomy and Earth Sciences, Hungarian Academy of Sciences (MTA CSFK GGI) and MBFSZ.

- Temperature gradient observation for geothermal studies has been started in 2010.
- Nonmagnetic temperature test hut was built in the observatory in order to study the most important source of temperature effect on magnetometers by using high amplitude thermal change (Hong et al. 2016).
- Tests of a suspended fast dIdD were performed in the observatory and during repeat station measurements (Šugar et al. 2015, Hegymegi et al. 2016).
- Checks of UXO detectors are performed from time to time in the observatory.
- A new site for measurement of absolute gravity was established in 2013.
- Member of the WWLLN global lightning detector network (University of Washington, Seatlle)
- Base station for magnetic surveys of Lake Balaton performed by the Department of Geophysics and Space Research Group of (ELTE) (Visnovitz et al. 2018).

3.4 New electric railway near Tihany observatory

A new governmental effort became known at the end of 2015. The railway approximately 4 km north of the observatory will be electrified. Up to now, the level of electromagnetic noises in the DC to ELF frequency band has been amongst the lowest in Europe. With the appearance of EM noises and transients generated by the electric locomotives, most of the experiments will be exposed to high risk. The observatory had to face a similar challenge in the 1980's, when the railway at a similar distance south of the observatory was electrified. In that case the AC railway was carefully designed applying 2X25 kV solution at that time in order to protect the nearby underground communication lines. We believe that the local geological structure also plays a role in protecting Tihany from the stray currents. We have no detectable artificial noise caused by the trains now.

Infrastructural projects including the electrification of the northern railway was delayed by the government for several months so we had some chance to defend the measurements in Tihany observatory. We asked international communities and our research partners to write supporting letters in this issue.

From the AC technologies, that had risen up as potential options of innovation, we only found the 2X25 kV (50Hz) technology acceptable. We initiated the idea of using only this well-tried method of electrification in a letter. The supporting letters also formed a part of our petition.

After receiving sceptical response the process ended up in a situation, where we made all the difference. That time we wrote a detailed technical report for the decision-makers, which made them accept our point of view. What is more, according to the current plans, the trains are going to approach the observatory only with seven kilometres instead of four.

3.5 Geological and geophysical investigations on the site of Tihany observatory

An appearance of little systematic baseline instability with large spatial differences motivates us to perform a detailed geophysical survey on the site of Tihany observatory including electric resistivity tomography (ERT), geomagnetic measurements and susceptibility measurements. Soil samples were also collected based on the measurement results; on them an X-ray powder diffraction (XRD) measurement was completed to identify the minerals of the sediments. After these investigations deposits with different magnetic properties could be linked to structures created by hydrothermal processes so the impoundment of magnetic anomalies of the crust were performed. As a consequence of our study we verified, that the absolute control of the geomagnetic observatory is not influenced by strong crust anomalies (Csontos et al. 2017).

4 Nagycenk Geophysical Observatory

Besides regular geomagnetic observations and continuous data services for IGRF and main field modelling, the main objectives of the ground based electric and magnetic observations are monitoring the solar-terrestrial environment and development of models to specify and predict the state of the Sun-Earth system (space weather and climate). Measurements include the monitoring of geomagnetic field variation, ionospheric parameters, solar emissions and determination of solar wind and radiation environment parameters. Model developments are required for the propagation of coronal mass ejection and energetic particle radiation, interaction between the interplanetary medium and the Earth's magnetosphere, the filling and depleting of the radiation belts, ionospheric composition, density, diffusion and convection, induced electric fields.

4.1 Geomagnetic observations

Continuous observation of geomagnetic elements with control of the absolute observations started in 1961. The observatory equipped with 3 sets of triaxial fluxgate magnetometers. The temperature variations of the triaxial fluxgates are maintained within 0.5 °C between the weekly absolute observations. The fluxgate variometer sensors are aligned in X, Y, Z directions. For better time resolution one of them is run with 1 second sampling rate. Simultaneous low altitude satellite and meridional magnetometer array ($1.56<L<1.88$) measurements were used to interpret the controversial relation between space and ground ULF signal, evaluate the effect of the ionosphere on the transmission and study the field line resonance phenomenon and study the expected ULF precursors of seismic activity.

In the frame of the INTERMAGNET data service 10 second samples are used to provide minute values centred on the minute, by means of a 7-point cosine filter. Geomagnetic indices and transient events are also scaled from these data.

Protonmagnetometer (Overhauser- effect magnetometer) in dIdD configuration consists of two orthogonal sets of coils (proton head is mounted at the centre). Coils orientated so that one provides bias fields approximately perpendicular to F vector in the magnetic meridian and the other provides bias fields approximately perpendicular to F in the horizontal plane. ΔD and ΔI relative to the initial values (D_0 , I_0) are calculated. dIdD proton magnetometer samples at 1Hz from which F (total force) and quasi absolute values of D and I are obtained. To ensure continuous recording a high stability torsion photoelectric magnetometer (type PSM-8711) is run as backup system. Data along with telluric data are logged by a DR-02 type digital recording system. The PSM magnetometer records the H, D and Z component with exceptionally high parameter stability. The baseline variation never exceeds 1.5 nT/year. Maximum resolution is 3 pT, sampling rate applied is 10°s, frequency response: 0.3 Hz to DC, sensitivity to tilting: less than 10 nT/'.

Baselines of the variometer systems are derived from absolute observations of F, D and I. The standard instrument for absolute measurements are the proton magnetometer (type: GSM 19 of GEM Systems) and the new fluxgate theodolite. To determine the momentary angle of declination four observations (four null positions in the horizontal plane) are taken and it is repeated at least twice. Inclination angle is determined in the plain of the momentary magnetic meridian in the same way as D. Total intensity is measured simultaneously with I-measurements on the next (F) pillar with an Overhauser magnetometer. Absolute values of all geomagnetic elements are referred to the same pillar of the absolute hut. Observations are made weekly, occasionally more often. Baseline determination was improved by new Overhauser effect protonmagnetometer, a Theo 020A based fluxgate theodolite, also called DI-flux.

4.3 GIC recording

Continuous measurement of the geomagnetically induced currents (telluric currents) started in 1957. The value of the telluric data of the observatory lies in the exceptional length of data series. The long-term stability of the observations had been ensured by the reconstruction of the electrode

system. This nearly sixty years long telluric recording forms an unique data set for statistical analysis of the long-term variation of the geomagnetic activity and its induction effect. Occurrence of high geomagnetically induced electric fields and their coincidence with the phases of solar activity is less clear than that of maximum magnetic activity. As the weights of variations with different periods are rather different in geomagnetic and earth-current indices, there are also differences between the two kinds of activities.

References

Aczél E, Stomfai R (1969): The variations of the geomagnetic elements according to the secular measurements in the year 1966 (in Hungarian with English summary). Geofizikai Közlemények, 18(1-2), 3-11.

Arneitz P, Leonhardt R, Schnepp E, Heilig B, Mayrhofer Kovács Hejda P, Valach F, Vadász G, Hammerl C, Egli R, Fabian K, Kompein N (2017): The HISTMAG database: Combining historical, archaeomagnetic and volcanic data. Geophysical Journal International, 210(3), 1347-1359, doi:10.1093/gji/ggx245.

Csontos A (2017) A geomágneses AE, ap és Dst indexek között korábban feltárt kapcsolatok vizsgálata a 24. napfoltciklus kiválasztott időszakaira. Magyar Űrkutatási Fórum 2017 válogatott közleményei MUF2017-K-07.

Csontos A, Tildy P, Kónya P (2017): Geoelectric and geomagnetic field survey on a geyser cone to measure the resistivity and magnetic properties of the sediments. 9th Congress of Balkan Geophysical Society. M. Smith, M. Wesson, ext. abstract published in earthdoc.org, DOI: 10.3997/2214-4609.201702626 2017.

De Santis A (1992): Conventional spherical harmonic analysis for regional modelling of the geomagnetic field. Geophys. Res. Lett., 19, 10, 1065-1067.

Hegymegi L, Csontos A, Merényi L (2016) Monitoring of long term mechanical stability of a suspended dIdD sensor applying optical observation. Proceedings of the 16th IAGA Workshop on Geomagnetic Observatory Instruments in Journal of Indian Geophysical Union Special, 2, 19-23.

Hong S, Kim JH, Marusenkov A, Hegymegi L, Csontos A (2016): The temperature stability of LEMI-025 1-second variometer: Case study in the icheon observatory. Proceedings of the XVI th IAGA Workshop on Geomagnetic Observatory Instruments in Journal of Indian Geophysical Union JIGU-IAGA Special Volume, 2, 42-46.

Kovács P, Csontos A, Heilig B, Koppán A (2012): Hungarian repeat station survey. Annals of Geophysics, 55(6), 1113-1119, DOI: 10.4401/ag-54502010.

Newitt LR, Barton CE, Bitterly J (1996): Guide for magnetic repeat station surveys. IAGA, Boulder, Colorado.

Šugar D, Csontos A, Brkić M (2015): Geomagnetic suvey on Sinjsko Polje repeat station and data reduction using the onsite dIdD variometer. Tecnical Gazette, Osijek, Croatia, 615 - 622.

Thébault E, Finlay CC, Beggan CD at al. (2015): International geomagnetic reference field: the 12th generation. Earth, Planets and Space. 67, 79 doi: 10.1186/s40623-015-0228-9.

Visnovitz F, Hegyi B, Balázs A, Raveloson A, Rozman G, Lenkey L, Lenkey-Bőgér Á, Király Á, Pethe M, Kudo I, Kovács P, Csontos A, Heilig B, Vadász G, Horváth F (2018): Mágneses mérések a Balatonon: Észlelt anomáliák és az eredmények értelmezése. Magyar Geofizika, 59(3), 117-128.

HUNGARIAN NATIONAL REPORT ON IAHS (2015-2018)

Zoltán Gribovszki[*]

1 Introduction

Every four years, the Hungarian National Committee of IUGG prepares a national report detailing the activities of the International Association for Hydrological Sciences. This paper summarizes the most important hydrology-related projects and research performed by universities, scientific institutions, and government agencies in Hungary during the period of 2015-2018. The National Representative of IAHS was entrusted to review the relevant water-related activities and their publication background.

Traditionally, the Environmental Protection and Water Resources Research Institute (Hungarian acronym VITUKI) managed hydrological research, but VITUKI dissolved in 2013 due to reorganization. Other organizations have since taken over its main research tasks and projects. These organizations include the General Directorate of Water Management (Hungarian acronym OVF) and universities such as the Budapest University of Technology, the National University of Public Service, the Pannon University, the Széchenyi István University, the University of Miskolc, and the University of Sopron, among others.

2 Selected research and development activities in Hungary

2.1 Budapest University of Technology

The Department of Hydraulic and Water Resources Engineering, and the Department of Sanitary and Environmental Engineering at the Budapest University of Technology and Economics conducted the following research activities.

The complementary relationship (CR) of evaporation has gone through a significant transformation in the past few years (Szilágyi 2015, Szilágyi et al. 2016). Based on empirical evidence it became clear that the CR is neither symmetric nor linear in nature between its two non-dimensional variables, $y = E / Ep$ and $x = Ew / Ep$ (or similarly between E / Ew and Ep / Ew). Here, E is the actual, Ep the potential, and Ew the wet-environment evapotranspiration rate.

The newly defined nonlinear CR (Crago et al. 2016, Szilágyi et al. 2017) employs a new rescaling for x, realizing that Ep is physically bounded; therefore, x cannot span the theoretical [0, 1] interval in general. With the properly rescaled non-dimensional variables, the nonlinear CR outperforms any previous versions of it (Szilágyi et al. 2017, Szilágyi 2018a). In fact, with the help of this new CR, unique and unprecedented relationships could be identified. For example, it could be shown that large-scale intensive irrigation affects the boundary layer of the atmosphere in a way that leads to reduced local precipitation rates (Szilágyi 2018b) and increased rates hundreds of kilometers farther downwind. Also, this new CR can express how the almost decade-long severe drought in California's Central Valley affected crop evapotranspiration rates, which is contrary to what hydrometeorologist had previously assumed to have happened (Szilágyi and Józsa 2018). It was discovered the crops could cope with the drought for several years due to intensified irrigation. This was valid only up to a point. When competition for irrigation water became fierce and water increased in price, many farmers cut back on irrigation and sold the water to the thirsty megacities of Los Angeles and San Francisco.

Current, ongoing research clearly demonstrates that one can obtain better evapotranspiration estimates with the help of the nonlinear CR than with any complex land surface (e.g., Noah, VIC, Mosaic), reanalysis (e.g., NCEP-II, ERA-Interim), remote-sensing based (e.g., GLEAM, PML) models, or even what a spatial upscaling of eddy covariance measurements (i.e., FLUXNET-MTE) can provide. In addition, this can be accomplished without calibration since the Szilágyi (2018)

[*]*Institute of Geomatics and Civil Engineering, Faculty of Forestry*
University of Sopron
E-mail: gribovszki.zoltan@uni-sopron.hu

version of the nonlinear CR is calibration-free. Employing the CR could be a great opportunity for climate scientists to upgrade land surface model components within global climate models. The future will determine if this happens or not.

To obtain a deeper understanding of the relationship between catchment morphometric parameters, rainfall event characteristics, and the corresponding response time (Tc), calculations were completed employing 736 events at 38 watersheds – with catchment sizes varying from 16 to 978 km^2. As a result, the root mean square error of the estimation was reduced from 8.6 to 2.3 hours, compared to the generally applied equation derived by Wisnovszky (1958). Out of 23 morphometric parameters, a principal component analysis identified four as the most important. A new polynomial equation was calibrated based on the parameters identified. Further improvement of the Tc estimation was achieved by applying a new catchment grouping method. A hyperbola was fit to the maximum rainfall intensity versus the Tc value for every watershed. The constant multiplier of the hyperbola displayed a linear correlation with the catchment area for each group, but the reason for this behavior has not yet been clarified. Study results were presented at the HydroCarpath Conference 2019 in Vienna, Austria.

Research at the Sanitary and Environmental Engineering Department covers a broad range of environmental topics: hydrology and water quality in natural catchments and in urban areas; public works and sanitation; and water and wastewater technologies. The department contributed to the implementation of the Second River Basin Management Plans of Hungary in two areas: (1) by developing and applying a novel bottom-up approach to estimate ecological water demand of groundwater dependent ecosystems, (2) by planning and carrying out water quality calculations for the surface water body classifications (Kardos and Koncsos 2017). The relationship of hydrological, land use, water quality and ecological conditions was analyzed at Lake Balaton and its watershed (Hatvani et al. 2015, Hatvani et al. 2017). To assist the country-scale analysis of diffuse source nutrient emissions, a new method was elaborated to estimate the base flow index in gauged and ungauged catchments (Jolánkai and Koncsos 2018). Multiple adaptation measures were investigated to mitigate the water-related consequences of climate change in general (Garnier et al. 2015) and to cope with hydrologic extremities (drought and inland excess water) in heavily cultivated lowland catchments (Ungvári et al. 2018). In the urban hydrology field, the performance of several existing sediment transport models were evaluated for a selected urban area in Budapest (Knolmár and Németh 2018), and a new automated approach for subcatchment delineation and parameterization to run the Storm Water Management Model (SWMM) more effectively was developed (Knolmár and Fülöp 2018). Field experiments were performed to analyze the transmission of traffic-emitted heavy metal pollution (Budai and Clement 2018), which is a significant environmental aspect of hydrologic processes.

2.2 National University of Public Service

The main research activities in the Faculty of Water Sciences (formerly Eötvös József College, Institute for Hydraulic Engineering and Water Management and Institute for Water Supply and Environmental Engineering) at the National University of Public Service are discussed below.
The Institute for Hydraulic Engineering and Water Management performed following research activities and projects.

The TÁMOP-4.1.1.F-14/1/Konv-2015-0003 "Development of Technical and Economic Education at Eötvös József College in the Field of Water Management through the Introduction of a Dual Education System" project was completed in 2015 to develop a dual education system for the engineering and business administration degree program at Eötvös József College. The project framework included improving practical education that was accomplished by involving water management professionals. For water management majors the introduction of dual higher education system and curriculum modernization were implemented. Some practice-oriented civil engineering curriculum subjects such as the modernization of the hydrometry field training, and the development of field training on river management and flood protection were accomplished (Tamás 2015).

The project InterFloodCourse 04_ECVII_PA05 "International Postgraduate Course on Flood Management" was another project related to training and curricula development. Together with the University of Belgrade, Faculty of Civil Engineering, a new and gap-filling postgraduate training has been developed. The program enables civil engineering graduates in the Danube River basin to apply a harmonized and coordinated flood and flood risk management and prevention process. The project addressed the lack of uniformly specialized training on flood management. This lack of dissemination of flood-related knowledge hinders the implementation of the EU Floods Directive (Oroszi et al. 2017).

In addition, there were several traditional – mostly applied – ongoing research activities:

1) Research on the investigation of riverine hydrological and morphological processes and the development of bathymetry techniques have been carried out (Göttlinger et al. 2017, Tamás and Ficsor 2018).
2) Application of remote sensing (Balázs et al. 2018) and precision technologies in agricultural uses have been investigated.
3) New model for design and evaluation for culverts was developed, and calibrated (Koch et al. 2017, Koch and Horvat 2018).

At the Institute for Water Supply and Environmental Engineering, a project aiming at the development of water management in higher education within the frame of intelligent, specialized decentralized wastewater treatment technologies founded by the EFOP-3.6.1-16-2016-00025 was evaluated and compared, and a feasibility study was performed to examine the applicability of such systems. The project scope was to determine the actual capacity of DEWATS options and map the capability of system upgrade. A decision-making system was developed applying a biokinetic simulation tool to provide customers a device to select suitable systems to meet their needs. Dissemination of this work was published in several articles (Karches and Orgoványi 2018, Karches 2018a).

Funded by TÉT_15_IL-1-2016-0013, the project handled smart chlorine dosage in water treatment process to reduce public health risk and optimize treatment process operations. The project revealed that using a smart process to control chlorine dosage the side products could be minimized. It was determined that the chemical added to the system may not cause corrosion in the drinking water supply system. In addition, the optimization and the organoleptic characteristics of the water could be improved. AquaNES-H2020-WATER 2014-2015 project "Demonstrating Synergies in Combined Natural and Engineered Processes for Water Treatment Systems" further developed this work. In this project, the membrane techniques were evaluated and reverse osmosis filter permeability was investigated (Salamon et al. 2018).

The KÖFOP-2.1.2.-VEKOP-15-2016-00001 István Egyed Postdoctoral Program aimed to investigate the reactor arrangement in wastewater treatment systems. Numerical tracer studies were applied to map the hydrodynamic conditions inside the reactors, the dead-zones, and the hydraulic short-cuts detected; with the help of computational fluid dynamic simulations (CFD), their effect was quantified on the treatment process. A number of completely stirred tank reactors in series were introduced and applied in biokinetic simulations. The project outcome was to improve the mass balance and hydrodynamic coupling model systems to improve the description of complex processes in wastewater technologies (Karches 2018b, 2018c).

At the Faculty of Water Sciences, extensive research has been done on the changes of runoff and catchment characteristics due to climate change (Bene et al 2015, Keve et al. 2015) and the possibilities of improvement in the monitoring of ice phenomena on the Danube River (Keve 2016, 2017).

2.3 Pannon University

At the Georgikon Faculty of Pannon University research focused on two main research activities during 2015-2019.

There were two goals in the GINOP-2.3.2-15-2016-00029 project to study the traditional water-soybean relationship to obtain the crop water demand during the whole vegetation period, and to investigate water stressed crop behavior during the most sensitive phenological stage (flowering). Dry period simulation through closing crop water supply and braiding the growing chambers from above produced full of water deprivation (Anda and Soós 2016). Among several methods to measure evapotranspiration (ET), compensation evapotranspirometers are the optimal devices as they produce accurate daily on-site results. Water use efficiency was also determined, which combines the analysis for dry matter and crop-water relation (Anda et al. 2018a). Results could contribute to more effective soybean growing practices (management) of end-users, be they farmers or decision makers.

The EFOP-3.6.1-16-2016-00015 project included the following research activities. Macrophyte's ET reveals the effects of annual water level fluctuations and allows for a more exact understanding of the impact of water losses. Water losses remain an elusive and substantial part of the hydrologic budget, particularly in wetland habitats. Information about annual variability of long-term ET values would assist in finding an ideal solution for determining the proper water level needed in strictly protected areas (Lake Balaton and Kis-Balaton Wetland System). It is recommended that for different wetland habitats the water balance should be continuously assessed to determine a suitable water level to sustain the most appropriate wetland ecological conditions (Anda et al. 2015a, 2015b, Anda et al. 2016, Anda et al. 2017, Anda et al. 2018b, 2018c, Menyhart et al. 2015, Kocsis et al. 2017, Kocsis and Anda 2017, Kocsis and Anda 2018, Kovács et al. 2017). The other aspect of the study is the investigation of decomposition processes, which are highly influenced by environmental factors (meteorological variables included). In the area of Lake Balaton and Kis-Balaton, wetland system decomposition is especially important for water quality (Kucserka et al. 2018, Simon et al. 2018a, 2018b, Hubai et al. 2017). While the environmental dependence of the process is well-known, the impact of meteorological parameters on decomposition processes are less known. Due to recent global climate change, the basic influencing factors will change as well, and the consequences for wetland habitats are unpredictable.

2.4 Széchenyi István University

At Széchényi István University the water resource program focused on three major areas for research; (1) water management and surface water hydrology, (2) unsaturated flow modelling with applications in transportation, geotechnical, and ecological areas, and (3) karst flow modelling.

1) In the water management and surface water hydrology area, we are modeling ungauged watersheds in western Hungary. Our efforts are directed at:
    - Determining similarity parameters (hydrological, watershed, and meteorological) for measured watersheds, using the available database in western Hungary. Using yearly and monthly flows as well as flow duration curves to develop index parameters.
    - Applying different geostatistical methods (kriging, and topkriging) to estimate yearly and monthly flow in western Hungary. Thirty-six gauged watersheds were selected to evaluate seasonal variability of runoff based on 15 years of measured data. The watersheds were clustered based on the Pardé distribution. Geostatistical interpolation methods were applied to predict regional monthly flows using point kriging at gauged and ungauged locations. The findings were presented at the EGU Conference 2018 in Vienna, Austria.
    - Modelling continuous rainfall-runoff processes by using daily measured data. Performing model selection and sensitivity analyses with available software (Nagy et al. 2016, Mátyás and Bene 2018). Evaluating models by applying different error

analysis methods. Searching for relationships between expanding window error analyses and meteorological, and watershed characteristic changes. In the first step of this study, rainfall-runoff models of four watersheds in the Kisalföld region were investigated. The models were applied to identify variations in runoff characteristics caused by climatic factors or fundamental alterations to the watershed itself through the application of numerical error analysis. By observing the continuous statistical error measurements, changes can be detected in either climatic conditions, watershed characteristics, or may indicate gauging or data collection errors (Mátyás and Bene 2018).

- Using calibrated models to assess the impact of climate change in selected regions. Investigating the effect of climate change on the flow factor, minimum and maximum yields, and annual distribution of water.

2) Applying measurement methods to develop soil water characteristic curves and evaluating measured data. Assessing the impact of unsaturated water movement on various structures in civil projects (railways, dams) and on the stability of natural loess bluffs. As a first step, we have built a realistic 2-dimensional infiltration and groundwater model that reflects the influence of river levels, rainfall patterns, and local pumping. Based on model results so far, initial and boundary conditions have a strong influence on seasonal pore pressures. (Murinkó and Bene 2017)
3) Describing karst spring flow using statistical methods. Karst spring flow plays an increasing important role in groundwater resources in Hungary. Three different estimation methods were evaluated to predict mean annual spring flows in the Aggtelek region, using GIS based catchment area. Neither method was found significantly better than the others. The Budyko curves gave a good estimation for annual spring flows, with average variance. The non-linear regression method gave the best result, with the smallest median error, and error variance (Mátyás and Bene 2017).

2.5 University of Miskolc

The Faculty of Earth Science and Engineering of the University of Miskolc had several national and international projects dedicated to sustainable water resource management and geothermal resource utilization challenges. The main research activities were performed to implement the following projects.

The KINDRA project (EC framework program H2020, Grant Agreement No. 642047) aims to achieve a better understanding of the societal challenge of groundwater by providing an overall view of the scientific knowledge that exists across Europe and classifying this knowledge in an open repository (Petitta et al. 2018). The six-member KINDRA consortium, led by the Sapienza University, conducted an EU-wide assessment of existing groundwater-related practical and scientific knowledge based on a new Hydrogeological Research Classification System (HRC-SYS). This classification was supported by a web-service – the European Inventory of Groundwater Research (EIGR) – which acts not only as a knowledge repository but also as a tool to help identify relevant research topics, existing research trends, and critical research challenges (Fernandez et al. 2017).

WaterWiseWays – Innovative Solutions for Sustainable Groundwater Resource Management project (GINOP-2.3.2-15-2016-00031) is implemented under the framework of the Széchenyi 2020 Plan, funded by the European Union, and is co-financed by the European Structural and Investment Funds. Its target is to support and work out new and innovative solutions in the following applications of groundwater management:

1) New procedures for discovering the effects of extreme weather conditions on natural groundwater recharge and flow regimes (Ilyés et al. 2018),
2) Analysis of soil-water interaction supporting precision agriculture activities,
3) Leakage detection and analysis of factors enhancing underground pipe-system failures (Hoang et al. 2017).

The program provides research infrastructure and human resources for the targeted research priorities to strengthen the international competitiveness of the Faculty of Earth Science and Engineering.

The project Combined Heat, Power, and Metal Extraction from Ultra-deep Ore Bodies (CHPM2030) has been submitted under the coordination of the University of Miskolc to the call: H2020-LCE-2015-1-two-stage of the Horizon 2020 program. The international consortium submitting the project is composed of 12 partners from 11 countries, also involving additional third parties under the umbrella of the European Federation of Geologists, thereby ensuring nearly full geographical coverage within the European Union. CHPM2030 aims to develop a novel and potentially disruptive technology solution that can help satisfy European needs for energy and strategic metals in a single interlinked process. Working at the frontiers of geothermal resources development, minerals extraction and electro-metallurgy, the project aims at converting ultra-deep metallic mineral formations into an "orebody-EGS" that will serve as a basis for the development of a new type of facility for "Combined Heat, Power and Metal extraction" (CHPM). In the technology envisioned, the metal-bearing geological formation will be manipulated in a way to make the co-production of energy and metals possible and optimized according to market demands at any given moment in the future.

2.6 University of Sopron

The following important research activities were implemented at the University of Sopron (formerly University of West Hungary), Faculty of Forestry, Institute of Geomatics and Civil Engineering.

Hydrological conditions in Hungary were analyzed in the context of the "Climate Change in Agrárklíma.2" (VKSZ_12-1-2013-0034) project.

1) A Thornthwaite-type monthly water balance model for seasonal estimations of climate change hydrological effects was developed by Herceg et al (2016). The model was calibrated using a remote sensing-based evapotranspiration. The key parameter of the model is soil water storage capacity (SOILMAX). During the calibration process, the maximal rooting depth is also projectable. Data of a mixed parcel of land near Mosonmagyaróvár and a small, forest-covered catchment in Sopron were successfully used for calibration of the model.
2) Csáki et al. (2018) projected the main components of the water balance for the Zala River Basin in Hungary. Increasing temperature (3.5° C) at the end the 21st century is projected to cause a 4% increase of evapotranspiration. On the other hand, this slight change in ET can cause a substantial reduction (53%) in long-term runoff especially for forested part of the watershed. The reducing runoff/recharge may limit manageable or extractable groundwater resources. Runoff decrease could lead to serious consequences for the watershed of Zala River (the main tributary of the Lake Balaton and adjoined wetlands) by further worsening the water balance.

Forest groundwater use was analyzed in project OTKA NN79835 (Statistical and Hydrological Modelling of Soil and Subsoil Salt-Accumulation Caused by Tree Plantations Established above Shallow Saline Groundwater) in collaboration with TAKI (Institute for Soil Sciences and Agricultural Chemistry, Centre for Agricultural Research, Hungarian Academy of Sciences) and ERTI (Forest Research Institute, National Agricultural Research and Innovation Centre).

1) Water table data under forest plantations and neighboring corn plots in groundwater discharge and recharge zones were analyzed by Móricz et al. (2016). A poplar (Populus tremula) plantation and adjacent corn field were surveyed in a local discharge area, while a black locust (Robinia pseudoacacia) forest and neighboring agricultural plot were evaluated in a recharge area.
2) Significant amount of groundwater uptake was detected by Csáfordi et al. (2017) during long dry periods in Hungarian Great Plain analyzing data from 20 groundwater wells with different vegetation cover. Comparing different vegetation covers low value of $ETgw$ was detected for black locust stands (mean 0.4 mm/day), with higher values for poplar planta-

tions (1.7–6.0 mm/day), and the highest rate of $ETgw$ for common oak forests (mean 8.2 mm/day). There were no or a very small amount of $ETgw$ on agricultural control plots, indicating lower groundwater consumption of control sites with herbaceous vegetation.

3) Groundwater evapotranspiration and salt accumulation of an oak forest, a poplar plantation, and grass covered plots were analyzed by Gribovszki et al. (2017). Groundwater uptake of a middle-aged oak forest was greater than that of younger poplar forest, but both forest types used significantly greater amounts of groundwater than adjacent grasslands during the summer monitoring period. Salt accumulation, which shows water use in the longer run, was slightly higher for the poplar plantation in both the vadose zone and groundwater. All in all, hybrid poplar, the most preferred species for afforestations in Hungarian Great Plain, is less favorable considering salinization effects.
4) Szabó et al. (2018) studied the effect of water table depth and clay content in the Great Hungarian Plain, where forest cover has been increasing for decades, by analyzing soil and groundwater samples from black locust (Robinia pseudoacacia, 11 plots) and poplar (Populus spp., 11 plots) stands. One herbaceous (control) and one or more forested plots were settled on all study sites. Greater amounts of $CaCO_3$ and Cl^- accumulated in the soil profile under tree cover than in the control.

Characteristics of natural and urbanized catchments were compared in the frame of the project TÁMOP 4.2.1/B-09/KONV-2010-0006. The urban soils from stream banks and the sediment of Rák Creek were analyzed within the context of the anthropogenic influence in the area of Sopron (Horváth et al. 2016). Results indicate covered parts of the watercourse were the most polluted; this is also confirmed by the enrichment factor (EF) of heavy metals. EF for Pb and Zn increased as we moved toward the city.

A new diurnal soil moisture fluctuation-based ET estimation method was validated using Hidegvíz Valley experimental catchment dataset. The method has a great advantage because it eliminates the need of specific yield (Sy). The ET rates of the proposed method lag behind the Penman–Monteith method by 30-60 minutes reference; otherwise, the two estimates compare favorably. ET rates of the new technique are 38% higher than the results of the original White method. By comparing the ET rates of the proposed method with traditional ET estimates from soil moisture, an almost magnitude difference can be detected. The proposed method has potential benefits in groundwater discharge areas, especially for warmer and drier growing seasons, which will likely result in limited water resources in the changing climate (Gribovszki 2018a).

Parallel soil-moisture profile and water table measurement were used by Gribovszki (2018b) to calculate Sy values, even on a sub-daily scale. Sy estimates were compared with values derived by traditional techniques. Slug-test-based Sy gave the most similar results to new estimations. So, slug-test methods, which are relatively cheap and quick, were most appropriate to estimate Sy for diurnal methods. The sub-daily dynamic characteristic of Sy (depending on the speed of drainage from the soil profile) was also analyzed, and a remarkable difference was found in Sy regarding water table changing speed. Research has been supported by the EFOP-3.6.2-16-2017-00018 in University of Sopron project.

2.7 OVF (General Directorate of Water Management)

General Directorate of Water Management had the following involvements in international co-operation and projects.

Flood protection and river management: Flood risk mapping and development of strategic risk management (KEOP-2.5.0/B/09-12-2013-0001) aims the revision of the Hungarian flood prevention strategy, considering the modern and remarkably changed social- economical demands on strategic and national level. The methodology of risk assessment was developed by considering relevant environmental, material and human life protection factors based on scientific methods of analysis and unified information background. In 2015, the General Directorate of Water Management drew up and published the hazard risk maps and strategic risk management plans based on preliminary

risk assessments, data acquisitions, and the determination and establishment of the applied methodology. From the year of 2017, in the framework of the compulsory revision of the developed flood risk management plans and maps (KEHOP-1.1.0-15-2016-00006), the reevaluation of measures and river basin management (RBM) plans are in progress. Regarding flood prevention issues, the elaboration of the strategical and scientific background of differentiated flood protection is also a deciding objective and task for sustainable and long-term effective flood protection and damage prevention. The development of the strategy and the preparation of legislative introduction are currently in progress. Within the framework of INTERREG Danube Transnational Program, dedicated to i) flood risk alleviation through floodplain restoration along the Danube River and its tributaries (DTP2-003-2.1), and; ii) develop tools contributing to the Danube basin wide floodplain restoration and preservation, a manual (addressed mainly to practitioners), called DRB Sustainable Floodplain management Strategic Guidance on ecological and flood protection features, is to be created.

The objective of another ongoing INTERREG project, called JOINTISZA, is to enhance the status of waters of the Tisza River Basin. It will focus on the interactions of two key aspects of water management — RBM and flood protection — while taking into account the relevant stakeholders who play a pivotal role in the Tisza RBM planning process. The main aim of the project is to further improve the integration of water management and flood risk prevention planning and actions for the next RBM planning cycle, in line with the relevant EU legislation.

Development of an Operational Drought and Water Scarcity Monitoring System in Hungary: The establishment of the monitoring network has been started with the aim of supporting Hungarian drought management (recently starting to emphasize prevention) and water resource management. The system incorporates novel detection and evaluation methods, based on which operational plans and legislation procedures will be elaborated. During the research activity preceding the development of the network a new, daily resolution drought index was elaborated. At present the input data for the index is provided by 47 monitoring stations, which were installed between 2016 and 2018. In the near future in total 150 stations will operate within the network. Beyond basic meteorological parameters the stations also provide soil moisture data from different depths, placing this way Hungarian water and drought management on new grounds. Novel information related to soil moisture can greatly support operational water resource management and the assessment of supplies and demands, being ultimately important for the agricultural sector to reach its goals concerning the development of irrigation and the facilitation of precision farming. A highly emphasized aim of the monitoring system is to bring into effect operational drought monitoring in Hungary, meaning that similarly to flood and excess water management, data and conditions become adequate to determine intervention levels, and to define precisely operational activities and related measures for legislative harmonization. The measured and calculated data provided by the monitoring network are published on a web portal, delivering information for decision makers, professionals or farmers free of charge, greatly supporting this was the everyday work of the most important stakeholders.

NEWADA duo project (Network of Danube Waterway Administrations - data and user) was a follow-up of the successful NEWADA project. Project objectives were: improved waterway management (integrated, sustainable and regionally coordinated), enhanced waterway maintenance (improved and coordinated performance), improved customer orientation of waterway related services, harmonized waterway infrastructure related basic data (defined quality, scope and availability of data), enhanced usage of Information and Communication Technologies (harmonized and up-to-date fairway information), increased visibility of waterway authorities, provide transition support from pilot implementation to regular operation, enable countries to tackle national priorities by involving partners.

DAREFFORT (Danube River Basin Enhanced Flood Forecasting Cooperation) is an international project launched officially in Budapest, Hungary on 13 September 2018. The three-year project aims at synchronizing and unifying the hydrological data information system for the Danube catchment. The most cost effective non-structural tangible solution which highly reflects the solidarity principle is the improvement of forecasting capabilities on basin-wide scale. The partners jointly work out the policy recommendations to be submitted to ICPDR in the interest of the establishment of the Danube Hydrological Information System (DanubeHIS) which is a fundamental step towards

flexible and sustainable data exchange. The focus is to enhance the access to the recorded hydrologic and ice data and to provide harmonized distribution for all the countries in the Danube catchment. For this purpose for all partners, interface software will be installed to provide standardized data services and as data source for EFAS.

The development of the hydrological forecasting system of the Hungarian Hydrological Forecasting Service (HHFS) is a continuous task. It includes the extension of the current system to previously not modelled subcatchments (Csík et al. 2017), introducing new elements to the methodology such as the fully dynamic hydraulic calculations and introducing alternative methods as seen in the case of river ice prediction. HHFS was also involved in the preparation works of the national water program (Barreto et al. 2017).

References

Anda A, Nagy K, Soós G, Kucserka T (2015a): Analyzing long-term evapotranspiration of Lake Fenéki wetland (Kis-Balaton, Hungary) between 1970 and 2012. Időjárás/Quarterly Journal of the Hungarian Meteorological Service, 119(1), 91-109.

Anda A, Soós G, Texeira da Silva J, Kozma-Bognár V (2015b): Regional evapotranspiration from a wetland in Central Europe, in a 16-year period without human intervention. Agricultural and Forest Meteorology, 205, 60-72.

Anda A, Simon B, Soós G, Teixira da Silva JA, Kucserka T (2016): Effect of submerged, freshwater aquatic macrophytes and littoral sediments on pan evaporation in the Lake Balaton region, Hungary. Journal of Hydrology, 542, 615-626.

Anda A, Soós G (2016): Some physiological responses of agricultural crops to global warming. Időjárás/Quarterly Journal of the Hungarian Meteorological Service, 120(1), 85-101.

Anda A, Soós G, Texeira da Silva J (2017): Practical use of Phragmites australis to study evapotranspiration in a wetland zone of Lake Balaton (southwest Hungary). Theoretical and Applied Climatology, 127(3), 899-909.

Anda A, Simon B, Soós G, Teixira da Silva JA, Kucserka T (2018a): Crop-water relation and production of two soybean varieties under different water supplies. Theoretical and Applied Climatology, https://doi.org/10.1007/s00704-018-2660-9.

Anda A, Simon B, Soós G, Kucserka T (2018b): Estimation of natural water body's evaporation based on Class A pan measurements in comparison to reference evapotranspiration. Időjárás/Quarterly Journal of the Hungarian Meteorological Service, 122(1), 41-58.

Anda A, Simon B, Soós G, Menyhárt L, Teixira da Silva JA, Kucserka T (2018c): Extending Class A pan evaporation for a shallow lake to simulate the impact of littoral sediment and submerged macrophytes: a case study for Keszthely Bay (Lake Balaton, Hungary). Agricultural and Forest Meteorology, 250-251, 277-289.

Balázs B, Bíró T, Dyke G, Singh SK, Szabó Sz (2018): Extracting water-related features using reflectance data and principal component analysis of Landsat images, Hydrological Sciences Journal, 63(2), 269-284.

Barreto S, Bártfai B, Engloner A, Liptay ZÁ, Madarász T, Vargha M (2017): Water in Hungary. Status overview for the National Water Programme of the Hungarian Academy of Sciences, 97. Link: https://mta.hu/data/dokumentumok/Viztudomanyi%20Program/Water_in_Hungary_2017_07_20.pdf.

Bene K, Torma P, Keve G, Hajnal G (2015): Impact of climate change on the Eger Creek watershed, In: Zoltán, Gribovszki; Kamila, Hlavčová; Péter, Kalicz; Silvia, Kohnová; Gemma, Carr (ed.) HydroCarpath-2015, Catchment processes in regional hydrology: Linking experiments and modelling in Carpathian drainage basins, Sopron, Magyarország, Nyugat-magyarországi Egyetem Kiadó, Paper: 11, 12.

Budai P, Clement A (2018): Spatial distribution patterns of four traffic-emitted heavy metals in urban road dust and the resuspension of brake-emitted particles: Findings of a field study. Transportation Research Part D: Transport and Environment, 62, 179-185, https://doi.org/10.1016/j.trd.2018.02.014.

Crago R, Szilágyi J, Qualls RJ, Huntington J (2016): Rescaling of the complementary relationship for land surface evaporation. Water Resources Research, doi:10.1002/2016WR019753.

Csáfordi P, Szabó A, Balog K, Gribovszki Z, Bidló A, Tóth T (2017): Factors controlling the daily change in groundwater level during the growing season on the Great Hungarian Plain: a statistical approach. Environ Earth Sci, 76:675, doi: 10.1007/s12665-017-7002-1.

Csáki P, Szinetár MM, Herceg A, Kalicz P, Gribovszki Z (2018): Climate change impacts on the water balance - case studies in Hungarian watersheds. Időjárás/Quarterly Journal of the Hungarian Meteorological Service, 122(1), 81–99, doi: 10.28974/idojaras.2018.1.6.

Csík A, Gauzer B, Gnandt B, Liptay ZÁ, Molnár K (2017): Extending the OLSER forecating system for small catchments in Hungary. In: Plamen Ninov, Elena Bojilova (ed.) Electronic book with full papers from XXVII Conference of the Danubian Countries on Hydrological Forecasting and Hydrological Bases of Water Management, 291-294, ISBN:978-954-90537-2-2.

Fernandez I, Petitta M, Hinsby K, Cseko A, Szűcs P, Padilla MG, Hartai E, Biševac V, Stein A, Bodo B, van der Keur P, Mikita V, Van Leijen G, García Alibrand CM (2017): The KINDRA project – towards Open Science in Hydrogeology for higher impact. European Geologist, 44, 38-43.

Garnier M, Harper DM, Blaskovicova L, Hancz G, Janauer GA, Jolánkai Zs, Lanz E, Lo Porto A, Mándoki M, Pataki B, Rahuel JL, Robinson VJ, Stoate C, Tóth E, Jolánkai G (2015): Climate Change and European Water

Bodies, a Review of Existing Gaps and Future Research Needs: Findings of the ClimateWater Project. Environmental Management, 56(2), 271-285, doi: 10.1007/s00267-015-0544-7.

Göttlinger I, Tamás EA, Varga Gy, Vas LT (2017): Case studies of 2D hydro-dynamic modelling of different Danube reaches in Hungary. In: Ninov P, Bojilova E (ed.) Electronic book with full papers from 27. Conference of the Danubian Countries on Hydrological Forecasting and Hydrological Bases of Water Management, Sofia, Bulgária, 339-345.

Gribovszki Z, Kalicz P, Balog K, Szabó A, Tóth T, Metwaly M, Szalai S (2017): Groundwater uptake of different surface cover and its consequences in great Hungarian plain. Ecological Processes 6:39, doi: 10.1186/s13717-017-0106-4

Gribovszki Z (2018a): Validation of diurnal soil moisture dynamic-based evapotranspiration estimation methods. Időjárás/Quarterly Journal of the Hungarian Meteorological Service, 122(1), 15–30, doi: 10.28974/idojaras.2018.1.2.

Gribovszki, Z (2018b): Comparison of specific-yield estimates for calculating evapotranspiration from diurnal groundwater-level fluctuations. Hydrogeol J, 26, 869-880, doi: 10.1007/s10040-017-1687-9.

Hatvani IG, Kovács J, Márkus L, Clement A, Hoffmann R, Korponai J (2015): Assessing the relationship of background factors governing the water quality of an agricultural watershed with changes in catchment property (W-Hungary). Journal of Hydrology, 521, 460-469, doi: 10.1016/j.jhydrol.2014.11.078.

Hatvani IG, Clement A, Korponai J, Kern Z, Kovács J (2017): Periodic signals of climatic variables and water quality in a river – eutrophic pond – wetland cascade ecosystem tracked by wavelet coherence analysis. Ecological Indicators, 83, 21-31, doi: 10.1016/j.ecolind.2017.07.018.

Hoang DT, Madarász T, Molnár J (2017): Investigation methods for pipe line tracing on University campus and leakage detecting in water utility networks: a case study in Miskolc. Advances in Environmental Sciences - International Journal of the Bioflux Society, 9(3), 193-206.

Herceg A, Kalicz P, Kisfaludi B, Gribovszki Z (2016): A monthly-step water balance model to evaluate the hydrological effects of climate change on a regional scale for irrigation design. Slovak Journal of Civil Engineering, 24(4), 27 – 35, doi: 10.1515/sjce-2016-0019.

Horváth A, Szita R, Bidló A, Gribovszki Z (2016): Changes in soil and sediment properties due the impact of the urban environment. Environ Earth Sci, 75:1211, doi: 10.1007/s12665-016-6012-8.

Hubai KE, Kucserka T, Karádi-Kovács K, Vass M, Kósa Á, Honti M, Padisák J (2017): Decoupling shredder activity and physical abrasion in leaf litter decomposition process: experiments in the Torna- stream (Hungary) affected by red-sludge disaster. Hydrobiologia, 785(1), 233-248.

Ilyés Cs, Turai E, Szűcs P (2018): Examination of rainfall data for 110 years using spectral and wavelet analysis. Central European Geology, 61(1), 1-15.

Jolánkai Zs, Koncsos L (2018): Base Flow Index Estimation on Gauged and Ungauged Catchments in Hungary Using Digital Filter, Multiple Linear Regression and Artificial Neural Networks. Periodica Polytechnica Civil Engineering, 62(2), 363-372, doi: 10.3311/PPci.10518.

Karches T, Orgoványi P (2018): Prediction of sludge reduction applying cascaded reactors in wastewater treatment. In: Feierabend M, Novytska O, Vouk D, Šabić M (ed.) 10th Eastern European IWA Young Water Professionals Conference Zagreb, Croatia: International Water Association (IWA), 223-225.

Karches T (2018a): Sewage Treatment Plant Upgrade Applying Wastewater Process Simulation. International Journal of Engineering Research and Development, 14(5), 22-26.

Karches T (2018b): Effect of Internal Recirculation on Reactor Models in Wastewater Treatment. WIT Transactions on Ecology and the Environment 228, 145-153.

Karches T (2018c): Effect of aeration on residence time in biological wastewater treatment. Pollack Periodica: An International Journal For Engineering And Information Sciences, 13(2), 97-106.

Kardos M, Koncsos L (2017): A stochastic approach for regionalscale surface water quality modeling. Pollack Periodica: An International Journal For Engineering And Information Sciences, 12(1), 17-27, doi: 10.1556/606.2017.12.1.2.

Keve G, Bene K, Hajnal G, Torma P (2015): Extrapolating water regime of Eger creek due to climate change. Sugo Szemle, 2, 18-25.

Keve G (2016): Space-time ice monitoring of the Hungarian Lower-Danube. Periodica Polytechnica Civil Engineering, 61(1), 27-38, doi: 10.3311/PPci.9116.

Keve G (2017): Utilization of gained experiences based on ice observation by webcameras. In: Ninov P, Bojilova E (ed.) Electronic book with full papers from XXVII Conference of the Danubian Countries on Hydrological Forecasting and Hydrological Bases of Water Management, Sofia, Bulgária, 68-78.

Knolmár M, Fülöp R (2018): Automation of SWMM Subcatchment Generation. International Journal of Advanced Engineering and Management Research, 3(2), 201-208, ISSN: 2456-3676.

Knolmár M, Németh A (2018): Application of Sediment Transport Models in a Sewer Network. International Journal of Advanced Engineering and Management Research, 3(4), 50-61, ISSN: 2456-3676.

Koch D, Horvat Z (2018): Field measuremenets and hydraulic computation of a culvert. Proceedings of the Faculty of Civil Engineering Subotica 34, 57-66.

Koch D, Bene K, Keve G (2017): Hydraulic design of culverts. In: Ninov P, Bojilova E (ed.) Electronic book with full papers from XXVII Conference of the Danubian Countries on Hydrological Forecasting and Hydrological Bases of Water Management, Sofia, Bulgária, 53-59.

Kocsis T, Anda A (2017): Analysis of precipitation time series at Keszthely, Hungary: (1871-2014). Időjárás / Quarterly Journal of the Hungarian Meteorological Service, 121(1), 63-78.

Kocsis T, Anda A (2018): Parametric or non-parametric: analysis of rainfall time series at a Hungarian meteorological station. Időjárás/Quarterly Journal of the Hungarian Meteorological Service, 122(2), 203-216.

Kocsis T, Kovács ISz, Anda A (2017): Comparison of parametric and non-parametric time-series analysis methods on a long-term meteorological data set. Central European Geology, 60(3), 1-17.

Kovács J, Tanos P, Várbíró G, Anda A, Molnár S, Hatvani IG (2017): The role of annual periodic behavior of water quality parameters in primary production: chlorophyll-a estimation. Ecological Indicators, 78, 311-321.

Kucserka T, Simon B, Anda A (2018): Decomposition of Salix and Populus leaves in standard class "A" evaporation pans in Hungary. In: Anežka, Čelková - 25th International Poster Day and Institute of Hydrology Open day: Transport of Water, Chemicals and Energy in the Soil-Plant-Atmosphere System: Proceedings of peer-reviewed contributors Bratislava: Institute of Hydrology SAS, 52-59.

Mátyás K, Bene K (2017): Comparison of Annual Prediction Methods for Spring Flow in the Aggtelek Region. Acta Technica Jaurinensis, 10(1), 70-83.

Mátyás K, Bene K (2018): Using numerical modeling error analyses methods to indicate changes in a watershed. Pollack Periodica: An International Journal For Engineering And Information Sciences, 13(3), 175-186.

Menyhart L, Anda A, Nagy Z (2015): A new method for checking the leveling of pyranometers. Solar Energy, 120, 25-34.

Móricz N, Tóth T, Balog K, Szabó A, Rasztovits E, Gribovszki Z (2016): Groundwater uptake of forest and agricultural land covers in regions of recharge and discharge. Iforest-Biogeosciences and Forestry &: 714-719, doi: 10.3832/ifor1864-009.

Murinkó LG, Bene K (2017): Modelling a loess bank hydrology along the Danube in Hungary. Pollack Periodica: An International Journal for Engineering and Information Sciences, 12(1), 3-15.

Nagy E, Torma P, Bene K (2016): Comparing methods for computing the time of concentration in a medium-sized Hungarian catchment. Slovak Journal of Civil Engineering, 24(4), 8-14.

Oroszi VGy, Tamás EA, Kosztyi B (2017): Flood management education in the Danube basin - needs and challenges. Hidrológiai Közlöny, 97(3), 24-31.

Petitta M, Del Bon A, Bodo B, Cseko A, Fernandez I, Muller P, Garcia Alibrandi C, Padilla M, Hartai E, Mikita V (2018): The KINDRA project: sharing and evaluating groundwater research and knowledge in Europe. Acque Sotterranee - Italian Journal of Groundwater, 7(1), 7-16.

Salamon E, Goda Z, Berek T (2018), Analysis of reverse osmosis filter permeability. Pollack Periodica: An International Journal For Engineering And Information Sciences, 13(3), 221-230.

Simon B, Simon Sz, Kucserka T, Anda A (2018a): Decomposition dynamics of willow and poplar leaf litter in the area of Lake Balaton and Kis-Balaton Wetland System. In: Anežka, Čelková - 25th International Poster Day and Institute of Hydrology Open day: Transport of Water, Chemicals and Energy in the Soil-Plant-Atmosphere System: Proceedings of peer-reviewed contributors Bratislava: Institute of Hydrology SAS, 143-148.

Simon B, Kucserka T, Anda A (2018b): Investigation of Salix alba and Populus tremula leaf litter decomposition in the area of Lake Balaton and Kis-Balaton Wetland. Acta Agraria Debreceniensis, 74, 159-162.

Szabó A, Gribovszki Z, Jobbagy EG, Balog K, Bidló A, Tóth T (2018): Subsurface accumulation of $CaCO_3$ and Cl^- from groundwater under black locust and poplar plantations. Journal of Forestry Research, Springer Nature, doi: 10.1007/s11676-018-0700-z.

Szilágyi J (2015): Complementary-relationship-based 30-year normals (1981-2010) of monthly latent heat fluxes across the contiguous United States. Water Resources Research, doi:10.1002/2015WR017693.

Szilágyi J, Crago R, Qualls R (2016): Testing the generalized complementary relationship of evaporation with continental-scale long-term water-balance data. Journal of Hydrology, 540, 914-922.

Szilágyi J, Crago R, Qualls RJ (2017): A calibration-free formulation of the complementary relationship of evaporation for continental-scale hydrology. Journal of Geophysical Research-Atmospheres, 122, doi:10.1002/2016JD025611.

Szilágyi J (2018a): A calibration-free, robust estimation of monthly land surface evapotranspiration rates for continental-scale hydrology. Hydrology Research, 49, doi:10.2166/nh.2017.078.

Szilágyi J (2018b): Anthropogenic hydrological cycle disturbance at a regional scale: state-wide evapotranspiration trends (1979-2015) across Nebraska, USA. Journal of Hydrology, 557, 600-612, doi:10.1016/j.jhydrol. 2017.12.062.

Szilágyi J, Józsa J (2018): Evapotranspiration Trends (1979–2015) in the Central Valley of California, USA: Contrasting Tendencies During 1981–2007. Water Resources Research, doi: 10.1029/2018WR022704.

Tamás EA (2015): Integration of sediment studies into the training of civil engineers at Eötvös József College. Sugó Szemle 2(2), 78-88.

Tamás EA, Ficsor J (2018): Questions in the quantitative analysis of sediment load - example of three major rivers in Hungary. E3S Web of Conferences 40 p. 04023.

Ungvári G, Jolánkai Zs, Kiss A, Kozma Zs (2018) The Feasibility of cooperation to comlpy with land use change obligations in the Marosszög area of South Hungary. Journal of Environmental Geography, 11(3-4), 35-45, doi: 10.2478/jengeo-2018-0011.

HUNGARIAN NATIONAL REPORT ON IAMAS (2015-2018)

László Bozó[*]

1 Introduction

In Hungary, the regular meteorological measurement activity begun in 1717 in Sopron. János Ádám Gensel, physician and scientist was the first Hungarian who recorded temperature and atmospheric pressure several times a day. In the past nearly 150 years our predecessors worked according to the scientific and technological standards of the time, thus Hungarian Meteorological Service (OMSZ) is facing the challenges of our days as an institute with large experience. OMSZ has diverse tasks in the areas of weather, climate and ambient air, ranging from daily operational duties through research and development to education of the general public (Buránszkiné et al. 2018).

2 Surface and Upper Air Observations, Radar Network

Our surface monitoring network is currently made up of 139 own, 142 jointly operated by General Directorate of Water Management and 12 other automatic weather stations and we have about 460 conventional rainfall stations. The automatic meteorological stations basically measure the weather parameters (air temperature and humidity, air pressure, wind, precipitation), but we also perform gamma-dose rate measurements at 28 sites for early detection of radioactive hazard, at three places aerosols with alpha, beta and gamma activity are monitored and at some dozen stations we measure soil temperature and soil moisture at several layers, which are important for agriculture. We make our best to meet the needs of reliable meteorological data by installing mobile measuring stations where we flexibly adjust the measuring program, communication and power supply to user requirements. For continuous operation the network inspectors of OMSZ regularly check the technical parameters of the stations and perform the necessary maintenance.

We started modernization and development of the meteorological stations at the civil airports in 2015, which enables operation of meteorological stations at all the 4 rural international airports (Pér, Pécs-Pogány, Debrecen, Sármellék) in compliance with the regulation of ICAO (International Civil Aviation Organization) and National Transport Authority so they are capable to prepare the airport weather reports (METAR) automatically.

To measure atmospheric state variables vertically, we regularly launch radiosondes in Budapest and Szeged at the same time as about other 750 radiosonde stations around the world. The sonde is lifted up by a hydrogen-filled meteorological balloon. The probe rises up to 25 to 30 km in about one and a half hours, while its electronic sensors are continuously measuring and its transmitter broadcasting the pressure (for certain type), temperature, relative humidity of the surrounding air and current GPS coordinates of the radiosonde to determine the direction and speed of the upper wind. The four daily ascents instead of the previous two resulted in significant progress, thanks to the recent testing and introduction of a new, more economical radiosonde, the developing and refining of which our staff were also involved in.

In recent years, we have put great emphasis on the development of the national weather radar network, which basically monitors rainfall, measures intensity of precipitation and tracks the atmospheric events. OMSZ operates a network of four radars, the latest of which was installed in the Southern Great Plain region near Szentes in October 2014. In addition to the installation of the new device, upgrade of the Budapest, Pogányvár and Napkor radars was also completed. We have not only developed our equipment, but also the products obtainable from the results of radar measurements. Instead of the former two-dimensional radar images, three-dimensional composite images are being made, enabling investigation of not only the horizontal properties of precipitation systems, but their vertical structure as well. The new products significantly contribute to severe weather forecasting and aviation meteorology.

[*]*Hungarian Meteorological Service, Budapest, H-1525 P.O.Box 38.*
E-mail: bozo.l@met.hu

The Government of Hungary decided on installation of a new radar in the South Hungarian region for the proper meteorological service of a national hail prevention system – applying updraft seeding by ground-based generators – designed to reduce the significant damage caused by hail in the national economy and therefore provided additional resources for Hungarian Meteorological Service. The network of five weather radars is anticipated to provide an outstanding technical base for detecting hazardous convective cells from 2019 (Buránszkiné et al. 2018).

3 Atmospheric Physical Measurements

Beside measuring and observing the weather parameters it is also our task to examine the other physical parameters of the atmosphere. We perform the measurements of the total ozone content of the atmosphere, the spectral UV-A radiation and the spectral UV-B radiation and the spectral solar radiation determining transmittance of the atmosphere, the results of which are transmitted to international data centres. We keep the population informed about the measured value and strength of the UV-B radiation in the summer season. In addition to the measurements of solar radiation, we started intensive development activity for examining the possibilities for short-term forecasting of solar radiation, which is of great importance in the production of solar energy as a renewable energy source. At the sixth meeting of the Regional Association VI of World Meteorological Organization held in October 1978, Marczell György Main Observatory was admitted to the regional radiation centers in RA VI.

4 Weather Forecasting

Besides the general forecasts we prepare severe weather warnings to protect life and property, detailed meteorological forecasts for the catchments of Tisza and Danube rivers (for flood and inland flood prevention) and we also provide meteorological services for the civil aviation. We satisfy requests of various users from both state and economic sectors, including media. Staff of our institution monitors the weather development for 24 hours a day, analyzes the latest model outputs and updates the forecasts. The aspect and the content of a weather forecast can significantly differ depending on whether that a severe weather warning, a general forecast or forecast with a special purpose prepared is. As for the time-range, we issue detailed forecasts for the following hours and days, but also outlooks for several weeks ahead. While some forecasts are issued for the entire country or regions, others focus on the weather characteristics of a specific location. Some users require forecast of special weather parameters, thus, a completely unique service is defined and provided upon their request. The quality of our forecasts is constantly verified, model and methodological developments are being carried out.

Nowadays meteorologists widely apply computer-based numerical weather prediction models, but in case of nowcasting (1-3 hour forecasts) it is very important to analyse the current weather situation of the possible highest accuracy.

Without meteorological measurements dense in both space and time it is almost impossible to tell what the weather will be, even for the next few hours. Therefore OMSZ is continuously developing the network of synoptic stations and expanding them with new instruments. Information about the course of temperature, wind, humidity and air pressure is provided by the automatic weather stations at every 10 minutes. The radar network updates the information on rainfall areas every 5 minutes, development of thunderstorms can be tracked by the help of the lightning detection network. High resolution satellite images also help the work of meteorologists owing to international cooperation. Several measurement data are processed and integrated in the MEANDER nowcasting system providing forecasts for a few hours ahead (László and Salavec 2018). For short and medium-range forecasts, we primarily use the model of European Centre for Medium-Range Weather Forecasts (ECMWF) and the AROME model, which is run by the supercomputer of OMSZ, but the results of other models (e.g. GFS, WRF) are also taken into account when preparing forecasts (Ihász et al. 2018, Lancz et al. 2018, Wang et al. 2018). With the

spread of the ensemble technique, the role of the probability forecasting and uncertainty information concerning forecasts is continuously increasing (Wastl et al. 2018).

The internationally acknowledged HAWK (Hungarian Advanced Workstation) developed at OMSZ is the most important tool in the operational forecasting. The system assimilates all information necessary for the forecast preparation. It displays the data interactively in customized maps or in a graph format (meteogram) at the selected points.

5 Severe Weather Forecasting and Storm Warning for Lakes

Severe weather forecasting is aimed at protecting lives and properties. The main purpose of the system is to ensure a credible source of information for the general public, media, disaster management and other state authorities in critical weather situations. The system provides a quick overview on current and future weather risks extended (from 2018 onwards) for the next four days, divided on districts or counties and emphasized by colour codes. The continuously updated severe weather warnings with a lead time of 1-3 hours are available on the website of OMSZ and on the Meteoalarm portal, which has been developed and operated in a frame of a European cooperation.

The pre-warnings or alerts can be related to heavy thunderstorm, torrential rain, wind gust, freezing rain, blowing snow. The severe weather warning system also consists of pre-warnings on long-lasting, high-amount rain or snow, as well as of so-called „special" warnings on occurrence of heat wave, extreme cold period or persistent dense fog.

The storm warning season at the lakes of our country lasts from 1 April to 31 October each year. During this period, we ensure the safety of tourists and water transport at the lakes Balaton, Velence and Tisza. The first degree of warning is issued when wind speed is expected between 40-60 km/h and the second degree of warning if wind speed may exceed 60 km/h. For decades, there have been no fatal accidents at the lakes which would have been a result of late or missing warning.

Starting from 2018, OMSZ is responsible to operate a supporting system to mitigate the atmospheric hail damage. Co-operating partner is the Hungarian Chamber of Agriculture. The model basis of the supporting system is WRF, optimized for the prediction of deep convections. In addition, diagnostic fields derived from the development of AROME and ECMWF models also contribute to hail damage mitigation efforts. It should also be noted, that new products from radar measurements could improve the reliability of forecasts related to this activity.

6 Aviation Meteorology

Meteorological information and products supporting a variety of air transport activities enable safer, more efficient and cost-effective operation of airspace users, air navigation service providers and air traffic management. Our forecasts for aviation meteorology are used in both national and international air traffic. Our forecasting activity is performed in accordance with international standards, but we also make several other forecasts tailored to the needs of our customers, which supplement the standard products. Based upon ICAO recommendations, we issue warning reports for the international aviation in case of conditions threatening the flights. We also prepare forecasts for four Hungarian international airports (Sármellék, Pér, Pécs, Debrecen). The meteorological support of national aviation is carried out by area forecasts, in which we provide information on severe weather events upon criteria established in cooperation with the aviation authorities.

In addition to the operational work, we are constantly improving our products to increase the safety of the flight. Since 2016, the new Aviation Meteorology website (aviation.met.hu) provides access to up-to-date and credible aviation weather reports and forecasts. On this site, special forecasts for the needs of sport aviation are also available (Buránszkiné et al. 2018).

To improve the service for the most vulnerable low level flights, we are participating in an international project aimed at providing uniform and harmonized meteorological information in Central and South-Eastern Europe through a common electronic interface for general purpose flight.

7 Statistical Climatology and Climate Modeling

Detection of climate change requires accurate comparison of the data measured nowadays and in the past, while the environment, instruments and methods of measurements have changed several times over the years (Babolcsai and Hirsch 2019). On the other hand, we are also curious about changes in areas where measured data are not available. Thus, it is essential to apply statistical methods to the carefully controlled data by which we get homogenized grid data series. During the regional CarpatClim project and the establishment of the Hungarian NAGiS (National Adaptation Geo-information System) database some years ago, we created daily homogenized grid data series at 0.1° spatial resolution using the homogenization and interpolation techniques developed by us (MASH-MISH systems).

Data series have been prepared for the most important meteorological variables (e.g. maximum, minimum and mean temperature, global radiation, wind, relative humidity, air pressure, clouds) and other derived parameters, indices (e.g. days with special rainfall and temperature thresholds, drought indices, tourism climate indices). We keep our databases up to date, taking into account additional stations can be used as a result of data recording, furthermore we extend them to other variables and to the last few years. Our climate specialists developing homogenisation and interpolation processes are internationally acknowledged and our methods are used in many other countries as well. Our recognition is also reflected in the fact that the great international assemble of meteorologists in this discipline has always been organized in Budapest.

The idea to initiate climate dynamics research at OMSZ (besides the traditional statistical climatology) had arisen in 2003, as modelling provides the only tool to explore the potential response of the climate system to a hypothetic anthropogenic forcing. Climate projections inherently include uncertainties arising from the chaotic nature of the climate system, from imperfections of the numerical models and also from the ambiguous future evolution of human activity (Gerhátné Kerényi, 2018). Therefore, the correct interpretation of the model simulations should contain information about their likelihood. This can be achieved with the ensemble technique, i.e., with the joint evaluation of several climate model experiments. For this reason, two regional climate models (RCMs) were adapted at our service: ALADIN-Climate, which was developed at Météo France, and REMO model of Max Planck Institute in Hamburg. Having established the modelling fundaments OMSZ joined to the European research network and participated in international cooperations investigating climate change effects. For the assessment of 21st century climate change in Hungary, several projections have been made by ALADIN-Climate and REMO applying different anthropogenic scenarios. Furthermore, other European climate model results produced under the framework of Euro-CORDEX international collaboration have been assessed in order to reveal whether the larger ensemble modifies the uncertainty range of the future changes. The National Adaptation Geo-information System (NAGiS) created in 2013 provides a harmonized data basis for the adaptation studies using locally run RCM results as inputs for the quantitative climate impact assessments. Given the efforts of the Regional Climate Modelling Group of OMSZ, the end users have become acquainted with the probabilistic climate information and the decision making based on them.

8 Air Quality Modelling

Neither financial nor technical possibilities exist to carry out measurements in every spatial point. However, continuous spatio-temporal distribution of air pollutant concentrations can be calculated based on the known characteristics of atmospheric flows and pollutants, the localization and yield of main sources (Németh et al. 2018). In addition, mathematical models describing the dispersion and transport of air pollutants make the evaluation of the eventual effects of supposed releases (impact studies and – combined with numerical weather prediction models – the estimation of the expected evolution of air pollution possible (Ferenczi et al. 2018, O-Groma et al. 2018). Different models are effective to use for different problems, on the one hand to keep the computation needs within

feasible limits, and on the other hand, because the relevance of individual processes varies depending on the target and spatio-temporal scale of their application (Blumberger et al. 2019).

Based on EU regulations, in addition to air pollution monitoring, Member States prepare national regional and urban air quality reports based on model calculations. These assessments contain identification of emission sources affecting air quality of a region. These kinds of calculations are based on multi-layer model systems. At Hungarian Meteorological Service, development of an evaluation model system started in 2015. First, the EMEP chemical transport model has been adapted to calculate concentrations over Europe using the gridded emission database of EMEP as well as the meteorological data of ECMWF. The EMEP model provides us with lateral and initial boundary conditions for air pollution concentration calculations. Based on this information, model calculations of finer spatial resolution (10 km x 10 km) can be done for Hungary, taking into account the transboundary long-range transport of air pollutants. Model calculations for the air quality of Budapest are performed with the CHIMERE chemical transport model. Another important condition of the model runs is an emission database of 0.1^0 x 0.1^0 resolution. Primarily in case of accidental releases from point sources, transport and dispersion of air pollutants is calculated for European, regional as well as local scales. Operative model runs are done twice a day for Paks nuclear power plant using the regional scale FLEXPART dispersion model and given emission values. Model runs can also be manually operated via the HAWK system of OMSZ, which means, that real emission data can be put into the system by the users in case of an accident.

References

Babolcsai G, Hirsch T (2019): Teleconnection between mean sea level pressure in the North Atlantic for September, the AMO phase and mean temperature in Central Europe for December (1896-2015). Meteorological Applications, 26(2), 267-274, Doi: 10.1002/met.1760.

Blumberger ZI, Vasanits-Zsigrai A, Farkas G, Salma I (2019): Mass size distribution of major monosaccharide anhydrides and mass contribution of biomass burning. Atmospheric Research, 220,1-9.

Buránszkiné Sallai M, Szabó D, Tölgyesiné Puskás M, Tóth R (2018): Tradition, Profession, Innovation. Hungarian Meteorological Service, Budapest.

Ferenczi Z, Imre K, Bozó L (2018): Application of trajectory clustering for determining the source regions of secondary inorganic aerosols measured at K-puszta background monitoring station, Hungary. Air Pollution Modeling and its Application XXV. Springer Proceedings in Complexity, DOI: 10.1007/978-3-319-57645-9_92.

Gerhátné Kerényi J (2018): Application of remote sensing for the determination of water management parameters. Hydrology SAF. Időjárás, 122(1), 1-13.

Ihász I, Mátrai A, Szintai B, Szűcs M, Bonta I (2018): Application of European numerical weather prediction models for hydrological purposes. Időjárás, 122, 59-79.

Lancz D, Szintai B, Honnert R (2018): Modification of a Parametrization of Shallow Convection in the Grey Zone Using a Mesoscale Model. Boundary-Layer Meteorology, 169(3), 483-503.

László E, Salavec P (2018): Relationship between weather conditions advantageous for the development of urban heat island and atmospheric macro-circulation changes. International Journal of Climatology, 38(8), 3224-3232.

Németh Z, Rosati B, Zíková N, Salma I, Bozó L, Dameto de España C, Schwarz J, Ždímal V, Wonaschütz A (2018): Comparison of atmospheric new particle formation events in three Central European cities. Atmospheric Environment, 178, 191-197.

O-Groma V, Ferenczi Z, Osán J, Török Sz, Steib R (2018): Verification of the EDMS model adapted to Budapest Liszt Ferenc Airport. Int. J. Environment and Pollution, 63(3), 137-153.

Wastl C, Simon A, Wang Y, Kulmer M, Baár P, Bölöni G, Dantinger J, Ehrlich A, Fischer A, Frank A, Heizler Z, Kann A, Stadlbacher K, Szintai B, Szűcs M, Wittmann C (2018): A seamless probabilistic forecasting system for decision making in Civil Protection. Meteorologische Zeitschrift, 27(5), 417-430.

HUNGARIAN NATIONAL REPORT ON IAPSO (2015-2018)

László Horváth[*], *Tamás Weidinger*[**]

In this compilation a brief summary is given on the activity of Hungarian scientists in the field of oceanography based on the summaries appeared in the articles. In the reported period, one review study and some research papers partly or fully dealing with aspects of oceanography were published by Hungarian authors or in co-authorship with Hungarians. We disregarded the papers dealing only with climate aspects unless the relation to the oceans is/was mentioned.

1 Review article

Oceanic research in Hungary has a long history. As Csernussi (2018) summarized in his review article the oceanography was developed in the Adriatic-Mediterranean region in a short time during the time of Austro-Hungarian monarchy (1867-1918). There was a need for stations to run scientific researches and to have bases for the expeditions. The Hungarian scientists were always among the firsts from the beginning, but they could get their own station only in 1905, at Fiume (Rijeka). Before the outbreak of World War I they were able to run a lot of research and two famous Adriatic expeditions. After World War I Hungary lost its sea and two-thirds of its ground but it has never lost the respect to the oceans' life.

2 Scientific research in connection with oceanography

Bozóki et al. (2019) reported a laboratory study on the large-scale ocean circulation in connection of Drake Passage. They reported a laboratory model of the large-scale flow phenomena in the Southern Ocean with a closed Drake Passage, imitating the situation before the Eocene-Oligocene transition (EOT) ca. 34 million years ago. In a differentially heated rotating annular wave tank an insulating 'meridional' barrier is installed to block zonal circulation. The obtained temperature fields and time series are compared to the ones from control runs with partially blocked and fully opened 'passages'. In the 'closed' case a persistent azimuthal temperature gradient emerges whose magnitude scales linearly with the 'meridional' temperature contrast. The anomalous temperature distribution is accompanied with perturbations of the background flow yielding significantly larger low-frequency variability than in the 'opened' configuration. The experimental findings have implications to the EOT but at present validation of results is hindered by the lack of deep-sea drilling data from the Southeast Pacific and adjacent parts of the Southern Ocean. The model may inspire further paleoceanographic research in this largely unexplored region.

Medjdoub et al. (2019) published an article on their laboratory investigations on the resonant feature of 'dead water' phenomenon. As they summarized interfacial internal wave excitation in the wake of towed ships is studied experimentally in a quasi-two layer fluid. At a critical 'resonant' towing velocity, whose value depends on the structure of the vertical density profile, the amplitude of the internal wave train following the ship reaches a maximum, in unison with the development of a drag force acting on the vessel, known in the maritime literature as 'dead water'. The amplitudes and wavelengths of the emerging internal waves are evaluated for various ship speeds, ship lengths and stratification profiles. The results are compared to linear two- and three-layer theories of freely propagating waves and lee waves. They find that despite the fact that the observed internal waves can have considerable amplitudes, linear theories can still provide a surprisingly adequate description of subcritical-to-supercritical transition and the associated amplification of internal waves.

Gravity waves play an essential role in the dynamics of oceans. In the paper of Vincze and Bozóki (2017) interfacial internal waves in a stratified fluid excited by periodic free-surface pertur-

[*]*IUGG-IAPSO National Representative*
E-mail: horvath.laszlo.dr@gmail.com
[**]*Department of Meteorology, Eötvös Loránd University,*
Pázmány Péter sétány 1/A, H-1117 Budapest, Hungary
E-mail: weidi@caesar.elte.hu

bations in a closed tank are studied experimentally. As they summarized barotropic-baroclinic energy conversion is induced by the presence of a bottom obstacle. The connection between horizontal surface velocities and internal wave amplitudes is investigated, the developing flow patterns are described qualitatively, and the wave speeds of internal waves are systematically analysed and compared to linear 2- and 3-layer theories. They find that, despite of the fact that the observed internal waves can have considerable amplitudes, a linear 3-layer approximation still gives fairly good agreement with the experimental results.

Tél et al. (2018) demonstrated experimentally the water-holding property of three-dimensional vortices. In summary when injecting dye into a vertical vortex generated by a commercial magnetic stirrer, one finds that dye remains captured around the vortex core over minutes, while it gets mixed with the water outside this region rather rapidly. Thus, considering its horizontal motion, the dye becomes trapped within a critical radius, even though the vortex structure (and the dyed region) is aperiodically time-dependent due to the oscillations of the position of the stirring bar. According to a recent paper by Haller et al. (2016), three-dimensional time-dependent vortices should be defined as rotating, material-holding tubular regions of the fluid. They reported a set of experiments carried out with magnetic-stirrer-generated vortices which appears to provide the first pieces of evidence supporting the theory in a very elementary set-up that is accessible even in high schools. Data also provide information about quantities not predicted by the theory, e.g., the lifetime of dye spent within the vortex. They showed that the maximum radius of the stable dye cylinders, i.e., the horizontal extent of the vortex, hardly depends on the rotational frequency of the stirrer bar - at least in the range investigated - but increases with the length of the bar. A generalization of this finding leads to the conclusion that the size of the material-holding region of the vortices in nature should be proportional to the size of the surface (or pressure) depression accompanying the vortex. As they concluded, their results may imply that the domain in which water parcels are transported by oceanic eddies is approximately of the size of the local Rossby radius.

Baroclinic instability is of fundamental importance in the atmosphere and in the oceans. Vincze et al. (2016) published an article on the basis of their laboratory investigations on the barostrat instability as the double-diffusive convection and baroclinic instability in a differentially heated and initially stratified rotating system. In summary, water-filled differentially heated rotating annulus with initially prepared stable vertical salinity profiles was studied in the laboratory. Based on two-dimensional horizontal particle image velocimetry data and infrared camera visualizations, they described the appearance and the characteristics of the baroclinic instability in this original configuration. First, they showed that when the salinity profile is linear and confined between two non-stratified layers at top and bottom, only two separate shallow fluid layers can be destabilized. These unstable layers appear nearby the top and the bottom of the tank with a stratified motionless zone between them. This laboratory arrangement is thus particularly interesting to model geophysical or astrophysical situations where stratified regions are often juxtaposed to convective ones. Then, for more general but stable initial density profiles, statistical measures are introduced to quantify the extent of the baroclinic instability at given depths and to analyse the connections between this depth-dependence and the vertical salinity profiles. They found that, although the presence of stable stratification generally hinders full-depth overturning, double-diffusive convection can lead to the development of multicellular sideways convection in shallow layers and subsequently to a multi-layered baroclinic instability. Therefore it has been concluded that by decreasing the characteristic vertical scale of the flow, stratification may even enhance the formation of cyclonic and anticyclonic eddies (and thus, mixing) in a local sense.

Another study also in connection with barostrat instability was published by Rodda et al. (2018) including a Hungarian co-author among others. As they summarized the differentially heated rotating annulus is a laboratory experiment historically designed for modelling large-scale features of the mid-latitude atmosphere. In the present study, they investigated a modified version of the classic baroclinic experiment in which a juxtaposition of convective and motionless stratified layers is created by introducing a vertical salt stratification. The thermal convective motions are suppressed in a central region at mid-depth of the rotating tank, therefore double-diffusive convection rolls can develop only in thin layers located at top and bottom, where the salt stratification is weakest. For

high enough rotation rates, the baroclinic instability destabilises the flow in the top and the bottom shallow convective layers, generating cyclonic and anticyclonic eddies separated by the stable stratified layer. Thanks to this alternation of layers resembling the convective and radiative layers of stars, the planetary's atmospheric troposphere and stratosphere or turbulent layers at the sea surface above stratified waters, this new laboratory setup is of interest for both astrophysics and geophysical sciences. More specifically it allows to study the exchange of momentum and energy between the layers, primarily by the propagation of internal gravity waves (IGW). PIV velocity maps are used to describe the wavy flow pattern at different heights. Using a co-rotating laser and camera, the wave field is well resolved and different wave types can be found: baroclinic waves, Kelvin and Poincaré type waves. The signature of small-scale IGW can also be observed attached to the baroclinic jet. The baroclinic waves occur at the thin convectively active layer at the surface and the bottom of the tank, though decoupled they show different manifestation of nonlinear interactions. The inertial Kelvin and Poincaré waves seem to be mechanically forced. The small-scale wave trains attached to the meandering jet point to an imbalance of the large-scale flow. For the first time, the simultaneous occurrence of different wave types is reported in detail for a differentially heated rotating annulus experiment.

In the reported period, many papers appeared by Hungarian authors concerning the atmosphere-ocean climate system. One of them has been published by Herein et al. (2015). Summarizing their findings a time series resulting from a single initial condition is shown to be insufficient for quantifying the internal variability in a climate model, and thus one is unable to make meaningful climate projections based on it. The authors argue that the natural distribution, obtained from an ensemble of trajectories differing solely in their initial conditions of the snapshot attractor corresponding to a particular forcing scenario should be determined in order to quantify internal variability and to characterize any instantaneous state of the system in the future. Furthermore, as a simple measure of internal variability of any particular variable of the model, the authors suggest using its instantaneous ensemble standard deviation. These points are illustrated with the intermediate complexity climate model Planet Simulator forced by a CO_2 scenario, with a 40-member ensemble. In particular, the levelling off of the time dependence of any ensemble average is shown to provide a much clearer indication of reaching a steady state than any property of single time series. Shifts in ensemble averages are indicative of climate changes. The dynamical character of such changes is illustrated by hysteresis-like curves obtained by plotting the ensemble average surface temperature versus the CO_2 concentration. The internal variability is found to be the most pronounced on small geographical scales. The traditionally used 30-yr temporal averages are shown to be considerably different from the corresponding ensemble averages. Finally, the North Atlantic Oscillation (NAO) index, related to the teleconnection paradigm, is also investigated. It is found that the NAO time series strongly differs in any individual realization from each other and from the ensemble average, and climatic trends can be extracted only from the latter. One of the conclusions of the paper is, authors argue that the only appropriate probabilistic description of the climate at any instant of time, which fully reflects the internal variability of the dynamics, is the natural distribution of the snapshot attractor corresponding to this time instant, applicable in practice even to GCMs. Thus the proper approach to characterize any climate change is to follow the temporal evolution of this distribution in time. An important consequence of the latter observation is that the individual 30-yr (or any multidecadal) averages might be misleading.

3 Studies on palaeoceanography

A study appeared in Hungarian on the palaeoceanographic history of the Hungarian Paleogene Basin by paleoecological analysis of benthic foraminifera by Ozsvárt (2018). According to his summary investigations of 16 late Palaeogene (Lutetian–Rupelian) boreholes and sections from the Hungarian Palaeogene Basin were investigated for their benthic foraminiferal faunas in order to reconstruct its palaeoecological and palaeoceanographic evolution. In the mentioned ecological interpretation of the temporal distribution of foraminiferal assemblages, multivariate statistical methods were used. These methods included Q-mode principal factor analysis (PFA) and BFOI

(Benthic Foraminiferal Oxygen Index) analysis. On the basis of the Q-mode principal factor analysis, the faunas are characteristic for inner neritic (0–30 m water depth) to upper bathyal environments (approximately 30–500 m water depth). The composition of the benthic foraminiferal fauna and the results of the Q-mode principal factor analysis indicate tropical–warm conditions from the beginning of the Middle Eocene. A change in the temperature of the bottom water can be detected from the late Middle Eocene time, and estimated temperatures indicate temperate–cold conditions during this period. On the basis of the BFOI (Benthic Foraminiferal Oxygen Index) analysis, the Middle and Late Eocene are characterised by two short eutrophic events (POMZ1 and POMZ3) and two significant eutrophic (POMZ2 and POMZ4) events. These periods are characterised by evidence of a low diversity of fauna, with a high dominance of low-oxygen tolerant (infaunal) species. The eutrophic events suggest that there was a second-order sea-level fall and restricted deep water circulation, while the oligotrophic and high oxic conditions might have been caused by colder, well-oxygenated bottom water masses from the SE Tethyan Realm. Evidence suggests that these oligo- to mesotrophic periods were characterised by a high diversity of fauna, with a significant dominance of epifaunal species. The initial stage of the significant subsidence history coincides with the POMZ2 period at the end of the NP17 zone. This demonstrates clearly that the evolution of the Hungarian Palaeogene Basin was strongly influenced by significant events.

Another paper has been published by Ozsvárt et al. (2018) in connection with palaeoceanography. They studied two boreholes (Cserépváralja-1 and Kiscell-1) with continuous sedimentary records across the Eocene-Oligocene climate transition from the Central Paratethyan area. Assemblages of benthic foraminifera display a shift in dominance by epifaunal taxa in the late Eocene to shallow and deep infaunal taxa in the early Oligocene. Using the benthic foraminiferal oxygen index (BFOI), a decreasing trend of bottom-water oxygen levels is established across the Eocene-Oligocene transition (EOT), leading to the development of dysoxic conditions later in the early Oligocene. Trends in δ18O and δ13C values measured on tests of selected benthic and planktic foraminifera roughly parallel those of the global record of stepped EOT δ18O increase and deviate only later in the early Oligocene, related to the isolation of the Paratethys. The overall similarity of the isotope curves and the presence of a planktic-benthic ecological offset suggest that the original isotope trends are preserved, despite the systematically more negative δ18O values. Of different scenarios, a quasi-uniform diagenetic overprint by fluids with low δ18O values, during burial or uplift, appears best supported. They concluded that the globally established isotopic expression of Antarctic ice sheet growth across the EOT may be recognizable in the Paratethys. Deviations from the global trends after the EOT were caused by regional palaeoceanographic changes induced by the progressing Alpine orogeny and sea level change, which led to a restricted connection with the open ocean, freshwater influx from increased precipitation, and gradual development of bottom-water oxygen depletion.

4 Other publications

We should mention here briefly some other ocean-related publications like a book used in the higher education from authors of Farkas and Németh (2016) Two articles appeared regarding to high school education of tropical cyclones, ocean streams and tide phenomena as the application of thermodynamics (Gróf 2016, Tasnádi 2016). A paper published on statistical relationships between large-scale oscillation phenomena and mesoscale atmospheric conditions over Central/Eastern Europe (Kristóf et al. 2018, Bottyán et al. 2017) investigated the marine source of moisture over Central Hungary on the basis of stable isotope analysis. A decade long investigation on simulation of sky-polarimetric Viking marine navigation has been finished successfully (Horváth et al. 2017, Száz et al. 2017). Finally, application of the 3D finite-volume, primitive equation community ocean model (FVCOM) developed for coastal areas was applied in the modelling of a Hungarian shallow lake (Balaton) (Torma and Krámer 2017).

References

Bottyán E, Czuppon Gy, Weidinger T, Haszpra L, Kármán K (2017): Moisture source diagnostics and isotope characteristics for precipitation in east Hungary: implications for their relationship. Hydrological Sciences Journal, 62, doi:10.1080/02626667.2017.1358450.

Bozóki T, Czelnai L, Horicsányi A, Nyerges A, Pál A, Pálfy J, Vincze M (2019): Large-scale ocean circulation in the Southern Hemisphere with closed and open Drake Passage – A laboratory minimal model approach. Deep Sea Research Part II: Topical Studies in Oceanography 160, 16-24, doi.org/10.1016/j.dsr2.2019.01.005.

Csernussi G (2018): Once Upon a Hungarian Oceanography on the Adriatic. Journal of Oceanography and Marine Research, Doi:06. 10.4172/2572-3103.1000178.

Farkas J, Németh Sz (2016): Wildlife of the Adriatic Sea – Introduction to Marine Biology (in Hungarian). Hungarian Marine Biology Association, Budapest, Second edition, 192 p. ISBN: 9639432156.

Gróf A (2016): Carousels to Coriolis, or how physics supports understanding geography. In: TPI-15 Conference Proceedings (Editors: Király A, Tél T), Budapest, 119−124, ISBN 978-963-284-925-6.

Haller G, Hadjighasem A, Farazmand M,Huhn F (2016): Defining coherent vortices objectively from the vorticity. Journal of Fluid Mechanics, 795, 136-173.

Herein M, Márfy J, Drótos G, Tél T (2015): Probabilistic Concepts in Intermediate-Complexity Climate Models: A Snapshot Attractor Picture. Journal of Climate 29, 151012111741001. 10.1175/JCLI-D-15-0353.1.

Horváth G, Takács P, Kretzer B, Szilasi Sz, Száz D, Farkas A, Barta A (2017): Celestial polarization patterns sufficient for Viking navigation with the naked eye: detectability of Haidinger's brushes on the sky versus meteorological conditions. Royal Society Open Science, 4:160688. rsos.royalsocietypublishing.org, doi.org/10.1098/rsos.160688.

Kristóf E, Pongrácz R, Bartholy J (2018): Statistical Relationships between Large-Scale Oscillation Phenomena and Mesoscale Atmospheric Conditions over Central/Eastern Europe and Their Representation in CMIP5 General Circulation Models. American Meteorological Society, 98th Annual Meeting, Austin, Texas, USA. 9p. file:///C:/Users/WEIDIN~1/AppData/Local/Temp/KE-PR-BJ-AMS2018-1.pdf.

Medjdoub K, Jánosi IM, Vincze M (2019): Laboratory investigations on the resonant feature of 'dead water' phenomenon. Fluid Dynamics. arXiv:1901.05931v1 [physics.flu-dyn].

Ozsvárt P (2018): Palaeoceanographic history of the Hungarian Palaeogene Basin using a palaeoecological analysis of benthic foraminifera (in Hungarian). Földtani Közlöny, 148, 235–254, 10.23928/foldt.kozl.2018.148.3.235.

Ozsvárt P, Kocsis L, Nyerges A, Győri O, Pálfy J, Dulai A (2017): The Eocene-Oligocene climate transition in the Central Paratethys. Palaeogeography, Palaeoclimatology, Palaeoecology, 459, 471–487, doi.org/10.1016/j.palaeo.2016.07.034.

Rodda C, Borcia I, Le Gal P, Vincze M, Harlander U (2018): Baroclinic, Kelvin and inertia-gravity waves in the barostrat instability experiment. Geophysical and Astrophysical Fluid Dynamics, Taylor Francis, <hal-01784584>.

Száz D, Farkas A, Barta A, Kretzer B, Blahó M, Egri Á, Szabó Gy, Horváth G (2017): Accuracy of the hypothetical sky-polarimetric Viking navigation versus sky conditions: revealing solar elevations and cloudinesses favourable for this navigation method. Proceeding of the Royal Society A, Mathematical, Physical and Engineering Sciences, doi.org/10.1098/rspa.2017.0358.

Tasnádi AM (2016): From heat pumps to hurricanes application of thermodynamics in secondary education. In: TPI-15 Conference Proceedings (Editors: Király, A, Tél, T), Budapest, 119−124, ISBN 978-963-284-925-6.

Tél T, Kadi L, Jánosi IM, Vincze M (2018): Experimental demonstration of the water-holding property of three-dimensional vortices. EPL (Europhysics Letters), 123(4), 1-7. doi:10.1209/0295-5075/123/44001.

Torma P, Krámer T (2017): Modelling wave induced vertical mixing and the vertical temperature distribution in a shallow lake. 4th International Symposium of Shallow Flows, Eindhoven University of Technology, NL, 26-28.

Vincze M, Bozóki T (2017): Experiments on barotropic–baroclinic conversion and the applicability of linear *n*-layer internal wave theories. Experiments in Fluids, 58(10), doi10.1007/s00348-017-2418-7.

Vincze M, Borcia I, Harlander U, Le Gal P (2016): Double-diffusive convection and baroclinic instability in a differentially heated and initially stratified rotating system: The barostrat instability. Fluid Dynamics Research, 48, doi10.1088/0169-5983/48/6/061414.

HUNGARIAN NATIONAL REPORT ON IASPEI (2015-2018)

István Bondár[*], Attila Galsa[**], Zoltán Gráczer[*], Katalin Gribovszki[*], Erzsébet Győri[*], János Kiss[***], Márta Kiszely[*], László Lenkey[**], Bálint Süle[*], Gyöngyvér Szanyi[*], Ernő Takács[***], Péter Varga[*], Zoltán Wéber[*]

1 Introduction

The past four years saw major developments in the IASPEI community in Hungary. Organizational changes include the merger of the Geological and Geophysical Institute of Hungary and the Hungarian Office for Mining and Geology into the Mining and Geological Survey of Hungary in 2017. The AlpArray experiment, with the Research Center for Astronomy and Earth Sciences, Geodetic and Geohysical Institute (MTA CSFK GGI) Kövesligethy Radó Seismological Observatory of the Hungarian Academy of Sciences as a core member, began in late 2015. In Hungary, 14 temporary three-component broadband stations have been deployed for the AlpArray temporary seismic network between December 2015 and July 2016. The first infrasound array in Hungary began operations in June 2017.

2 Observational seismology

Varga (2016) summarized the history of the Seismological Observatory of Budapest from its foundation in 1905 to date. The MTA CSFK GGI Kövesligethy Radó Seismological Observatory is a member of the International Federation of Digital Seismograph Networks (FDSN, http://www.fdsn.org), the Observatories & Research Facilities for European Seismology (ORFEUS, www.orfeus-eu.org), the International Seismological Centre (ISC, www.isc.ac.uk), the European-Mediterranean Seismological Center (EMSC, www.emsc-csem.org), and the Central and Eastern European Earthquake Research Network (CE3RN, http://www.ce3rn.eu) organizations as well as the AlpArray (http://www.alparray.ethz.ch) and the Atmospheric dynamics Research Infrastructure in Europe (ARISE, http://arise-project.eu) projects.

2.1 The Hungarian National Seismological Network

The MTA CSFK GGI Kövesligethy Radó Seismological Observatory operates the Hungarian National Seismological Network (HNSN, doi:10.14470/UH028726). The network has been significantly expanded with both permanent and temporary broadband stations since 2015. All HNSN stations are registered in the International Registry of Seismograph Stations, and the waveforms are archived at the GEOFON European Integrated Data Archive (EIDA) node (https://geofon.gfz-potsdam.de/doi/network/HU). Gráczer et al. (2018b) provides a detailed description of the HNSN permanent and temporary stations.

Between 2015 and 2018 two new permanent stations were added to the HNSN. KOVH (Kővágótöttös), equipped with a Streckeisen STS-2.5 seismometer and an Earthdata PS-6-24 digitizer, was deployed in southern Hungary in February 2015. ABAH (Abaújkér) was deployed in October 2016 and it is equipped with a Streckeisen STS-2.5 seismometer and a Guralp CMG-DM24S3EAM data acquisition unit. The short period station CSKK (Csókakő) was upgraded to a broadband Guralp CMG-3T 120s seismometer in January 2016. Finally, a Guralp Radian borehole seismometer was installed at 70 m depth next to the AMBH (Ambrózfalva) station in November 2018.

The MTA CSFK GGI contributed to the AlpArray Seismic Network (Hetényi et al. 2018) with 11 broadband seismic stations deployed in Western Hungary. Three additional stations were provided by the Swiss-AlpArray SINERGIA program (two of them were dismantled in October 2017).

[*]*Kövesligethy Radó Seismological Observatory, MTA CSFK Geodetic and Geophysical Institute*
E-mail: bondar.istvan@csfk.mta.hu
[**]*Department of Geophysics and Space Science, Eötvös Loránd University*
[***]*Mining and Geological Survey of Hungary*

The Hungarian AlpArray stations are equipped with Guralp CMG-3T 120s seismometers and Guralp DM24S3EAM digitizers, while the Swiss-AlpArray SINERGIA stations have Trillium Compact 120s sensors with Taurus 3 channel 24-bit digitizers.

All the HNSN waveforms are streamed to the Kövesligethy Radó Seismological Observatory. The automatic processing runs *SeisComP3* (www.seiscomp3.org), and the automatic bulletins are published on the website, www.seismology.hu. Automatic e-mail alerts on earthquakes in Hungary are sent to the Hungarian National Directorate General for Disaster Management. Automatic event notifications are published on twitter (http://twitter.com/szeizmologia). The manual review is also carried out with *SeisComP3*. The final hypocenter parameters in the annual Hungarian National Seismological Bulletin (HNSB) are determined by *iLoc*, a further developed version of the ISC location algorithm (Bondár and Storchak 2011). Besides the hypocenter and phase data of natural and anthropogenic events occurred in Hungary and its surroundings, HNSB lists the focal mechanism of several earthquakes as well as the macroseismic data of felt earthquakes in Hungary (Gráczer et al. 2015, 2016, 2017, 2018a). The automatic bulletins are reported to the ISC in real time; the annual HNSB is sent to the ISC once it is published. The HNSB can be downloaded from the Kövesligethy Radó Seismological Observatory website (www.seismology.hu). *iLoc*, together with the RSTT global 3D velocity model (Myers et al. 2010) is available for download from the IRIS software depository, https://seiscode.iris.washington.edu/projects/iloc.

2.2 The Hungarian National Infrasound Network

The Hungarian National Infrasound Network (HNIN, doi:10.14470/UA114590) was established by the MTA CSFK Kövesligethy Radó Seismological Observatory with the deployment of the PSZI (Piszkés-tető) infrasound array in 2017 (Czanik and Bondár 2017). The PSZI array is registered at the International Registry of Seismographic Stations, and waveforms are collected in real time at the GEOFON EIDA node (https://geofon.gfz-potsdam.de/doi/network/HN). The PSZI array is located in the Mátra Mountains. The array consists of four elements and has an aperture of approximately 300m. Each element of the array is equipped with a SeismoWave MB3d microbarometer with a built-in digitizer. The central element of the infrasound array is co-located with a permanent broadband seismological station, PSZ, jointly managed by the Kövesligethy Radó Seismological Observatory and the GFZ German Research Centre for Geosciences.

For data acquisition *SeisComP3* (www.seiscomp3.org) and for infrasound data processing *DTK-PMCC* (Cansi, 1995) are used. Both programs are found in the CTBTO NDC-in-a-Box software package. The seismo-acoustic and infrasound-only events are located with *iLoc* (Bondár et al. 2018). The first Hungarian Seismo-Acoustic Bulletin has been published by the MTA CSFK Kövesligethy Radó Seismological Observatory early 2019 (http://infrasound.hu/pdf/HSAB2017-2018.pdf).

3 Seismicity studies

3.1 Historical seismicity

The knowledge of past earthquakes of the Pannonian Basin is rather incomplete. Between 1000 and 1750, only about 200 significant events are known. Furthermore, up to the beginning of the 16th century, there are only five earthquakes with approximately known geographical locations. These are Savaria (Szombathely, Hungary, 455), Selmecbánya (Banská Štiavnica, Slovakia, 1441), Zólyomlipcse (Slovenská Ľupča, Slovakia, 1443), Temesvár (Timişoara, Romania, 1443) and Szeged (Hungary, 1444). Based on historical sources, the magnitude of the earthquake in Savaria appears to be significantly above M6. However, according to our present knowledge, this area is completely aseismic (Varga 2017).

Two distinguished professors, Pál Kitaibel and Ádám Tomcsányi of the Royal University of Pest published a book on Mór earthquake (1810, M5.4) in 1814. The "Dissertatio de terrae motu Mórensi" contains a number of useful field observations, such as the appearance of faults, variations in the

rate of spring water output, and water chemistry changes related to earthquake. Most notably, the book contains the first published isoseismal map in the world (Varga 2015a, Varga et al. 2015). Timár (2015) investigated the topographic base and georeference of the earthquake. Kiszely (2015) and Budai et al. (2018) determined the local seismic activity in the Vértes and Gerecse mountains.

3.2 Recent seismicity

Between 2013 June and 2015 January, 35 earthquakes with local magnitude ML ranging from 1.1 to 4.2 occurred in Nógrád county, Hungary. This earthquake sequence represents above average seismic activity in the region and is the first one that was recorded by a significant number of three-component digital seismographs in the county. Using the Bayesloc multiple-event location algorithm (Myers et al. 2007, 2009), Wéber (2016b) have estimated the hypocenters of 30 earthquakes with ML $\geq$ 1.5. The events occurred in two small regions of a few squared kilometers: one to the east of Érsekvadkert and the other at Iliny. The uncertainty of the epicenters is about 1.5–1.7 km in the E-W direction and 1.8–2.1 km in the N-S direction at the 95 % confidence level. The estimated event depths are confined to the upper 3 km of the crust. Kiszely et al. (2016) performed waveform correlation on the two closest stations and a cluster analysis using the correlation coefficients.

One of the largest recent earthquake sequences (ML 4.5) hit near Oroszlány in central Hungary in 2011, with more than 200 aftershocks. The Oroszlány sequence is one of the best recorded event clusters to date in Hungary. Kiszely and Győri (2015) attempted to separate quarry blasts from the aftershock sequence using waveform correlation and cluster analysis. Békési et al. (2017) relocated the Oroszlány cluster with the double difference multiple event location algorithm (Waldhauser and Ellsworth 2000). The improved locations of the events allowed to identify a N-S striking, steeply eastward dipping fault plane, in agreement with the N-S striking nodal plane of the moment tensor solution of the main shock. Owing to the favorable network geometry and the accurate relative locations, 7 earthquakes were identified as ground-truth (Bondár et al. 2004, Bondár and. McLaughlin 2009a).

The largest earthquake in the past decade occurred near Tenk, Hungary on 22 April 2013. The ML 4.8 event had two smaller foreshocks and 27 aftershocks. Czecze et al. (2017) relocated the Tenk cluster with the double difference multiple event location algorithm (Waldhauser and Ellsworth, 2000). The best fitting plane to the new hypocenters shows a good agreement with the focal mechanism solutions (Wéber 2016a).

Kiszely et al. (2017) analysed events in the Mecsek mountains to determine the best method to separate earthquakes and quarry blasts relying on ground truth information from reports of mining captains. They concluded that the spectral properties and waveform similarities of seismograms can be used to revise the classification of events in the HNSB and some 16% of the events that were originally identified as earthquakes between 2004 and 2016 were actually quarry blasts.

Bondár et al. (2018) relocated the seismicity of the Pannonian Basin for the entire digital instrumental period between 1996 and 2016 using the state-of-the-art location algorithm, *iLoc* (Bondár and Storchak 2011, Bondár and McLaughlin 2009b, Bondár et al. 2015). The relative abundance of ground-truth (Bondár et al. 2004, Bondár and McLaughlin 2009a) events (324 quarry blasts and earthquakes) allowed us to evaluate the performance of the 1D local velocity models used in the past and the global 3D upper-mantle and crustal regional seismic travel time (RSTT, Myers et al. 2010) velocity models. They demonstrated that the RSTT model captures the major 3D velocity heterogeneities and provides an improved view of the seismicity in the region. Figure 1 shows the resulting seismicity map after the relocations.

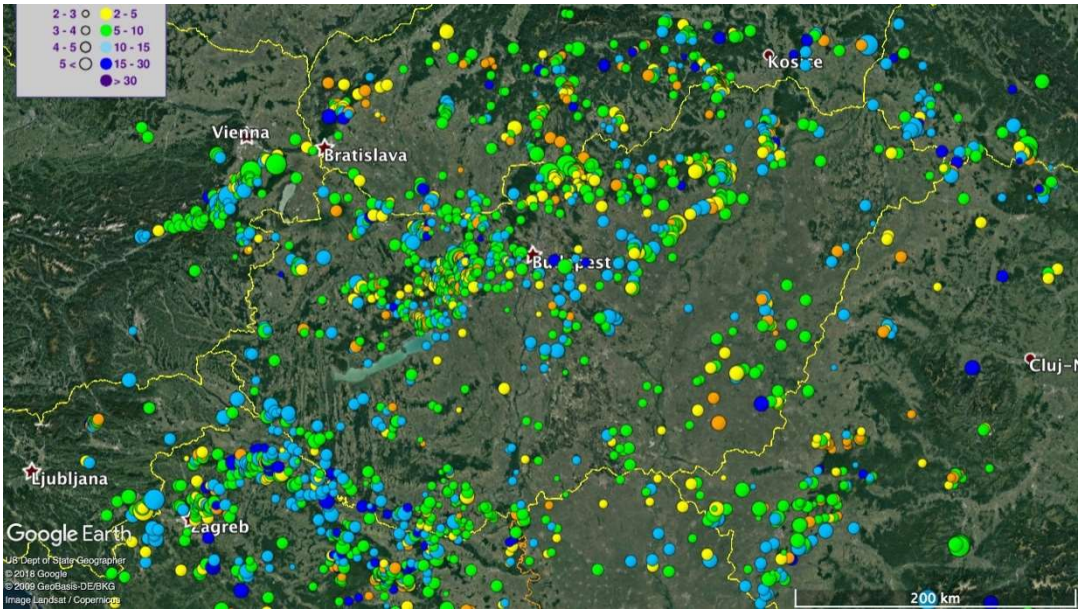

Figure 1. Seismicity of the Pannonian Basin relocated using the upper mantle and crust global 3D RSTT model. Known anthropogenic events are excluded from the map. Events are scaled by magnitude and color-coded by depth

Varga et al. (2017) studied the waveforms of one of largest of deep earthquakes, the May 24, 2013 Mw 8.3 event under the Sea of Okhotsk, recorded at the Russian and Hungarian seismological networks and concluded that event was preceded by an earthquake swarm that consisted of 58 $M \geq 5$ events that occurred between May 15 and 24, 2013 in the higher part of the sinking slab east of Kamchatka in an area of increased historical seismicity. The aftershock activity after the Okhotsk Sea earthquake was moderate: twelve events with magnitudes above M4 were observed till June 27. Although, in comparison with shallow events, the number of aftershocks is unusually small, these events determine a fault area of 2.64×10^4 km^2.

4 Earthquake hazard studies

4.1 Seismic microzonation

Local geological conditions can considerably amplify damages occurring during earthquakes. To determine site amplification, numerous measurements were performed in Budapest, in connection with seismic hazard assessment and microzonation of the capital. The studied areas were delineated on the basis of different types of engineering geological maps, available geotechnical data and macroseismic intensities observed during the 1956 Dunaharaszti earthquake.

Microseismic noise measurements were performed to identify and delineate the areas where resonance of subsurface sedimentary layers can occur. Resonance frequencies and the strength of the resonance were determined by computing horizontal-to-vertical spectral ratio (H/V) curves. Beside average H/V curves, their azimuthal variations were also computed.

Areas where soil resonance can occur during earthquakes have been found mainly in the valleys and hill-side areas in the Buda side. Strong resonance was found in some locations; in some cases, coincidence of soil and building resonance frequencies also occurred. Computing directivity, lateral amplification could be detected in some cases that originates from the inhomogeneous local geology and topography. Drawing the polarity diagrams onto a topographic map, amplification of topography moreover the effect of the valley edge could be also detected.

Microseismic noise measurements were performed in different types of buildings (brick and panel buildings with different number of floors) measuring the background noise in different levels

of the building. Fundamental mode was determined from the peak on the H/V curve whose amplitude was increased with the floor number.

Active (MASW) and passive (ESAC, ReMi) seismic measurements based on the dispersion properties of surface waves were carried out in several locations to determine the S wave velocities in the near surface layers. The S wave velocity profiles have been computed by the joint inversion of complementary (MASW, ReMi, ESAC, H/V) measurements. At these places, local applicability of seismic interferometry was also studied. The method gave mixed results, its applicability mainly has depended on the distribution of noise sources.

Microseismic noise measurements were also performed to map the resonant frequencies of upper geological layers in the locality of Zlaté Hory, Northern Moravia. The cause of the significant harmonic vibrations that was recorded in the vicinity of the winding tower during its demolition was determined on the basis of resonant frequencies that were analysed together with the results of geophysical measurements and borehole documentation (Lednická et al. 2015).

4.2 Small scale ambient seismic noise tomography at Dunaszekcső high bank

High banks are prone to landslides, therefore passive measurements have to be used when studying them by seismic methods. As a pilot project, small scale ambient noise tomography was successfully applied at the Dunaszekcső high bank, where significant landslides occurred in the last decade. The aim of the study was to map near surface velocity anomalies since it is assumed that the formation of tension cracks which precedes landslides are represented by low velocity anomalies.

Szanyi et al. (2016) performed microseismic noise measurements at the top of the Castle Hill in October 2014 and June 2015. The study area was chosen to be at the surroundings of presently active head scarp formed in April 2011. Phase cross-correlation and time-frequency phase weighted stacking were applied to calculate the cross-correlation functions that were used to retrieve the dispersion curves. A Rayleigh wave group velocity map was constructed for 0.1 s period. The average Rayleigh wave group velocity was found to be 171 m/s. The group velocity map revealed a region of negative velocity anomaly; its location coincided with a highly creviced area, where slope failure had taken place along a several metre-wide area. Another low velocity zone was also detected at a previously unknown weakened area. The noise source distribution was also studied and it was found that the most energetic noise is originated not from the Danube, but from the residential area of Dunaszekcső.

4.3 Liquefaction hazard assessment

Although the seismicity of Hungary is moderate, soil liquefaction have been observed and documented at least eight times during historical earthquakes in Hungary. Their surface manifestations were reported from Komárom (1763, 1783, 1822), Mór (1810), Érmellék (1829, 1834), Kecskemét (1911) and Dunaharaszti (1956) earthquakes. Győri et al. (2015) studied contemporary macroseismic observations that demonstrated the occurrence of soil liquefaction. Building or structural damage caused by the phenomenon is proven only in the case of 1763 Komárom earthquake. Local subsoil conditions and information regarding ground water level were also studied. Distributions of horizontal ground accelerations possibly caused by these historical earthquakes were modelled by *ShakeMap*. The ground accelerations simulations show horizontal PGA of 0.2 – 0.3 g in areas where liquefaction occurred.

Liquefaction and post-liquefaction settlement as a secondary earthquake effect are one of the main concerns during site characterization of major industrial/nuclear installations in Hungary. Katona et al. (2015) showed that the practicable empirical methods for definition of liquefaction susceptibility provide rather controversial results. Selection of method for assessment of soil behaviour that affects the integrity of structures requires specific considerations. The case of nuclear power plant at Paks, Hungary, was used as an example for demonstration of practical importance of the presented results and considerations.

Significant part of epistemic uncertainties in evaluation of liquefaction potential arise from the application of different methods. In practice, the probability of liquefaction is usually determined using empirical correlations that are based one of the in situ measurements (SPT, CPT, shear wave velocity measurements). Bán et al. (2016) have developed an empirical method where the results of CPT and V_S measurements are used in parallel. The two types of measurements can supplement each other and more and more frequently these are carried out in parallel. Bán et al. (2018) evaluated the prediction capability of the method on an independent dataset of the 2010-2011 Canterbury earthquake sequence and compared it with commonly used empirical procedures. It was found that the error index defined to quantify the false predictions is the largest for the recommended method but regarding the number of false predictions, it outperforms the other methods used for comparison.

4.4 Speleoseismology

Gribovszki et al. (2017a, 2017b) presented the result of a stalagmite-based case study from the Little Carpathians of Slovakia. A specially-shaped (candlestick type), intact and vulnerable stalagmite (IVSTM) in Plavecká priepast cave has been examined since 2013. This formation survived all earthquakes that have occurred over thousands of years, depending on the age of the stalagmite. This stalagmite is suitable for estimating the upper limit of horizontal peak ground acceleration generated by prehistoric earthquakes. Such type of stalagmites exists at many different caves in Earth.

The investigation consists of the following steps: (i) in-situ non-destructive determination of the natural frequencies, and measuring the dimensions of the IVSTM; (ii) laboratory measurements of the geomechanical and elastic properties of stalagmite samples; (iii) calculation of the natural frequencies of the IVSTM and the static horizontal ground acceleration value (a_g), which would break the IVSTM; (iv) age determination of core samples taken from speleothems; (v) determination of seismic wave attenuation with depth; (vi) construction of a critical horizontal ground acceleration curve going back into the past.

Figure 2 presents the critical horizontal ground acceleration (HGA) value as a function of time determined from the stalagmite in the Plavecká Priepast cave. Gribovszki et al. (2017a, 2017b) compared the effect of the Jókő earthquake (1906) on the location of the Plavecká priepast cave to the critical horizontal ground acceleration value provided by the stalagmite we investigated and claimed that the effect of Jókő earthquake (1906) is consistent with the critical HGA value provided by the stalagmite. At the time of Jókő event (1906) the critical HGA value could not have been higher than 1 m/s^2, and 1.3 m/s^2 at the time of the assumed Carnuntum event (~340 A.D.).

The approach used in Gribovszki et al. (2017a, 2017b) yields significant new constraints on the seismic hazard, as tectonic structures close to Plavecká priepast cave did not generate strong earthquakes in the last few thousand years. The results of this study are highly relevant given that the two capitals, Vienna and Bratislava are located within 40 and 70 km of the cave, respectively.

The approach to determine to HGA by using stalagmites is very conservative. In order to get a more sophisticated threshold for HGA several different investigations are required, such as numerical and analogue modeling of the stalagmites' vibration and failure process; model computation for determining the depth-dependent attenuation of seismic waves above the cave, detailed investigation of geomechanical and elastic properties of stalagmites (Konečný et al. 2015). The pattern of oscillation of the investigated stalagmites should be fully understood as well since at the resonance frequency the stalagmites can break more easily than in the static case. During our cave observations we observed that the harmonic oscillations of the investigated stalagmites split into two parts. Therefore, Gribovszki et al. (2018) simulated the oscillation by setting up four simplified models of the stalagmites. The eigenfrequencies of the different stalagmite models have been calculated numerically, by the finite element method, and compared with the measured in situ values. The splitting of eigenfrequencies were reproduced by the numerical model calculations, taking into account the asymmetric shape of the stalagmite.

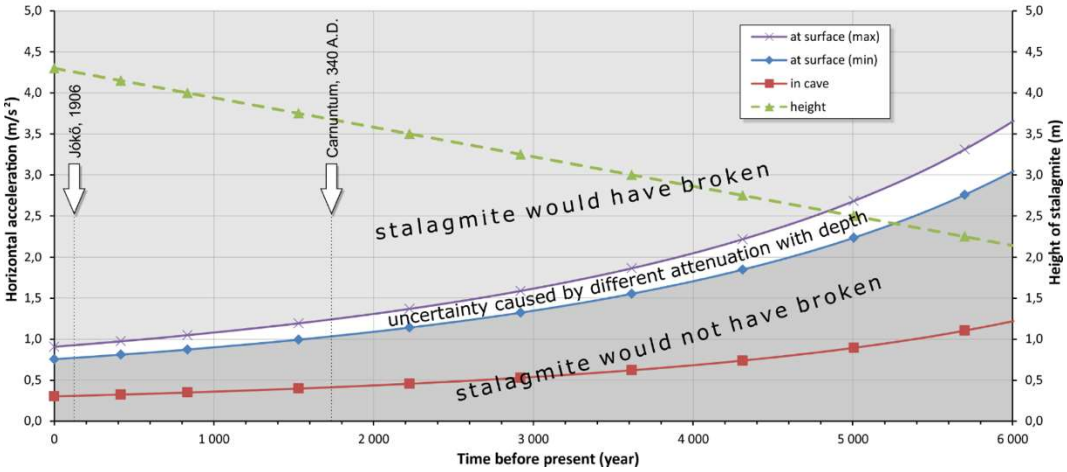

Figure 2. Constraint on critical horizontal ground acceleration at the surface (purple and blue curves) and in the cave (red curve) provided by the height of the investigated stalagmite (green line) as a linear function of time going back into the past. The arrows show the ages of the assumed and real moderate size or large earthquakes occurred in the past. The uncertainty of the critical HGA at the surface is given by the white region

5 Earthquake source mechanism studies

Wéber (2016a) has estimated the full moment tensors of 22 local earthquakes in Hungary with local magnitude ranging from 1.2 to 4.8 that occurred between 1995 and 2014. The probabilistic waveform inversion procedure (Wéber 2006) takes into account the effect of the random noise contained in the seismograms, the uncertainty in the hypocenter and the inaccurate knowledge of the velocity structure, while estimating the error affecting the derived focal parameters. The probabilistic approach maps the posterior probability density functions for both the hypocentral coordinates and the moment tensor components. This waveform inversion method is equally suitable to recover the source mechanism for low-magnitude events using short-period local waveforms as well as for moderate-size earthquakes using long-period seismograms. Only strike-slip and thrust faulting events have been found, giving further support to the hypothesis that the Pannonian basin is currently experiencing a compressional regime of deformation. The orientations of the obtained focal mechanisms are in good agreement with the present-day stress field derived by Bada et al. (2007). The azimuth of the subhorizontal P principal axis varies from about NNE-SSW in SW Hungary through NE-SW well inside the basin to around E-W in the NE part of the country.

Wéber (2006, 2016b) estimated the full moment tensors of four earthquakes in the Nógrád sequence with Mw ≥ 3.6 using a probabilistic waveform inversion procedure. All of the analyzed earthquakes have strike-slip mechanism with either right-lateral slip on an approximately N-S striking or left-lateral movement on a roughly E-W striking nodal plane. Both the P and T principal axes are horizontal, and the P axis is oriented along a NE-SW direction.

Estimating the mechanisms of small (M < 4) earthquakes is quite challenging. A common scenario is that neither the available polarity data alone nor the well predictable near-station seismograms alone are sufficient to obtain reliable focal mechanism solutions for weak events. To handle this situation, Wéber (2018) has developed a novel method that jointly inverts waveforms and polarity data following a probabilistic approach. The joint waveform and polarity (JOWAPO) inversion maps the posterior probability density of the model parameters and estimates the maximum likelihood double-couple mechanism, the optimal source depth and the scalar seismic moment of an event. The uncertainties of the solution are described by confidence regions. The method was validated on two earthquakes for which well-determined focal mechanisms are available. The validation tests demonstrated that including waveforms in the inversion considerably reduces the uncertainties of the usually poorly constrained polarity solutions. The JOWAPO method performs best when it

applies waveforms from at least two seismic stations. If the number of the polarity data is large enough, even single-station JOWAPO inversion can produce acceptable solutions.

6 Lithospheric studies

6.1 Deep seismic and geophysical potential field data

The Geological and Geophysical Institute of Hungary and Hungarian Office for Mining and Geology were merged into Mining and Geological Survey of Hungary in 2017. However, the transformation did not cause any difficulties in the continuation of our lithospheric investigations. Several important results published in the last four years are summarized below.

To refine the geological model of southeast Hungary, we reprocessed historical data of the international Pannonian Geotraverse program as well as reflection data along five additional profiles, recently made available by the oil and gas industry. During the data reprocessing, we aimed to preserve the true seismic amplitudes. To perform reliable depth imaging, we applied pre-stack depth migration (PSDM). Figure 3 shows a presumed magmatic intrusion under the Derecske Trough. Furthermore, the spatial orientation of two master faults intersecting the whole crust with different origins was determined. The first one is dipping towards northeast beneath the Makó Trough and the Battonya High, and the strike of the other one is near parallel with the Szolnok Flysch Belt. The Moho depth map of the study area was also significantly refined (Gúthy et al. 2018).

The CELEBRATION 2000 large-scale refraction experiment covered a significant part of eight Central European countries, and provided substantial coverage for a subsequent 3D velocity tomography over approximately a 100 × 150 km area in northeast Hungary. The area was located between the eastern rim of the Mátra Mountains and the eastern border of the Nyírség region, the penetration of the inversion was about 10 km. By means of the velocity tomography a batholite-like formation was detected under the Mátra Mountains (Figure 4), and three other well defined volcanic bodies were observed beneath the Nyírség area.

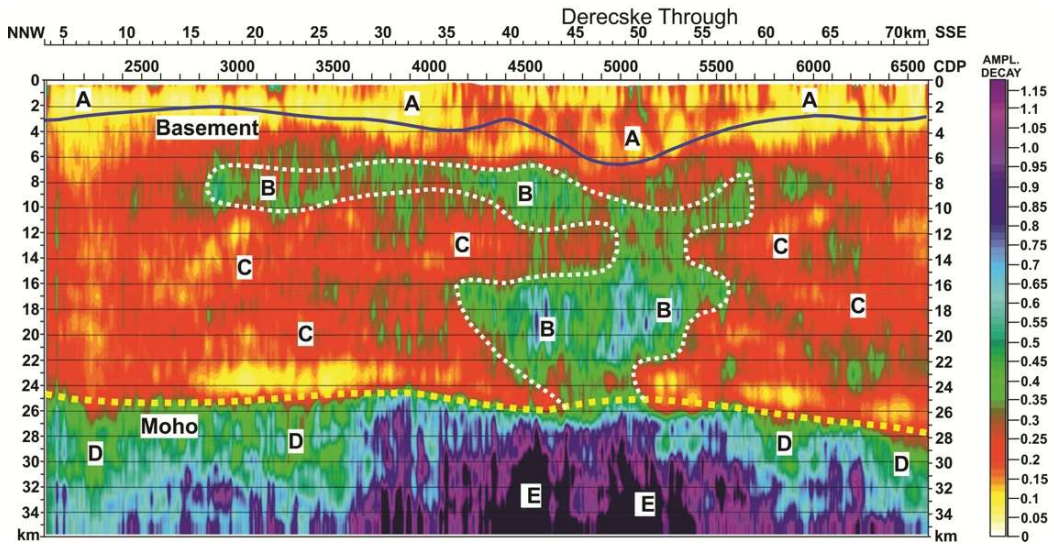

Figure 3. Presumable magmatic intrusion under the Derecske Trough based on the reflection energy decay. (A) Sedimentary and metasedimentary formations, (B) Magmatic intrusion, (C) Older crustal portions, (D) Uppermost transitional part of the mantle, (E) Supposedly higher temperature mantle material

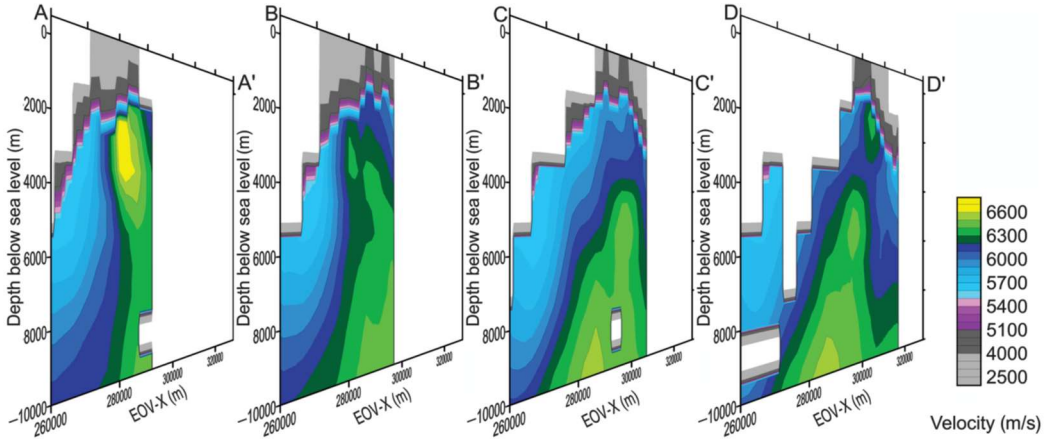

Figure 4. Velocity slices obtained from 3D refraction tomography beneath the Mátra Mountains showing a high-velocity anomaly (6.3–6.7 km/s). The anomaly might be due to the batholithic source of the volcanic material

Kiss and Bodoky (2015) performed an integrated interpretation on the available geophysical potential field and deep seismic data to understand the lithospheric processes forming the Carpathian-Pannonian region. Kiss (2016) interpreted gravity and magnetic anomalies together with the seismic data to identify regional faults, deep structures, and shear zones. Kiss (2017) studied the effect of isostasy, including regional isostasy, using the "parachute model" beneath the region.

Kiss et al. (2015), applying Airy's isostatic model, defined the surface of the Moho beneath Hungary. Figure 5 shows that the map corresponds well with the data obtained from deep seismic surveys; however, it provides a much denser spatial coverage. The new surface map enabled to compensate the gravity impact of the Moho, preserving only the effects of the density variations in the upper crust. That has a great importance in the surface geological investigations and in determination of the depth of basement.

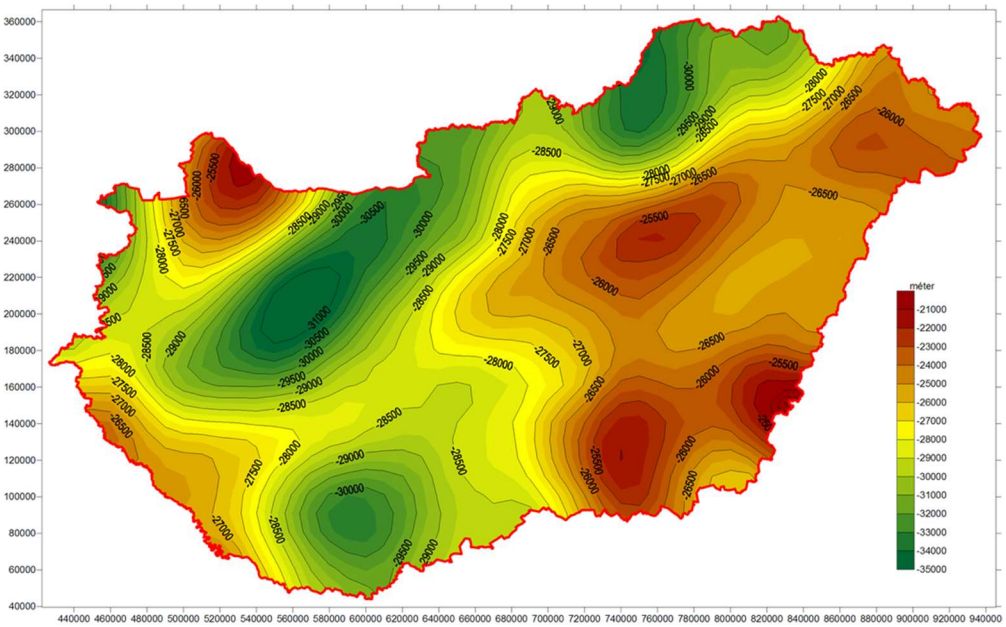

Figure 5. Moho depth map beneath Hungary calculated using Airy's isostatic model

We also studied the regional, low amplitude anomaly zones of the national geomagnetic map (Figure 6). Based on borehole data, the lithological sources of the anomalies could be identified only partially, because their sources are usually located deeper than the bottom of the holes (Kiss 2015). However, the deep refraction profiles of the CELEBRATION 2000 experiment permitted to examine the global lithospheric structure beneath Hungary (Kiss et al. 2017). The regional velocity models obtained by seismic refraction tomography indicated several high velocity intrusions, with a velocity range of the lower crust, in the upper crust. Almost all of the velocity anomalies are correlated with high magnetic features (Figure 7). Those magnetic lineaments demonstrate the global fabric of the subsurface of Hungary, and are in a good correlation with the regional faults, main shear zones, and often with the Moho surface (Kiss 2016). Finally, Kiss and Prácser (2016) and Kiss et al. (2017) implemented magnetic body detection by Naudy deconvolution along the deep refraction profiles that lead to new results to locate buried intermediate and mafic formations (Figure 8).

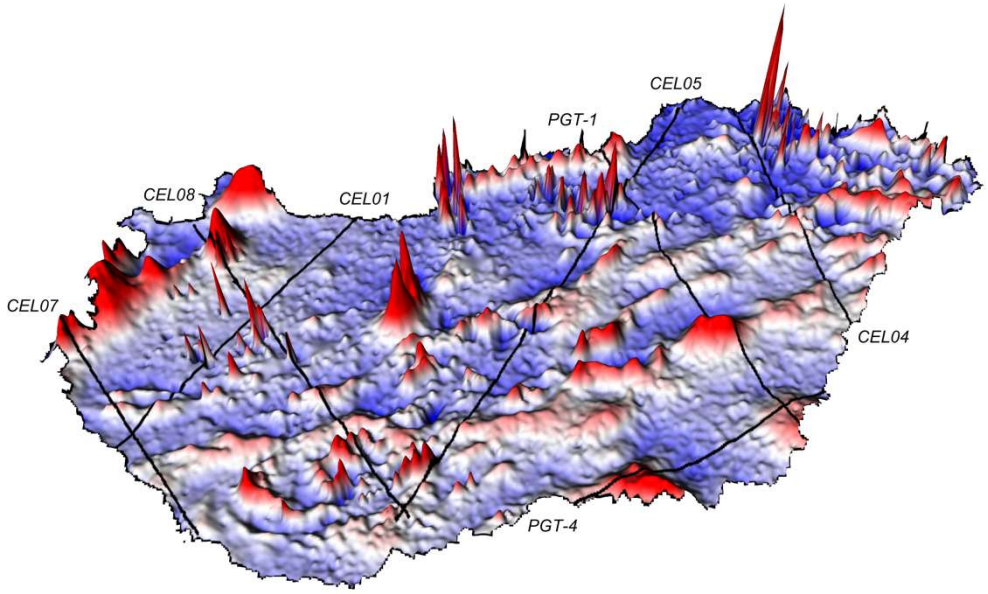

Figure 6. Magnetic anomaly map of Hungary showing the CELEBRATION 2000 deep refraction profiles

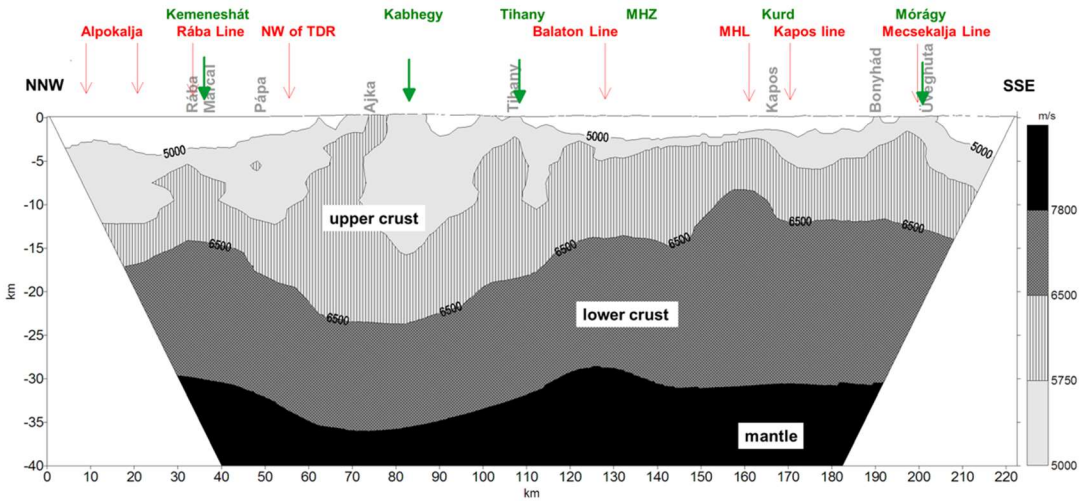

Figure 7. Crustal structure based on the CEL08 lithospheric velocity section obtained by seismic refraction tomography

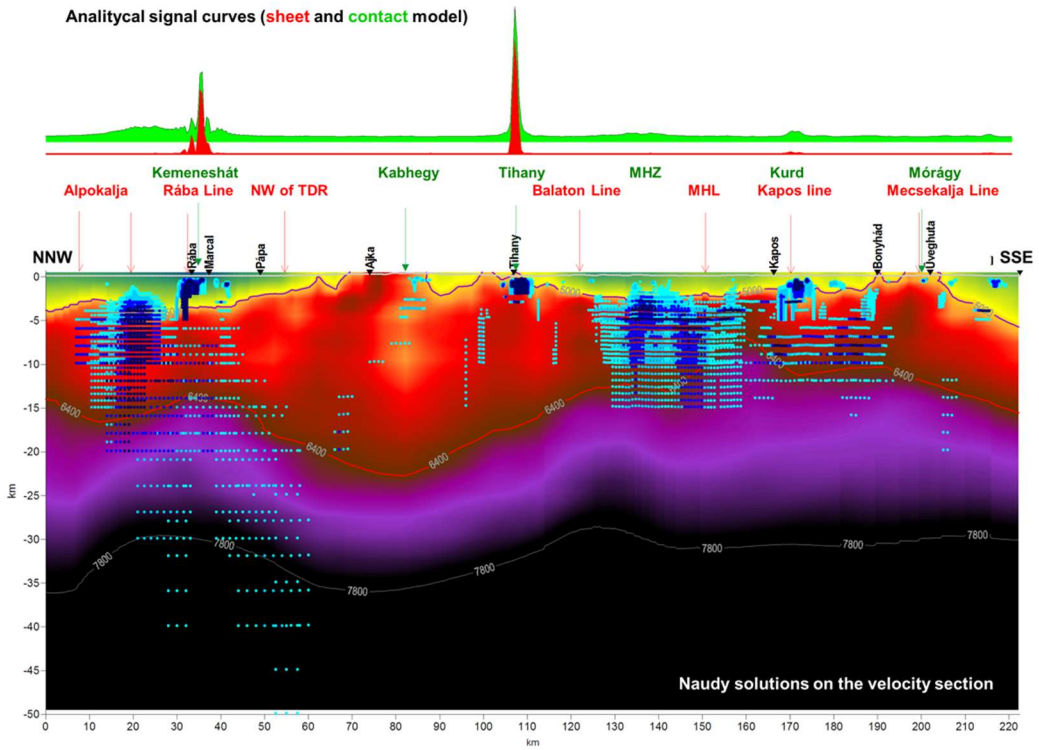

Figure 8. CEL08 lithospheric velocity section displaying the results of the magnetic body detection (below) and computed magnetic gradient curves for sheet and contact models (above)

6.2 Receiver function analysis and ambient noise tomography

Kalmár et al. (2018) performed P receiver function analysis for the West Pannonian Basin. The unprecedented station density owing to the AlpArray network allowed us to map the Moho depth in great details.

Szanyi (2016) performed ambient noise tomography for Hungary. Fundamental mode Rayleigh wave group velocity maps were prepared with a spatial resolution of around 70 km for the periods 7–26 s for almost the whole territory of the country. First, a four-layer, average S wave velocity profile was created for the region. According to this 1D model, the average basin depth is 3 km and the thickness of the upper and lower crust is 8 and 16 km, respectively. The average S wave velocity in the crustal layers are 2.34 km/s, 3.10 km/s and 3.53 km/s, respectively, while in the uppermost mantle it can be estimated as 4.16 km/s. Then a three-dimensional S wave velocity structure of the Pannonian basin was computed down to the depth of approximately 35 km.

6.3 Thermal modeling

During the report period we carried out thermal modeling of the lithosphere of the Alp-Carpathian-Pannonian regions. The Pannonian basin is characterized by high heat flow density of 80-120 mW/m^2 and elevated geothermal gradient of 40-50 °C/km. The 200 °C isotherm is situated in 4 km depth or less, which makes the basin favorable for deep geothermal exploration. In order to reveal the deep thermal conditions we carried out conductive heat transport modelling.

Lenkey et al. (2017) developed a three-layer model consisting of Tertiary sediments, underlying crust and lithospheric mantle in the Alpine-Pannonian transition zone including the Vienna, Danube, Styrian and the Mura-Zala basins. The crust and mantle were homogenous with constant thermal properties, and the thermal conductivity of sediments varied horizontally and vertically based

on laboratory measurements. The area underwent lithospheric stretching during the Early-Middle Miocene time (Horváth 1993), therefore the 3D time-dependent conductive heat transport equation was solved. We calculated the initial temperature distribution in the lithosphere at the end of rifting using non-homogeneous stretching factors (Lenkey 1999), and we modeled the present-day thermal field. The results of the model fit to the observed heat flow density and temperatures, except in those areas where intensive groundwater flow occurs in the carbonatic basement of the Transdanubian Range and Northern Calcareous Alps, and the metamorphic basement high between the Mura trough and Styrian basin.

Békési et al. (2018) constructed a similar 3D conductive thermal model for Hungary. The model consists of six sedimentary layers, upper crust, lower crust, and lithospheric mantle, where each layer has its own thermal properties. The prior thermal properties and basal condition of the model is updated through the ensemble smoother with multiple data assimilation technique. The model is able to reproduce the thermal effect of lithospheric extension and sediment infill of the Pannonian basin. Results suggest that the hottest areas below 3 km are linked to the basement highs surrounded by deep sub-basins of the Great Hungarian Plain.

In contrast to the Pannonian basin the Transylvanian basin has an anomalously low heat flow density of 30-40 mW/m^2 (Demetrescu et al. 2001). 2D lithospheric scale heat flow modelling, simulating the present-day thermal regime of the basin shows the great importance of paleoclimate and sedimentation during the evolution of the basin. Heat flow densities corrected for these processes are 20% higher compared with observed heat flow. The modelling implies that the low values of heat flow density are the result of a combination of thermal effects of Middle – Upper Miocene sedimentation and the presence of ophiolitic rocks, depleted in radioactive isotopes, located in the basin basement (Tiliţă et al. 2018).

Kovács et al. (2017) put up the hypothesis that the depths for the lithosphere–asthenosphere boundary (LAB) and the mid-lithospheric discontinuities (MLD) evolve because the upper mantle contains pargasitic amphibole. The dehydration solidus of the pargasitic amphibole may result in a very small degree of partial melting in the upper mantle at temperatures in excess of 1050°C (for geochemically more depleted) or 1100 °C (for geochemically less depleted upper mantle) within the depth range from 30 to 90 km. The partial melt may be responsible for changes in geophysical properties (e.g. lower seismic velocity, higher attenuation of seismic waves, higher electrical conductivity) attributed to the LAB and MLD. This simple petrologic model was tested using geophysical data of the Carpathian–Pannonian region (CPR). Geotherms in the lithosphere were calculated using Royden and Keen's (1980) non-homogeneous stretching model in the basin in a grid with 5 km spacing, and the depths to intersection of the geotherms with the dehydration solidus temperatures (1050 and 1100 °C isotherms) were obtained. The depth of the intersection agrees with the geophysically determined LAB in the central area of the CPR with an error of 5 km. The good fit to the observations supports the hypothesis that the dehydration solidus determines the depth of the LAB in young continental rift areas. Towards the basin margins, where the heat flow is lower (70 mW/m^2), the predictive capability of the dehydration solidus model deteriorates. This is because, for lower geothermal gradients, pargasitic amphibole breaks down at 90 km before temperature exceeds the dehydration solidus temperatures.

7 Mantle plumes

Süle (2015) performed 3D numerical calculations to investigate the effect of Rayleigh number and temperature- and depth-dependent viscosity on the radius and temperature anomaly of mantle plumes and on surface observable characteristics such as topography and geoid anomaly. Depth-dependent models were chosen, then the addition of weak and stronger temperature-dependence was studied. The Rayleigh number changed between 10^5 and 10^7. If viscosity decreases with temperature the convection becomes more vigorous and thermally weaker plumes rise from the bottom boundary layer. The radius and temperature anomaly of the upwelling decreases with increasing temperature-dependence. Topographic uplift significantly decreases with increasing temperature-dependence. For weak depth-dependent models the geoid decreases together with the topography as Rayleigh

number increases. However, strongly depth-dependent models show negative geoid anomaly above the hot plume. In case of temperature- and depth dependent models the geoid have a maximum in the function of Rayleigh number. The amplitudes of topographic uplift in the case of stronger temperature-dependence and high Rayleigh number are not far from the observed values, but the geoid signal is higher by a factor of about 2.

Galsa et al. (2015) investigated numerically the process of thermo-chemical mixing in the Earth's mantle in a 2D cylindrical shell domain. A new parameter, the effective buoyancy ratio was defined to quantify the evolution of a primordial dense layer around the core-mantle boundary. It was established that the effective buoyancy ratio, B_{eff} decreases monotonically with time due to four physical processes: (1) warming of the deep, compositionally dense layer, (2) cooling of the overlying mantle, (3) eroding of the dense layer through thermal convection in the overlying mantle and (4) diluting of the dense layer through inner convection. When the value of B_{eff} reaches 1, the instability point (when stabilizing chemical and destabilizing thermal buoyancy is balanced) the pattern of the flow system changes considerably; the two-layer convection is replaced with a one-layer thermo-chemical mixing. The time of B_{eff}=0 defines the time when the two layers are mixed. Larger initial density difference between the dense layer and the overlying mantle, β results in more resistive dense layer and delays the occurrence of the thermo-chemical mixing and homogenization. Figure 9 illustrates the effect of β on the evolution of the deep dense layer. When the initial density difference is β=0.5%, 600 Myr is enough to mix the two layers. But in the case of β=2%, the dense layer is more resistant, two-layer convection can slightly deform the surface of the dense layer. Nevertheless, the phase of the effective thermo-chemical mixing and homogenization occurred in each calculation. Although, for large values of β (β>6%), this time exceeded the age of the Earth.

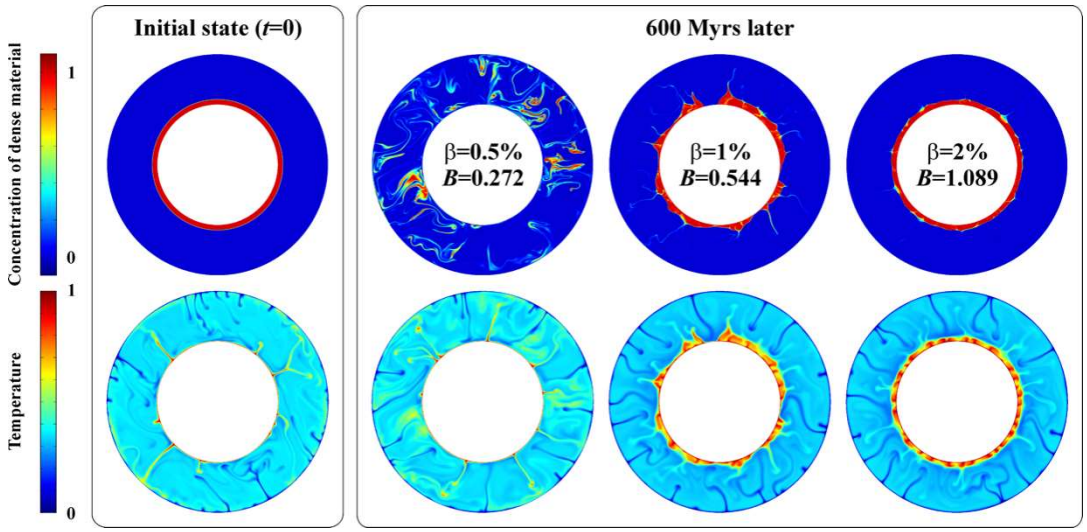

Figure 9. The non-dimensional concentration of the dense material and the temperature at the initial stage (t=0) and 600 Myrs later at different initial compositionally density contrast between the dense layer and the overlying mantle (β). B denotes the buoyancy ratio in its classical meaning (Davaille et al. 1999)

Bozóki et al. (2017) carried out numerical model calculations to study the effect of the centrifugal force on the compositionally dense material accumulated in the lowermost mantle. The deformation of an initial dense layer encircling the core was investigated systematically as a function of the density difference between the lower dense and the overlaying mantle, β and the angular velocity of the planet, Ω in a two-dimensional cylindrical shell domain. It was established that increasing β does not influence the magnitude of the deformation of the dense layer but decreases the velocity of the deformation. The relaxation time of the deformation is inversely proportional to β similarly to post-glacial rebound. On the other hand, increasing Ω enhances the magnitude of the deformation but does not affect the deformation relaxation time. The magnitude of the deformation is approximately proportional to Ω^2. It was pointed out that for the present-day mantle parameters, β=2–4% and

$\Omega=7.3\cdot10^{-5}$ 1/s the equatorial elevation of the dense layer is about 2 km which more than two orders of magnitude less than the height of the seismically observed large low shear velocity provinces beneath Africa and Pacific (e.g. Garnero et al. 2007).

8 Geodynamic studies

Schreider et al. (2015, 2016) and Varga (2015b) reconstructed the movement of the virtual dipole moment (VDM) of the earth's magnetic field through the Paleoarchean–Phanerozoic. The VDM change over time is characterized by a positive linear trend in the interval of 4.1×10^{22} Am^2 (3.5 Ga ago) to 5.5×10^{22} Am^2 (to date). This background linear growth of the field strength is complicated by irregularly distributed VDM variations ranging in the amplitude from 1.7×10^{22} to 3.7×10^{22} Am^2 with the wavelength varying from 220 to 920 Ma. The average wavelength of such fluctuations is estimated to be 570 Ma, which is approximately equal by duration to the Wilson geological cycles. The interval of 0.84–1.3 Ga before present is first established to be characterized by the relatively calm VDM region of 4.7–4.9 × 10^{22} Am^2. The first defined deep minimum with the extremum of 2.3×10^{22} Am^2 (2.15 Ga ago) corresponds to the terminal phase in the formation of the Earth's core geometry and initiation of the formation of the modern dipole field.

There are various equations that describe relations between different classes of Love–Shida numbers. Varga et al. (2018) obtained an integral relation with the use of the time-varying gravitational potential, which connects tidal Love–Shida numbers, load numbers, and potential-free Love–Shida numbers generated by normal and horizontal stresses. Varga et al. (2018) obtained the equations without any considerations concerning the boundary conditions at the surface and centre of the Earth. Therefore, they are valid both for tidal, load and potential free Love–Shida numbers. Furthermore, they do not follow from the sixth-order differential equation system of motion that are usually applied to calculate the Love–Shida numbers, and they can used in stress calculations both at the surface and within the Earth's mantle.

Varga and Grafarend (2018) calculated the lunisolar stress tensor in terms of their components along the latitude of the spherical surface of the Earth as well as inside the Earth (up to the core-mantle boundary) for the PREM. Results of calculations prove that increase of stress as a function of depth reaching a value around some kPa at the depth of 900-1500 km, well below the zone of deep earthquakes. At the depth of the overwhelming part of seismic energy accumulation (around 50 km) the stresses of lunisolar origin are only $(0.0\text{-}1.0)\cdot10^3$ Pa. Despite the fact that these values are much smaller than the earthquake stress drops (1-30 MPa) they do not exclude the possible impact of tidal forces on outbreak of seismic events. Since the tidal potential and its derivatives are coordinate dependent and the zonal, tesseral and sectorial tides have different distributions from the surface down to the CMB, the lunisolar stress cannot influence the break-out of every seismological event in the same degree. The influencing lunisolar effect of the solid earth tides on earthquake occurrences is connected with its radial stress components acting parallel to the surface of the Earth. The influence of load tides is limited to the loaded area and its immediate vicinity.

The distribution of great earthquakes ($M\geq7.0$) and their released seismic energy along the Earth radius is asymmetric, as 90% of energy release occurs relatively close to the Earth's surface. The vast majority of the remaining 10% is associated with seismic events that occur at great depths. These very deep earthquakes (depth ≥ 350 km) differ significantly from the shallow events, their source, in contrast to the shallow focus events, is located inside the plate. Varga et al. (2017) examined seven source zones of deep events, and showed that (except for one, Honsu-Kamchatka where both shallow and deep $M\geq 7.0$ earthquakes occur) linear distribution of deep earthquakes is considerably shorter than that found for the shallow earthquakes, which determine the length of the zone. In case of two further zones of deep earthquakes (Solomon Islands and Izu-Bonin-Mariana arc) there are no seismic events $M\geq 7.0$ deeper than 450 km, where the aforementioned shortening occurs. For the remaining four zones (Indonesia, Philippines, Tonga-Kermadec and Chile-Peru) the length of shortening at the top of the lower mantle relative to the length of zone observed close to the surface unequivocal. Their emergence, as demonstrated by the spatial distribution of hypocenters, is controlled not only by slab stagnation but also by their penetration into the lower mantle

influenced by the Venturi effect. The position of very deep (≥ 500 km) earthquakes foci indicate where the downgoing lithospheric plates conflict with the upper boundary of lower mantle, and where they in some cases cross it. This passage generates compression - elongation inside the slab. A comparison of temporal distribution of shallow and deep seismic events suggests that there is no direct relationship in the distribution of these two different earthquake activities.

References

Bada G, Horváth F, Dövényi P, Szafián P, Windhoffer G, Cloetingh S (2007): Present-day stress field and tectonic inversion in the Pannonian basin. Glob. Planet. Change, 58, 165-180.

Bán Z, Mahler A, Katona TJ, Győri E (2016): Liquefaction assessment based on combined use of CPT and shear wave velocity measurement. In: Barry, M Lehane; Hugo, E Acosta-Martínez; Richard, Kelly (eds.) Geotechnical and Geophysical Site Characterisation, 5, Australian Geomechanics Society, 597-602.

Bán Z, Mahler A, Győri E (2018): Performance of liquefaction assessment method based on combined use of cone penetration testing and shear wave velocity measurement. ce/papers, 2(2-3), 193-198.

Békési E, Süle B, Lenkey L, Lenkey Á, Bogér I, Bondár I (2017): Double-difference relocation of the 29 January 2011 ML 4.5 Oroszlány earthquake and its aftershocks and its relevance to the rheology of the lithosphere and geothermal prospectivity. Acta Geod. Geophys., 52, 229-242, doi:10.1007/s40328-017-0195-7.

Békési E, Lenkey L, Limberger J, Porkoláb K, Balázs A, Bonté D, Vrijlandt M, Horváth F, Cloetingh S, van Wees JD (2018): Lithospheric-scale subsurface temperature model of the Hungarian part of the Pannonian Basin. Glob. and Planet. Change, 171, 48-64.

Bondár I, Myers SC, Engdahl ER, Bergman EA (2004): Epicenter accuracy based on seismic network criteria. Geophys. J. Int., 156, 483-496, doi: 10.1111/j.1365-246X.2004.02070.x.

Bondár I, McLaughlin K (2009a): A new ground truth data set for seismic studies. Seism. Res. Let., 80, 465-472, doi:10.1785/gssrl.80.3.465.

Bondár I, McLaughlin K (2009b): Seismic location bias and uncertainty in the presence of correlated and non-Gaussian travel-time errors. Bull. Seism. Soc. Am., 99, 172-193, doi:10.1785/0120080922

Bondár I, Storchak D (2011): Improved location procedures at the International Seismological Centre. Geophys. J. Int., 186, 1220-1244.

Bondár I, Engdahl ER, Villasenor A, Harris J, Storchak D (2015): ISC-GEM: Global instrumental earthquake catalogue (1900-2009), II. Location and seismicity patterns. Phys. Earth. Planet. Int., 239, 2-13, doi:10.1016/j.pepi.2014.06.002.

Bondár I, Mónus P, Czanik Cs, Kiszely M, Gráczer Z, Wéber Z, and the AlpArrayWorking Group (2018): Relocation of Seismicity in the Pannonian Basin Using a Global 3D Velocity Model. Seism. Res. Let., 89, 2284-2293, doi:10.1785/0220180143.

Bozóki T, Herein M, Galsa A (2017): Numerical evolution of the asymmetry in the compositionally inhomogeneous lower mantle driven by Earth's rotation. Acta Geod. Geophys., 52, 331-343.

Budai T, Fodor L, Sztanó O, Kercsmár Z, Császár G, Csillag G, Gál N, Kele S, Kiszely M, Selmeczi I, Babinszki E, Thamóné Bozsó E, Lantos Z (2018): Geology of the Gerecse Mountains, Explanatory book to the geological map of the Gerecse Mountains (1:50 000) (edited Budai T). Mining and Geological Survey of Hungary, Budapest.

Cansi Y (1995): An automated seismic event processing for detection and location: The P.M.C.C. method. Geophys. Res. Lett., 22, 1021-1024.

Czanik Cs, Bondár I (2017): The First Infrasound Array in Hungary. CTBT: Science and Technology Conference: Book of Abstracts, p. 9., 26-30 June 2017, Vienna, Austria.

Czecze B, Süle B, Bondár I (2017): A 2013. évi Heves megyei földrengéssorozat helymeghatározása többeseményes algoritmussal (Multiple event relocation of the 22 April 2013, ML = 4.8 Tenk (Hungary) earthquake aftershocks). in Hungarian, Magyar Geofizika, 58, 162-174.

Davaille A, Girard F, Le Bars M (2002): How to anchor hotspots in a convecting mantle? Earth Planet. Sci. Lett., 203, 621-634.

Demetrescu C, Nielsen SB, Enea M, Şerban DZ, Polonic G, Andreescu M, Pop A, Balling N (2001): Lithosphere thermal structure and evolution of the Transylvanian Depression — insights from new geothermal measurements and modelling results. Phys. Earth Planet. Int., 126, 249-267.

Galsa A, Herein M, Lenkey L, Farkas MP, Taller G (2015): Effective buoyancy ratio: A new parameter for characterizing thermo-chemical mixing in the Earth's mantle. Solid Earth, 6, 93-100.

Garnero EJ, Lay T, McNamara A (2007): Implication of lower-mantle structural heterogeneity for existence and nature of whole-mantle plumes. Geol. Soc. Am. Spec. Pap., 430, 79-101.

Gráczer Z (ed.), Bondár I, Czanik Cs, Czifra T, Győri E, Kiszely M, Mónus P, Süle B, Szanyi Gy, Tóth L, Varga P, Wesztergom V, Wéber Z (2015): Hungarian National Seismological Bulletin 2014. Kövesligethy Radó Seismological Observatory, MTA CSFK GGI, Budapest, p. 563.

Gráczer Z (ed.), Bondár I, Czanik Cs, Czifra T, Győri E, Kiszely M, Mónus P, Süle B, Szanyi Gy, Szűcs E, Tóth L, Varga P, Wesztergom V, Wéber Z (2016): Hungarian National Seismological Bulletin 2015. Kövesligethy Radó Seismological Observatory, MTA CSFK GGI, Budapest, p. 278.

Gráczer Z (ed.), Bondár I, Czanik Cs, Czifra T, Győri E, Kiszely M, Mónus P, Süle B, Szanyi Gy, Szűcs E, Tóth L, Varga P, Wesztergom V, Wéber Z (2017): Hungarian National Seismological Bulletin 2016. Kövesligethy Radó Seismological Observatory, MTA CSFK GGI, Budapest, p. 353.

Gráczer Z (ed.), Bondár I, Czanik Cs, Czifra T, Győri E, Kiszely M, Mónus P, Süle B, Szanyi Gy, Tóth L, Varga P, Wesztergom V, Wéber Z (2018): Hungarian National Seismological Bulletin 2017. Kövesligethy Radó Seismological Observatory, MTA CSFK GGI, Budapest.

Gráczer Z, Szanyi G, Bondár I, Czanik Cs, Czifra T, Győri E, Hetényi Gy, Kovács I, Molinari I, Süle B, Szucs E, Wesztergom V, Wéber Z and AlpArray Working Group (2018): AlpArray in Hungary: temporary and permanent seismological networks in the transition zone between the Eastern Alps and the Pannonian basin. Acta Geod. Geophys., 53, 221-245, https://doi.org/10.1007/s40328-018-0213-4

Gribovszki K, Kovács K, Mónus P, Bokelmann G, Konecny P, Lednická M, Moseley G, Spötl C, Edwards RL, Bednárik M, Brimich L, Tóth L (2017a): Estimating the upper limit of prehistoric peak ground acceleration using an in-situ, intact and vulnerable stalagmite from Plavecká priepast cave (Detrekői-zsomboly), Little Carpathians, Slovakia - first results. J. Seismol., 21(5), 1111-1130, doi: 10.1007/s10950-017-9655-3.

Gribovszki K, Kovács K, Mónus P, Bokelmann G, Konecny P, Lednická M, Moseley G, Edwards,RL, Spötl C, Bednárik M, Brimich L, Hegymegi E, Tóth L, Kegyes-Brassai Cs, Szeidovitz Gy (2017b): Contraints on long-term seismic hazard from vulnerable stalagmite in Plavecká priepast cave, Slovakia (in Hungarian). Magyar Geofizika, 58(1), 1-16.

Gribovszki K, Esterhazy S, Bokelmann G (2018): Numerical modeling of stalagmite vibration. Pure Appl. Geophys., 175(12), 4501-4514, doi: 10.1007/s00024-018-1952-4.

Gúthy T, Takács E, Kovács ACs, Fancsik T, Csabafi R, Török I, Hegedűs E (2018): Recent developments in imaging the earth's crust by deep seismic data beneath the eastern parts of the Pannonian Basin Interpretation. 6(1), SB23–SB35, doi: 10.1190/INT-2016-0206.1.

Győri E, Tóth L, Mónus P (2015): Secondary effects generated by earthquakes: liquefaction occurrences in and around Hungary. Acta Geod. Geoph. Hung., 50(1), 79-95.

Hetényi Gy, Molinari I, Clinton J, Bokelmann G, Bondár I, Crawford WC, Dessa JX, Doubre C, Friederich W, Fuchs F, Giardini D, Gráczer Z, Handy MR, Herak M, Jia Y, Kissling E, Kopp H, Korn M, Margheriti L, Meier T, Mucciarelli M, Paul A, Pesaresi D, Piromallo C, Plenefisch T, Plomerová J, Ritter J, Rümpker G, Sipka V, Spallarossa D, Thomas C, Tilmann F, Wassermann J, Weber M, Wéber Z, Wesztergom V, Zivcic M, AlpArray Seismic Network Team, AlpArray OBS Cruise Crew, AlpArray Working Group (2018): The AlpArray Seismic Network: A Large-Scale European Experiment to Image the Alpine Orogen. Surv. Geophys., 39, 1009-1033, doi: 10.1007/s10712-018-9472-4.

Horváth F (1993): Towards a mechanical model for the formation of the Pannonian basin. Tectonophysics, 226, 333-357.

Kalmár D, Süle B, Bondár I, AlpArray Working Group (2018): Preliminary Moho depth determination from receiver function analysis using AlpArray stations in Hungary. Acta Geod. Geophys., 53, 309-321, doi: 10.1007/s40328-018-0218-z

Katona TJ, Bán Z, Győri E, Tóth L, Mahler A (2015): Safety Assessment of Nuclear Power Plants for Liquefaction Consequences. Science and Technology of Nuclear Installations. Paper: 727291.

Kiss J (2015): Connection between geomagnetic anomalies and map of geological formations penetrated by wells in the Pannonian Basin (in Hungarian). Magyar Geofizika, 56(1), 21-42.

Kiss J, Bodoky T (2015): What starts and what is driving subductions of lithospheric plates (in Hungarian)? Magyar Geofizika, 56(4), 197-208.

Kiss J, Gúthy T, Zilahi-Sebess L (2015): Research of the Mohorovičić discontinuity in Hungary (methods, measurements and results (in Hungarian). Magyar Geofizika, 56(3), 152-178.

Kiss J, Vértesy L, Gulyás Á, Madarasi A (2015): TISIA — in the mirror of geophysics. in Hungarian, Abstract Book of TISIA conference, 25-28, ISBN 978-963-8221-56-8.

Kiss J (2016): Comprehensive interpretation of gravity and magnetic anomalies in Carpathian–Pannonian Region (in Hungarian). Földtani Közlöny, 146(3), 275-298.

Kiss J, Prácser E (2016): Data processing along a profile – semi-automated source detection, frequency filtering and depth slicing (CEL08 profile (in Hungarian). Magyar Geofizika, 57(2), 69-87.

Kiss J, Vértesy L, Gulyás Á (2017): Geomagnetic case studies from the Balaton Highland, the Danube–Tisza interfluve and the Tokaj Mountains (in Hungarian). Magyar Geofizika, 57(4), 126-151.

Kiss J (2017): An alternative model for the development of the Carpathian Basin and its environment (in Hungarian). Magyar Geofizika, 58(2), 66-75.

Kiss J, Vértesy L, Fancsik T, Kovács ACs, Madarasi A, Gulyás Á (2017): Tisia – in the light of geophysics and the interpretation of high seismic velocity zones in the crust (in Hungarian). Magyar Geofizika, 58(4), 209-229.

Kiszely M (2015): Earthquakes in Vértes—What Happens below our Feet (in Hungarian)? Magyar Tudomány, 3, 298-310.

Kiszely M, Győri E (2015): Separation of quarry blasts from the aftershock sequence of the Oroszlány (Hungary) January 29, 2011. Acta Geod. Geophys., 50, 97-107.

Kiszely M, Mónus P, Tóth L, Győri E (2016): Cluster analysis of earthquakes occurred in Érsekvadkert, Iliny Heves, between 2013 and 2015 (in Hungarian). Magyar Geofizika, 57(1), 35-46.

Kiszely M, Mónus P, Kalocsai L, Süle B, Győri E, Tóth L (2017): Revision of the Hungarian earthquake catalogs for seismic events occurred in the vicinity of the Mecsek Hill (in Hungarian). Magyar Geofizika, 58(3), 151-162.

Konečný P, Lednická M, Souček K, Staš L, Kubina L, Gribovszki K (2015): Determination of dynamic young's modulus of vulnerable speleothems. Acta Mont. Slov., 20(2), 156-163.

Kovács I, Lenkey L, Green DH, Fancsik T, Falus Gy, Kiss J, Orosz L, Angyal J, Vikor Zs (2017): The role of pargasitic amphibole in the formation of major geophysical discontinuities in the shallow upper mantle. Acta Geod. Geophys., 52(2), 183-204.

Lednická M, Kaláb Z, Győri E (2015): Mapping the resonant frequencies of upper geological layers in the vicinity of abandoned mining pit at the Zlaté Hory locality, Northern Moravia. Acta Geodyn. Geomat., 12(2), 157-167.

Lenkey L, Raáb D, Goetzl G, Lapanje A, Nádor A, Rajver D, Rotár-Szalkai Á, Svasta J, Zekiri F (2017): Lithospheric scale 3D thermal model of the Alpine-Pannonian transition zone. Acta Geod. Geophys., 52(2), 161-182.

Lenkey L (1999): Geothermics of the Pannonian Basin and its bearing on the tectonics of basin evolution. Vrije Universiteit Amsterdam, p. 215.

Myers SC, Johannesson G, Hanley W (2007): A Bayesian hierarchical method for multiple-event seismic location. Geophys. J. Int., 171, 1049-1063.

Myers SC, Johannesson G, Hanley W (2009): Incorporation of probabilistic seismic phase labels into a Bayesian multiple-event seismic locator. Geophys. J. Int,, 177, 193-204.

Myers SC, Begnaud ML, Ballard S, Pasyanos ME, Phillips WS, Ramirez AL, Antolik MS, Hutchenson KD, Dwyer JJ, Rowe CA, Wagner GS (2010): A crust and upper-mantle model for Eurasia and North Africa for Pn travel-time calculation. Bull. Seism. Soc. Am., 100, 640-656.

Royden L, Keen CE (1980): Rifting process and thermal evolution of the continental margin of Eastern Canada determined from subsidence curves. Earth Planet. Sci. Let., 51, 343-361.

Schreider AA, Schreider AlA, Varga P, Denis C (2015): Evolution of the virtual dipole moment through the Paleoarchean–Phanerozoic. Oceanology, 55(2), 245-252.

Schreider AA, Ignatova AA, Schreider AlA, Sajneva AA, Varga P, Denis C (2016): Evolution of the virtual dipole moment calculation for reconstruction of the oceanic inversion magnetic layer parameters. Oceanology, 56(3), 463-470.

Süle B (2015): Mantle plume characteristics in three-dimensional depth- and temperature-dependent models. Acta Geod. Geophys., 50, 403-417.

Szanyi Gy (2016): A Pannon-medence S-hullám-sebességterének vizsgálata. PhD thesis, Eötvös Loránd Tudományegyetem, Budapest, p. 135., doi:10.15476/ELTE.2016.118

Szanyi Gy, Gráczer Z, Győri E, Kaláb Z, Lednická M (2016): Ambient Seismic Noise Tomography of a Loess High Bank at Dunaszekcső (Hungary). Pure Appl. Geophys., 173(8), 2913-2928.

Tiliţă M, Lenkey L, Mațenco L, Horváth F, Surányi G, Cloetingh S (2018): Heat flow modelling in the Transylvanian basin: implications for the evolution of the intra-Carpathians area. Global Planet. Change, 171, 148-166.

Timár G (2015): Topographic Base and Georeference of Kitaibel's and Tomcsányi's 1810 Mór Earthquake Map. in Hungarian, Magyar Tudomány, 3, 289-297.

Varga P (2015a): Bicentenary of Kitaibel's and Tomcsányi's Book on the 1810 Mór Earthquake. in Hungarian, Magyar Tudomány, 3, 276-288.

Varga P (2015b): Long-term variations of the gravitational potential and of the geodynamical properties of a deformable Earth due to axial despinning. Leibniz Online, 19, 1-8.

Varga P, Timár G, Kiszely M (2015): Two Hundred Years Ago the Dissertatio de terrae motu Mórensi and the First Isoseismal Map Appeared. Seism. Res. Lett., 86(5), 1432-1437, doi: 10.1785/0220150076

Varga P (2016): From the Earthquake Observatory to the Radó Kövesligethy Seismological Observatory. in Hungarian, Ma-gyar Tudomány, 10, 1192-1217.

Varga P (2017): Old Hungarian earthquakes, with particular regard to Budapest. in Hungarian, Magyar Geofizika, 58(2), 76-87.

Varga P, Rogozhin EA, Süle B, Andreeva NV (2017): A Study of the Energy Released by Great ($M \geq 7$) Deep Focus Seismic Events with Allowance for the Mw 8.3 Earthquake of May 24, 2013 in the Sea of Okhotsk, Russia. Phys. Solid Earth, 53(3), 385-409.

Varga P, Grafarend E, Engels J (2018): Relation of Different Type Love–Shida Numbers Determined with the Use of Time-Varying Incremental Gravitational Potential. Pure Appl. Geophys., 175, 1643-1648.

Varga P, Grafarend E (2018): Influence of Tidal Forces on the Triggering of Seismic Events. Pure Appl. Geophys., 175, 1649-1657.

Waldhauser F, Ellsworth WL (2000): A double-difference earthquake location algorithm: method and application to the northern Hayward fault, California. Bull. Seism. Soc. Am., 90, 1353-1368.

Wéber Z (2006): Probabilistic local waveform inversion for moment tensor and hypocentral location. Geophys. J. Int., 165, 607-621.

Wéber Z (2016a): Probabilistic waveform inversion for 22 earthquake moment tensors in Hungary: new constraints on the tectonic stress pattern inside the Pannonian basin. Geophys. J. Int., 204, 236-249.

Wéber Z (2016b): Source parameters for the 2013–2015 earthquake sequence in Nógrád county, Hungary. J. Seismol., 20, 987-999.

Wéber Z (2018): Probabilistic joint inversion of waveforms and polarity data for double-couple focal mechanisms of local earthquakes. Geophys. J. Int., 213, 1586-1598.

HUNGARIAN NATIONAL REPORT ON IAVCEI (2015-2018)

Gábor Dobosi[*] *, Szabolcs Harangi*[**,***]

Introduction

This report covers the research activity between 2015 and 2018 which belongs to the topics of IAVCEI. The most significant results have been obtained in the volcanological, petrological and geochemical investigation of the Miocene and Plio-Pleistocene calc-alkaline and alkali volcanism of the Carpathian-Pannonian Region and in the study of upper mantle xenoliths found in alkali basalts. The research topics and new results will be presented in the following order:

1) The Mesozoic Ditrău alkaline massif in the Eastern Carpathians
2) Neogene to Quaternary calc-alkaline volcanism
3) Plio-Pleistocene alkali basalt volcanism
4) Upper mantle and lower crustal xenoliths
5) Most significant studies based on international collaboration.

1 The Mesozoic Ditrău Alkaline Massif in the Eastern Carpathians

Mafic–ultramafic cumulates enclosed in gabbroic-dioritic rocks of the Mesozoic Ditrău Alkaline Massif were investigated by Pál-Molnár et al. (2015a). Using major and trace element compositions of minerals and whole-rock samples the origin of these cumulates is determined and the parental magma composition and depth of emplacement are calculated. Lamprophyre dykes are proposed to reflect multiple basanitic parental magma batches from which the cumulus olivine and clinopyroxene crystallised. The evolution of poikilitic olivine-and pyroxene-rich cumulates, and the amphibole-rich mesocumulates is the result of closed system crystallisation at temperature and pressure of ~1000–1050 °C and ~ 0.7 GPa (i.e. lower crustal depths).

In addition to a series of ultramafic to mafic and alkaline igneous rocks, a granite body also occurs in the Ditrău Alkaline Massif. Pál-Molnár et al. (2015b) presented and discussed mineral chemical data, and major and trace element compositions of the granites in order to define their nature and origin and to determine the depth of the magma emplacement. Geochemical data are consistent with A1-type granites and mantle differentiates correspond to an intra-plate environment. The Ditrău granites were emplaced at middle – upper crustal levels between 14 and 4 km depth (370 ± 40 MPa).

Trace element content of clinopyroxene was investigated by Batki el al. (2018) in the different igneous rock types of the Ditrău Alkaline Massif. Clinopyroxenes record two major magma sources as well as distinct magma evolution trends. The primitive high-Cr Fe-diopside population is derived from an early camptonitic magma related to basanitic parental melts, whilst the intermediate Na-diopside-hedenbergite crystals represent a Na-, Nb- and Zr-rich magma source recognised for the first time in the Ditrău magmatic system. Repeated recharge events of the two principal magmas resulted in multiple interactions between more primitive and more fractionated coexisting magma batches.

The Tarniţa Complex (ultramafic and mafic rock assemblage of the northern part of the Ditrău Alkaline Massif) was investigated by Heincz et al. (2018). Mingling and mixing processes occurred between magmas (a) in the former magma storage system and (b) during the incorporation of the earlier crystallized magmatic fragments entrained during the new magma intrusions. The studied minerals show several micro textural features which can be related to crystal transfer process

[*]*Department of Mineralogy and Geology, University of Debrecen, Egyetem tér 1, H-4032 Debrecen. E-mail: gabor.dobosi@gmail.com*
[**]*Department of Petrology and Geochemistry, Institute of Geography and Earth Sciences, Eötvös Loránd University (ELTE), Pázmány Péter sétány 1/C, H-1117 Budapest, e-mail: szabolcs.harangi@geology.elte.hu*
[***] *MTA-ELTE Volcanology Research Group, Pázmány Péter sétány 1/C, Budapest 1117, Hungary*

between the intruding magma and the host magma, as well as between the intruding magma and the recycled cumulates.

2 Neogene to Quaternary calc-alkaline volcanism in the Carpathian-Pannonian Region

2.1 Ignimbites and other calc-alkaline volcanic rocks

Biró et al. (2015) performed detailed petrographic investigation and twofold fabric study including image analysis and low-field anisotropy of magnetic susceptibility (AMS) on the Mid-Miocene Rám Hill Pumiceous Sandstone (RHPS; Visegrád Mountains) introduced by Karátson and co-workers in 2007. Based on petrographic features the formation consists of heterogeneous pyroclastic material from a single phreatomagmatic eruption period, which emplaced in a shallow subaqueous environment around the Keserűs Hill lava dome group. The RHPS show 'quasi-radial' flow pattern around the Keserűs Hill volcano, which was the central volcanic edifice of the Visegrád Mountains around 15 Ma. Sediment heterogeneity as a major factor influencing the magnetic fabric strength of laharic deposits was highlighted.

Magma/wet sediment interaction (e.g. autobrecciation, magma-sediment mingling, hyaloclastite and peperite-forming, etc.) was studied by Csámer (2015) in the Eastern Borsod Basin (NE-Hungary) where relatively small (2–30 m) subvolcanic bodies with contact lithofacies zones were found.

A detailed characterization of structural hydroxyl concentration of quartz phenocryst fragments from various pumiceous pyroclastic density current deposits (ignimbrites) at the Bükk Foreland Volcanic Area was performed. Biró et al. (2016) revealed that the structural hydroxyl content of quartz from the interior of several ten meters thick ignimbrites is just ~3 ppm. Further investigations showed that the structural hydroxyl content is decreasing from the base of thick ignimbrites towards their interior part from ~12 ppm to 3 ppm (Biró et al. 2017a). Such results indicate that the high emplacement temperature and slow cooling of massive ignimbrites cause post-depositional diffusional dehydration of nominally anhydrous minerals. This study highlighted the importance of careful sampling, when the water content representing magma chamber conditions prior to explosive eruptions should be probed: basal parts of ignimbrites and rapidly cooled fallout pyroclastics are the best candidates.

Based on a self-consistent K-Ar database completed with up-to-date geochronological information, Szakács et al. (2018) reviewed the general time–space evolution of Neogene magmatism in the Carpathian–Pannonian region, aiming at identifying significant patterns and trends. A petrographical and geochemical analysis was carried out on intrusive rocks along the Outer Carpathians from the Pieniny and Moravian areas (south Poland) by Pécskay et al. (2015), with special attention to boron content and K-Ar radiometric ages. The low boron concentration of the andesitic rocks in the Pieniny area is in the range measured in back-arc, intraplate basalts of the Bakony-Balaton Highland volcanic field, whereas the higher boron content of the Moravian rocks overlaps with that of the Western Carpathian andesites. K-Ar ages of the Moravian rocks are 14.8 Ma to 11.0 Ma and those of the Pieniny Mts. are 13.5-10.8 Ma.

Biró et al. (2017b, 2017c) described the field volcanological characteristics and presented granulometrical data of a bedded pyroclastic succession which was deposited at the Bükk Foreland Volcanic Area in the Mid-Miocene. The basal part of the succession is dominated by well-sorted coarse tuffs and lapilli tuffs with laterally constant thickness indicating fallout events. On the contrary, the fine grain size and high amount of ash aggregates at the upper part indicate wet-surge activity from hydromagmatic eruptions.

Márton et al. (2018) presented paleomagnetic results correlating the ignimbrites of the Mátra and Bükk Foreland volcanic areas. Based on the absence of CCW rotation and reversed polarity, the non-welded ignimbrites of the former (e.g. Tar quarry, Mátrabérc) can be traced as far as the western part of the latter (e.g., Sirok castle hill and Demjén–Nagyeresztvény quarry). In this case, biotite trace element geochemistry reinforces the correlation based on paleomagnetism. Further east in the foreland of the Bükk Mts, a number of outcrops are considered to be coeval, as demonstrated

by their physical volcanological features, and are proposed to belong to the youngest "tuff complex". These outcrops often comprise products deposited from several eruption pulses separated by paleosol horizons. The paleomagnetic results support a perfect correlation between the studied outcrops, since all have normal polarity and similar declinations. However, they must belong to the middle "tuff complex" due to the declinations suggesting about 30° CCW rotation.

2.2 Zircon geochronology and tectonic relationships of silicic volcanism

A comprehensive zircon geochronological study (Lukács et al. 2015, 2018a, 2018b) was undertaken for the Miocene silicic volcanism of the Pannonian Basin that resulted in an accurate eruption chronology framework for the volcanic activity. The in-situ LA-ICP-MS U-Pb zircon ages were confirmed by single zircon CA-ID-TIMS and sanidine Ar-Ar age determinations. On the contrary of the former three-fold distinction of the silicic volcanic products, Lukács et al. (2018a) identified at least 8 eruption units. The volcanism covers about 4 Myrs, from 18.2 Ma to 14.4 Ma. Within this, four large eruption events were recognized at 14.358 ± 0.015 Ma (Harsány ignimbrite), 14.880 ± 0.014 Ma (Demjén ignimbrite), 16.816 ± 0.059 Ma (Bogács unit) and 17.055 ± 0.024 Ma (Mangó ignimbrite), which are found in areas across the Pannonian Basin and elsewhere in central Europe. Considering all the potential sources of silicic ash found in the Paratethys sub-basins around the Pannonian Basin and along the northern Alps and in central Italy, Lukács et al. (2018a) suggested that they were probably derived almost exclusively from the Pannonian Basin as shown by zircon U-Pb dates presented in this paper and published comparable age data from several localities. These new zircon U-Pb data could help refining also the Miocene stratigraphy in the Pannonian Basin and could help to construct a high-resolution chronostratigraphic framework to achieve a better correlation of different Paratethys stages in the Mediterranean and to yield precise age proxies that could contribute to connect these sequences to global events. The cumulative volume of the volcanic material formed during this 4 Myr long silicic volcanism is estimated to be>4000 km^3, consistent with a significant ignimbrite flare-up event. This volcanism is regarded as the largest one in Europe for the last 20 Myr.

The silicic volcanism occurred coeval with the thinning of the lithosphere beneath the Pannonian basin. During this period, long-lived silicic magma reservoirs developed in the upper crust, mostly kept as high-crystallinity mushes for several 100' kyrs (Lukács et al. 2015). This affected considerably the thermal condition of the continental crust and could have an influence also to the crustal thinning and contributed to the maturation of organic material in the upper crust. Zircon Hf isotope and bulk rock Sr-Nd isotopic data indicate a sharp decrease of crustal and/or increase of asthenospheric mantle input after 16.2 Ma, suggesting that by this time the crust, and the lithospheric mantle was considerably thinned (Lukács et al. 2018a). This magmatism appears to have had a structural relationship to tectonic movements characterized by strike-slip and normal faults within the Mid-Hungarian Shear Zone as well as vertical axis block rotations, when the two microplates were juxtaposed. Based on the new eruption age data, the age of the two major block rotation events in Northern Hungary was refined: the first rotation event occurred between 17.05 Ma and 16.8 Ma, whereas the second one between 16.2 Ma and 14.9 Ma. This was accompanied also with a temporal change in the stress field orientation (Petrik et al. 2016).

2.3 Ciomadul (Csomád) volcano

Ciomadul the youngest volcano in the Carpathian-Pannonian Region. It is a long-dormant, seemingly inactive volcano where the radiometric dating suggested that the last eruption occurred around 30 ka.

To constrain the eruption chronology, a novel methodology, i.e. zircon (U-Th)/He dating combined with U-Th and U-Pb ages was applied (Harangi et al. 2015a, Molnár et al. 2017, 2018, Lukács et al. 2018c). It was demonstrated that such a technique can be successfully used for young (i.e. < 1 Ma) volcanic rocks (Molnár et al. 2017).In contrast to the former K/Ar age data, eruption ages were significantly refined. The volcanism of the Ciomadul lava dome field started at 1 Ma and

occurred intermittently until ca. 300 ka (Molnár et al. 2018). This was accompanied by a significant change in the composition of the erupted magmas compared to the older Pilisca volcanic rocks. Remarkably, volcanic activity resumed even after protracted, more than 100 ka long quiescence time. Development of the Ciomadul volcanic complex started at 160 ka and the last eruptions occurred at around 30 ka. This volcanism was characterized also long, i.e. several 10's ka repose periods between the active phases. The youngest eruption stage from 57 ka to 30 ka was dominantly explosive.

Zircon U-Th and U-Pb ages suggest that crystallization of zircons occurred more than 200 ka before the onset of eruptions (Harangi et al. 2015b, Lukács et al. 2018c). Most of the zircons are thus regarded as antecrysts and indicate a protracted lifetime of the subvolcanic magma storage. Noteworthy, crystallization took place even during the quiescence periods. Harangi et al. (2015a) used combined magnetotelluric and petrologic constrains for the nature of the magma storage system beneath the Ciomadul volcano. Combination of the identified electrical resistivity anomaly in the upper crust with thermobarometry results coming from the phenocrysts of the dacites, they suggested the presence of a melt-bearing crystal mush body in 8 to 20 km depth range. Summarizing these new results, Harangi et al. (2015a, 2015b) proposed that a new term is necessary for those volcanoes, which erupted last time >10 ka and therefore they cannot be regarded as potentially active. They introduced the term PAMS volcano, i.e. 'volcano with potentially active magma storage' for such volcanic systems, where there are observations that melt-bearing magma body is still present in the upper crust. There are an increasing number of studies showing that such crystal mush with some melt fraction can be rapidly rejuvenated and formation of eruptible magma could result in volcanic activity even after long quiescence.

Kis et al. (2017) provided the first high-resolution CO_2 flux data for the Neogene to Quaternary volcanic regions of the entire Carpathian-Pannonian Region, and estimated the CO_2 emission of the seemingly inactive Ciomadul volcanic complex. The CO_2 fluxes of focused emissions range between 277 and 8172 g d^{-1}, corresponding to a CO_2 output into the atmosphere between 0.1 and 2.98 t per year. The highest CO_2 focused gas fluxes at Ciomadul were found at the periphery of the youngest volcanic complex, which could be explained either by tectonic control across the brittle older volcanic edifices or by degassing from a deeper crustal zone resulting in CO_2 flux at the periphery of the supposed melt-bearing magma body beneath Ciomadul. The estimate of the total CO_2 output in the area is 8.70 × 103 t y^{-1}, and it is consistent with other long (>10 ka) dormant volcanoes with similar age worldwide.

At Ciomadul, other studies have also addressed both the late-stage explosive activity which formed the present structure of the twin-cratered dome complex and the extending (<1 My-long) extrusive lava dome-forming history. During the past ca. 60 ka, violent explosive eruptions occurred at Ciomadul, the youngest volcano in the Carpathian-Pannonian Region. Its tephra, oriented to the east, has been recovered as far as in the Dniester delta (Wulf et al. 2016). Detailed field volcanology, major element pumice glass geochemistry, optically stimulated luminescence and radiocarbon dating helped to establish a detailed tephrostratigraphy (Karátson et al. 2016, 2017a, 2017b; Veres et al. 2018). The explosive stage, related to the older Mohos and the younger St. Ana crater which decapitated the central domes, resulted in thick successions of pyroclastic-fall and -flow deposits in both proximal and medial/distal localities around the volcano. In particular, a significant two-phase eruption occurred at ca. 31.5 ka, producing a plinian pumiceous fallout and pyroclastic flows from vulcanian explosions. The latest eruptive phase, associated possibly with dome disruption at St. Ana crater, produced violent phreatomagmatic eruptions. According to radiocarbon age constraints and Cassignol-Gillot (unspiked) K-Ar dating on fragmented dome blocks, the youngest volcanic events terminated at ca. 28-29 ka (Karátson et al. 2016, 2018a, Karátson 2017).

Volumetric analysis and Cassignol-Gillot K/Ar dating have been used to infer the rates of long-term magma output (Karátson et al. 2018a, 2018b). The volcano showed an extended eruptive history from ~850 ka to <30 ka. A dominantly effusive activity took place during the first several hundred thousand years, producing isolated, peripheral domes and, subsequently, a central dome cluster. The calculated ~8.00 km^3 cumulative total volume of the lava domes, which includes an

erosionally removed volume of ~0.2 km^3, matches the dimensions of medium-sized dacitic lava domes worldwide. Such a volume was produced in the long term at a rate of 9.7 km^3/My (0.0097 km^3/ka). However, most of the domes (7.52 km^3) formed between 200-30 ka, implying a significantly increased lava extrusion rate of 44.2 km^3/My (0.0442 km^3/ky) in the second stage. Within this, individual lava domes with volumes between 0.02 and 0.4 km^3 could have been emplaced at much higher rates in the order of 1-10 km^3/ky.

3 Plio-Pleistocene alkali basalt volcanism

The mineral-scale textural and geochemical studies of the Late Miocene to Quaternary basalts of the Pannonian Basin resulted in a new insight into the pre-eruptive deep crustal magma evolution beneath monogenetic volcanic fields (Jankovics et al. 2015, 2016, Sági et al. 2018) and combining these results with bulk rock composition data, this led to a new model for the basaltic volcanism of the Carpathian-Pannonian Region (Harangi et al. 2015c).

Jankovics et al. (2015) studied the chemical composition, zoning and texture of the minerals from Kissomlyó Pliocene alkaline basaltic eruptive centre (Little Hungarian Plain, western Pannonian Basin. The high-resolution mineral-scale analyses provided a unique, more detailed insight into the evolution of these "simple" magmatic system. Five types of olivine crystals and three distinct compositional groups of olivine-hosted spinel inclusions were recognized which represent four magmatic environments. This implies that the petrogenesis of a single magma batch(usually defined as representing a particular eruptive unit) can be complex involving several magmas and various, closed- and open-system magmatic processes which finally result in the whole-rock (erupted magma) composition. The trace element patterns of clinopyroxene crystals of various origins occur were investigated by Jankovics et al. (2016) in the unusually crystal- and xenolith-rich alkaline basalts of the Bondoró-hegy and the Füzes-tó scoria cone (Bakony-Balaton Highland). The detailed study revealed that most of the clinopyroxenes are xenocrysts of diverse origins. The different clinopyroxene populations derived from the upper mantle, the lower crust and Type II. cumulates. The abundance of foreign crystals incorporated in the ascending basaltic magmas, and their potential for contamination of the host magma, must be taken into account when whole-rock geochemical data are interpreted.

Volcanological description and interpretation have been given about the Late Pliocene Badacsony Hill basalt volcano (Bakony–Balaton Highland Volcanic Field) by Hencz et al. (2017). The pyroclast/lithics ratio of the pyroclastics was investigated by using point-counting image analysis methodology on the surfaces of hand-cut specimens. It was possible to infer the relative depth of explosions with respect to the synvolcanic surface and the syneruptive morphology; moreover, the effusive and explosive phases of the volcanism have been identified. Hencz et al. (2017) pointed out that the Badacsony volcano was a monogenetic (probably polycyclic) tuff ring or shallow maar volcano, terminated by hawaiian and strombolian eruptions.

Three-dimensional geophysical modelling of the early Late Miocene Pásztori volcano (ca. 11–10 Ma) and adjacent area in the Little Hungarian Plain Volcanic Field of the Danube Basin was carried out by Panisova et al. (2018) in order to get an insight into the most prominent intra-crustal structures here. The volcanic series comprise alkaline trachytic and trachyandesitic volcanoclastic and effusive rocks. The uppermost 0.3–1.8 km thick layer of volcanoclastics underlain by a trachytic-trachyandesitic volcanoclastic rock units of a maximum 2 km thickness, and a deeper magmatic pluton in a depth range of 5–15 km.

Based on some alkaline basaltic rocks from the Carpathian-Pannonian Region, Sági et al. (2018) suggested a new fractionation calculation method for olivine and/or clinopyroxene phyric intracontinental alkaline basalts, using only the major elements and the Ni concentration of the basaltic rock, as well as the forsterite and Ni content of its olivine phenocrysts.

Harangi et al. (2015c) discussed the origin and geodynamic relationships of the Late Miocene to Quaternary alkaline basalt volcanism in the Pannonian basin and provided a new model for it. They estimated the mantle potential temperature as well as the depth range of the melting columns. The final pressure values of melting corresponds well the seismically identified lithosphere-

asthenosphere boundary beneath the region. Basaltic magmas formed by low-degree (2–3 %) melting in the convective asthenosphere. Existence of a mantle plume beneath the region was excluded, instead the Harangi et al. (2015c) proposed that plate tectonic processes controlled the magma generation. The Pannonian basin acted as a thin spot after the 20–12 Ma syn-rift phase and provided suction in the sublithospheric mantle, generating asthenospheric flow from below the adjoining thick lithospheric domains. A near-vertical upwelling along the steep lithosphere–asthenosphere boundary beneath the western and northern margins of the Pannonian basin could result in decompressional melting producing low-volume melts. The youngest basalt volcanic field (Persani) in the region is inferred to have been formed due to the dragging effect of the descending lithospheric slab beneath the Vrancea zone that could result in narrow rupture at the base of the lithosphere.

A novel model was proposed by Kovács et al. (2017a, 2018a) to explain the genesis of Plio-Pleistocene alkaline basaltic rocks in the Carpathian-Pannonian region. The new results indicate that there is enough water (>>300 ppm wt.) in the asthenosphere to keep the upper mantle in partially molten state even after the cessation of extension. The driving force for the formation of alkaline basalts is the convergence between the Adriatic indenter and the stable European platform in the tectonic inversion stage. In this period the foliation in the upper mantle became subvertical and the compression facilitated the rise of the partial melt to the surface, which was further enhanced by the deep fractures in the lithosphere having been formed during coeval lithospheric scale folding.

4 Upper mantle and lower crustal xenoliths from the Carpathian-Pannonian region

4.1 General studies on xenoliths

Berkesi et al. (2017) developed a method to detect minor amount (less than 1 mol. %) of nitrogen in high-density CO_2 fluid inclusions from mantle rocks using confocal Raman spectroscopy. The Raman signal of the N_2 appeared as two adjacent, partially overlapping bands. The band at higher Raman shift is identical with the nitrogen-in-air band, meanwhile the band at lower Raman shift is the nitrogen within the fluid inclusions. They proposed that N_2 may be a minor but common component in subcontinental lithospheric mantle fluids.

The role of melt depletion versus refertilization in the spinel peridotite xenoliths was discussed by Embey-Isztin (2016). In this study, a modified version of Ti-in-Cpx versus Mg#-in-olivine plots was applied to ~1,500 spinel peridotite xenoliths from worldwide localities. The results showed that the vast majority of shallow mantle samples are consistent with the partial melting model; however, a minority of samples may indicate refertilization of formerly refractory mantle domains.

Kovács et al. (2017b) demonstrated the importance of pargasitic amphibole (a hydrous chain silicate) in the formation of major geophysical discontinuities in the upper mantle. In particular, the authors showed that the pargasite dehydration solidus at ~ 1100 °C below ~ 100 km is responsible for the lithosphere-asthenosphere boundary beneath young oceanic plates and continental rift areas.

4.2 Mantle xenoliths from the Styrian Basin and Bakony-Balaton Highland Volcanic Fields

Aradi et al. (2015) studied upper mantle peridotite xenoliths from the Styrian Basin (Western Pannonian Basin, Austria). They concluded that the deformation of the lithospheric mantle took place during the transpressional phase of the Alpine orogeny after the breakoff of the suspected Penninic slab. Combining the microstructural data and structural OH^--content of olivine they suggest that an extensive annealing process of the lithospheric mantle was caused by a late metasomatic event. A possible source for the metasomatic fluid/melt could be the subducted Penninic slab.

Créon et al. (2016) investigated secondary fluid and melt inclusions, melt pockets and veins found in mantle xenoliths from the Bakony-Balaton Highland, in order to study the connection between subduction of carbon-bearing continental crust and intraplate CO_2 emission. Based on CO_2/silicate melt ratios, they concluded that the metasomatic agent could have been a CO_2

supersaturated melt or a carbonate melt that reacted with the lithospheric mantle resulting in a CO_2 enriched silicic melt. Crystallization of the melt caused CO_2 exsolution. A minimal 2000 ppm CO_2 bulk concentration of the lithosphere was proposed as rest of the CO_2 degassed through the Mid-Hungarian Shear Zone.

Kovács et al. (2016) studied water concentrations and H-isotope compositions of basalt hosted clinopyroxene megacrysts and amphibole clinopyroxenites, mostly from the Bakony-Balaton Highland, and other localities worldwide. The authors found that the structural hydroxyl concentration correlates positively with the δD values of clinopyroxene megacrysts for each locality. This indicates that structurally bond hydrogen in clinopyroxenes may have δD values higher than molecular water in nano-inclusions. This, in turn, implies that there may be a significant hydrogen isotope fractionation for structural hydroxyl during crystallization of clinopyroxene.

Bali et al. (2018) described a composite xenolith from Szigliget (Bakony Balaton Highland) that consist of a zircon-bearing, apatite-rich olivine-pyroxene hornblendite and an amphibole harzburgite. The amphibole of the olivine-pyroxene hornblendite is enriched in incompatible elements. Based on the mineral compositions, condition of pressure (1.2-1.4 GPa), temperature (~1000-1015 °C) and oxygen fugacity (ΔlogfO2(FMQ)~+1.3) were estimated. The amphibole-rich mantle segment crystallized from a phonolitic-trachitic melt that was enriched in volatile and incompatible elements.

4.3 Mantle xenoliths from the Nógrád-Gömör Volcanic Field

Klébesz et al. (2015) studied the average seismic properties of the lithospheric mantle beneath the Nógrád-Gömör Volcanic Field focusing on mantle xenoliths from Bárna-Nagykő. Based on the geophysical observations, petrology and CPO data, it can be estimated that the thickness of a layer (140-330 km if one layer is assumed) that generates the seismic anisotropy beneath the region. The layer is greater than the lithospheric mantle, thus most of the delay accumulates in the sublithospheric mantle, namely in the asthenosphere.

Liptai et al. (2017) studied 51 mantle upper mantle spinel peridotite xenoliths from the Nógrád-Gömör Volcanic Field, representing the whole volcanic area. Based on major and trace element data, the xenoliths could be divided into different groups showing evidence of different metasomatic events. They suggest that the metasomatic agents in all cases were basaltic silicate melts (with different equilibrium temperatures) interacted with the mantle rocks during the Miocene extension of the Pannonian Basin.

4.4 Mantle xenoliths from the Transylvanian Basin

Kovács et al. (2018b) presented a detailed study in which the authors combined geochemical and geophysical methods on mantle xenoliths from the Persány Mountains, Transylvania (Eastern CPR). They explain that with the help of modal composition of mantle xenoliths it is possible to estimate seismic velocities (Vp and Vs) which can be compared with the data provided by geophysical surveys. Crystal preferred orientation (CPO) of rock-forming minerals combined with SKS wave splitting data help to understand the seismic anisotropy generated in the lithospheric mantle. Structural OH^--content of nominally anhydrous minerals increase the conductivity of the mantle, which can be measured with magnetotellurics. Thus volatile content of the lithospheric mantle could be estimated based on geophysical data.

Nédli et al. (2015) present petrography and geochemistry data of a lherzolite-websterite xenolith series and of clinopyroxene xenocrysts hosted in Upper Cretaceous - Paleogene basanites from Poiana Ruscă (Transylvania). The xenoliths have slightly deformed porphyroclastic-equigranular textures. In many xenoliths notable orthopyroxene growth and poikilitic texture was observed. The calculated melt composition in equilibrium with clinopyroxenes was mafic, Al-Na-rich and volatile-poor. This melt is associated with Late Cretaceous—Paleogene subdution-related andesitic magmatism of the Poiana Ruscă causing crystallization of orthopyroxene and forming poikilitic texture in the lithospheric mantle.

4.5 Lower Crustal xenoliths

Németh et al. (2015) studied mafic garnet granulite xenoliths from the Bakony-Balaton Highland Volcanic Field to trace fluid-melt-rock interactions in the lower crust. Two unique xenoliths were selected for analyses (microthermometry, electron microprobe, Raman and IR spectroscopy). Petrography, fluid and melt inclusion study suggests that at least three fluid events occurred in the deep crust. Water content of the rock forming minerals implies a highly dry lower crust, locally hydrated by percolating fluids and melts.

Downes et al. (2015) determined the U-Pb ages for zircons separated from a lower crustal granulite-facies metasedimentary xenolith from the Bakony-Balaton Highland, using LA-ICPMS and SHRIMP techniques. The ages are highly variable from late Devonian to Pliocene (5.1-4.2 Ma) which coincide with the age of host basalt eruptions. This suggests that the heat flow in the base of the Pannonian Basin was sufficiently high to keep many of zircons close or above to their blocking temperature.

5 Geoheritage

The concept of geodiversity involving abiotic elements of the environment arose as a scientific topic in the last decade of the 20th century. The increasing number of geological exhibition sites and the public interest in the two domestic UNESCO Global Geoparks in Hungary (Novohrad–Nógrád, Bakony–Balaton) indicated that geodiversity-based geotourism had become a development tool for disadvantaged peripheral regions. Such developments require multi-faceted professional inventory and assessment of the elements of geodiversity.Szepesi et al. (2017, 2018) discussed the geoheritage and geotourism perspectives in Hungary. The Tokaj Wine Region (TWR) Historic Cultural Landscape (inscribed on the World Heritage List in 2002 as a cultural site) is characterized also by high geodiversity due to complex volcanic settings (andesite–dacite composite cones, silicic pyroclastites, lava domes, hydrothermal activity) and specialized viticultural land use of the cultural landscape. They performed a quantitative assessment to evaluate the scientific, cultural/historical, aestheticand socio-economic values of the Tokaj and other volcanic areas in the Pannonian Basin that could help to define priorities in site management. They suggested a 900 km long, cross-Hungary volcano route which starts in the TWR and involves 50 more planned stations all along the country. They represent various volcanological phenomena from silicic ignimbrite sheets through andesitic stratocones to basaltic volcanic fields. These include significant historic, cultural, gastronomic tourism attractions to support the promotion of volcanic geoheritage.

6 Most significant studies based on international collaboration

6.1 Igneous petrology and geochemistry

Guzmics et al. (2015) studied the compositional evolution of both the silicate and carbonate melt in the subvolcanic reservoir of the Kerimasi Volcano in the East African Rift. Geochemistry of the studied silicate and carbonate melt inclusions trapped in nepheline, apatite and magnetite from plutonic afrikandite and calciocarbonatite rocks show that liquid immiscibility occurred during the generation of carbonatite magmas from a CO_2-enriched melilite–nephelinite magma formed at ~1100 °C. The evolution of the Kerimasi carbonate magma could have led to the formation of natrocarbonate melts with similar composition to those of Oldoinyo Lengai. Moreover, in this paper Guzmics et al. provided partition coefficients between carbonate and silicate melt for a wide range of elements. Káldos et al. (2015) reported a new model for the melt evolution of the Kerimasi Volcano based on carbonate melt inclusions in magnetite and clinopyroxene from a jacupirangite rock. Petrographic observations and geochemical data suggest that during the crystallization a CaO-rich and alkali-"poor" carbonate melt existed, similar in composition to the parental melt of the Kerimasi calciocarbonatite. Jacupirangite was most probably formed when the immiscible silicate

and carbonate melts separated from the afrikandite body, although the carbonate melt was not separated completely from the silicate melt fraction.

Klébesz et al. (2015) determined major and trace element and volatile compositions of reheated melt inclusions (RMI) and their clinopyroxene hosts from a selected "sub-effusive" nodule from the uppermost layer of the Sarno (Pomici di Base; PB) plinian eruption of Mt. Somma-Vesuvius (Italy). Based on RMI and clinopyroxene composition they constrain processes associated with the origin of the nodule, its formation depth, and hence the depth of the magma chamber associated with the Sarno (PB) eruption.

6.2 Peridotite xenoliths

Park et al. (2017) studied fluid inclusions in xenoliths derived from the lithospheric mantle beneath the Rio Grande Rift. Based on petrography, two generations of fluid-inclusion assemblages can be distinguished, both hosted in orthopyroxenes. An earlier fluid infiltration, containing mainly C–O–N–S, was trapped in the cores of orthopyroxenes, whereas a later fluid infiltration (C–O–H–S) was trapped as inclusions after the formation of the orthopyroxene porphyroclasts with exsolution lamellae.

Pintér et al. (2015) studied ultramafic xenoliths from Nyos and Barombi Mbo Lakes in the continental sector of the Cameroon Volcanic Line. The authors concluded that the Barombi Mbo xenoliths originated from a juvenile segment of the upper mantle, which has asthenospheric origin. It became a part of the lithosphere in response to thermal relaxation following the extension, forming a weakly deformed lower lithospheric mantle region along the Cameroon Volcanic Line. On the other hand, the Nyos xenoliths represent a shallow lithospheric mantle with imprints of several depletion and enrichment events.

6.3 Geochronology

Systematic collaborative geochronological studies have been carried out in the Institute of Nuclear Research in Debrecen (Hungarian Academy of Sciences). These studies include: the Rudnik Mts. volcano-intrusive complex, central Serbia (Cvetkovic et al. 2016), Calimani-Gurghiu-Harghita volcanic range, Eastern Transylvania, Romania (Seghedi et al. 2017), Neogene Vepor stratovolcano, Central Slovakia (Konecny et al. 2015), Ciomadul, South Harghita Mts., Romania (Szakács et al. 2015), Oaş-Gutâi Volcanic Zone, Romania (Kovacs et al. 2017), Izmir-Balikesir transfer zone, Western Anatolia, Turkey (Seghedi et al. 2015), western Mongolian Altai (Zacek et al. 2016).

6.4 Volcanology

Karátson et al. (2018c, 2018d) attempted to reconstruct the topography of Santorini before the cataclysmic Late Bronze Age (Minoan) eruption which, according to many authors, contributed to the decline of the Minoan civilisation. During the Late Bronze Age, the island of Santorini had a semi-closed caldera harbour in the northern part of the present-day caldera, inherited from the 22 ka Cape Riva Plinian eruption, and a central island similar to the present-day Kameni Islands, which is referred to as 'Pre-Kameni'.

Pre-Kameni and other parts of Santorini were destroyed during the Minoan eruption, and their fragments were incorporated as lithic clasts in the Minoan pyroclastic deposits. Photo-statistical analysis and granulometry of these lithics, differentiated by lithology, constrain the volume of Pre-Kameni to 2.2–2.5 km^3. Applying the Cassignol-Gillot K-Ar dating technique to the most characteristic black glassy andesite lithics, we propose that the island started to grow at 20.2±1.0 ka soon after the Cape Riva eruption. This implies a minimum long-term lava extrusion rate of ~0.13–0.14 km^3/ka during the growth of Pre-Kameni. However, because this value is only one seventh of the average growth rate during the much shorter lifetime of the present-day Kameni Islands (~0.9 km^3/ka since the Minoan eruption), it is possible that Pre-Kameni grew up in a short

period at higher lava extrusion rates. If so, the extrusive activity may have declined, and possibly the island of Pre-Kameni was dormant by the Late Bronze Age.

6.5 Geoheritage

Geoheritage and geoconservation has become more and more accepted by scientists as a mean for protecting and improving our urban environment. The Limagne fault and Chaîne des Puys, the alignment of 80 volcanoes of a large rift margin is next to the city of Clermont-Ferrand, France. It is currently (2018) inscribed for the UNESCO World Heritage title. The ongoing UNESCO project is outside the urban city limits, but diverse and valuable geology also continues below the fault escarpment limit into the city. Vereb et al. (2018) presented a wide variety of geological features inside the metropolitan area, such as lava flows, river channels and sediments, inverted relief, landslides and even travertine with CO_2 vents. The delineation of features based on a high resolution lidar-based DEM will be a guideline for the further extension of inventories and pinpoint areas for protection and development.

Acknowledgements. The authors are thankful to the researchers who supported the compilation of this report: L. Aradi, T. Bíró, É. Jankovics, D. Karátson, L. Lange, E. Pál-Molnár, I. Kovács and Cs. Szabó.

References

Aradi LE, Hidas K, Kovács IJ, Tommasi A, Klébesz R, Garrido CJ, Szabó Cs (2015): Fluid-Enhanced Annealing in the Subcontinental Lithospheric Mantle Beneath the Westernmost Margin of the Carpathian-Pannonian Extensional Basin System. Tectonics, 36, 2987–3011.

Bali E, Hidas K, Guðfinnsson GH, Kovács Z, Török K, Román-Alpiste MJ (2018): Zircon and apatite-bearing pyroxene hornblendite mantle xenolith from Hungary, Carpathian-Pannonian region. Lithos, 316–317, 19–32.

Batki A, Pál-Molnár E, Jankovics MÉ, Kerr AC, Kiss B, Markl G, Heincz A, Harangi Sz (2018): Insights into the evolution of an alkaline magmatic system: An in situ trace element study of clinopyroxenes from the Ditrău Alkaline Massif, Romania. Lithos, 300–301, 51–71.

Berkesi M, Káldos R, Park M, Szabó Cs, Váczi T., Török K, Czuppon Gy (2017): Detection of small amounts of N2 in CO2-rich high-density fluid inclusions from mantle xenoliths. European Journal of Mineralogy, 29, 423-431.

Biró T, Karátson D, Márton E, Józsa S, Bradák B (2015): Paleoflow directions of a subaqueous lahar deposit around the Miocene Keserűs Hill lava dome complex (North Hungary) as constrained by photo-statistics and anisotropy of magnetic susceptibility (AMS). Journal of Volcanology and Geothermal Research, 302, 141-149.

Biró T, Kovács IJ, Király E, Falus G, Karátson D, Bendő Z, Fancsik T, Sándorné JK (2016): Concentration of hydroxyl defects in quartz from various rhyolitic ignimbrite horizons: results from unpolarized micro-FTIR analyses on unoriented phenocryst fragments. European Journal of Mineralogy, 28, 313-327.

Biró T, Kovács IJ, Karátson D, Stalder R, Király E, Falus G, Fancsik T, Sándorné JK (2017a): Evidence for post-depositional diffusional loss of hydrogen in quartz phenocryst fragments within ignimbrites. American Mineralogist, 102, 1187-1201.

Biró T, Hencz M, Karátson D, Márton E, Bradák-Hayashi B, Szalai Z (2017b): First physical volcanological description of a Miocene, silicic, phreatomagmatic fall complex in the Carpatho-Pannonian Region (CPR). Geophysical Research Abstract, 19, Paper 6616.

Biró T, Hencz M, Karátson D, Márton E, Szalai Z, Bradák-Hayashi B (2017c): Middle Miocene silicic phreatomagmatism at the Bükk Foreland Volcanic Area. Romanian Journal of Earth Sciences, 91, Special Issue, p. 60.

Créon L, Rouchon V, Youssef S, Rosenberg E, Delpech G, Szabó Cs, Remusat L, Mostefaoui S, Asimow PD, Antoshechkina PM, Ghiorso MS, Boller E, Guyot F (2016): Highly CO_2-supersaturatedmelts in the Pannonian lithospheric mantle – A transient carbon reservoir? Lithos, 286–287, 519–533.

Csámer Á (2015): Interaction between a Late Miocene andesitic dyke swarm and wet sediment in the Szoros Valley, Eastern Borsod Basin, Northeast Hungary. Central European Geology, 58, 246-267.

Cvetkovic V, Saric K, Pécskay Z, Gerdes A (2016): The Rudnik Mts. volcano-intrusive complex (central Serbia): An example of how magmatism controls metallogeny. Geologia Croatica, 69, 89-99.

Downes H, Carter A, Armstrong R, Dobosi G, Embey-Isztin A (2015): Lower crustal zircons reveal Neogene metamorphism beneath the Pannonian Basin (Hungary). Open Geosciences, 7, 223-233.

Embey-Isztin A (2016): The role of melt depletion versus refertilization in the major element chemistry of four-phase spinel peridotite xenoliths. Central European Geology, 59, 60-86.

Guzmics T, Zajacz Z, Mitchell RH, Szabó Cs, Wälle M (2015): The role of liquid–liquid immiscibility and crystal fractionation in the genesis of carbonatite magmas: insights from Kerimasi melt inclusions. Contributions to Mineralogy and Petrology, 169(2), Article 17.

Harangi Sz, Novák A, Kiss B, Seghedi I, Lukács R, Szarka L, Wesztergom V, Metwaly M, Gribovszki K (2015a): Combined magnetotelluric and petrologic constrains for the nature of the magma storage system beneath the Late Pleistocene Ciomadul volcano (SE Carpathians). Journal of Volcanology and Geothermal Research, 290, 82-96.

Harangi Sz, Lukács R, Schmitt AK, Dunkl I, Molnár K, Kiss B, Seghedi I, Novothny Á, Molnár M (2015b): Constraints on the timing of Quaternary volcanism and duration of magma residence at Ciomadul volcano, east–central Europe, from combined U–Th/He and U–Th zircon geochronology. Journal of Volcanology and Geothermal Research, 301, 66-80.

Harangi Sz, Jankovics MÉ, Sági T, Kiss B, Lukács R, Soós I (2015c): Origin and geodynamic relationships of the Late Miocene to Quaternary alkaline basalt volcanism in the Pannonian basin, eastern–central Europe. International Journal of Earth Sciences, 104, 2007-2032.

Heincz A, Pál-Molnár E, Kiss B, Batki A, Almási EE, Kiri L (2018): Nyílt rendszerű magmás folyamatok: magmakeveredés, kristálycsere és kumulátum-recirkuláció nyomai a Ditrói alkáli masszívumban (Orotva, Románia). Földtani Közlöny, 148(2), 125–142.

Hencz M, Karátson D, Németh K, Biró T (2017): The phreatomagmatic pyroclastic sequence of the Badacsony Hill: implications for the processes and landforms of monogenetic basaltic volcanism (in Hungarian with English abstract). Földtani Közlöny, 147, 297-310.

Jankovics MÉ, Harangi Sz, Németh K, Kiss B, Ntaflos T (2015): A complex magmatic system beneath the Kissomlyó monogenetic volcano (western Pannonian Basin): evidence from mineral textures, zoning and chemistry. Journal of Volcanology and Geothermal Research, 301, 38-55.

Jankovics MÉ, Taracsák Z, Dobosi G, Embey-Isztin A, Batki A, Harangi Sz, Hauzenberger CA (2016): Clinopyroxene with diverse origins in alkaline basalts from the western Pannonian Basin: implications from trace element characteristics. Lithos, 262, 120-134.

Káldos R, Guzmics T, Mitchell RH, Dawson JB, Milke R, Szabó Cs (2015): A melt evolution model for Kerimasi volcano, Tanzania: Evidence from carbonate melt inclusions in jacupirangite. Lithos, 238, 101-119.

Karátson D (2017): Volcanic evolution and morphology of the Late Quaternary Ciomadul lava dome complex, the youngest center within the Inner Carpathian Volcanic Range. In: 4th Central European Geomorphology Conference, Bayreuth, Germany, Session O 2.1 (Cretaceous and Cenozoic volcanism in Europe, relations to geomorphology), Abstract Volume, Universität Bayreuth, p. 17.

Karátson D, Telbisz T, Lahitte P, Dibacto S, Veres D, Szakács A, Gertisser R, Jánosi Cs (2018a): Magma output rates of the Late Quaternary Ciomadul (Csomád) lava dome complex using digital elevation model (DEM) volumetry and Cassignol - Gillot K-Ar dating. In: Mattoni, S. (ed.) Abstracts Volume of the International meeting "Cities on Volcanoes 10": Millenia of Stratification between Human Life and Volcanoes: strategies for coexistence (Naples, Italy). Istituto Nazionale di Geofisica e Vulcanologia, Rome, p. 355.

Karátson D, Telbisz T, Dibacto S, Lahitte P, Szakács S, Veres D, Gertisser R, Jánosi Cs, Timár G (2018b): Volcanic evolution of Ciomadul – long-term magma output rates on the basis of new K-Ar dating and volumetry (in Hungarian). In: Papucs A, Dénes R (ed.) XXth Székelyföldi Geológus Találkozó, Sepsiszentgyörgy, Abstract Volume, 24-26.

Karátson D, Gertisser R, Telbisz T, Vereb V, Quidelleur X, Druitt T, Nomikou P, Kósik Sz (2018c): Reconstructing 'Atlantis', the Late Bronze Age island of Santorini. In: Mattoni, S. (ed.), Abstracts Volume of the International meeting "Cities on Volcanoes 10": Millenia of Stratification between Human Life and Volcanoes: strategies for coexistence (Naples, Italy). Istituto Nazionale di Geofisica e Vulcanologia, Rome, p. 661.

Karátson D, Gertisser R, Telbisz T, Vereb V, Quidelleur X, Druitt T, Nomikou P, Kósik Sz (2018d): Towards reconstruction of the lost Late Bronze Age intra-caldera island of Santorini, Greece. Scientific Reports 8(1), Paper 7026.

Karátson D, Veres D, Wulf S, Gertisser R, Magyari E, Bormann M (2017a): The youngest volcanic eruptions in East-Central Europe—new findings from the Ciomadul lava dome complex, East Carpathians, Romania. Geology Today, 33, 60-65.

Karátson D, Veres D, Wulf S, Gertisser R, Lahitte P, Dibacto-Kamwa S, Novothny Á, Magyari E, Jánosi Cs (2017b): Explosive eruptions and tephra dispersal from Ciomadul (Csomád) volcano, Easth Carpathians. In: La Monica, M, Corsale, L (eds.) Explosive eruptions and the Mediterranean Civilizations through prehistory and history (Ustica, Italy). Istituto Nazionale di Geofisica e Vulcanologia, Rome, p. 49.

Karátson D, Wulf S, Veres D, Magyari EK, Gertisser R, Timar-Gabor A, Novothny Á, Telbisz T, Szalai Z, Anechitei-Deacu V, Appelt O, Bormann M, Jánosi Cs, Hubay K, Schäbitz F (2016): The latest explosive eruptions of Ciomadul (Csomád) volcano, East Carpathians: a tephrostratigraphic approach for the 51–29 ka BP time interval. Journal of Volcanology and Geothermal Research, 319, 29-51.

Kis BM, Ionescu A, Cardellini C, Harangi Sz, Baciu C, Caracausi A, Viveiros F (2017): Quantification of carbon dioxide emissions of Ciomadul, the youngest volcano of the Carpathian-Pannonian Region (Eastern-Central Europe, Romania). Journal of Volcanology and Geothermal Research, 341, 119-130.

Klébesz R, Esposito R, De Vivo B, Bodnar RJ (2015): Constraints on the origin of sub-effusive nodules from the Sarno (Pomici di Base) eruption of Mt. Somma-Vesuvius (Italy) based on compositions of silicate-melt inclusions and clinopyroxene. American Mineralogist, 100, 760-773.

Klébesz R, Gráczer Z, Szanyi Gy, Liptai N, Kovács I, Patkó L, Pintér Zs, Falus Gy, Wesztergom V, Szabó Cs (2015): Constraints on the thickness and seismic properties of the lithosphere in an extensional setting (Nógrád-Gömör Volcanic Field, Northern Pannonian Basin). Acta Geodaetica et Geophysica, 50, 133–149.

Konecny V, Konecny P, Kubes P, Pécskay Z (2015): Paleovolcanic reconstruction of the Neogene Vepor statovolcano (Central Slovakia), part I. Mineralia Slovaca, 47, 1-76.

Kovacs M, Seghedi I, Yamamoto M, Fülöp A, Pécskay Z, Jurje, M (2017): Miocene volcanism in the Oaş–Gutâi Volcanic Zone, Eastern Carpathians, Romania: Relationship to geodynamic processes in the Transcarpathian Basin. Lithos, 294, 304-318.

Kovács I, Demény A, Czuppon Gy, Lécuyer C, Fourel F, Xia QK, Szabó Á (2016): Water concentrations and hydrogen isotope compositions of alkaline basalt-hosted clinopyroxene megacrysts and amphibole clinopyroxenites: the role of structural hydroxyl groups and molecular water. Contributions to Mineralogy and Petrology, 171(5), Article 38.

Kovács I, Kiss J, Török K, Király E, Karátson D, Fancsik T, Biró T, Pálos Zs, Aradi L, Patkó L, Liptai N, Falus Gy, Hidas K, Wesztergom V, Szabó Cs (2018a):A new conceptual model for the genesis of Plio-Pleistocene alkaline basalts in the Pannonian Basin. Geophysical Research Abstracts, 20, Paper 9929.

Kovács I, Patkó L, Falus Gy, Aradi LE, Szanyi Gy, Gráczer Z, Szabó Cs (2018b): Upper mantle xenoliths as sources of geophysical information: the Perşani Mts. area as a case study. Acta Geodaetica et Geophysica, 53, 415–438.

Kovács I, Kiss J, Falus Gy, Hidas K, Aradi L, Patkó L, Liptai N, Török K, Biró T, Karátson D, Pálos Zs, Király E, Fancsik T, Sándorné Kovács J, Szabó Cs (2017a):A Kárpát–Pannon régió „tercier" bazaltképződésének új geodinamikai modellje. In: Dégi, Júlia; Király, Edit; Kónya, Péter; Kovács, István János; Pál-Molnár, Elemér; Thamóné, Bozsó Edit; Török, Kálmán; Udvardi, Beatrix (szerk.) Ahol az elemek találkoznak: víz, föld és tűz határán : 8. Kőzettani és Geokémiai Vándorgyűlés Budapest, Magyarország: Geological and Geophysical Institite of Hungary, 93-96.

Kovács I, Lenkey L, Green DH, Fancsik T, Falus Gy, Kiss J, Orosz L, Angyal J, Vikor Zs (2017b):The role of pargasitic amphibole in the formation of major geophysical discontinuities in the shallow upper mantle. Acta Geodaetica et Geophysica, 52, 183-204.

Liptai N, Patkó L, Kovács IJ, Hidas K, Pintér Zs Jeffries T, Zajacz Z, O'Reilly SY, Griffin WL, Pearson NJ, Szabó Cs (2017): Multiple Metasomatism beneath the Nógrád–Gömör Volcanic Field (Northern Pannonian Basin) Revealed by Upper Mantle Peridotite Xenoliths. Journal of Petrology, 58, 1107–1144.

Lukács R, Harangi S, Bachmann O, Guillong M, Danišík M, Buret Y, von Quadt A, Dunkl I, Fodor L, Sliwinski J, Soós I, Szepesi J (2015): Zircon geochronology and geochemistry to constrain the youngest eruption events and magma evolution of the Mid-Miocene ignimbrite flare-up in the Pannonian Basin, eastern central Europe. Contribultions to Mineralogy and Petrology, 170(5-6), Article 52.

Lukács R, Harangi Sz, Guillong M, Bachmann O, Fodor L, Buret Y, Dunkl I, Sliwinski J, von Quadt A, Peytcheva I, Zimmerer M (2018a): Early to Mid-Miocene syn-extensional massive silicic volcanism in the Pannonian Basin (East-Central Europe): Eruption chronology, correlation potential and geodynamic implications. Earth Science Reviews, 179, 1-19.

Lukács R, Guillong M, Sliwinski J, Dunkl I, Bachmann O, Harangi Sz (2018b): LA-ICP-MS U-Pb zircon geochronology data of the Early to Mid-Miocene syn-extensional massive silicic volcanism in the Pannonian Basin (East-Central Europe). Data in Brief, 19, 506-513.

Lukács R, Guillong M, Schmitt AK, Molnár K, Bachmann O, Harangi Sz (2018c): LA-ICP-MS and SIMS U-Pb and U-Th zircon geochronological data of Late Pleistocene lava domes of the Ciomadul Volcanic Dome Complex (Eastern Carpathians). Data in Brief, 18, 808-813.

Márton E, Karátson D, Biró T, Hencz M (2018): Correlation of the deposits of an extensive Miocene silicic explosive volcanism by combining paleomagnetic marker horizons and magnetic polarities: new results from the Mátra and Bükk Mts, NE Hungary. Geophysical Research Abstracts, 20, Paper EGU 2018-6716.

Molnár, K., Dunkl, I., Harangi, Sz., Lukács, R. (2017): A cirkon (U-Th)/He kormeghatározás módszertani alapjai és alkalmazása fiatal (<1M év) vulkánkitörések datálására. Földtani Közlöny 147, 225-244.

Molnár K, Harangi Sz, Lukács R, Dunkl I, Schmitt AK, Kiss B, Garamhegyi T, Seghedi I (2018): The onset of the volcanism in the Ciomadul Volcanic Dome Complex (Eastern Carpathians): Eruption chronology and magma type variation. Journal of Volcanology and Geothermal Research, 354, 39-56.

Nédli Z, Szabó Cs, Dégi J (2015): Orthopyroxene-enrichment in the lherzolite-websterite xenolith suite from Paleogene alkali basalts of the Poiana Ruscă Mountains (Romania). Geologica Carpathica, 66, 499-514.

Németh B, Török K, Kovács I, Szabó C, Abart R, Dégi J, Mihály J, Németh C (2015): Melting, fluid migration and fluid-rock interactions in the lower crust beneath the Bakony-Balaton Highland volcanic field: a silicate melt and fluid inclusion study. Mineralogy and Petrology, 109, 217-234.

Pál-Molnár E, Batki A, Almási E, Kiss B, Upton BGJ, Markl G, Odling N, Harangi Sz (2015a): Origin of mafic and ultramafic cumulates from the Ditrău Alkaline Massif, Romania. Lithos, 239, 1–18.

Pál-Molnár E, Batki A, Ódri Á, Kiss B, Almási E (2015b): Geochemical implications of the magmatic origin of granitic rocks from the Ditrău Alkaline Massif (Eastern Carpathians, Romania). GeologiaCroatica, 68, 51–66.

Panisova J, Balázs A, Zalai Z, Bielik M, Horváth F, Harangi Sz, Schmidt S, Gotze HJ (2018): Intraplate volcanism in the Danube Basin of NW Hungary: 3D geophysical modelling of the Late Miocene Pásztori volcano. International Journal of Earth Sciences, 107, 1713-1730.

Park M, Berkesi M, Jung H, Kil Y (2017): Fluid infiltration in the lithospheric mantle beneath the Rio Grande Rift, USA: a fluid-inclusion study. European Journal of Mineralogy, 29, 807-819.

Petrik, A; Beke, B.; Fodor, L.; Lukács,R. (2016): Cenozoic structural evolution of the southwestern Bükk Mts. and the southern part of the Darnó Deformation Belt (NE Hungary). Geologica Carpathica, 67(1), 83-104.

Pécskay Z, Gméling K, Molnár F, Benkó Zs (2015): Neogene calc-alkaline intrusive magmatism of post-collisional origin along the Outer Carpathians: A comparative study of the Pieniny Mountains and adjacent areas. Annales Societatis Geologorum Poloniae, 85, 77-89.

Pintér Z, Patkó L, Djoukam JFT, Kovács I, Tchouankoue JP, Falus G, Németh C (2015): Characterization of the sub-continental lithospheric mantle beneath the Cameroon volcanic line inferred from alkaline basalt hosted peridotite xenoliths from Barombi Mbo and Nyos Lakes. Journal of African Earth Sciences, 111, 170-193.

Sági T, Jankovics MÉ, Kiss B, Ntaflos T, Harangi Sz (2018): A new method for the olivine- and clinopyroxene fractionation modelling of alkaline basaltic magmas (in Hungarian with English abstract). Földtani Közlöny, 148, 273-292.

Seghedi I, Helvaci C, Pécskay Z (2015): Composite volcanoes in the south-eastern part of Izmir-balikesir transfer zone, Western Anatolia, Turkey. Journal of Volcanology and Geothermal Research, 291, 72-85.

Seghedi I, Szakács A, Pécskay Z, Mirea V, Luffi P (2017): The significance of debris avalanche deposits in the architecture of the Calimani-Gurghiu-Harghita volcanic range (Eastern Transylvania, Romania). Romanian Journal of Earth Sciences, 91 (Spec Iss), 78-79.

Szakács A, Pécskay Z, Gál Á (2018): Patterns and trends of time–space evolution of Neogene volcanism in the Carpathian–Pannonian region: a review. Acta Geodetica et Geophysica, 53, 347-367.

Szakács A, Seghedi I, Pécskay Z, Mirea V (2015): Eruptive history of a low-frequency and low-output rate Pleistocene volcano, Ciomadul, South Harghita Mts., Romania. Bulletin of Volcanology, 77, 2, Paper 12.

Szepesi J, Harangi Sz, Ésik Zs, Novák TJ, Lukács R, Soós I (2017): Volcanic Geoheritage and Geotourism Perspectives in Hungary: a Case of an UNESCO World Heritage Site, Tokaj Wine Region Historic Cultural Landscape, Hungary. Geoheritage, 9, 329-349

Szepesi J, Ésik Zs, Soós I, Novák TJ, Sütő L, Rózsa P, Lukács R, Harangi Sz (2018): Földtani objektumok értékminősítése: módszertani értékelés a védelem, bemutatás, fenntarthatóság és a geoturisztikai fejlesztések tükrében. Földtani Közlöny, 148, 143-160.

Vereb V, Karátson D, van Wyk de Vries B (2018): Geoheritage is coming to town: preservation of geological features in an urban environment with the example of geomorphological mapping on Clermont-Ferrand. Geophysical Research Abstracts, 20, Paper EGU 2018-11647.

Veres D, Cosac M, Schmidt C, Murătoreanu G, Hambach U, Hubay K, Wulf S, Karátson D (2018): New chronological constraints for Middle Palaeolithic (MIS 6/5-3) cave sequences in Eastern Transylvania, Romania. Quaternary International, 485, 103-114.

Wulf S, Fedorowicz S, Veres D, Karátson D, Gertisser R, Bormann M, Magyari E, Appelt O, Łanczont M, Gozhy PF (2016): The 'Roxolany Tephra' (Ukraine - new evidence for an origin from Ciomadul volcano, East Carpathians. Journal of Quaternary Science, 31, 565-576.

Zacek V, Burianek D, Pécskay Z, Skoda R (2016): Astrophyllite-alkali amphibole rhyolite, an evidence of early Permian A-type alkaline volcanism in the western Mongolian Altai. Journal of Geosciences, 61, 93-103.